Analysis and functional characterisation of the zDHHC9/GCP16 protein complex

A thesis presented by

Despoina Allagioti

In fulfilment of the requirement for the degree of

Doctor of Philosophy

2025

University of Strathclyde

Strathclyde Institute of

Pharmacy and Biomedical Sciences

Declaration of authenticity and author's rights

This thesis is the result of the author's original research. It has been composed by the author and has not been previously submitted for examination which has led to the award of a degree.

Signed: 

Date: 30/09/2025

Acknowledgements

I would like to express my sincerest thanks to my supervisor, Professor Luke H. Chamberlain, for being an exceptional mentor. Luke, I am deeply grateful for your support, guidance, and unwavering optimism during the past four years. Thank you for giving me the opportunity to be part of your lab – I genuinely could not have imagined a better mentor for this journey. The thumbs-up emojis will be missed!

To Dr. Christine Salaun, thank you for always making yourself available, no matter how busy you were. Thank you for helping me grow as a researcher, it was an honour to learn from you, and most importantly, thank you for all the chats. I would also like to thank Dr. Kimon Lemonidis, the AlphaFold master, for his valuable contribution and expertise.

A million thanks to Professor Shernaz Bamji for her incredible kindness and generosity, and of course to Taika for being an amazing friend. Thanks to Andrew for all his help during my time in Canada, and to Dr. Angie Wild for all the laughs and for being the best desk mate ever.

Special thanks to Dr. Liam Butler, my favourite lab buddy and very first PhD friend. Thank you for all the squash tournaments, the burgers, the simple lab tasks we turned into two-man jobs, and for making workdays fun. To Dr. Carla Busquets Hernández, I am so lucky you chose to be a guiri in Scotland. Thank you for bringing the sunshine in every single day. See you in April and in every April after that, mi amiga. Thanks to everyone who came through the lab and all the friends I made in SIPBS over the years. A big thank you to the SIPBS staff who made me feel so welcome, especially Gayle and Anne.

To all the people who made gloomy Glasgow feel like home, thank you from the bottom of my heart. I never could have imagined how many memories I would create in a place so far from everything I am used to. Thank you for making it special.

To Steph, my biggest bellyish, from Italian GCSE to PhD. Thank you for always being on the other end of the phone, whether it’s for a rant or just to be a body double. I can’t wait to be neighbours. To Filio, thank you for always being up for exhausting every topic, for getting on a plane every single year to fangirl with me and for always making it the funniest time ever. To Kate, thank you for being so close to me no matter

how many countries come between us. Thank you for the joy you transmit, I am so lucky to be in your orbit. I can’t wait for our big adventure! To my couch friends who became family, Nagia and Maria, thank you for always believing in me. To Nullis, my forever friend, thank you for everything.

To Janka, I can’t possibly describe how grateful I am for you. Thank you for your endless patience and support and for always saving the day, sometimes with just a single matcha.

Στην οικογένειά μου, ευχαριστώ για όλα όσα έχετε κάνει για μένα όλα αυτά τα χρόνια. Στην ΄Υζμα μου, που καταφέρνει πάντα να με κάνει να χαμογελάω. Στην πολυαγαπημένη μου γιαγιά, αμφιβάλλω αν θα είχα καταφέρει όσα έχω πετύχει μέχρι σήμερα αν δεν μου είχες μάθει τους πίνακες πολλαπλασιασμού. Μακάρι να μπορούσα να το μοιραστώ μαζί σου.

It would not have been the same without every one of you, thank you.

Publications

Research articles

Butler, L., Locatelli, C., Allagioti, D., Lousa, I., Lemonidis, K., Tomkinson, N. C. O., Salaun, C., & Chamberlain, L. H. 2023. S-acylation of Sprouty and SPRED proteins by the S-acyltransferase zDHHC17 involves a novel mode of enzyme-substrate interaction. *The Journal of Biological Chemistry*, 299(1), 102754. https://doi.org/10.1016/j.jbc.2022.102754.

Oral communications

Allagioti, D., Tomkinson, N. C. O., Salaun, C., & Chamberlain, L. H. 2025. Analysis of the interaction of zDHHC9 with its accessory protein GCP16. Cellular Basis of Disease (CBD) Seminar. University of Strathclyde, Glasgow, UK.

Allagioti, D., Tomkinson, N. C. O., Hannoush, R. N., Salaun, C., & Chamberlain, L. H. 2022. Targeting zDHHC9 interactions as a novel therapeutic strategy. Medical Research Scotland (MRS) PhD Studentship Researcher Development Event 25th – 26th April 2022. Crieff, UK.

Poster communications

Allagioti, D., Tomkinson, N. C. O., Hannoush, R. N., Salaun, C., & Chamberlain, L. H. 2024. Analysis of the interaction of zDHHC9 with its accessory protein GCP16. The Federation of American Societies for Experimental Biology (FASEB) Science Research Conference, Protein Lipidation: Enzymology, Signalling and Therapeutics 21st – 25th July 2024. Tucson, Arizona, USA. Appendix I.

Allagioti, D., Tomkinson, N. C. O., Salaun, C., & Chamberlain, L. H. 2024. Analysis of the interaction of zDHHC9 with its accessory protein GCP16 - Developing novel inhibitors to target oncogenic Ras. Strathclyde Institute of Pharmacy and Biomedical Sciences (SIPBS) PhD Research Day. University of Strathclyde, Glasgow, UK.

Allagioti, D., Tomkinson, N. C. O., Hannoush, R. N., Salaun, C., & Chamberlain, L. H. 2023. Targeting zDHHC9 interactions as a novel therapeutic strategy. The Biochemical Society: New Insights into Lipidation in Cell Biology 29th August – 1st September 2023. Liverpool, UK. Appendix II.

Allagioti, D., Tomkinson, N. C. O., Hannoush, R. N., Salaun, C., & Chamberlain, L. H. 2023. Targeting zDHHC9 interactions as a novel therapeutic strategy. Medical Research Scotland (MRS) PhD Studentship Researcher Development Event 24th – 25th April 2023. Pitlochry, UK.

Funding

This research was funded by a PhD studentship from Medical Research Scotland (MRS), in collaboration with Genentech, whose support is gratefully acknowledged.

Table of Contents

List of figures

CHAPTER 1

CHAPTER 3

CHAPTER 4

CHAPTER 5

List of tables

CHAPTER 1

CHAPTER 2

List of abbreviations

2-BP	2-Bromopalmitate (S-acylation inhibitor)
aa	Amino acid
ABHDs	α/β hydrolase domain-containing proteins
AMP	Adenosine 5′-monophosphate
AMPK	AMP-activated protein kinase
Ank	Ankyrin-repeat
APS	Ammonium persulfate
APT	Acyl-protein thioesterase
ATP	Adenosine triphosphate
Az	Azide
Bcl-2	B-cell lymphoma 2
BSA	Bovine serum albumin
Caax	Caax box prenylation motif
CCR5	C-C chemokine receptor type 5
CHX	Cycloheximide (protein synthesis inhibitor)
CMA	Cyano-myracrylamide
CoA	Co-enzyme A
COPI	Coat protein complex I
CRD	Cysteine-rich domain
CRISPR	Clustered regularly interspaced short palindromic repeats
CSP	Cysteine-string protein
DAPI	4’,6-diamidino-2-phenylindole
DHHC	Aspartic acid-Histidine-Histidine-Cysteine
DIFP	Diisopropyl fluorophosphonate
DMEM	Dulbecco's modified eagle medium
DMSO	Dimethyl sulfoxide
DNA	Deoxyribonucleic acid
DPG	Aspartate – proline – glycine motif
DTT	Dithiothreitol
E1	Ubiquitin-activating enzyme
E2	Ubiquitin-conjugating enzyme
E3	Ubiquitin ligase
EDTA	Ethylenediaminetetraacetic acid

EGFP	Enhanced green fluorescent protein
EGFR	Epidermal growth factor receptor
eNOS	Endothelial nitric oxide synthase
ER	Endoplasmic reticulum
ERAD	ER-associated degradation
FBS	Fetal bovine serum
FRET	Fluorescence resonance energy transfer
FSEC	Fluorescence-detection size-exclusion chromatography
FTase	Farnesyltransferase
FTI	Farnesyl transferase inhibitors
Gag	Group-specific antigen
GAPDH	Glyceraldehyde 3-phosphate dehydrogenase
GAPs	GTPase-activating proteins
GCP16	Golgi complex-associated protein of 16 kDa
GDP	Guanosine diphosphate
GEFs	Guanine nucleotide exchange factors
GGTase	Geranylgeranyltransferase
GPCR	G protein-coupled receptor
GS	Goat serum
GTP	Guanosine triphosphate
HA	Human influenza hemagglutinin
HATs	Histone acetyltransferases
HBSS	Hanks' Balanced Salt Solution
HDFP	Hexadecylfluorophosphonate
HEK293T	Human embryonic kidney 293 cells, expressing the SV40 large T antigen
HIV-1	Human immunodeficiency virus 1
HPLC	High-performance liquid chromatography
HTT	Huntingtin
ICMT	Isoprenylcysteine carboxyl methyltransferase
IFN	Interferon
IL	Interleukin
IP	Immunoprecipitation
ipTM	Predicted template modelling score
ipTM	Interface predicted template modelling score
IR680	Infrared reporter of 680 nm
IR800	Infrared reporter of 800 nm

KATs	Lysine acetyltransferases
kDa	KiloDalton
KDAC	Lysine deacetylase
KO	Knockout
LRP6	Low-density lipoprotein receptor-related protein 6
MAP6	Microtubule-associated protein 6
MC1R	Melanocortin-1 receptor
MEM	Minimum Essential Medium
mPEG	Monomethoxy polyethylene glycol
mRNA	Messenger ribonucleic acid
mSH	Metabolic serine hydrolase
NADH	Nicotinamide adenine dinucleotide hydrogen)
NCLs	Neuronal ceroid lipofuscinoses
NF-κB	Nuclear Factor-kappa-light-chain-enhancer of activated B cells
NLSDI	Neutral Lipid Storage Disease with Ichthyosis
NMT	N-myristoyltransferase
PaCCT	Palmitoyltransferase conserved C-terminal motif
PAE	Predicted aligned error
PBM	PDZ-binding motif
PBS	Phosphate buffered saline
PBS-T	Phosphate buffered saline containing 0.1% Tween® 20
PCR	Polymerase chain reaction
PEI	Polyethylenimine
PFA	Paraformaldehyde
pLDDT	Predicted local distance difference test
PLM	Phospholemman
PMSF	Phenylmethylsulfonyl fluoride
PolyQ	Expanded polyglutamine
PPII	Polyproline-II
PPTs	Palmitoyl-protein thioesterases
PSA	Prostate-specific antigen
PSD-93	Postsynaptic density protein-93
PSD-95	Postsynaptic density protein-95
PTMs	Post-translational modifications
Ras	Rat sarcoma
Rce1	Ras converting Caax endopeptidase 1
REP	Rab escort protein

RNA	Ribonucleic acid
RNAi	Ribonucleic acid interference
RT-PCR	Reverse Transcription Polymerase Chain Reaction
RUSH	Retention using selective hooks
SDS-PAGE	Sodium Dodecyl Sulphate-Polyacrylamide Gel Electrophoresis
Selk	Selenoprotein K
SEM	Standard error of mean
SH3	Src homology 3
siRNA	Small interfering RNA
SNAP23	Synaptosomal-associated protein of 23 kDa
SNAP25	Synaptosomal-associated protein of 25 kDa
SNARE	Synaptosomal-associated protein receptors
SPRED	Sprouty-related EVH1 domain containing protein
STRIPAK	Striatin-interacting phosphatase and kinase
STRN4	Striatin-4
SUMO	Small ubiquitin-like modifier.
TBTA	Tris(benzyltriazolylmethyl)amine.
TEM8	Tumour endothelial marker 8, or anthrax toxin receptor 1
TEMED	N,N,N',N'-tetramethylethylenediamine
TM	Transmembrane
TMDs	Transmembrane domains
TNFR	Tumour necrosis factor receptor
TPS	Total protein stain
TTxE	Threonine – threonine – x – glutamate motif
Tul1	Transmembrane ubiquitin ligase 1
VSV-G	Vesicular stomatitis virus
WT	Wild-type
XLID	X-linked intellectual disability
Yck	Yeast casein kinase
zDABM	zDHHC ankyrin-binding motif
zDHHC	Zinc finger DHHC motif-containing acyltransferase

Abstract

S-Acylation is a reversible post-translational modification that affects many proteins, influencing their localisation, interactions, stability and activity. S-Acylation is mediated by 23 zinc finger DHHC enzymes (zDHHCs), which are predominantly catalytically autonomous. However, zDHHC9 requires an accessory protein, GCP16, for S-acylation activity. We hypothesise that interfering with the zDHHC9/GCP16 interaction offers a novel approach for selective inhibition of this enzyme. However, before inhibitors of the zDHHC9/GCP16 complex can be rationally designed, it is important to understand the mechanisms and regulatory consequences of this interaction. This thesis characterises the bidirectional effects of zDHHC9/GCP16 complex formation on the S-acylation and stability of both proteins in mammalian cells, also highlighting critical residues in the binding interfaces at the N- and C-terminal regions of GCP16. The stabilisation of GCP16 required S-acylation by zDHHC9 and, indeed, non-acylated GCP16 mutants were more rapidly degraded by the proteasome; interestingly, the presence of non-acylated cysteines appeared to be linked to GCP16 degradation. Furthermore, comparison of non-acylated GCP16 mutants with either intact cysteines or cysteine-to-alanine substitutions suggested that the cysteine residues in GCP16 are also important for membrane association before S-acylation. This suggests a model where cysteines and surrounding hydrophobic residues initially target GCP16 to the membrane and subsequent S-acylation (perhaps by driving deeper membrane insertion) protects the protein from degradation – this may provide a mechanism to ensure that GCP16 is always complexed with partner zDHHC enzymes by ensuring the rapid degradation of non-complexed protein. Finally, analysis of mutant forms of GCP16 with disrupted interaction with zDHHC9, demonstrated that the formation of an intact zDHHC9/GCP16 complex is critical for dendritic growth in hippocampal neurons. Overall, this study provides a detailed characterisation of the bidirectional regulation of the zDHHC9/GCP16 interaction, providing new insights that can underpin development of selective inhibitors of zDHHC9.

CHAPTER 1

GENERAL INTRODUCTION

Chapter 1 - General introduction

Introduction

There are approximately 20 thousand protein-coding genes in mammalian cells, making up only a small fraction of the genome (Khan and Smith, 2021). However, these genes can undergo modifications that expand the protein repertoire and can give rise to thousands more proteins. Each gene can code for multiple protein isoforms through alternative splicing, a process in which the coding regions of a gene, known as exons, are joined to form multiple combinations giving rise to different mRNA transcripts that are then translated into proteins. Additionally, each of these newly synthesised proteins can undergo chemical changes referred to as post-translational modifications (PTMs), giving rise to different forms of the same protein. One single protein can undergo multiple PTMs that can regulate a range of processes like protein activity, stability, localisation and interactions with other proteins.

There are hundreds of different PTMs, with the most commonly studied being phosphorylation and glycosylation (Ramazi and Zahiri, 2021). Protein lipidation, a general term characterising a group of modifications where lipids, or lipid-like groups, are attached to protein substrates is of particular relevance to this project. Lipidation can impact protein hydrophobicity, regulate protein trafficking, facilitate membrane association, and influence protein structure and stability (Chamberlain and Shipston, 2015, Anwar and van der Goot, 2023). S-Acylation is one of the main subsets of lipid modifications and it involves the reversible attachment of fatty acids to protein substrates via acyltransferase enzymes, while acyl protein thioesterases catalyse their removal (Ramazi and Zahiri, 2021).

S-acylation influences an array of proteins, including receptors, signalling molecules, ion channels and transporters (Zmuda and Chamberlain, 2020) and affects several biological pathways, such as Ras/MAPK (Swarthout *et al.*, 2005), and epidermal growth factor receptor (EGFR) signalling (Bollu *et al.*, 2015). Acyltransferase enzymes mediating the S-acylation of substrates belong to the zDHHC family of enzymes (Roth *et al.*, 2006). The activity of these zDHHC enzymes can be regulated by a number of factors including other PTMs (Zmuda and Chamberlain, 2020), fatty acyl-coenzyme A (CoA) availability, or by the activity of accessory or regulatory co-factors (Salaun *et al.*, 2020). For example, zDHHC9, the main focus of this thesis, requires the

accessory protein GCP16 (Golgi complex-associated protein of 16 kDa) for its activity *in vitro* (Swarthout *et al.*, 2005, Salaun *et al.*, 2020). Dysregulation of S-acylation is linked to several diseases, including neurological disorders such as X-linked intellectual disability (XLID), epilepsy (Shimell *et al.*, 2019), Alzheimer's disease (Natale *et al.*, 2024), and cancer (Resh, 2017), and therefore, zDHHC enzymes are of significant pharmacological importance.

1.1 Post-translational modifications

PTMs are chemical modifications of amino acid side chains that can regulate protein stability, and impact protein activity, interactions, localisation, and function. PTMs are thereby crucial in maintaining proteostasis, the dynamic and tight regulation of a functional proteome (Samarzija, 2021). Common PTMs include phosphorylation, glycosylation, ubiquitination, methylation, acetylation, SUMOylation, and lipidation (Figure 1.1) (Ramazi and Zahiri, 2021). These modifications take place at various locations within the cell and can either be reversible or irreversible (Ramazi and Zahiri, 2021). Although hundreds of different types of PTMs have been described, only a small fraction have been studied in detail at the proteome level (Samarzija, 2021). As PTMs play a major role in regulating protein behaviour, they are widely recognised as potential sites of intervention in disease states where protein activity is dysregulated.

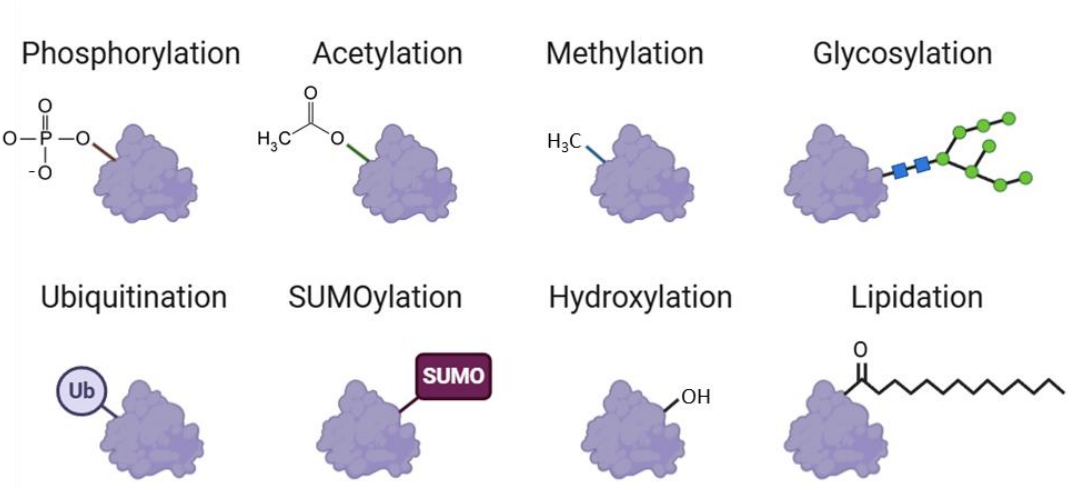

Figure 1.1 Common post-translational modifications.

The illustration highlights some of the most common protein modifications. Ubiquitination and SUMOylation involve the addition of small protein molecules to target proteins. There are various types of lipidation, the figure shows S-acylation (the attachment of a fatty acyl chain) as an example of a common lipidation modification. Created using BioRender.com.

Phosphorylation is the reversible attachment of a phosphate group derived from the hydrolysis of adenosine triphosphate (ATP), onto a serine, threonine, or tyrosine residue by kinase enzymes (Ardito *et al.*, 2017, Ramazi and Zahiri, 2021). According to the dbPTM database (https://biomics.lab.nycu.edu.tw/dbPTM/), serine phosphorylation is the most widely recorded PTM after ubiquitination (Ramazi and Zahiri, 2021). Amongst the myriads of proteins that undergo phosphorylation is the tumour suppressor protein p53 that regulates cell division. Phosphorylation of p53 takes place at multiple sites in the protein. In this case, phosphorylation affects the stability and activation of the protein to regulate the cell cycle, to allow for DNA repair or to induce apoptosis (MacLaine and Hupp, 2011).

Protein acetylation involves the reversible transfer of an acetyl group ($COCH_3$) from an acetyl donor, such as acetyl-CoA, onto predominantly lysine residues of substrate proteins. This process is catalysed by lysine acetyltransferases (KATs) or otherwise referred to as histone acetyltransferases (HATs) (Ramazi and Zahiri, 2021). Protein acetylation is a highly specific PTM, and it was first described as a regulator of gene

transcription, acting as a transcriptional co-activator. HAT enzymes located in the nucleus act on lysine residues present on histones, changing their positive charge and allowing for the packaged DNA to unwind and be transcribed. This process is reversible, and subsequent removal of the acetyl group is catalysed by lysine deacetylase (KDAC) enzymes (Samarzija, 2021).

Methylation is another reversible PTM which is also heavily involved in histone regulation in the nucleus. Methylation is catalysed by methyltransferase enzymes and involves the addition of a methyl group (CH_3) to a substrate protein. This modification largely occurs on lysine and arginine residues (Ramazi and Zahiri, 2021). Histone methylation can either activate or repress transcription by making DNA more or less accessible to transcription factors and RNA polymerase enzymes. Demethylases reverse the effects of methylation.

Glycosylation, which can be reversible or irreversible, characterises the covalent attachment of oligosaccharide chains by glycosyltransferase enzymes. Common types of glycosylation include the addition of a glycan group to the amide group of an asparagine residue, termed as N-glycosylation, or to the hydroxyl oxygen of serine or threonine residues, known as O-glycosylation (Samarzija, 2021). This PTM affects approximately 50% of all proteins found in blood plasma (Ramazi and Zahiri, 2021). Changes in protein glycosylation patterns are linked to diseases, making them a useful tool for disease diagnosis. In fact, altered glycosylation of prostate-specific antigen (PSA) is linked to prostate cancer, and PSA glycoform profiling using mass spectrometry offers a more specific screening test that distinguishes between cancerous and benign cases, in contrast to screening for elevated serum PSA levels (Butler and Huang, 2021).

Ubiquitination involves the covalent ligation of ubiquitin, a small regulatory protein, primarily to lysine residues via an isopeptide bond, but it can actually involve all 20 amino acids. The process is mediated by a protein complex consisting of ubiquitin-activating (E1), ubiquitin-conjugating (E2) and ubiquitin ligase (E3) enzymes, while deubiquitinase enzymes reverse ubiquitination. Polyubiquitination occurs when more ubiquitin molecules are successively linked to one of the seven lysine residues within ubiquitin (Song and Luo, 2019, Ramazi and Zahiri, 2021). Monoubiquitination mainly affects protein trafficking, while polyubiquitination also results in protein degradation by the proteasome (Samarzija, 2021). However, essentially every cell process is

regulated by this modification, including cell proliferation, DNA repair, innate immune signalling, and apoptosis (Karve and Cheema, 2011, Samarzija, 2021).

SUMOylation is the reversible covalent addition of small ubiquitin-related modifier (SUMO) proteins to the amino group of lysine residues of substrate proteins. The processes of SUMOylation and ubiquitination are mechanistically similar and often target the same residues within substrate proteins (McClurg and Robson, 2015). SUMOylation is also catalysed by a multi-enzyme complex of E1, E2 and E3 enzymes and is reversed by SUMO proteases (Ramazi and Zahiri, 2021). In contrast to ubiquitination, SUMOylation does not trigger protein degradation, but instead is often involved in protein localisation and activity regulation. An example of a SUMOylation substrate is the transcription factor NF-κB, whose p65 RelA subunit is SUMOylated at lysine-37, lysine-121 and lysine-122, repressing its activity and NF-κB-mediated gene expression (Liu *et al.*, 2012).

Hydroxylation is the addition of a hydroxyl group (OH) by hydrolase enzymes, typically on proline and lysine residues. A well-known hydroxylated protein is collagen. Hydroxylation is crucial for the stability of the triple helix of collagen, and it is also proposed to influence the flexibility of the protein and uncover functional sites required for protein interactions (Rappu *et al.*, 2019).

In addition to these PTMs, there is a diverse array of other modifications that occur on cellular proteins and of particular relevance to this thesis is protein lipidation, a general term characterising a group of modifications where lipids, or lipid-like groups, are attached to protein substrates. The modifying groups include fatty acids, isoprenoids, phospholipids and sterols (Chamberlain and Shipston, 2015).

1.2 Protein lipidation

Protein lipidation can impact substrates in various ways, including increasing protein hydrophobicity, regulating protein trafficking, facilitating membrane association, and influencing protein structure and protein stability (Chamberlain and Shipston, 2015, Anwar and van der Goot, 2023). Common lipid modifications include N-terminal glycine N-myristoylation, C-terminal cysteine prenylation that is comprised of farnesylation and geranylgeranylation, and cysteine S-acylation (Samarzija, 2021).

N-Myristoylation is the covalent and irreversible transfer of myristic acid, a 14-carbon fatty acid (C14:0), to the N-terminal glycine residues of substrate proteins, forming an amide bond (Jiang *et al.*, 2018). N-Myristoylation is catalysed by the N-myristoyltransferase (NMT) enzymes, NMT-1 and NMT-2. Proteins do not naturally have an N-terminal glycine, and hence, N-myristoylation is primarily considered a co-translational modification, where the myristate is added to glycine-2, following removal of the initiating methionine of the nascent peptide during protein translation (Yuan *et al.*, 2020). Examples of co-translationally N-myristoylated proteins include Gα subunits that are then localised to the membrane, where they associate with the β and γ subunits to form the heterotrimeric G protein complex involved in G-protein coupled receptor (GPCR) signalling (Preininger *et al.*, 2012). Another example is the human immunodeficiency virus type 1 (HIV-1) group-specific antigen (Gag) protein that also requires N-myristoylation for membrane association and virus assembly (Lindwasser and Resh, 2002). However, post-translational N-myristoylation has also been documented to occur during apoptosis when proteins have undergone caspase-mediated cleavage, exposing amine groups of internal glycines that can be modified by NMTs (Yuan *et al.*, 2020). An example of a post-translationally N-myristoylated protein is BH3-interacting domain death agonist of the B-cell lymphoma 2 (Bcl-2) family of pro-apoptotic proteins. After proteolytic cleavage, the protein is post-translationally N-myristoylated and targeted to the mitochondrial membrane, where it triggers apoptosis (Zha *et al.*, 2000).

A further type of lipidation is prenylation, or isoprenylation, which characterises the attachment of either a 15-carbon (farnesyl) or a 20-carbon (geranylgeranyl) isoprenoid lipid to cysteine residues at the C-terminal region of protein substrates. This modification is catalysed by either farnesyltransferase (FTase), or geranylgeranyltransferase 1 and 2 (GGTase-1 and -2), and always occurs post-translationally (Wang and Casey, 2016). Well-characterised substrates include Ras proteins whose prenylation is important for their initial targeting to the cell membrane (Anwar and van der Goot, 2023).

N-Myristoylation and prenylation both have defined consensus sequences. N-Myristoylation is dependent upon the presence of an N-terminal glycine residue in the consensus sequence MGxxxS/T (where x = any amino acid), while prenylation typically requires a C-terminal Caax motif, where A represents an aliphatic (hydrophobic) amino acid and X represents any amino acid, the latter determining

whether a farnesyl or a geranylgeranyl isoprenoid group will be added to the protein substrate (Nadolski and Linder, 2007, Zverina *et al.*, 2012). Specifically, where X is alanine, glutamine, methionine, or serine, then the isoprenoid group added will be farnesyl, whereas a geranylgeranyl group is added if X is isoleucine, leucine, or phenylalanine. However, FTase and GGTase-1 enzymes have also been shown to have some overlapping substrate specificity. In the case of K-Ras, the CVIM motif tends to be farnesylated, but it can also be geranylgeranylated if FTase is inhibited. Another example is Rho B, whose CKVL motif is both farnesylated and geranylgeranylated (Palsuledesai and Distefano, 2015). Rab proteins, on the other hand, contain C-terminal motifs different from the classic Caax motif found in Ras and Rho protein families. The prenylated motifs in Rab proteins are CC or CxC, which are strictly recognised by GGTase-2 in association with a Rab escort protein (REP), resulting in a geranylgeranyl lipid group being added to each cysteine residue. The double geranylgeranylation mediates the membrane association of Rab, where the protein is activated (Farnsworth *et al.*, 1994, Homma *et al.*, 2021). Rab8 however is atypical, since it ends in a Caax motif, CVLL, and can be prenylated by both GGTase-1 and REP-dependent GGTase-2 (Wilson *et al.*, 1998).

In contrast to N-myristoylation and prenylation, S-acylation has no defined consensus sequence, and thus the study of S-acylation using prediction models is very limited. Instead, any free cysteine residues in soluble or transmembrane proteins that are positioned at the cytoplasmic surface of cell membranes and accessible to membrane-bound S-acylation enzymes are possible S-acylation sites (Nadolski and Linder, 2007, Chamberlain and Shipston, 2015). S-acylation sites are located throughout the protein sequence but are frequently found in pairs or as longer stretches of cysteine residues and can be positioned close to transmembrane domains or other hydrophobic amino acids (Nadolski and Linder, 2007).

1.3 Protein S-acylation

S-Acylation is an exclusively post-translational modification that involves the reversible addition of a fatty acid onto one or more cysteine residues of a protein substrate, resulting in the formation of a thioester bond. The discovery of S-acylation was reported in 1979 by Schmidt and Schlesinger in Sindbis virus-infected cells. The

authors used radiolabelled [^{3}H] palmitate, followed by membrane protein isolation and sodium dodecyl sulphate-polyacrylamide gel electrophoresis (SDS-PAGE), to demonstrate the incorporation of palmitate onto viral envelope glycoproteins. They discovered that the modification was attached by a thioester bond using hydroxylamine cleavage. This study was the first direct demonstration of lipid attachment to proteins (Schmidt and Schlesinger, 1979).

The most frequently added fatty acid is palmitate (C16:0), and thus, S-acylation is often referred to as palmitoylation. However, other saturated and unsaturated fatty acyl chains can be transferred to S-acylation substrates, including myristic acid (C14:0), palmitoleic acid (C16:1), stearic acid (C18:0), oleic acid (C18:1), linoleic acid (C18:2), and arachidonic acid (C20:4) (Chamberlain and Shipston, 2015, West *et al.*, 2022). The first experimental demonstration that fatty acids other than palmitate can be incorporated into proteins via S-acylation was reported by Olson *et al.* (1985). Their study indicated that even though most radiolabelled [^{3}H] myristic acid was linked to substrates via an amide bond, some was linked via ester linkage, which was released by hydroxylamine treatment and determined by high-performance liquid chromatography (HPLC) in a BC3H1 muscle cell line. In addition, the proteins labelled with palmitate and myristate differed, exhibiting fatty acid specificity (Olson *et al.*, 1985). Since then, advancements in mass spectrometry (MS) have allowed for a more accurate profiling of the S-linked lipids.

A recent study by Busquets-Hernández *et al.* (2024) has reported a novel hydroxylamine-based mass spectrometry workflow for the identification of fatty acid species attached via S-acylation in cells and tissues. In this study, hydroxylamine treatment released the attached fatty acids, which were then converted into more stable fatty acid hydroxamate derivatives and were finally analysed by liquid chromatography mass spectrometry, which enabled quantitative detection of attached fatty acids in a proteome-wide manner. This innovative approach can also allow for the simultaneous profiling and quantification of acyl-CoA substrate availability, demonstrating a direct association of endogenous acyl-CoA levels and substrate S-acylation lipid profiles. This study also revealed differences in the lipid profile of the S-acylated proteome in different tissues, along with enzyme-specific acyl chain preferences (Busquets-Hernandez *et al.*, 2024).

Since the discovery of S-acylation, there have been great advances made in both the knowledge and the methodologies to study this modification. These breakthroughs

include the discovery of the relevant enzymes controlling this process. In addition, proteomic studies have identified a diverse array of S-acylation substrates. Indeed, it is estimated that at least 20% of the human proteome might be S-acylated, including membrane receptors, signalling proteins, ion channels, transporters, and structural proteins (Chamberlain and Shipston, 2015, Blanc *et al*., 2019, West *et al*., 2022).

The hydrophobic nature of the fatty acid chains that are added can have a substantial impact on the biochemical properties and functions of the S-acylated protein substrates. S-acylation increases the hydrophobicity of the substrate proteins, thereby increasing their membrane affinity, impacting their localisation, protein-protein interactions, and interactions with membrane domains (Blaskovic *et al*., 2013, Blanc *et al*., 2019).

1.4 The zDHHC family of acyltransferases

Protein S-acylation is catalysed by a family of zDHHC acyltransferase enzymes, first identified in 2002 in the yeast *Saccharomyces cerevisiae*. More specifically, ankyrin repeat-containing protein (Akr) 1 and Erf2 were the first identified yeast proteins with S-acyltransferase activity (Lobo *et al*., 2002, Roth *et al*., 2002). Akr1 was reported as the S-acyltransferase for the yeast casein kinase (Yck) 2, since deletion of Akr1 abolished labelling of Yck2 with [^{3}H] palmitate, similarly to a Yck2 cysteine-to-serine mutant (Roth *et al.*, 2002). Erf2 was first shown to be linked to S-acylation of Ras2 in a genetic screening study, where deletion of Erf2 resulted in decreased Ras2 S-acylation and protein mis-localisation (Bartels *et al.*, 1999). Further studies revealed that Erf2 co-purifies with Erf4 in both yeast and *E.coli*, and provided evidence of a direct role in Ras2 S-acylation (Lobo *et al.*, 2002).

Akr1 and Erf2 are not evolutionary similar, except for a shared conserved 51-amino acid zinc finger Asp-His-His-Cys cysteine-rich domain (DHHC-CRD) (Roth *et al.*, 2002). Mutagenesis analysis of Erf2 proved the importance of the DHHC-CRD domain for its function (Bartels *et al.*, 1999). Alanine substitution of the conserved histidine-201 in the DHHC domain of Erf2 abolished Ras S-acylation directly, while serine substitution of cysteine-189 disrupted the interaction with Erf4, which then abolished Ras S-acylation (Lobo *et al.*, 2002). Similarly, mutations of the DHYC tetrapeptide motif in Akr1 disrupted the incorporation of [^{3}H] palmitate in Yck2 and the

autoacylation of Akr1, proving the requirement of an intact DHHC motif for both autoacylation and substrate S-acylation activity (Roth *et al.*, 2002). Subsequently, a total of seven proteins with a DHHC-CRD were identified in *Saccharomyces cerevisiae* (Lobo *et al.*, 2002, Roth *et al.*, 2006), while 23 distinct zDHHC-encoding genes have now been identified in the human genome (Fukata *et al.*, 2004) (Figure 1.2). Fukata *et al.* (2004) isolated and sequenced all 23 mouse zDHHC proteins and studied their S-acyltransferase activity towards postsynaptic density protein-95 (PSD-95), a synaptic scaffolding protein, and other proteins using [^{3}H] palmitate in COS7 and HEK293 cells. The results of this study further highlighted the S-acylation activity of zDHHC enzymes, as well as their substrate specificity, since not all zDHHCs were able to catalyse PSD-95 S-acylation (Fukata *et al.*, 2004).

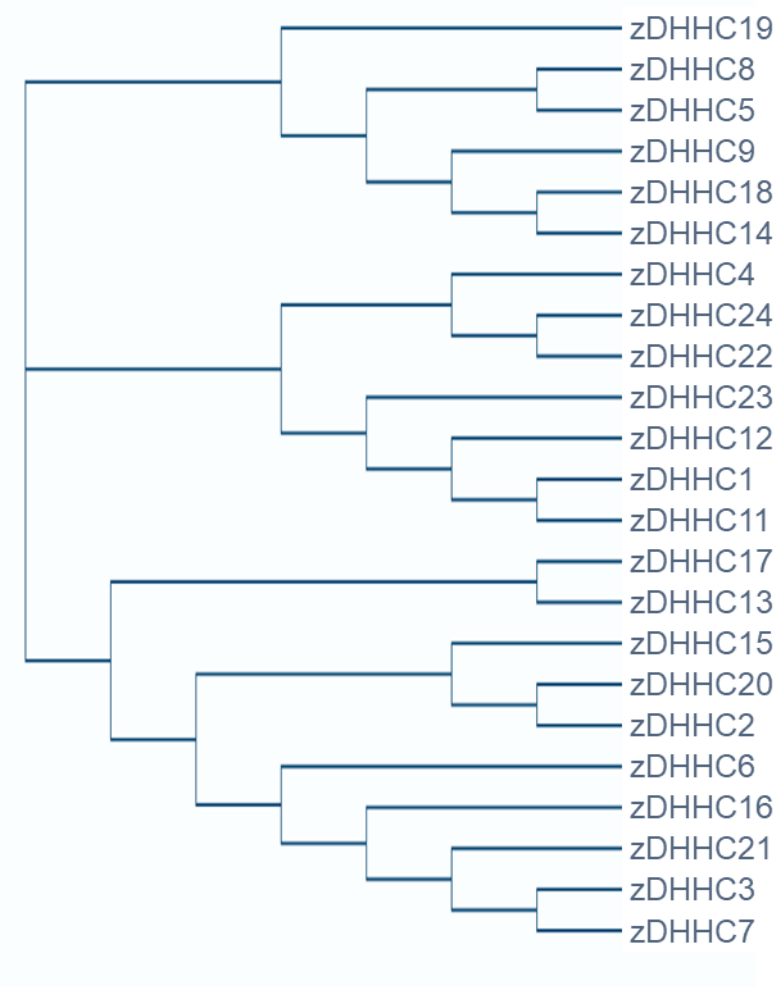

Figure 1.2 The evolutionary relationship between the 23 human zDHHC enzymes.

Phylogenetic cladogram tree of all 23 human zDHHC acyltransferase enzymes, based on full-length sequence homology, generated using the Clustal Omega multiple sequence alignment tool on Uniprot (https://www.uniprot.org/align) (UniProt, 2025).

zDHHC enzymes are present in all eukaryotic species, mediating the S-acylation of around 10% of the proteomes in yeasts, protozoans, plants, and mammalian systems (Zhang and Hang, 2017). A fundamental study by Roth *et al.* (2006) indicated that zDHHC enzymes mediate essentially all S-acylation in yeast. The group developed strains in which zDHHC protein encoding genes were deleted and discovered that the S-acylation of 29 out of 30 substrates analysed was abolished. Residual S-acylation seen could be due to a lack of a strain with all seven zDHHC genes deleted included

in the analysis, along with overlapping substrate S-acylation activity between isoforms. The same study also allowed the pairing of some protein substrates with certain zDHHC enzymes since strains deficient in individual zDHHC enzymes uncovered isoform-dependent substrates (Roth *et al.*, 2006).

1.4.1 The structure of zDHHC enzymes

All zDHHC enzymes are integral, polytopic membrane proteins with four to six transmembrane domains (TMDs). Most zDHHC enzymes are predicted to have four TMDs and the DHHC-CRD active site is located in a cytosolic loop between TMDs 2 and 3 (Figure 1.3A) (Malgapo and Linder, 2021). However, isoforms zDHHC13, zDHHC17 and zDHHC23 are predicted to have six TMDs, with the DHHC-CRD active site located between TMDs 4 and 5 (Figure 1.3B), while zDHHC4 and zDHHC24 are predicted to have five TMDs (Figure 1.3C and D) (Salaun *et al.*, 2020, Malgapo and Linder, 2021). In addition, zDHHC13 and zDHHC17 have a cytosolic ankyrin repeat (Ank) domain at their N-terminal region which is involved in substrate recognition (Figure 1.3B) (Lemonidis *et al.*, 2015b, Malgapo and Linder, 2021). A conserved feature of zDHHC enzymes is the positioning of the catalytic DHHC-CRD in the cytoplasm, consistent with S-acylation taking place at the cytoplasmic face of the membrane lipid bilayer (Lemonidis *et al.*, 2015b, Rana *et al.*, 2018a). Most zDHHC isoforms are predicted to also have both their N- and C- terminal domains in the cytoplasm (Philippe and Jenkins, 2019), with zDHHC4 and zDHHC24 being the exceptions. The N-terminal domain of zDHHC4 and the C-terminal of zDHHC24 are thought to face the lumen (Rana *et al.*, 2018b).

The multipass transmembrane nature of zDHHC proteins makes them challenging targets for structural characterisation. The first high-resolution molecular structure of a zDHHC enzyme was published by the Banerjee group in 2018. The group solved the molecular structure of human zDHHC20 and a catalytically inactive mutant of zebrafish zDHHC15 using X-ray crystallography. These isoforms were selected after screens for protein stability, yield and monodispersity using fluorescence-detection size-exclusion chromatography (FSEC) analysis of their autoacylation activity through a coupled-enzyme assay using the free CoA to form fluorescently detected NADH,

and analysis of their S-acylation activity using appropriate substrates in an *in vitro* assay using purified proteins (Rana *et al.*, 2018a).

The crystal structures published revealed that the four TMDs of zDHHC20 and zDHHC15 have a “teepee-like” membrane topology, with the TMDs tilting closer to each other on the luminal interface and being further away from each other on the cytosolic interface. The DHHC-CRD active site and the C-terminal domain were facing the cytosolic interface in both models (Rana *et al.*, 2018a). Moreover, it was confirmed that two CCHC-coordinated zinc fingers bind to the DHHC-CRD (Rana *et al.*, 2018a). Although the zinc ions do not directly interact with the catalytic cysteine (Rana *et al.*, 2018a), it was assumed that they have a structural role relating to its optimal orientation, as mutation of the conserved cysteine and histidine residues in CCHC decreased the stability and catalytic activity of zDHHC3 (Gottlieb *et al.*, 2015). The zinc finger motifs, however, are not required for substrate S-acylation, since Akr1, Akr2, and Pfa5 in yeast, along with zDHHC22 in humans lack almost all the cysteines and histidines coordinating the two zinc fingers (Mitchell *et al*., 2010, Gottlieb *et al*., 2015). The DHHC tetrapeptide motif of zDHHC20 is positioned on the β5 and β6 hairpins coordinating the zinc ions, with histidine-155 coordinating the zinc ion on one face of the hairpin and aspartate-153 and histidine-154 forming a hydrogen bond, facing the membrane on the other side of the hairpin. The catalytic cysteine-156 is also facing the membrane bilayer, and a cross section of zDHHC20 indicated a hydrophobic cavity formed right above the active site. This orientates the catalytic cysteine at a favourable position to accommodate a long hydrophobic acyl chain into the hydrophobic part of the membrane bilayer during autoacylation (Rana *et al.*, 2018a).

It has been shown that different zDHHC enzymes prefer different fatty acyl CoA substrates (Jennings and Linder, 2012). The results of an *in cellulo* S-acylation assay using different fatty acids in click chemistry experiments showed that zDHHC3 and zDHHC7 display a variable fatty acid selectivity, despite their structural similarity. Chimeric mutant analyses pinned this down to a single isoleucine residue, isoleucine-182, on TMD3 of zDHHC3, in contrast to a serine-185 residue present at the same position in zDHHC7. The bulky isoleucine is thought to restrict zDHHC3 to only using fatty acid ligands shorter than 16-carbons, while zDHHC7 can use longer chain ligands (Greaves *et al.*, 2017).

Rana *et al.* (2018a) also used the S-acylation inhibitor 2-bromopalmitate (2-BP) which covalently interacts with the catalytic cysteine-156 of zDHHC20 to study the crystal structure of the enzyme when the active site is occupied. This analysis showed that 2-BP is incorporated into the hydrophobic cavity formed by the TMDs, right above the catalytic cysteine and also identified highly conserved residues lining the cavity. These residues include tryptophan-28, tryptophan-158 and phenylalanine-171, which are found near the base of the cavity and whose alanine substitution compromises the enzyme's catalytic activity, and phenylalanine-174 and leucine-227, which are located further into the membrane and are conserved as hydrophobic residues within the zDHHC family. Substitution of leucine-227 with tryptophan, a bigger and bulkier amino acid, also reduced catalytic activity. Other residues found in the zDHHC20 cavity enclosing the acyl chain are only conserved in a subfamily of zDHHCs. An example is isoleucine-22, whose substitution with tryptophan decreases the enzymatic activity of zDHHC20, because the bulkier tryptophan replacement results in a new interaction with the acyl chain. Other than their size, the polarity of the residues found in the hydrophobic cavity of zDHHC enzymes and their interacting with the acyl-chain during the autoacylation step, can affect the chemical properties of the cavity that then influences the acyl chain selectivity profile of the enzyme (Rana *et al.*, 2018a).

In zDHHC20, tyrosine-181 is the homologous residue to isoleucine-182 in TMD3 of zDHHC3, which was reported to restrict the length of acyl chain that can be used by this enzyme (Greaves *et al.*, 2017). Tyrosine-181 in zDHHC20 forms a H-bond with serine-29 found in TMD1 at the top of the fatty acid binding cavity. Substitution of serine-29 in zDHHC20 with a bulkier residue altered the preferred fatty acid ligand to ones with shorter acyl chains, while mutation of tyrosine-181 to a smaller residue resulted in longer fatty acid ligands being incorporated, like stearic acid (C18:0). In zDHHC3, isoleucine-182 forms a H-bond with phenylananine-53, while in zDHHC7 serine-185 forms a H-bond with leucine-56. Both pairs are found at the top end of the cavity, and their positioning and size can explain the increased ability of zDHHC7 to use C18:0 as a substrate (Rana *et al.*, 2018a). In agreement with this finding, substituting isoleucine-182 in zDHHC3 with serine, a smaller amino acid, showed an increased ability to use C18:0 as a substrate (Greaves *et al.*, 2017). The space within the membrane cavity of zDHHC enzymes is therefore the main determining factor for acyl chain length selectivity. However, detailed computational analyses are required to fully understand and define the fatty acid chain interactions with the TMD lipid-binding cavity in different zDHHC enzymes (Rana *et al.*, 2018a).

Other identified conserved motifs within the zDHHC family, outside of the DHHC-CRD, include an aspartate – proline – glycine (DPG) motif, a threonine – threonine – x – glutamate (TTxE) motif, and a palmitoyltransferase conserved C-terminal (PaCCT) motif (Mitchell *et al.*, 2006, Gonzalez Montoro *et al.*, 2009, Rana *et al.*, 2018a). These three short motifs are present at the cytosolic side of the membrane; DPG is located right before the DHHC-CRD, while TTxE and PaCCT are downstream of the catalytic site (Figure 1.3). The TTxE and PaCCT motifs in the C-terminal region have been shown to mediate interactions of the DHHC-CRD and the TMDs. The first threonine of TTxE stabilises the C-terminal helix by capping a main-chain amide nitrogen, the second threonine directly interacts with the aspartate in the DHHC motif, while the glutamate interacts with a conserved arginine in the DHHC-CRD of zDHHC20. Hence, mutation of the TTxE motif decreases the S-acylation activity of the enzyme. As for the PaCCT C-terminal motif, the highly conserved asparagine-266 maintains the structural integrity of zDHHC20 through the interaction with nearby residues of TMD3 and TMD4, and alanine substitution of this residue decreases enzymatic activity (Rana *et al.*, 2018a).

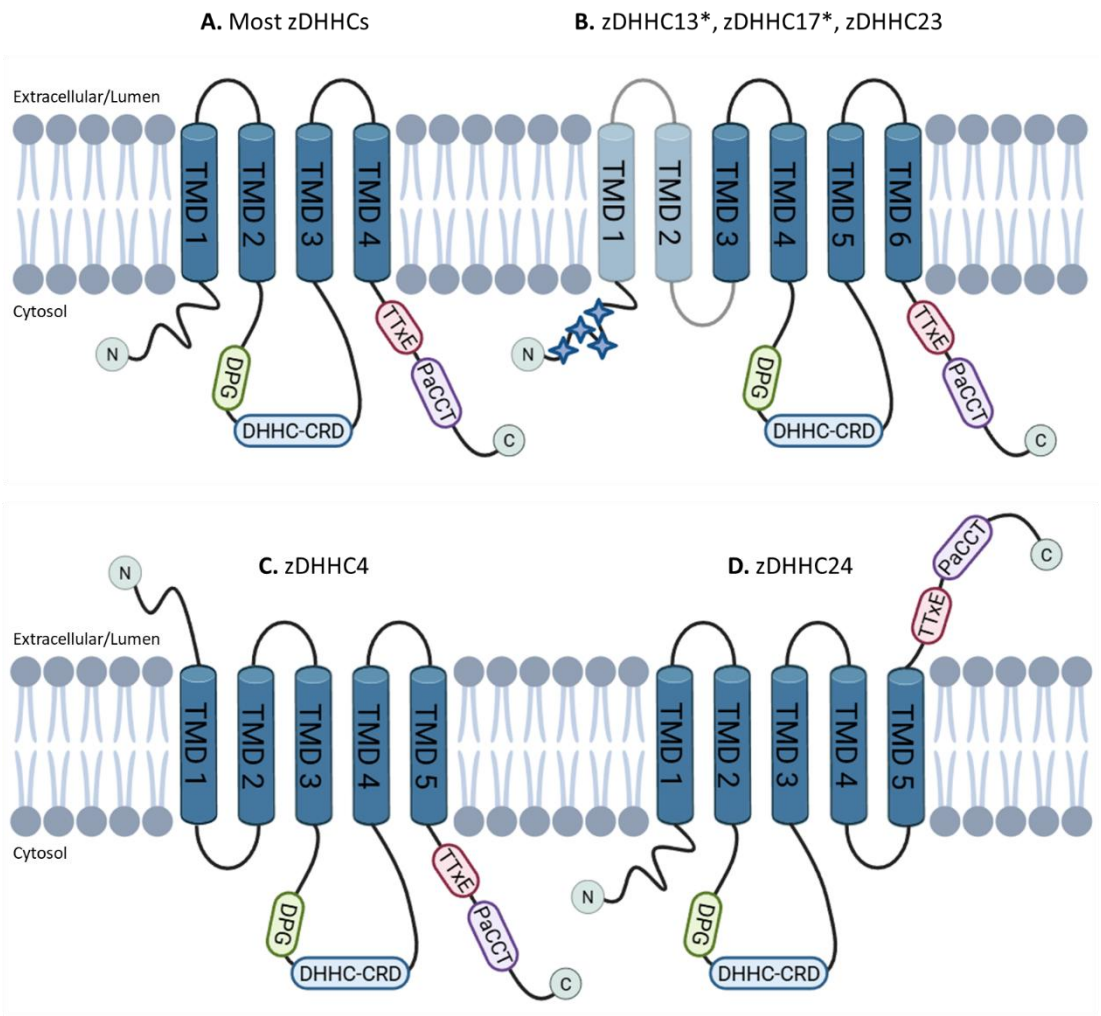

Figure 1.3 Schematic of the membrane topology and conserved motifs of zDHHC enzymes.

(A) *zDHHCs with 4 TMDs: the DHHC-CRD is located between TMD2 and TMD3. Both the N- and C-terminal domains are located in the cytosol.* ***(B)*** *zDHHCs with 6 TMDs - zDHHC13, zDHHC17 and zDHHC23: the DHHC-CRD is located between TMD4 and TMD5. The N-terminal ankyrin repeat (Ank) domain of zDHHC13 and zDHHC17 is indicated with an asterisk and is displayed with the use of star shapes. Note that zDHHC23 does not have an Ank domain. Both the N- and C-terminal domains are located in the cytosol.* ***(C)*** *zDHHC4 has 5 TMDs and the DHHC-CRD is located between TMD3 and TMD4. The N-terminal region is positioned in the extracellular space, while the C-terminal domain is found in the cytosol.* ***(D)*** *zDHHC24 has 5 TMDs and the DHHC-CRD is located between TMD2 and TMD3. The N-terminal region is located in the cytosol, while the C-terminal domain is found in the extracellular space.*

The DHHC-CRD catalytic region is positioned at the cytosolic face of the lipid bilayer in all zDHHC enzymes. The conserved DPG short motif is located at the cytosol right before the DHHC-CRD, while TTxE and PaCCT are found at the C-terminal region. Created using BioRender.com.

1.4.2 The catalytic mechanism of zDHHC enzymes

As previously mentioned, zDHHC enzymes are defined by their conserved zinc finger cysteine-rich domain, containing the DHHC tetrapeptide motif. This tetrapeptide motif forms the enzymes' catalytic site and is responsible for their S-acylation activity (Greaves and Chamberlain, 2011, Philippe and Jenkins, 2019).

The catalytic mechanism of S-acylation is a nucleophilic substitution reaction, and it takes place via a two-step "ping-pong" mechanism, using a CoA derivative as the activated lipid substrate. The first step involves the three catalytic residues of the DHHC region, referred to as the catalytic triad: aspartate and histidine, which form a H-bond, and the catalytic cysteine. Histidine is polarised by aspartate, which then deprotonates the cysteine, which then acts as a nucleophile and attacks the carbonyl carbon of the fatty acyl-CoA. This results in the transfer of the acyl group from acyl-CoA to the DHHC motif cysteine residue, and the release of CoA-SH. This is defined as the "autoacylation step". The other histidine of the DHHC motif, although not directly involved in the autoacylation step, is important for the coordination of one of the two zinc ions, which are crucial for maintaining the functional and structural integrity of the enzyme (Mitchell *et al.*, 2010, Jennings and Linder, 2012, Rana *et al.*, 2018a). During the intermediate autoacylation step, the acyl chain is enclosed in the hydrophobic cavity formed by the four TMDs of the zDHHC enzymes (Rana *et al.*, 2018a, Meng *et al.*, 2023). Subsequently, the second step of this ping-pong mechanism involves the transfer of the acyl group from the DHHC motif to a cysteine residue of a protein substrate and the regeneration of the zDHHC enzyme (Figure 1.4) (Jennings and Linder, 2012). The crystal structure of the 2-BP–treated zDHHC20 revealed that the carbonyl oxygen of the acyl chain incorporated onto the cysteine of the DHHC motif is positioned in close proximity to histidine-154. This suggests that the protonated histidine, which received a proton in the first step, now mediates the activation of the autoacylated intermediate via donating a proton to the carbonyl

oxygen. The crystal structure also demonstrated that the substrate can only interact with the autoacylated intermediate via the front side, as the other sides of the attached acyl group are enclosed by hydrophobic residues. However, it is possible that substrate interaction results in conformational changes that allow the second catalysis step to occur through a different angle (Rana *et al.*, 2018a).

Mitchell *et al.* (2010) uncovered the kinetics of the Erf2/Erf4 protein complex by measuring the rate of CoA-SH generated as a result of autoacylation in a coupled enzyme assay using thin-layer chromatography. This served as an indirect method of studying the association between the acyl-chain donor and the S-acyltransferase enzyme. They found that autoacylation occurs in a burst within the first 5 seconds and then becomes linear, while release of the acyl chain via hydrolysis is slower. This was the first study to propose the two-step ping-pong S-acylation model. They demonstrated that substrate addition resulted in an increased use of acyl-CoA, while the release of free fatty acid was decreased, suggesting that the acyl group was transferred to the substrate (Mitchell *et al.*, 2010). Furthermore, Jennings and Linder (2012) were the first to prove that the fatty acid is transferred from the autoacylated enzyme to a protein substrate. The authors added substrate to purified zDHHC2 and zDHHC3 labelled with [^{3}H] palmitate, in the presence of unlabelled palmitoyl-CoA, and they observed that the radioactive palmitate was transferred from the enzyme to the substrate. If a substrate is not available, the autoacylated intermediate undergoes hydrolysis and returns to its original state, releasing a free fatty acid, which was depicted by a slower release of palmitate from the labelled zDHHC enzymes (Jennings and Linder, 2012).

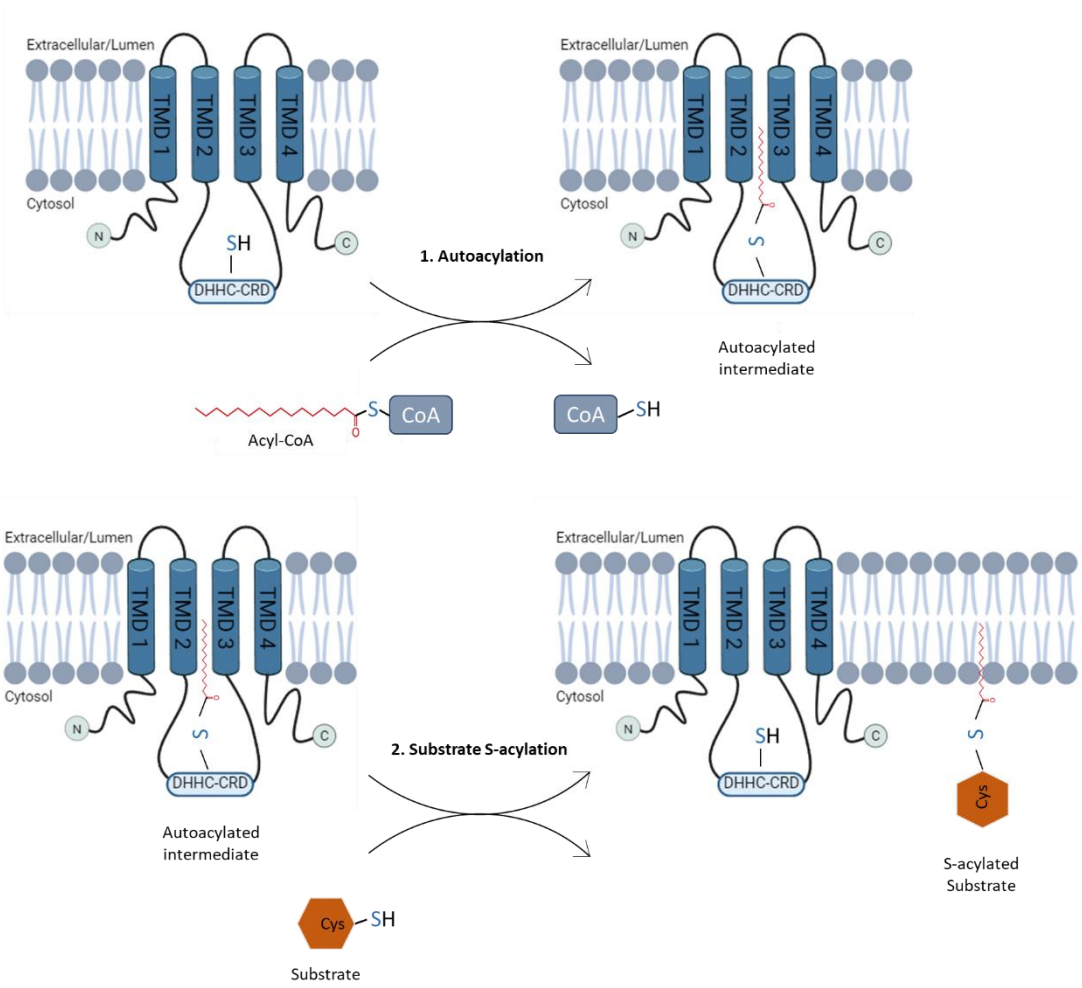

Figure 1.4 Schematic of the S-acylation ping-pong mechanism of zDHHC enzymes.

The first step involves the transfer of the acyl group from acyl-CoA to the cysteine residue of the DHHC motif, forming a zDHHC autoacylated intermediate and releasing CoA. The second step involves the transfer of the acyl group from the autoacylated DHHC motif to a cysteine residue of a protein substrate, resulting in substrate membrane association. The zDHHC enzyme is then regenerated for another round of catalysis. Created using BioRender.com.

The highly conserved DHHC motif is crucial for both the autoacylation step and the transfer of the fatty acid group to the substrate. However, some atypical catalytic motifs have also been reported, like the DHYC motif in yeast Akr1p, Akr2p and Pfa5 (Tabaczar *et al.*, 2017). The zDHHC13 mammalian isoform is also characterised by a unique DQHC motif, while maintaining its S-acylation activity (Malgapo and Linder, 2021). The cysteine residue within the tetrapeptide catalytic motif was long regarded as critical for S-acylation activity. Mutation of the cysteine residue to serine (DHHS) or alanine (DHHA) results in loss of both enzyme autoacylation and substrate S-acylation, both *in vitro* and *in vivo*, and these mutants are regularly used as catalytically inactive controls (Mitchell *et al*., 2010, Jennings and Linder, 2012, Gonzalez Montoro *et al*., 2015, Lemonidis *et al*., 2015b). However, based on mutagenesis experiments of the DHHC catalytic motif, it was suggested that there may be alternative mechanisms for S-acylation. Yeast S-acyltransferase mutants of Swf1 and Pfa4 displaying atypical catalytic motifs, DHHR, or DHHA and DHHR, respectively, were reported to remain partially active in substrate S-acylation, possibly by stabilising the transition state intermediate (Gonzalez Montoro *et al*., 2015, Tabaczar *et al*., 2017, Rana *et al*., 2018b).

1.4.3 The intracellular localisation of zDHHC enzymes

Ohno *et al.* (2006) investigated the intracellular localisation and tissue distribution of all zDHHC enzymes from human and the yeast *Saccharomyces cerevisiae.* For the seven yeast zDHHC enzymes, immunofluorescent microscopy of HA-tagged constructs demonstrated that Akr1 and Akr2 had discontinuous patterns indicative of Golgi localisation, Erf2 was shown as two ring patterns suggesting nuclear and cortical ER localisation, while Pfa3 was shown as a ring pattern similar to the vacuolar dye FM4-64. HA-tagged Pfa4 and Pfa5, on the other hand, were undetectable and were therefore fused with EGFP. EGFP-Pfa4 was shown as two rings, suggesting ER localisation, and EGFP-Pfa5 was mostly found at the plasma membrane and less so at vacuole-vacuole junctions (Ohno *et al.*, 2006). Immunofluorescent microscopy of either EGFP-tagged or HA-tagged Swf1 indicated that it is found at the ER (Valdez-Taubas and Pelham, 2005).

Analysis of the intracellular localisation of human zDHHC protein constructs in HEK293 cells via immunofluorescent microscopy demonstrated that zDHHC1, zDHHC6, zDHHC11, zDHHC14, zDHHC19, zDHHC23 and zDHHC24 are located in the ER, co-localising with the ER-resident protein calreticulin. On the other hand, perinuclear staining patterns were seen for zDHHC3, zDHHC4, zDHHC7, zDHHC8, zDHHC15, zDHHC17, and zDHHC18, along with co-localisation with the Golgi marker GM130. Isoforms zDHHC2, zDHHC9, zDHHC12, and zDHHC13 exhibited both ER and Golgi localisation, merging with both calreticulin and GM130. Additionally, a smaller subset of zDHHC enzymes, consisting of zDHHC5 and zDHHC20 showed plasma membrane localisation, while zDHHC21 was found both at the plasma membrane and at the ER (Ohno *et al.*, 2006). The localisation of zDHHC16 could not be identified in this study, however, subsequent confocal microscopy mapped zDHHC16 to the ER (Ernst *et al.*, 2018). Furthermore, zDHHC17 was also found in recycling and late endosomes, associating with vesicular structures in neurons, and at the plasma membrane (Huang *et al.*, 2004), whereas zDHHC2 and zDHHC5 were subsequently shown to cycle between the plasma membrane and recycling endosomes in neurons and neuroendocrine cells (Greaves *et al.*, 2011, Brigidi *et al.*, 2015, Salaun *et al.*, 2017).

Ernst *et al.* (2018) investigated the distribution of Golgi-localised human zDHHCs in more detail using super-resolution microscopy. They used probes for endogenously expressed *cis*- and *trans*-Golgi protein markers in stimulated emission depletion (STED) microscopy experiments. This revealed that the majority of Golgi-localised zDHHC enzymes, including zDHHC3, zDHHC7, zDHHC13, zDHHC17, zDHHC21, and zDHHC24, are concentrated at the *cis*-Golgi, while zDHHC9, zDHHC15, and zDHHC23 are found in the *trans*-Golgi compartment and in post-Golgi structures (Ernst *et al.*, 2018).

Table 1.1 summarises the subcellular localisation of all zDHHC isoforms. It is important to note that some zDHHC enzymes have been localised to different intracellular compartments in different studies. These studies all used overexpression of zDHHC enzymes and often different cell types, for example, HEK293 cells and neurons. It will be important to explore the localisation of endogenous zDHHC enzymes when suitable antibodies and higher sensitivity detection are available.

zDHHC isoform	Intracellular localisation
zDHHC1	ER, Golgi
zDHHC2	ER, Golgi, plasma membrane, recycling endosomes
zDHHC3	*cis*-Golgi
zDHHC4	ER, Golgi, nuclear envelope
zDHHC5	plasma membrane, recycling endosomes
zDHHC6	ER
zDHHC7	*cis*-, *medial*-, (low) *trans*-Golgi
zDHHC8	Golgi, plasma membrane
zDHHC9	ER, (low) *cis*-, *medial*-, *trans*-Golgi
zDHHC11	ER, Golgi
zDHHC12	ER, Golgi
zDHHC13	ER, *cis*-Golgi
zDHHC14	ER, Golgi, plasma membrane, recycling endosomes
zDHHC15	*trans*-Golgi
zDHHC16	ER
zDHHC17	*cis*-, *medial*-Golgi, plasma membrane, recycling endosomes
zDHHC18	Golgi, plasma membrane, recycling endosomes
zDHHC19	ER, Golgi
zDHHC20	ER, Golgi, plasma membrane
zDHHC21	ER, *cis*-Golgi, plasma membrane
zDHHC23	ER, *trans*-Golgi
zDHHC24	ER, *cis*-Golgi
zDHHC25	Golgi

Table 1.1 The intracellular localisation of zDHHC enzymes.

The table shows the intracellular localisation reported for mammalian zDHHC enzymes in different studies, with all reported localisations shown for each enzyme (Huang *et al*., 2004, Ohno *et al*., 2006, Greaves *et al*., 2011, He *et al*., 2014, Salaun *et al*., 2017, Ernst *et al*., 2018).

Although there is little information on the mechanisms that determine the subcellular localisation of zDHHC enzymes, specific sorting signals have been identified in the sequence of some zDHHCs. ER membrane-targeting lysine-based sorting signals Kxx and KKxx (where x = any amino acid) have been identified in the extreme C-terminal tails of zDHHC4 and zDHHC6, respectively (Gorleku *et al.*, 2011). The retention mechanism of these lysine-based sorting signals is based on the association with coat protein complex I (COPI) proteins that mediate retrograde transport from the Golgi to the ER. Truncated zDHHC4 and zDHHC6 mutants in which 5 C-terminal amino acids, including the lysine-based sorting signals are removed lost their ER localisation, while addition of these sorting signals onto the C-terminal tail of zDHHC3 shifted the enzyme's localisation from the Golgi to the ER, confirming their identity as ER retention signals (Gorleku *et al.*, 2011). Furthermore, two endocytic signals - SxxxLL and NP – have been identified at the C-terminal tail of zDHHC2, and proposed to be endocytic sorting signals as their mutation increased the plasma membrane accumulation of the enzyme (Greaves *et al.*, 2011, Salaun *et al.*, 2017). Another example is that of zDHHC20-long, an extended version of the canonical zDHHC20 isoform, which is found to be exclusively localised to the ER instead of the typical Golgi, vesicular and plasma membrane localisation seen with canonical zDHHC20. This variation in intracellular localisation is a result of an N-terminal tetrapeptide PERW motif present in the sequence of zDHHC20-long. This PERW motif appears to mediate ER retention, rather than retrograde retrieval. This was demonstrated when the two isoforms were used in a retention using selective hooks (RUSH) assay using zDHHC20 reporters fused to a streptavidin-binding peptide and a streptavidin-tagged ER hook that traps the protein to the ER membrane. Biotin-induced release of the zDHHC20 reporters, followed by live microscopy to monitor protein transport, indicated that zDHHC20 trafficked to the Golgi, while zDHHC20-long was retained in the ER (Mesquita *et al.*, 2023).

Analysis of the tissue distribution of human zDHHC mRNAs using reverse transcription-PCR (RT-PCR) by Ohno *et al.* (2006) allowed the categorisation of the isoforms into (i) highly ubiquitous: zDHHC4, zDHHC5, zDHHC7, zDHHC8, zDHHC11, zDHHC12, zDHHC13, zDHHC17, and zDHHC24, (ii) nearly ubiquitous: zDHHC1, zDHHC3, zDHHC6, zDHHC9, zDHHC14, zDHHC16, zDHHC18, and zDHHC21, and (iii) tissue-specific: zDHHC19, zDHHC20, and zDHHC23. More specifically, zDHHC19 and zDHHC23 were detected in testis, while zDHHC20 was detected in

the placenta and testis. The isoforms zDHHC2 and zDHHC15 were not detected in any of the tissues examined (Ohno *et al.*, 2006).

1.5 zDHHC9

zDHHC9 is the focus of this study, and was identified based on sequence homology of its DHHC domain to Akr1, a yeast S-acyltransferase protein (Fukata *et al.*, 2004). It has a molecular mass of 40,916 Dalton (Da), consisting of 364 amino acids (Uniprot ID: Q9Y397). The enzyme has the common zDHHC structure composed of four TMDs. The N-terminal region of zDHHC9 is present in the cytoplasm (aa 1-35) and is followed by the four TMDs: TMD1 – aa 36-56, TMD2 – aa 64-84, TMD3 – aa 184-204, and TMD4 – aa 229-249, with two luminal loops (aa 57-63 and aa 205-228) and one cytoplasmic loop (aa 85-183). The C-terminal region is also cytoplasmic (aa 250-364). The DHHC-CRD (aa 139-189) is found in the cytosolic loop between TMD2 and TMD3 (Figure 1.5) (UniProt, 2025).

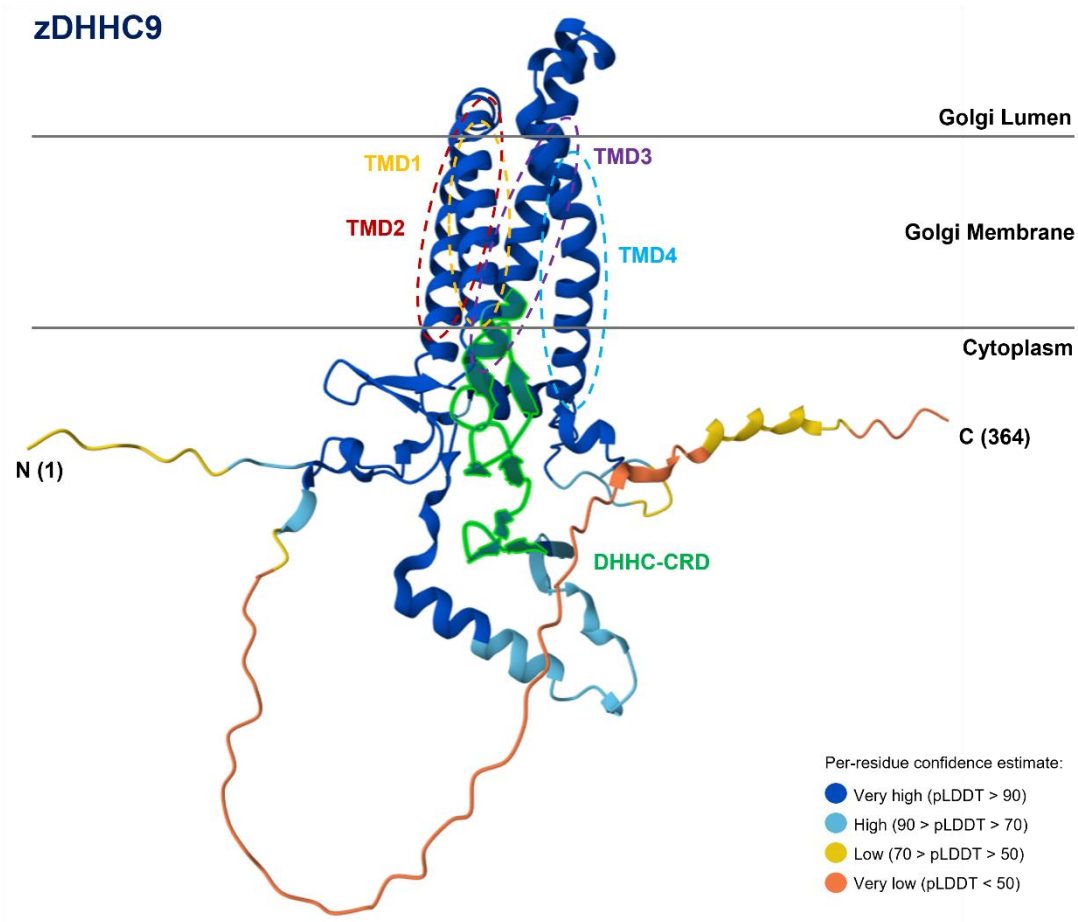

Figure 1.5 The AlphaFold-predicted structure of zDHHC9.

AlphaFold structural prediction model of zDHHC9 (Human) (AF-Q9Y397-F1-v4). The protein structure is designed based on a per-residue confidence estimate score that is scaled from 0 to 100 and measured by the predicted local distance difference test (pLDDT). The residues within the structure are also colour-coded based on their pLDDT. The schematic highlights the approximate spatial orientation of the DHHC-CRD domain, transmembrane domains 1-4 (TMD1-4), and the N- and C-terminal regions relative to the Golgi. The AlphaFold protein structure database was developed by DeepMind and EMBL-EBI (Jumper et al., 2021, Varadi et al., 2022, Varadi et al., 2024).

Confocal microscopy subcellular localisation experiments in HEK293 cells have shown that zDHHC9 is localised to the ER and Golgi (Swarthout *et al.*, 2005, Ohno *et al.*, 2006). Northern blot analysis revealed that zDHHC9 is expressed in various human tissues, such as the brain, skeletal muscle, kidney, liver, lung, and, to a lesser extent in the heart, colon, small intestine, and placenta, while it was not detected in the thymus, spleen, and peripheral blood leukocyte tissues (Swarthout *et al.*, 2005, Ohno *et al.*, 2006, Raymond *et al.*, 2007).

Mutation of the conserved cysteine-169 residue of the DHHC motif to a serine residue results in loss of zDHHC9 autoacylation and, therefore, subsequent substrate acylation (Swarthout *et al.*, 2005), as reported for other zDHHC enzymes. Interestingly, zDHHC9 was the first zDHHC isoform with an obligatory accessory protein to be discovered. The catalytic activity of zDHHC9 seems to be dependent on the association with an accessory protein named GCP16, also known as GOLGA7 (Golgin subfamily A member 7). Enzymatic assays have demonstrated that in the absence of GCP16, zDHHC9 is inactive (Swarthout *et al.*, 2005).

zDHHC9 has received much interest as a novel anti-cancer target since it was reported to have activity towards H- and N-Ras proteins, contributing to their plasma membrane association and downstream cell signalling effects (Swarthout *et al.*, 2005). Additionally, mutations in *ZDHHC9* cause X-linked intellectual disability (XLID) and childhood epilepsy (Raymond *et al.*, 2007). Individuals with XLID caused by mutations in *ZDHHC9* also demonstrated hypoplasia of the corpus callosum (Baker *et al.*, 2015).

1.6 GCP16 (Golgi complex-associated protein of 16 kDa)

GCP16, or Golga7, is a small, peripheral Golgi complex-associated protein consisting of 137 amino acids and with a molecular weight of 15,824 Da (Uniprot ID: Q7Z5G4) (UniProt, 2025). GCP16 was discovered in a yeast two-hybrid screen for GCP170 interactors. GCP170 is a member of the golgin family of proteins associated with the cytoplasmic face of the Golgi membrane whose cleavage is involved in the breakdown of the Golgi during programmed cell death. The association of GCP16 with GCP170 was also validated in a co-immunoprecipitation assay using Triton X-100 lysates of HeLa cells. GCP16 is implied to be involved in secretory pathway processes, as

overexpression of GCP16 in COS-1 cells inhibited protein transport of the G protein of vesicular stomatitis virus (VSV-G) from the Golgi to the cell surface, without impacting Golgi morphology (Ohta *et al.*, 2003).

GCP16 is most widely known for its role as an accessory protein for zDHHC9 (Swarthout *et al.*, 2005). Immunofluorescent analysis of GCP16 localisation in HeLa or COS-1 cells showed that the protein is found in the Golgi complex, co-localising with giantin and GCP170. Northern blot analysis revealed that GCP16 is ubiquitously expressed in various human tissues, including the brain, heart, testis, ovary, skeletal muscle, spleen, kidney, liver, small intestine, placenta, lung, and peripheral blood cells, but not in the colon and thymus. This highlights a high overlap in the tissue expression of GCP16 and zDHHC9 (Ohta *et al*., 2003, Swarthout *et al*., 2005), consistent with them functioning as a protein complex.

GCP16 can also interact with zDHHC5 and zDHHC8 in co-immunoprecipitation experiments performed in HEK293 cells (Ko *et al.*, 2019, Salaun *et al.*, 2020). Moreover, Golga7b (Golgin subfamily A member 7B), a protein with 75% sequence homology to GCP16 consisting of 167 amino acids and with a molecular weight of 18,335 Da (Uniprot ID: Q2TAP0) (UniProt, 2025), has also been identified as an interactor of zDHHC5 in a protein interactome study (Huttlin *et al.*, 2015, Salaun *et al.*, 2020). Golga7b is characterised by longer and distinct N- and C-terminal regions, compared to GCP16, while the central region of the proteins, including the cysteine residues, are highly conserved (Figure 1.6) (UniProt, 2025). The association of Golga7b with zDHHC5 has been validated in co-immunoprecipitation experiments. The protein was also shown to regulate the localisation of zDHHC5 in HeLa cells, and this could not be recovered by expression of GCP16 in Golga7b siRNA knockdown cells, suggesting that the distinct N- and C-terminal regions of Golga7b might be involved in the functional interaction with zDHHC5 (Woodley and Collins, 2019).

Figure 1.6 Amino acid sequence alignment of GCP16 and Golga7b.

*Amino acid sequence alignment of human GCP16 (amino acids 1-137) (*Uniprot ID: Q7Z5G4) *and Golga7b (amino acids 1-167)* (Uniprot ID: Q2TAP0)*, generated using the Clustal Omega multiple sequence alignment program through the align tool from UniProt (UniProt, 2025). Identical amino acids are highlighted in purple.*

GCP16 is not predicted to contain any transmembrane regions but yet it does exhibit integral membrane protein behaviour. This was shown to be linked to the S-acylation of the protein, predominantly at cysteine-69 and cysteine-72 (Ohta *et al.*, 2003, Swarthout *et al.*, 2005). Specifically, it was shown that there was reduced incorporation of [^{3}H] palmitic acid into GCP16 mutants with either cysteine-69 or cysteine-72 substituted to alanine, while a double mutant removed almost all S-acylation signal. Immunofluorescence microscopy experiments in HeLa cells using mutant GCP16 proteins lacking these acylation sites showed that the double cysteine mutant failed to localise to the Golgi and was distributed into the cytoplasm instead. In contrast, mutants with only a single substitution of either cysteine-69 or cysteine-72 were still observed at the Golgi complex. This highlighted the importance of GCP16 S-acylation of cysteine-69 and cysteine-72 for membrane association (Ohta *et al.*, 2003). The two S-acylation sites of GCP16 have also proved to be essential for the formation of the zDHHC9/GCP16 complex, as mutation of C69 and C72 in GCP16 resulted in failure to interact with zDHHC9 (Mitchell *et al.*, 2014). GCP170 also failed to co-immunoprecipitate with the C69A/C72A mutant of GCP16 in HeLa cells (Ohta *et al.*, 2003).

1.7 The zDHHC9/GCP16 and Erf2/Erf4 protein complexes

zDHHC9 was characterised as the human orthologue of Erf2 (the Ras S-acyltransferase enzyme in yeast) based on the high sequence identity of their DHHC-CRD and predicted structural similarity (Swarthout *et al.*, 2005). Work on *Saccharomyces cerevisiae* showed that the S-acyltransferase activity of Erf2 was dependent on the association with an accessory protein named Erf4 (Lobo *et al.*, 2002, Zhao *et al.*, 2002). Subsequently, Swarthout *et al.* (2005) identified GCP16 as a possible mammalian orthologue of Erf4 (Swarthout *et al.*, 2005). zDHHC9 was further confirmed as a human orthologue of Erf2 in a functional assay in yeast, after the phenotype of Erf2 mutant strains was partially rescued by zDHHC9 and GCP16 co-expression. The assay indicated that although zDHHC9 or GCP16 alone are not functionally interchangeable with Erf2 and Erf4 respectively, the zDHHC9/GCP16 complex can partially substitute for the loss of Erf2/Erf4 activity (Mitchell *et al.*, 2014).

Expression levels of Erf2 were found to be significantly reduced in cells lacking Erf4, suggesting that the accessory protein might stabilise the enzyme (Lobo *et al.*, 2002). A later study by Mitchell *et al.* (2012) using cycloheximide inhibition of protein synthesis, showed that Erf2 degradation was indeed enhanced in Erf4 mutant cells. It was proposed that Erf4 association shields Erf2 from ubiquitylation and subsequent degradation by the ubiquitylation-mediated ER-associated degradation (ERAD) system. In support of this hypothesis, the authors used a C-terminal lysine-to-arginine mutant of Erf2 to show that the decrease in stability was a result of ubiquitylation-dependent degradation. They also detected Erf2 polyubiquitylation in Erf4 mutant cells and highlighted that the stability of Erf2 in the absence of Erf4 in yeast strains with mutations in crucial ERAD genes was comparable to that of wild-type Erf2 (Mitchell *et al.*, 2012).

GCP16 has also been suggested to have a similar stabilisation effect on zDHHC9, at least in purified systems. Swarthout *et al.* (2005) noted that zDHHC9 was more unstable when expressed and purified from Sf9 insect cells in the absence of GCP16, as a lot of the purified enzyme was degraded (Swarthout *et al.*, 2005). Furthermore, FSEC analysis of HEK293 cell lysates showed that zDHHC9 forms aggregates in the absence of GCP16 co-expression (Nguyen *et al.*, 2023).

The regulatory effects of Erf4 are not limited to stabilisation of Erf2. In fact, experiments using fluorescently labelled acyl-CoA indicated that the autoacylation of Erf2 was reduced in the absence of Erf4. This was shown to be a result of increased hydrolysis of the thioester bond between the catalytic cysteine and the attached acyl chains, examined by measuring CoA-SH release. A C-terminal truncation mutant of Erf2 lacking 58 amino acids also showed increased hydrolysis even with Erf4 co-expression, suggesting that Erf4 stabilisation of DHHC autoacylation might be mediated through an interaction with the C-terminus of Erf2 (Mitchell *et al.*, 2012). Moreover, it is believed that Erf4 may also be involved in the transfer of the acyl chain to substrates, either by direct involvement in the acyl transfer, substrate recognition, or both (Mitchell *et al.*, 2012, Salaun *et al.*, 2020).

Similarly to Erf2/Erf4, GCP16 is also thought to be involved in regulating zDHHC9 activity. In an experiment using radioactive palmitate and Ras as a substrate, GCP16 expression was essential for both the autoacylation and the catalytic activity of zDHHC9 against Ras. Furthermore, the zDHHC9/GCP16 complex exhibits substrate selectivity, as a purified zDHHC9/GCP16 complex from infected Sf9 insect cells showed S-acylation activity against H- and N-Ras with C-terminal cysteines, but not against known S-acylation substrates with N-terminal motifs, such as $G\alpha_{i1}$ and GAP-43 (Swarthout *et al.*, 2005). Further analysis of purified proteins revealed that the autoacylated intermediate of zDHHC9 is more susceptible to hydrolysis in the absence of GCP16 (Mitchell *et al.*, 2014), which is consistent with findings made with the Erf2/Erf4 complex. As the C-terminus of Erf2 was suggested to be important for functional interaction with Erf4, it was also proposed that GCP16 might be interacting with the C-terminal tail of zDHHC9 for DHHC domain stabilisation (Salaun *et al.*, 2020). In fact, a later study identified a conserved C-terminal cysteine motif with the “CCxxxC” sequence at amino acid positions 283, 284 and 288 whose mutation abolished GCP16-mediated stabilisation of zDHHC9 in an FSEC screening analysis, with cysteine-288 being the most critical of this motif (Nguyen *et al.*, 2023).

1.7.1 The cryo-EM structures of the zDHHC9/GCP16 and Erf2/Erf4 protein complexes

Yang *et al.* (2024) recently solved the cryo-EM structures of the Erf2/Erf4 and zDHHC9/GCP16 protein complexes (Figure 1.7). The zDHHC9/GCP16 complex excludes amino acids 304-364 that form the C-terminal region of zDHHC9. However, the authors demonstrated that these residues are not important for activity as a truncated mutant of zDHHC9 (aa 1-305) has the same S-acylation activity as the full-length protein (Yang *et al.*, 2024).

The Erf2/Erf4 and zDHHC9/GCP16 complexes show high structural similarity; they both consist of four TMDs, a large cytoplasmic region including three anti-parallel β-sheets forming the two zinc finger motifs between TMD2 and TMD3, and a second cytoplasmic region with two conserved α-helices found after TMD4 (Figure 1.7). As previously stated, both GCP16 and Erf4 lack a transmembrane domain but behave like integral membrane proteins. The cryo-EM structure revealed that two α-helices, α5' and α6' in Erf4 and α2' and α3' in GCP16, are inserted into the membrane (Figure 1.7). These helices seem to account for the fact that zDHHC9 lacks a membrane-inserted α-helix like that of zDHHC20 (Yang *et al.*, 2024). Mutation of the α5' helix of zDHHC20 (W278A/L279A) reduced the catalytic activity of the enzyme (Rana *et al.*, 2018a), highlighting its importance and the requirement for an accessory partner for Erf2 and zDHHC9.

In both complexes, the accessory proteins GCP16 or Erf4 interact with zDHHC9 or Erf2 through a surface located opposite to the DHHC domain, which is present between TMD2 and TMD3, proposing that they are not directly involved in catalysis but exert their regulatory effects through stabilisation of the complex. The cryo-EM maps showed a H-bond forming between the carbonyl oxygen of the acyl group added during autoacylation and the first histidine of the DHHC domain. The acyl chain hydrophobic binding pockets in Erf2 and zDHHC9 are primarily formed by residues in TMD1, TMD3, and TMD4, with amino acids in close proximity to the catalytic cysteine being highly conserved between Erf2, zDHHC9 and zDHHC20, while those around the acyl chain are more variable. The CRD is important for the optimal positioning of the DHHC domain. The zinc finger motifs found in the CRD are stabilised by H-bonds with helix α2' and the linker region found between TMD2 and helix α1' in both Erf2 and zDHHC9. zDHHC9 has an additional region stabilising the zinc finger motifs by

H-bonding between residues in the N-terminus and residues found around the zinc finger domains (Yang *et al.*, 2024). The overall structures of Erf2/Erf4 and zDHHC9/GCP16 protein complexes can be seen in Figure 1.7.

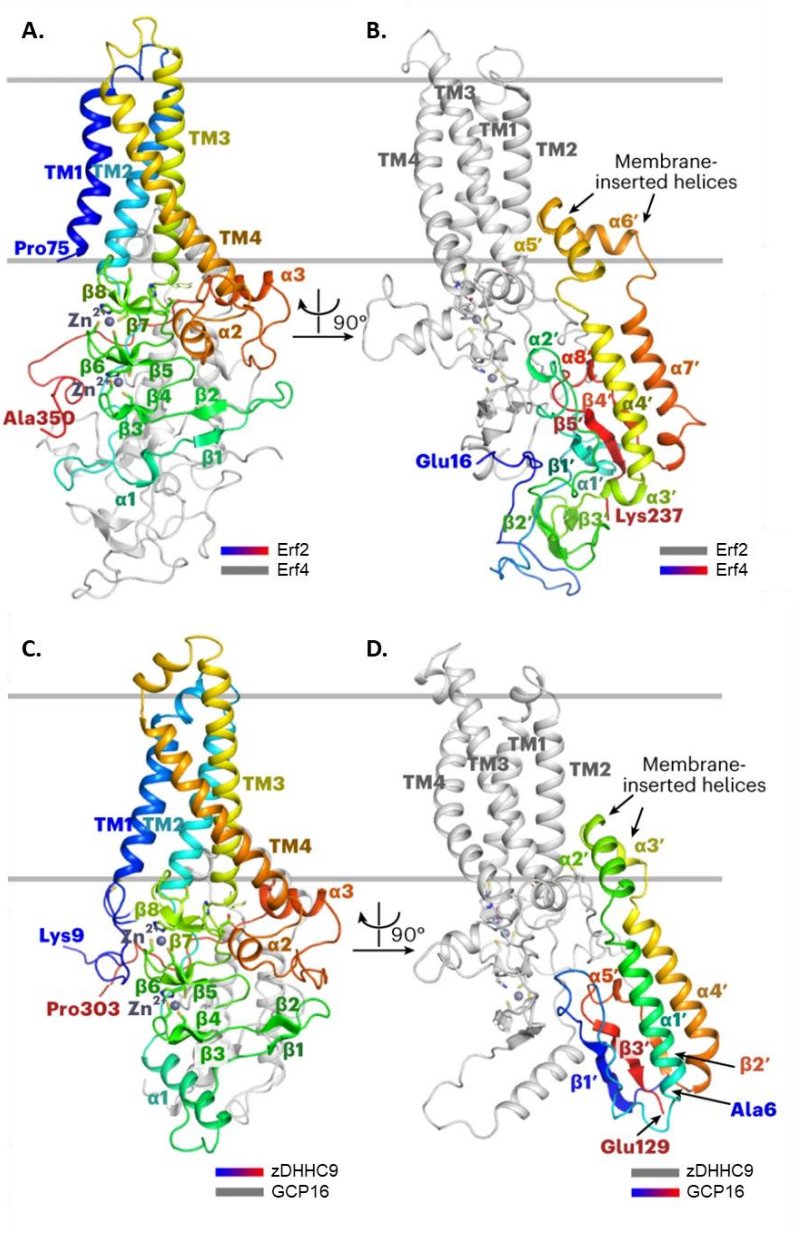

Figure 1.7 Cryo-EM structures of the Erf2/Erf4 and zDHHC9/GCP16 protein complexes.

(A-B) *Cryo-EM structure of the Erf2/Erf4 protein complex. In panel (A), Erf2 is multicoloured, with the N-terminus shown in blue and the C-terminus shown in red, while the sequence of Erf4 is shown in grey. In panel (B), the colouring is reversed.* ***(C-D)*** *Cryo-EM structure of the zDHHC9/GCP16 protein complex. In panel (C), zDHHC9 (aa 1-303) is multicoloured, with the N-terminus shown in blue and the C-terminus shown in red, while GCP16 is shown in grey. In panel (D), the colouring is reversed. Adapted from (Yang et al., 2024).*

1.7.2 The binding interfaces within the zDHHC9/GCP16 protein complex

The cryo-EM structure of the zDHHC9/GCP16 complex revealed four binding interfaces between the two proteins, as shown in Figure 1.8. The first one involves Y76 in α3' helix of GCP16 forming a H-bond with R85 in TMD2 of zDHHC9 and a π-π stacking interaction with Y183 in TMD3 of zDHHC9 (Figure 1.8A). The second binding interface consists of an interaction formed between two negatively charged pockets created by α1'-α2' and α4'-α5' helices of GCP16 and residues P290 and P293 found in the polyproline-II (PPII) helix of zDHHC9. Another component of the second binding interface is the formation of a CH-π H-bond between Y86 in the α3' helix of GCP16 and P292 in the PPII helix of zDHHC9 (Figure 1.8B). The third interface involves Y18 in GCP16 forming a CH-π interaction with P150 of zDHHC9 and a π-π stacking interaction with F129 of zDHHC9, while R16 of GCP16 also forms a charge-charge interaction with E163 of zDHHC9 (Figure 1.8C). Finally, the fourth interface involves D100 of zDHHC9 forming a charge-charge interaction with K11 of GCP16 and an anion-π interaction with F13 of GCP16, E101 of zDHHC9 forming a charge-charge interaction with R118 of GCP16 and a H-bond with R121 of GCP16, and F104 of zDHHC9 forming a π-π stacking interaction with F13 of GCP16 as well (Figure 1.8D). In summary, the first and second binding interfaces mediate zDHHC9 stabilisation by keeping TMD2, TMD3 and PPII helix together, while the third and fourth interfaces stabilise the zinc finger domains of zDHHC9 (Yang *et al.*, 2024).

The authors also found that R85, R179, and R298 of zDHHC9 create a positively charged patch that accommodates a phospholipid molecule. In fact, mass spectrometry analysis of small molecules taken from the purified proteins revealed that phosphatidic acid species interact with the complex and the S-acylation activity of the complex is reduced once the lipids are removed by washing with Triton X-100. Mutation of either R85 or R298 also reduced the S-acylation activity of zDHHC9, whereas mutating R298 reduced the autoacylation of the enzyme. The importance of the bound phospholipid seems to come through the stabilisation of TMD2, TMD3 and the PPII helix of the protein (Figure 1.8A). Another important finding was that zDHHC9 is S-acylated on Cys-24, Cys-25, and Cys-288, and that these PTMs are required for efficient catalytic activity of the complex. The mutation of Cys-288 in particular, abolished the S-acylation activity against H-Ras (Yang *et al.*, 2024). These findings agree with the observations by Nguyen *et al.* (2023) who highlighted the involvement

of Cys-288 of the C-terminal cysteine motif of zDHHC9 for S-acylation acitvity (Nguyen *et al.*, 2023). Attachment of an acyl chain on Cys-288 located on the α3' helix of zDHHC9 facilitates the membrane association of the zDHHC9 helix through a hydrophobic pocket found between TMD2 and TMD3, bringing all these components of the enzyme closer together and stabilising the complex. Residues Cys-69 and Cys-72 located on the α2' helix of GCP16 are part of a cysteine cluster, together with Cys-283, Cys-284, and Cys-288 of zDHHC9, which (in addition to mediating membrane association of GCP16) are also important for the stability and hence the catalytic activity of the complex (Ohta *et al.*, 2003, Yang *et al.*, 2024).

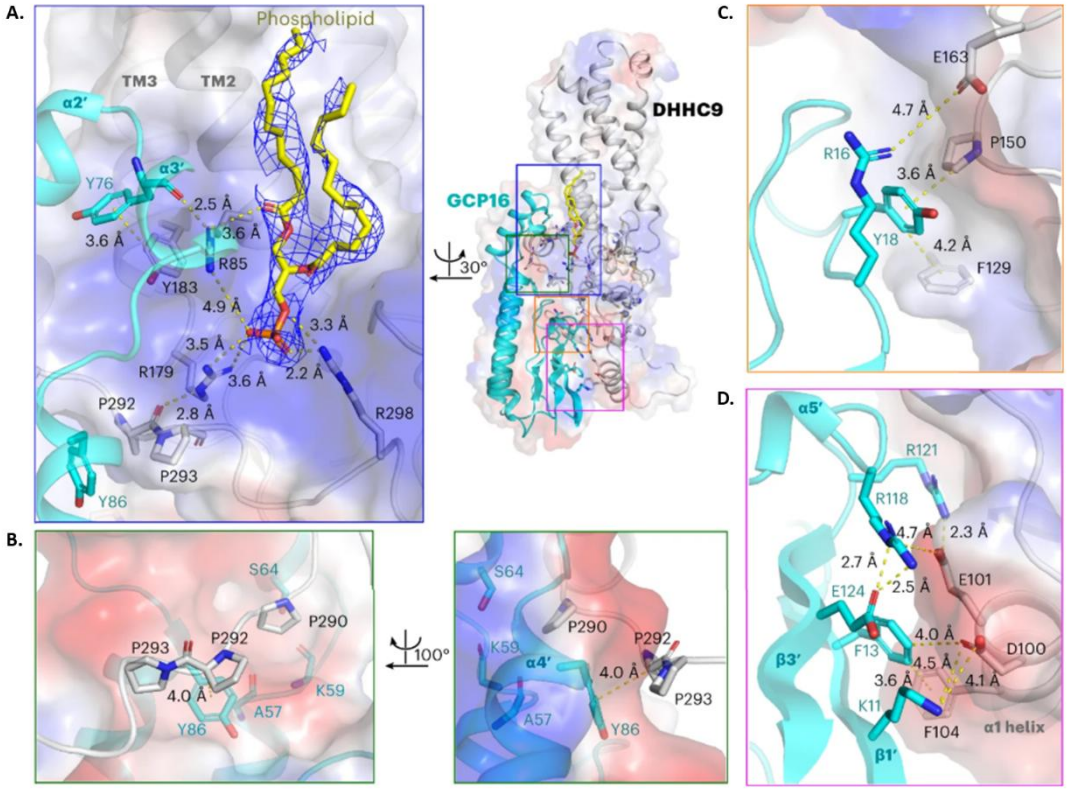

Figure 1.8 Binding interfaces within the cryo-EM structure of the zDHHC9/GCP16 protein complex.

(A) *First binding interface: R85 and Y183 in TMD2 and TMD3 of zDHHC9 interact with Y76 in the α3' helix of GCP16. Attachment of a phospholipid (shown as a stick, in yellow) via the interaction with R85, R179 and R298 of zDHHC9.* ***(B)*** *Second binding interface: Proline residues P290 and P293 of the PPII helix of zDHHC9 dock into two charged pockets formed in GCP16. P292 of the PPII helix interacts with Y86 in the α3' helix of GCP16.* ***(C)*** *Third binding interface: P150 and E163 in the zinc finger motifs and F129 of zDHHC9 interact with R16 and Y18 found in the loop after GCP16 β1' strand.* ***(D)*** *Fourth binding interface: D100, E101, and F104 found in the α1' helix of zDHHC9 interact with residues in the β1', β3' strands and in a loop following the α5' helix of GCP16 - K11, F13, R118, and R121. The hydrogen bonds formed are depicted using yellow dashed lines (Yang et al., 2024).*

1.8 Regulation of zDHHC S-acyltransferases

Although zDHHC enzymes are generally intrinsically active, their activity can be regulated at several levels via emerging mechanisms (Chamberlain and Shipston, 2015, Salaun *et al.*, 2020).

1.8.1 Accessory proteins as regulators of zDHHC enzymes

Association of zDHHC enzymes with accessory proteins can regulate their localisation, stability, interactions with substrate proteins and catalytic activity (Salaun *et al.*, 2020). The regulatory effects of Erf4 and GCP16 as co-factors of Erf2 and zDHHC9 have already been discussed in detail; however, GCP16 has also been proposed to be an accessory protein of another four human zDHHC enzymes, which are evolutionary related to zDHHC9: zDHHC5, zDHHC8, zDHHC14, and zDHHC18 (Ko *et al*., 2019, Salaun *et al*., 2020, Nguyen *et al*., 2023, Yang *et al*., 2024). Nguyen *et al.* (2023) reported that GCP16 interaction with these enzymes involves their C-terminal cysteine motifs, which are highly conserved in the zDHHC9 subfamily. GCP16 expression increased the monodispersity of these enzymes and prevented their aggregation in FSEC analysis, while it had no effect on more evolutionary distant zDHHCs. Experiments using purified proteins and [^{3}H] palmitoyl-CoA showed that GCP16 also affects the autoacylation and catalytic activity of both zDHHC14 and zDHHC18 (Nguyen *et al.*, 2023). In addition to these effects of GCP16 on this set of zDHHC enzymes, a different study also reported that GCP16 regulates the plasma membrane localisation of zDHHC5 (Ko *et al.*, 2019).

Golga7b is closely related to GCP16 and was previously identified as an accessory protein of zDHHC5 (Huttlin *et al.*, 2015, Salaun *et al.*, 2020). Golga7b can stabilise both zDHHC5 and zDHHC8 but does not affect the stabilisation of zDHHC9, zDHHC14, or zDHHC18 in FSEC experiments, exhibiting the specificity of accessory protein interactions, even for closely related homologs (Nguyen *et al.*, 2023). The association of Golga7b with zDHHC5, also involving the three S-acylated C-terminal cysteine residues, has been reported to stabilise the plasma membrane localisation of zDHHC5 by inhibiting its endocytosis. In addition, Golga7b also regulates the

protein interactions of zDHHC5, and promotes its association with cell adhesion proteins (Woodley and Collins, 2019).

Other reported accessory/regulatory proteins of the zDHHC enzyme family include huntingtin (HTT) and selenoprotein K (SelK). These proteins have been proposed to regulate the autoacylation of zDHHC17 and zDHHC6, respectively. HTT, an S-acylated protein involved in Huntington's disease, promoted a 70% increase in the catalytic activity of zDHHC17 against synaptosomal-associated protein of 25 kDa (SNAP25) *in vitro*, while mice lacking one allele of the *HTT* gene showed decreased zDHHC17 S-acylation, suggesting that HTT regulates the autoacylated intermediate of the enzyme (Huang *et al.*, 2011). SelK, a cellular protein with incorporated selenocysteines is involved in store-operated calcium entry in immune cells (Verma *et al.*, 2011) and also affects the expression levels of the IP_3 receptor, has been reported as a modulator of zDHHC6. zDHHC6 depletion does, in fact, result in decreased IP_3 receptor S-acylation and expression in Jurkat T-cells (Fredericks *et al.*, 2014). The role of SelK as a modulator of zDHHC6 was investigated using a purified zDHHC6 construct including the DHHC-CRD domain and the C-terminal Src homology 3 (SH3) domain, which interacts with the SH3-binding domain of SelK. The results revealed that SelK enhanced zDHHC6 autoacylation, suggesting that SelK may stabilise the autoacylated intermediate of zDHHC6 (Fredericks *et al.*, 2018).

1.8.2 Post-translational modifications of zDHHC enzymes

Another mechanism of regulating the activity of zDHHC enzymes is through post-translational modifications. As previously discussed, S-acylation of the zDHHC9/GCP16 complex at cysteine residues Cys-288 of zDHHC9 or Cys-69 and Cys-72 of GCP16 regulates the stability and catalytic activity of the complex. Moreover, Cys-288 is a conserved residue in zDHHC5, zDHHC8, zDHHC14, zDHHC18, and zDHHC19, further suggesting that S-acylation has a wider regulatory role in the zDHHC enzyme family (Nguyen *et al.*, 2023, Yang *et al.*, 2024). zDHHC6 is also regulated by S-acylation mediated by the activity of another S-acyltransferase, zDHHC16, as part of a so-called "S-acylation cascade". The investigation of S-acylation dynamics using biochemical analysis and mathematical modelling revealed that the stability and catalytic activity of zDHHC6 is enhanced by zDHHC16

overexpression through the S-acylation of three C-terminal cysteines - Cys-328, Cys-329 and Cys-343 (Abrami *et al.*, 2017).

Other examples of PTMs controlling the activity of zDHHCs include the phosphorylation of zDHHC13 by the adenosine 5′-monophosphate (AMP)-activated protein kinase (AMPK), which enhances the interaction with the melanocortin-1 receptor (MC1R), which leads to increased S-acylation of the receptor, and increased downstream signalling, DNA damage repair and suppression of melanocyte transformation, decreasing the risk of skin cancer. Indeed, it was shown that AMPK-mediated phosphorylation of zDHHC13 can rescue defects in MC1R signalling that are linked to increased susceptibility to melanoma both *in vitro* and *in vivo* (Sun *et al.*, 2023). Another example of phosphorylation-mediated regulation of zDHHCs is the phosphorylation of zDHHC5. Here, the modification of Tyr-61, located near the active site, results in the inhibition of the enzyme's catalytic activity (Hao *et al.*, 2020). In contrast, Src-dependent phosphorylation of Tyr-533 serves to anchor zDHHC5 at the plasma membrane in neurons through increased association with PSD-95 (Brigidi *et al.*, 2015).

Another PTM that has been shown to control zDHHC enzyme activity is ubiquitination, which regulates zDHHC enzyme degradation via the proteosome. The degree of S-acylation of zDHHC6 (by zDHHC16) impacts lysine ubiquitination and subsequent enzyme degradation through ERAD (Abrami *et al.*, 2017), while Erf4 protects Erf2 from ERAD-mediated degradation as previously discussed (Mitchell *et al.*, 2012). Moreover, attachment of ubiquitin, a bulky molecule, to the lysine residue in the amphipathic α2' helix of zDHHC20 or zDHHC9, which mediates stabilisation by bringing the TMDs together (Yang *et al.*, 2024), could disrupt the catalytic activity of the enzymes. Lysine ubiquitination has also been identified to occur close to other important domains of zDHHC enzymes, including the TTxE C-terminal motif, and the zinc-binding motifs, and conformational changes in these domains induced by this PTM might also result in significant effects on catalytic activity (Zmuda and Chamberlain, 2020). These latter examples highlight potential effects of ubiquitination on protein conformation, in addition to the well known effects of polyubiquitination on protein degradation.

1.9 Specificity of zDHHC substrate interactions

The lack of a universal substrate recognition motif for zDHHC enzymes increases the complexity of investigating zDHHC-substrate specificity. S-acylation was previously thought to be non-specific and solely based on proximity (Rocks *et al.*, 2010), while a generic assumption is that any cysteine residues accessible to membrane-bound zDHHC enzymes could be S-acylated (Nadolski and Linder, 2007, Chamberlain and Shipston, 2015). It is clear that in some cases multiple zDHHC isoforms can S-acylate the same substrate, reflecting the plasticity of S-acylation, for example the modification of Gα protein subunits by zDHHC3 and zDHHC7 (Tsutsumi *et al.*, 2009), or S-acylation of PSD-95 by zDHHC2, zDHHC3, zDHHC7, and zDHHC15 (Noritake *et al.*, 2009). However, knockdown studies have also indicated that the S-acylation of other substrates appears to be specific to one zDHHC enzyme (Huang *et al.*, 2009).

The mechanisms underlying substrate specificity in the zDHHC enzyme family are not generally well understood (Malgapo and Linder, 2021). The subcellular localisation of zDHHC enzymes presents a method of spatially restricted substrate specificity, as it limits the ability of zDHHC enzymes to encounter specific proteins. An example of this is the cycling of zDHHC2 between the plasma membrane and recycling endosomes, which dictates its activity against PSD-95 through facilitating access to the substrate at the plasma membrane of dendritic spines (Noritake *et al.*, 2009, Malgapo and Linder, 2021).

A study by Lemonidis *et al.* (2014) examined the differences in substrate S-acylation between different Golgi-localised zDHHC enzymes. The authors found that in co-expression experiments in HEK293 cells, zDHHC3 and zDHHC7 showed increased S-acylation against SNAP25 and cysteine-string protein (CSP) compared to zDHHC17 or zDHHC13 (which was unable to S-acylate the substrates), despite their significantly weaker interaction with these substrates. This suggests an increased intrinsic ability of zDHHC3 and zDHHC7 to transfer their acyl chains to protein substrates, along with a reported increased autoacylation compared to zDHHC17 and zDHHC13. This study demonstrated a disproportional relationship between substrate binding affinity and S-acylation efficiency. Therefore, the zDHHC3 and zDHHC7 isoforms were classified as high activity/low specificity enzymes, exhibiting more flexibility towards substrate interactions in the absence of any recognition motifs. In contrast, zDHHC13 and zDHHC17 are considered low activity/high specificity

isoforms, with direct binding affinity likely dictating the substrates that can be modified by these enzyme (Lemonidis *et al.*, 2014).

Notably, specific substrate-binding domains and residues have been identified in the sequence of several zDHHC isoforms. These include the C-terminal SH3 domain of zDHHC6 interacting with SH3-binding domain proteins containing proline-rich regions (Malgapo and Linder, 2021), the N-terminal ankyrin repeat (ANK) domain of zDHHC13 and zDHHC17 interacting with zDHHC ankyrin-binding motifs (zDABM) (Lemonidis *et al.*, 2015a) on substrates such as HTT (Singaraja *et al.*, 2002), SNAP25b, or CSPα (Lemonidis *et al.*, 2014), as well as the PDZ-binding motif (PBM) of zDHHC3, zDHHC5, zDHHC7, zDHHC8, zDHHC14, zDHHC16, zDHHC17, zDHHC20 and zDHHC21 which bind to PDZ domain-containing substrates such as Pick1 (Thomas *et al.*, 2012), PSD-93 and PSD-95 (Thomas and Hayashi, 2013, Malgapo and Linder, 2021). For these enzyme-substrate pairs, S-acylation activity is dependent on the coordinated activity of the DHHC catalytic motif and their defined substrate-binding domains (Chamberlain and Shipston, 2015). Indeed, the addition of the ANK domain of zDHHC17 to the N-terminal region of zDHHC3 allowed the new construct to S-acylate zDHHC17 substrates, solidifying the importance of the identified substrate binding domains for substrate recognition (Huang *et al.*, 2009, Chamberlain and Shipston, 2015). Interestingly, SPRED3 S-acylation by zDHHC17 does not require the ANK domain of the enzyme (Butler *et al.*, 2023), suggesting that zDHHC17 can also recognise substrates independently of the ANK domain, and that different modes of binding and substrate recognition exist (Butler *et al.*, 2023).

A study by Salaun *et al.* (2023) identified zDHHC6 as the only ER-resident zDHHC isoform that can broadly S-acylate ER-localised type I and type II transmembrane proteins in which the cytosolic cysteine residue is in close proximity to the TMD. Indeed, they showed that all that was required for S-acylation of these proteins by zDHHC6 was the transmembrane domain and adjacent cysteine. The results suggested that the SH3 domain of zDHHC6 was not involved in the interaction with the TMD constructs studied, since they lack any accessible proline-rich regions on the cytoplasmic membrane face. Subsequently, the authors proposed that while the SH3 domain of zDHHC6 might be important for some specific substrate interactions, it is not essential for all zDHHC6-mediated substrate S-acylation (Salaun *et al.*, 2023). In this case, there might also be some weak interactions between the TM sequences of

zDHHC6 and the TMDs of substrate proteins that enable substrate recognition or specificity.

All in all, it is likely that the S-acylation machinery uses both high and low specificity interactions to enable the modification of a large and diverse set of cellular proteins. High activity/low specificity enzymes are suggested to mediate the S-acylation of bulk proteins exiting the ER or Golgi (Ernst *et al.*, 2018), whereas low activity/high specificity enzymes may be involved in the S-acylation of soluble proteins to facilitate their trafficking to the plasma membrane and endocytic compartments (Salaun *et al.*, 2023).

1.10 Protein deacylation

S-acylation is reversible, and protein deacylation is catalysed by members of the metabolic serine hydrolase (mSH) enzyme superfamily, which includes palmitoyl-protein thioesterases (PPTs), acyl-protein thioesterases (APTs), and α/β hydrolase domain-containing proteins (ABHDs). Metabolic serine hydrolases are characterised by an active site serine responsible for substrate hydrolysis, along with an α/β hydrolase fold, composed of a central β-sheet of 5-8 strands surrounded by α-helices. The active site serine is part of a catalytic dyad (Ser-Lys, or Ser-Asp), or triad (Ser-His-Asp, or Ser-Ser-Lys), which is located on a tight loop near the end of a β-strand referred to as the “nucleophilic elbow” (Long and Cravatt, 2011, Lord *et al.*, 2013). The catalytic mechanism involves the formation of an acyl-enzyme intermediate via attachment to the catalytic serine, followed by water-induced saponification that results in the regeneration of the free serine, now available for another catalytic cycle. The activity of mSHs can be studied using affinity labels directed at the active site serine, such as fluorophosphonates (Long and Cravatt, 2011).

1.10.1 Palmitoyl-protein thioesterases (PPTs)

Palmitoyl-protein thioesterase 1 (PPT1) was the first deacylation enzyme discovered, purified from a soluble fraction of bovine brain. PPT1 showed deacylation activity against H-Ras and Gα protein subunits *in vitro* (Camp and Hofmann, 1993), and since

endogenously expressed PPT1 co-sedimented with lysosomal enzyme markers in Madin-Darby bovine kidney cells, the enzyme was characterised as a lysosomal glycoprotein (Verkruyse and Hofmann, 1996). PPT2, a homolog of PPT1, was also identified as a lysosomal enzyme with similar catalytic thioesterase activity (Soyombo and Hofmann, 1997). The two thioesterases were proposed to deacylate substrates during protein degradation in the lysosomes (Hellsten *et al.*, 1996). However, while most PPT1 co-localised with a lysosomal marker in confocal microscopy analysis of mouse cerebral cortex neuronal cultures, a small fraction co-localised with synaptic vesicle markers in the pre-synaptic compartment, and also in mouse brain tissues analysed by immunoelectron microscopy (Kim *et al.*, 2008), suggesting that this enzyme might also have deacylase activities outside of the lysosomal system. Gorenberg *et al.* (2022) identified PPT1 substrates in a proteome-wide screening study, based on differences between WT and PPT1 KO mice S-acylated synaptic profiles, followed by PPT1-mediated deacylation assays for validation. PPT1 substrates exhibited increased S-acylation in PPT1 KO synaptosomes and were directly deacylated by recombinant mouse PPT1 expression in HEK293 cells. The proteins identified included both cytosolic and membrane proteins like G-proteins, mitochondrial proteins, ion channels and transporters, synaptic adhesion proteins, endocytic and lysosomal proteins. In the same study, the trafficking of PPT1 in neurons was also described. The group stated that PPT1 is secreted, endocytosed, and then trafficked to lysosomes. After endocytosis in the presynaptic compartment, some of it is released to the cytosol, where it can access cytosolic protein substrates (Gorenberg *et al.*, 2022). This model explained how PPT1 can act on both lysosomal and cytosolic substrates.

PPT1 was shown to exhibit an unusual insensitivity to the common serine-reactive inhibitors phenylmethylsulfonyl fluoride (PMSF) and diisopropyl fluorophosphonate (DIFP) (Camp and Hofmann, 1993), something that was later explained by the enzyme's crystal structure, which showed the presence of a narrow hydrophobic channel that blocks access to the active site serine (Das *et al.*, 2000). PPT1 can cleave long acyl-CoA chains, exhibiting a preference for myristoyl to stearoyl acyl chains of 14 to 18 carbons, while PPT2 can bind shorter and longer acyl chain lipids. However, it was shown that PPT2 cannot hydrolyse fatty acids with branched or bulky head groups, or S-acylated protein substrates such as H-Ras, due to limited space in between the loops above the lipid binding site accommodating the substrate to be hydrolysed (Calero *et al.*, 2003).

The importance of PPT1 is emphasised by the finding that mutations in the *PPT1* gene underlie the neurodegenerative disorder infantile neuronal ceroid lipofuscinosis (INCL), a lysosomal storage disease exhibiting abnormal neurotransmission, accumulation of lipofuscin, and neuronal degeneration. Patients experience seizures, blindness, and premature death at around the age of 10 years old (Long and Cravatt, 2011).

1.10.2 Acyl-protein thioesterases (APTs)

APT1 and APT2, also known as LYPLA1 and LYPLA2, were identified after PPT1 in two independent studies (Duncan and Gilman, 1998, Toyoda *et al.*, 1999). The crystal structure of APT1 and APT2 revealed that, in addition to the canonical α/β hydrolase fold and catalytic triad, that these enzymes have an additional four short antiparallel β-strands (Abrami *et al.*, 2021). The crystal structure also demonstrated the presence of a hydrophobic pocket in APT2 in which the acyl chain from the S-acylated substrate is inserted once extracted from the membrane, resulting in the optimal positioning of the thioester bond at the catalytic site to be hydrolysed (Abrami *et al.*, 2021). APT1 and APT2 predominantly localise to the cytosol and despite their high amino acid similarity of more than 60%, they show deacylase activity against different substrates (Chamberlain and Shipston, 2015). Specifically, APT1 catalyses the hydrolysis of endothelial nitric oxide synthase (eNOS) (Yeh *et al.*, 1999), H- and N-Ras, Gα protein subunits (Duncan and Gilman, 1998), and BK potassium channels (Tian *et al.*, 2012), while substrates of APT2 include tumour necrosis factor receptor (TNFR) (Zingler *et al.*, 2019), MC1R (Chen *et al.*, 2019), GAP43 (Tomatis *et al.*, 2010), and zDHHC6 (Abrami *et al.*, 2017). A few examples of substrate specificity include APT2 being unable to deacylate BK potassium channels in overexpression experiments in HEK293 cells (Tian *et al.*, 2012), while APT1 overexpression had no effects on GAP43 deacylation in CHO-K1 and HeLa cells (Tomatis *et al.*, 2010), or on the S-acylation of zDHHC6 in HeLa cells (Abrami *et al.*, 2017).

APT enzymes have been reported to undergo S-acylation in biochemical labelling experiments, and bioinformatics analysis revealed a conserved cysteine residue at position 2 (Kong *et al.*, 2013). Experiments using APT1 and APT2, along with Cys-2 serine substitution mutants, indicated that wild-type APTs are found in the cytosol and

the Golgi in mammalian cells, while the cysteine mutant constructs were entirely localised in the cytosol. The loss of Golgi localisation was also demonstrated when wild-type APT constructs were treated with the 2-BP S-acylation inhibitor (Vartak *et al.*, 2014). Another study identified the zDHHC enzymes responsible for the S-acylation of APTs in an siRNA assay. Silencing of both zDHHC3 and zDHHC7 resulted in the relocalisation of APT2 from the Golgi, and this observation was also confirmed using radiolabelled [^{3}H] palmitate (Abrami *et al.*, 2021). Interestingly, inhibition of the thioesterase activity of APTs with palmostatin B treatment resulted in their localisation to the plasma membrane (Kong *et al.*, 2013). It was proposed that the nonphysiological plasma membrane localisation is a result of prolonged Golgi membrane association of APTs, mediated by their stabilised S-acylation, which is then followed by vesicular trafficking to the plasma membrane (Vartak *et al.*, 2014). Furthermore, APT1 can catalyse its own deacylation, and also that of APT2, resulting in the relocalisation of the enzymes to the cytosol, where they can be S-acylated again. Therefore, cycles of S-acylation and deacylation of APTs provide tight regulation of their activity, especially against membrane-associated S-acylated substrates (Kong *et al.*, 2013, Vartak *et al.*, 2014). Soluble APT2 C2S mutant has also shown decreased stability and increased susceptibility to proteasomal degradation due to the exposure of Lysine-69 that undergoes ubiquitination, further highlighting the importance of S-acylation of this enzyme (Abrami *et al.*, 2021).

1.10.3 α/β hydrolase domain proteins (ABHDs)

There are multiple human ABHD proteins reported, named ABHD1-19, that act as regulators of lipid metabolism. These enzymes exhibit different expression patterns and act on several groups of substrates. Most ABHDs have a conserved HxxxxD motif, in addition to the canonical α/β hydrolase fold structure and the catalytic triad. ABHD5 is the most well-studied member of the family, implicated in triacylglycerol metabolism and identified as the mutated gene in Neutral Lipid Storage Disease with Ichthyosis (NLSDI), or otherwise referred to as Chanarin–Dorfman Syndrome, a non-lysosomal disorder of excessive ectopic triacylglycerol accumulation (Lord *et al.*, 2013). However, the ABHD17 isoform has been identified as the predominant deacylation enzyme of N-Ras and PSD-95 (Lin and Conibear, 2015), boosting its significance in the field of S-acylation. Lin and Conibear (2015) discovered that

although the S-acylation turnover of some substrates was reduced upon selective inhibition of APT1 and APT2 or double RNAi knockdown, this was not the case for N-Ras and PSD-95. The authors then identified additional enzymes that are sensitive to both palmostatin B and hexadecylfluorophosphonate (HDFP), since treatment with either inhibited the deacylation of both N-Ras and PSD-95, and then used pulse-chase click chemistry to examine if overexpression of these enzymes resulted in increased S-acylation turnover. The results indicated that expression of ABHD17A, ABHD17B, or ABHD17C significantly enhanced the turnover of both protein substrates (Lin and Conibear, 2015). Overexpression of ABHD17 isoforms in primary neuronal cultures also decreased the S-acylation of microtubule-associated protein 6 (MAP6) involved in microtubule stability (Tortosa *et al.*, 2017).

The ABHD17 protein isoforms are anchored to membranes by the S-acylation of an N-terminal cysteine cluster (Martin and Cravatt, 2009, Lin and Conibear, 2015, Won *et al*., 2018). ABHD17A is the isoform with the strongest effect on N-Ras and PSD-95 S-acylation, and this enzyme is localised to the plasma membrane and to Rab5- and Rab11-positive endosomes. Truncation of the N-terminal cysteine-rich domain abolishes ABHD17A plasma membrane association and relocalises the enzyme to the cytosol, while also compromising its catalytic activity. Overexpression of inactive or N-terminal truncated mutants of ABHD17A did not affect the S-acylation of N-Ras or PSD-95 (Lin and Conibear, 2015). Other ABHD isoforms like ABHD12 and ABHD13 only had a minor effect on PSD-95 deacylation when overexpressed in HEK293 cells, COS-7 cells, and primary neuronal cultures, suggesting a degree of substrate specificity in the enzyme family (Won *et al.*, 2018).

The discovery of selective inhibitors for certain ABHD isoforms is challenging but necessary to avoid any undesirable off-target effects. A recent study reported the identification of general chemical determinants for the reversible and selective inhibition of ABHD16A, which could be beneficial in gastric cancer and neuroinflammation cases among others (Ahonen *et al.*, 2023). The study used reversible inhibitor compounds 12-thiazole abietanes as a starting point as these had previously shown ABHD16A selectivity (Ahonen *et al.*, 2018, Ahonen *et al.*, 2023). The newly synthesised compound inhibitors were tested via competitive activity-based protein profiling to explore their ability to selectively inhibit ABHD16A over ABHD12. In this assay, if the synthesised compounds interfere with the binding of the reactive probe, it means that they successfully interact with and inhibit their target enzyme.

Five of the tested compounds exhibited significant inhibition of ABHD16A, with compound 35 being characterised as the most potent and selective against the enzyme. On the other hand, out of these five compounds, only compound 28 was able to inhibit the activity of ABHD12. Notably, the study identified that structural differences found in compound 28 switched its preference towards ABHD12, successfully disrupting the enzyme. Specifically, incorporation of an ester group on ring A in the presence of a 1-hydroxyethyl group at the C2' position of the thiazole ring shifted target selectivity for ABHD12. Docking analysis using AlphaFold revealed that the thiazole ring of compound 28 is positioned close to the catalytic serine residue in both ABHD16A and ABHD12, along with some differences in how the thiazole ring of the inhibitor interacts with the two enzymes. However, the two predicted models show similar docking of the inhibitor and do not explain the experimental selectivity observed. Although future work is required to determine the mechanism of inhibition of these compounds and to test their potential in disease models, this study provided insights for developing more potent and selective ABHD16A inhibitors and demonstrated how small modifications can fine-tune target preference, as in compound 28 (Ahonen *et al.*, 2023).

1.11 Effects of S-acylation on substrate proteins

The reversible nature of S-acylation allows for rapid cycles of S-acylation and deacylation events that regulate the properties of a plethora of protein substrates, including both soluble and transmembrane proteins. S-acylation can affect various stages of a protein's life cycle, from its assembly to its degradation, as zDHHC enzymes reside in multiple membranes within the cell. The main effect of lipid attachment onto substrates is increased hydrophobicity that correlates with membrane association and can influence protein trafficking, protein-protein interactions, localisation to cholesterol-rich membrane domains, protein folding, stability, and protein activity (Linder and Jennings, 2013, Chamberlain and Shipston, 2015, Anwar and van der Goot, 2023). The effects of S-acylation on protein trafficking are broad and influence movement through the secretory and endocytic pathways, although how this is achieved is not always clear. Interestingly, the effects of S-acylation on protein movement through the Golgi were suggested to reflect association with cholesterol-rich domains that are present at the rims of Golgi

cisternae, from where vesicle budding occurs (Linder and Jennings, 2013, Ernst *et al.*, 2018).

A prominent effect of S-acylation is preventing the premature degradation of both soluble and transmembrane proteins (Linder and Deschenes, 2007). The C-C chemokine receptor type 5 (CCR5), a cell surface GPCR primarily involved in the chemokine response and white blood cell migration during inflammation but also serving as a co-receptor for the entry of the human immunodeficiency virus (HIV) into cells, is regulated by S-acylation. The receptor is S-acylated on three adjacent cysteine residues in the C-terminal tail, crucial for protein trafficking, surface expression at the plasma membrane, stability and efficient signal transduction activity. Non-acylated cysteine mutants of CCR5 or 2-BP treatment resulted in reduced cell surface expression, and this was later attributed to a reduced stability of mutant CCR5. Moreover, the protein levels of mutant CCR5 were increased after treatment with lysosomal inhibitor Bafilomycin A1, indicating that S-acylation prevents the lysosomal degradation of the protein (Percherancier *et al.*, 2001).

Additionally, S-acylation-deficient mutants of the yeast transmembrane SNARE protein Tlg1 exhibit increased ubiquitination as a result of a pair of acidic amino acid residues preceding the TMD coming into membrane contact and being recognised by the transmembrane ubiquitin ligase 1 (Tul1), which mediates ubiquitination of proximal lysines. S-acylation of Tlg1 shields the protein from degradation by fixing the position of the TMD in a way that prevents the acidic residues from approaching the lipid bilayer, avoiding recognition by Tul1 (Valdez-Taubas and Pelham, 2005).

Another mechanism through which S-acylation protects against premature degradation is seen with the anthrax toxin receptor TEM8. S-acylation deficient mutants of TEM8 are targeted to lipid rafts where they are ubiquitinated, while S-acylation of TEM8 restricts its membrane distribution to non-raft domains (Abrami *et al.*, 2006). This is an interesting example as S-acylation is generally thought to mediate protein association with lipid rafts, rather than preventing raft association as seen with TEM8 (Chamberlain and Shipston, 2015).

1.11.1 S-acylation of soluble protein substrates

For cytosolic protein substrates that are intrinsically hydrophilic, S-acylation usually facilitates their stable association with the membrane, and the subcellular localisation of the S-acyltransferase enzyme dictates where substrate membrane binding will initially occur, before either being retained at that compartment or transported to other compartments by vesicle-mediated trafficking (Nadolski and Linder, 2007). Even though all lipid modifications mediate membrane interaction, one lipid group is usually insufficient for membrane attachment. Instead, myristoyl or prenyl groups often mediate weak and transient membrane binding, which brings proteins to the membrane and facilitates S-acylation of neighbouring cysteines, leading to a marked increase in membrane affinity (Chamberlain and Shipston, 2015).

An example of a widely studied peripheral protein that undergoes dual lipidation is Ras. There are four Ras protein isoforms: H-Ras, N-Ras, K-Ras4A, and K-Ras4B. Ras proteins are small GTPases that switch between active guanosine triphosphate (GTP)-bound and inactive guanosine diphosphate (GDP)-bound states (Simanshu *et al.*, 2017, Busquets-Hernandez and Triola, 2021). Activation of Ras proteins is catalysed by guanine nucleotide exchange factors (GEFs), while inactivation by GTP hydrolysis is facilitated by GTPase-activating proteins (GAPs). Activated RAS proteins are involved in intracellular signal transduction pathways controlling cell growth and proliferation, differentiation and survival (Simanshu *et al*., 2017, Prior *et al*., 2020, Busquets-Hernandez and Triola, 2021). The membrane association of Ras proteins is essential for their activation and for their role in activating signal transduction pathways. Initial membrane attachment of Ras proteins is facilitated by farnesylation of their C-terminal Caax motif in the cytosol, followed by cleavage of the aax residues by Ras converting Caax endopeptidase 1 (Rce1), and subsequent methylation of the farnesylated cysteine by isoprenylcysteine carboxyl methyltransferase (Icmt). Farnesylated Ras proteins can transiently interact with membranes. Transient interaction with the Golgi brings N-Ras into proximity with the zDHHC9/GCP16 complex, which mediates S-acylation at Cys-181 (N-Ras) or Cys-181 and Cys-184 (H-Ras). While mutation of the S-acylated cysteine residues in Ras proteins results in a weak and transient membrane interaction, mutation of the farnesylated cysteine results in complete loss of S-acylation and membrane association (Hancock *et al.*, 1989), revealing the necessity of farnesylation for subsequent S-acylation.

After dual lipidation, Ras proteins become trapped on the membrane and are transported to the plasma membrane via vesicular transport, where they become activated (Daniotti *et al.*, 2017, Busquets-Hernandez and Triola, 2021). Deacylation releases farnesylated Ras back to the cytosol, and further transient interactions with the Golgi complex lead to another round of S-acylation, and therefore constant cycling of N/H-Ras between the plasma membrane and Golgi (Rocks *et al.*, 2005, Daniotti *et al.*, 2017, Busquets-Hernandez and Triola, 2021). Because N-Ras is S-acylated on a single cysteine, its release from membranes is faster than that of H-Ras. This results in N-Ras having a more pronounced Golgi localisation, whereas H-Ras has a stronger distribution at the plasma membrane (Raymond *et al.*, 2007, Busquets-Hernandez and Triola, 2021). Interestingly, the K-Ras4B isoform does not undergo S-acylation but instead binds to the phospholipid groups of the cytosolic face of the plasma membrane through a C-terminal polybasic domain containing multiple lysine residues (Daniotti *et al.*, 2017, Busquets-Hernandez and Triola, 2021).

S-acylation of Ras proteins has also been associated with their microlocalisation at the plasma membrane. The different Ras isoforms exhibit defined microdomain localisation and nonoverlapping nanocluster formation, influenced by their distinct lipidation profiles. For example, H-Ras is found in a dynamic equilibrium between cholesterol-rich lipid rafts and other non-cholesterol-dependent microdomains, while K-Ras is enriched in non-raft microdomains (Prior *et al.*, 2003). The plasma membrane clustering of different Ras isoforms to different microdomains could affect the assembly of signal transduction complexes and the interaction with effector proteins, therefore explaining their functional differences and distinct signal outputs (Prior *et al.*, 2003, Janosi *et al.*, 2012).

Other reported soluble protein substrates are exclusively S-acylated and do not have myristoylation or prenylation sites to mediate initial membrane binding. Instead, they use weakly hydrophobic domains to mediate membrane contact and subsequent S-acylation. An example is SNAP25, a soluble protein involved in synaptic transmission in neurons through exocytosis, whose non-acylated CRD mediates initial membrane contact before S-acylation (Greaves *et al.*, 2010, Kadkova *et al.*, 2019). CSPα is also involved in synaptic vesicle exocytosis and, like SNAP25, has a hydrophobic CRD that mediates membrane binding prior to S-acylation and stable membrane attachment (Greaves and Chamberlain, 2006).

1.11.2 S-acylation of transmembrane protein substrates

Transmembrane proteins are intrinsically irreversibly embedded in membranes and therefore have no requirement for S-acylation for stable membrane binding. However, this modification can still have significant effects on their trafficking, stability and structure, as highlighted above for effects on CCR5 and TME8 (Chamberlain and Shipston, 2015). It has been suggested that S-acylation of TM proteins is determined by cysteine accessibility, independently of any recognition motifs, and that any cysteine residue in proximity to the DHHC domain of a zDHHC enzyme is a potential modification site (Rodenburg *et al.*, 2017).

S-acylation of the ER transmembrane protein calnexin occurs on three cysteine residues. This modification alters the structure of the protein by changing the conformation of its cytoplasmic tail, which then enhances the targeting of calnexin to different ER subdomains; the perinuclear rough ER, where it assists in the folding of nascent glycoproteins, and the mitochondrial-associated membrane, where it interacts with sarcoendoplasmic reticulum Ca^{2+} transporter ATPase 2b and regulates mitochondrial calcium uptake (Chamberlain and Shipston, 2015, Paskevicius *et al.*, 2023). Another study also noted that S-acylation significantly increases the stability of calnexin in pulse-chase experiments by comparing wild-type and cysteine mutant constructs (Dallavilla *et al.*, 2016). Therefore, in the case of calnexin, S-acylation regulates the spatial distribution of the protein, increases its stability, and also enhances its association with other proteins (Chamberlain and Shipston, 2015, Dallavilla *et al.*, 2016, Paskevicius *et al.*, 2023).

Low-density lipoprotein receptor-related protein 6 (LRP6), a monotopic transmembrane protein that acts as a co-receptor for the Wnt signalling pathway, is another example of an S-acylated transmembrane protein. LRP6 is S-acylated on cysteines adjacent to the transmembrane domain, and S-acylation-deficient LRP6 is trapped at the ER and fails to traffic to the plasma membrane. Interestingly, shortening the TMD of S-acylation-deficient LRP6 allowed ER exit and plasma membrane delivery of the protein. Therefore, it was proposed that hydrophobic mismatching of the long 23-residue TMD and the thin ER membrane prevents the non-acylated protein from exiting the ER, whereas S-acylation shifts the orientation of the TMD and improves hydrophobic matching and reduces aggregation, allowing for its trafficking to the plasma membrane (Abrami *et al.*, 2008, Chamberlain and Shipston, 2015).

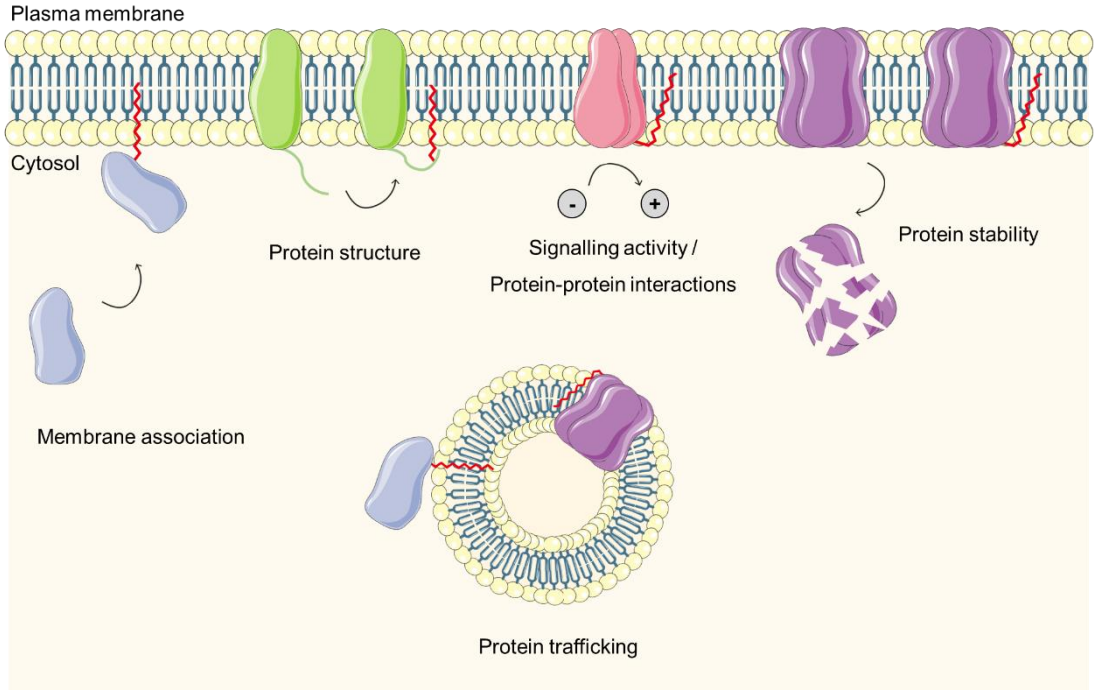

Figure 1.9 The regulatory effects of S-acylation.

S-acylation can take place on the plasma membrane or at different cell membrane compartments, regulating multiple stages in the life cycle of both soluble and transmembrane protein substrates. Some regulatory effects of S-acylation are illustrated in this figure, including membrane association, altered protein structure, signalling activity, protein-protein interactions, increased protein stability and protein trafficking. Created using Servier Medical Art (https://smart.servier.com/).

1.12 Links between S-acylation and disease

Given the impact that S-acylation has on the behaviour of a diverse array of cellular proteins involved in multiple physiological cell processes, it is not surprising that dysregulation of this modification is linked to a number of diseases, including neurodegenerative diseases, cancer, and metabolic disorders, amongst others (Nguyen *et al.*, 2023).

1.12.1 Neurological disorders

Huntington's disease

S-acylation is ubiquitous in the brain, regulating synaptic function, plasticity, and neuronal development. zDHHC17 and zDHHC13 have been linked to the huntingtin (HTT) protein, which is mutated in Huntington's disease, an autosomal dominant neurodegenerative disorder with motor, cognitive and behavioural decline characteristics. Huntington's disease is caused by the expansion of the polyQ region of the HTT protein that decreases protein stability and increases proteolysis, resulting in the accumulation of protein fragments that become aggregated and form toxic cytoplasmic and nuclear inclusions in neurons (Bates *et al.*, 2015). The disease-associated mutant of HTT displays decreased association with zDHHC17 and therefore decreased S-acylation, whereas knockdown of zDHHC17, or mutation of the S-acylated cysteine of HTT are associated with increased formation of nuclear inclusions (Yanai *et al.*, 2006). As mutant HTT is not able to enhance the activity of zDHHC17, it has been suggested that some features of Huntington's disease may also arise due to decreased S-acylation of zDHHC17 substrates (Huang *et al.*, 2011).

Neuronal ceroid lipofuscinosis

Neuronal ceroid lipofuscinoses (NCLs) are a group of rare, inherited neurodegenerative lysosomal storage disorders that can affect people of all ages and are classified as early or late infantile, juvenile, or adult NCL. Dysfunctional lysosomes in NCLs cause defects in waste removal, resulting in the excessive accumulation of lipofuscin in tissues, primarily in the brain and retina (Simonati and Williams, 2022). As mentioned previously, infantile NCL is caused by mutations in the *CLN1* gene encoding the deacylation enzyme PPT1 (Long and Cravatt, 2011). Adult NCL, on the other hand, has been linked to mutations in the *DNAJC5* gene encoding CSPα, one of the most highly S-acylated proteins in the brain. CSPα contains a conserved cysteine-rich motif of 14 cysteine residues which is extensively S-acylated and mediates stable membrane attachment, and trafficking to the plasma membrane and secretory vesicles. The disease-associated mutations are within the cysteine-rich motif and lead to the substitution of leucine-115 by arginine or the deletion of leucine-116. Both of these mutants form SDS-resistant aggregates that are S-acylation

dependent and susceptible to hydroxylamine treatment. It was proposed that the formation of these aggregates might contribute to the neurodegeneration seen in this condition (Greaves *et al.*, 2012).

Schizophrenia

Additionally, other zDHHC enzymes have also been associated with different neurological disorders. For example, the zDHHC5 isoform is associated with PSD-95, a key protein in synaptic development and plasticity found in excitatory synapses (Brigidi *et al.*, 2015). A mutation in zDHHC5 that results in a truncated form of the protein lacking the last 68 amino acids of its C-terminal tail, which includes the PDZ-binding motif involved in substrate binding, has been reported in cases of schizophrenia (Fromer *et al.*, 2014). Knockdown of zDHHC5 resulted in a decrease in the density of excitatory synapses, which could not be rescued by the expression of the catalytically inactive zDHHS5 mutant, nor the expression of the C-terminal truncated zDHHC5 mutant lacking the final 68 amino acids. Moreover, a mutant with decreased surface localisation also failed to reverse the zDHHC5 knockdown phenotype. These observations suggested that excitatory synapse formation and/or maintenance is dependent on the S-acylation activity of zDHHC5 and its association with PDZ domain-containing proteins via its C-terminal tail, such as PSD-95, as well as the plasma membrane association of the enzyme (Shimell *et al.*, 2021).

Moreover, zDHHC20, highly expressed in both neurons and immune cells, is important for synaptic integrity and for regulating immune signalling. A recent study used Mendelian randomisation to study the causal effects of S-acylation on schizophrenia. Their results showed an association between increased zDHHC20 expression and increased risk of schizophrenia, mediated through the expression of CCR7 on naive $CD8^+$ T-cells. Specifically, zDHHC20 induces an inflammatory response via CCR7-mediated T-cell activation, aggravating chronic inflammation that disrupts the crosstalk between the nervous system and the immune system and contributes to the progression of the disease (Guo *et al.*, 2025).

1.12.2 Cancer

Altered expression of several zDHHC enzymes, both upregulation and downregulation, has been observed in various cancer types, and zDHHC isoforms can have opposing roles in cancer disease states, acting as potential oncoproteins or as tumour suppressors. For example, overexpression of zDHHC14 has been observed in leukaemia, while the same enzyme is downregulated in prostate cancer (Chamberlain and Shipston, 2015).

zDHHC15 has been linked to glioma malignancy, the most common primary brain tumour characterised by high aggressiveness and low survival rates. The enzyme levels are dramatically upregulated in glioma tissues, compared to normal brain tissues, and levels are higher in patients with high-grade glioma. zDHHC15 knockdown experiments demonstrated decreased glioma cell proliferation and migration, whereas overexpression had opposing effects that were later linked to the overactivation of the STAT3 signalling pathway, which promoted the transcription of oncogenic proteins (Liu *et al.*, 2023).

The regulatory role of zDHHC7 has also been highlighted in prostate cancer, a significant contributor to mortalities among the male population. Androgen-dependent prostate cancers are reliant on the effect of androgen hormones that activate the androgen receptor, which then acts as a transcription factor for a number of genes involved in cell division. Overactivation of the androgen receptor results in the progression of prostate cancer. zDHHC7 is highly expressed in prostate tissues, and experiments using prostate cancer cells demonstrated a significant reduction of androgen receptor protein levels after zDHHC7 overexpression. This reduction is a result of transcriptional inhibition mediated by decreased recruitment of RNA Polymerase II to the androgen receptor promoter, negatively regulating the receptor's protein levels and attenuating its signalling activity in prostate cancer. zDHHC7 overexpression in experiments using human prostate cancer cell lines limited cell growth and prostate cancer cell invasion, whereas *in vivo* experiments demonstrated significantly reduced tumour growth in mice overexpressing zDHHC7. However, these tumour suppressor effects of zDHHC7 are limited in prostate cancer patients, as zDHHC7 expression is significantly downregulated in patient tissues, and therefore, androgen signalling is enhanced, driving disease progression (Lin *et al.*, 2023).

In addition to the examples above, there are several other zDHHC enzymes that have been linked to cancer, including zDHHC3, zDHHC9, and zDHHC19 (Ko and Dixon, 2018). Indeed, 26% of 299 validated cancer-driving genes are either known to be or predicted to be S-acylated, highlighting the broad relevance of S-acylation to cancer (Ko and Dixon, 2018).

1.12.3 Metabolic disorders

Diabetes mellitus is a major metabolic disorder that costs the NHS in excess of £10 billion per year. This condition is defined by sustained high blood sugar levels and categorised as either type 1 diabetes, an autoimmune form of the disease manifested by the loss of pancreatic β-cells responsible for the production of insulin (Berchtold *et al.*, 2011) and type 2 diabetes, often linked to lifestyle and defined by insulin resistance and defective insulin secretion (Du *et al.*, 2017).

zDHHC17 has been identified as a type 1 diabetes candidate protein in an *in silico* phenome-interactome network analysis to identify disease-causing genes. Proinflammatory cytokines IL-1β and IFN-γ impair β-cell function and facilitate the progression of type 1 diabetes, and these cytokines also cause a decrease in the expression of zDHHC17. Loss of expression of this enzyme could be linked to pathophysiology of diabetes as zDHHC17 is critical for pancreatic β-cell survival and insulin secretion in knockdown experiments, while the enzyme also exhibited anti-apoptotic effects against IL-1β-induced β-cell death in overexpression experiments. Therefore, downregulation of zDHHC17 in type 1 diabetes contributes to the disease phenotype of decreased insulin secretion and β-cell apoptosis (Berchtold *et al.*, 2011).

While type 1 diabetes is caused by β-cell death and loss of insulin secretion, the underlying factor that leads to the development of type 2 diabetes is insulin resistance in liver, adipose and skeletal muscle (the main insulin-responsive tissues). In adipose and skeletal muscle, a major target of insulin is glucose transporter 4 (Glut4), which is important for regulating glucose homeostasis. This transporter is stored intracellularly in these cells, and insulin stimulates its movement to the cell surface where it drives glucose uptake, clearing excess glucose from the bloodstream (Du *et al.*, 2017). The S-acylation of Glut4 is essential for its insulin-dependent translocation to the cell surface, since a cysteine-to-serine mutant exhibited decreased

responsiveness to insulin stimulation, due to interfering with the correct sorting to storage vesicles (Ren *et al.*, 2015). Glut4 S-acylation is mediated by zDHHC7, and silencing of the enzyme inhibited Glut4 S-acylation and significantly decreased the insulin-induced plasma membrane levels of Glut4. *Zdhhc7* knockout mice were shown to be hyperglycaemic, further validating the role of zDHHC7 in glucose homeostasis (Du *et al.*, 2017). GLUT4 translocation to the cell surface involves the interaction of SNARE proteins on the Glut4 vesicles with SNAREs at the plasma membrane. The plasma membrane SNARE proteins include SNAP23, which requires S-acylation for plasma membrane delivery. As zDHHC17 mediates S-acylation and membrane targeting of SNAP23, this enzyme is also likely to be functionally significant for insulin-stimulated glucose uptake in adipose and skeletal muscle tissues (Chamberlain *et al.*, 2021).

1.13 zDHHC9 and disease

1.13.1 zDHHC9 in Ras-dependent cancers

The substrate specificity of the zDHHC9/GCP16 protein complex for the oncoproteins H- and N-Ras makes it especially relevant to Ras-driven cancers. *RAS* has been characterised as a hallmark cancer gene due to its prevalence in human cancers. Ras proteins are part of a fundamental signal transduction cascade, in which initial extracellular signals from the EGFR activate Ras proteins (via GDP-GTP exchange), which then activate the Raf/MEK/ERK pathway, transducing the signal to the cell nucleus (Figure 1.10). Activated Ras signals for prolonged cell survival and proliferation, and reported oncogenic mutations in Ras trap the protein in a constitutively active GTP-bound state, resulting in tumorigenesis. In fact, it is estimated that *RAS* is mutated in approximately 20% of all human cancers, with each isoform being linked to different types of cancer (Busquets-Hernandez and Triola, 2021). Specifically, H-Ras is mostly associated with bladder carcinomas, while N-Ras mostly correlates with skin melanomas and haematological malignancies (Ward *et al.*, 2012, Busquets-Hernandez and Triola, 2021).

As previously discussed, Ras trafficking, membrane attachment, and signalling activity are regulated by post-translational lipid modifications. Farnesyl transferase

inhibitors (FTIs) emerged as a novel way to restrict mutant Ras activity, since FTase catalyses the initial farnesylation of Ras proteins for transient membrane attachment. Although FTIs initially showed promising pharmacological properties in animal cancer models, such as low ID50, cancer regression, low toxicity, and high membrane permeability, they failed to inhibit oncogenic Ras activity (Rajalingam *et al.*, 2007). It is thought that inhibition of farnesylation is not sufficient to block Ras activation due to compensatory geranylgeranylation by the related GGTase-1 enzyme (Appels *et al.*, 2005, Palsuledesai and Distefano, 2015).

S-acylation and deacylation cycles mediate the rapid movement of farnesylated H- and N-Ras between the plasma membrane, where EGFR is localised, and the Golgi apparatus. Considering their regulatory importance, there is a growing interest in targeting S-acylation enzymes responsible for modifying Ras proteins (Busquets-Hernandez and Triola, 2021). In fact, *in vivo* experiments using *Zdhhc9* knockout mice demonstrated that zDHHC9 inhibition reduced the S-acylation and plasma membrane association of oncogenic N-Ras. Most importantly, the same study demonstrated that zDHHC9 inhibition decreased the cellular transformation of haematopoietic cells by oncogenic N-Ras and its potential to cause leukaemia, without impairing normal haematopoiesis (Liu *et al.*, 2016).

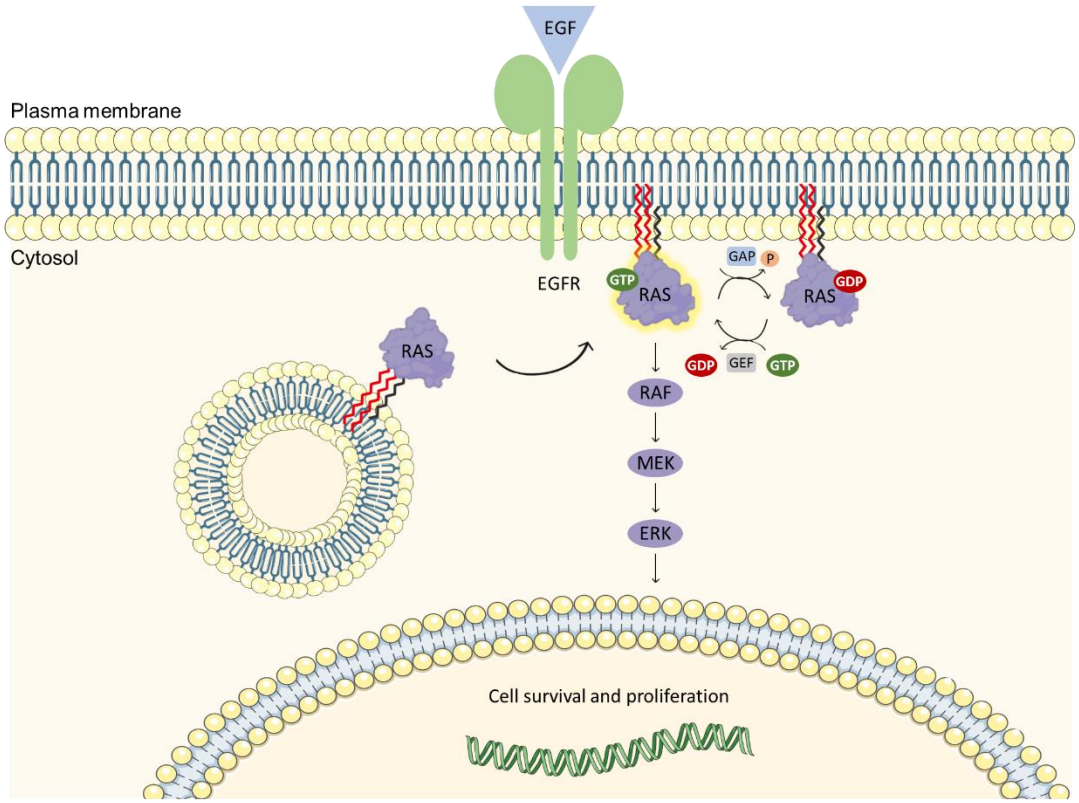

Figure 1.10 The Ras/Raf/MEK/ERK signalling pathway.

S-acylation of farnesylated Ras (S-acylation is shown in red and farnesylation is shown in black) allows trafficking from the Golgi to the plasma membrane via vesicular transport. Upon EGFR activation, Ras is switched from the inactive GDP-bound state to the active GTP-bound state, regulated by GEF and GAP enzymes. Activated Ras initiates a signalling cascade and transduces the signal to the cell nucleus to promote cell survival and proliferation. Created using BioRender.com and Servier Medical Art (https://smart.servier.com/).

1.13.2 zDHHC9 and X-linked intellectual disability (XLID)

Mutations in *ZDHHC9* have long been known to cause XLID, a term describing the impairment of various complex processes in brain development and function (Raymond *et al.*, 2007). Mutations in *ZDHHC9* have been identified in 2% of XLID patients, and these patients also demonstrated an increased risk of childhood

epilepsy (Baker *et al.*, 2015, Shimell *et al.*, 2019). Raymond *et al.* (2007) identified two single amino acid missense mutations within the highly conserved DHHC-CRD of zDHHC9: R148W and P150S (Raymond *et al.*, 2007).

The mechanisms underlying the loss of function effects of the zDHHC9 R148W and P150S mutants were uncovered by Mitchell *et al.* (2014). Their group demonstrated that the R148W and P150S mutations within zDHHC9 do not affect the stability of the enzyme, nor complex formation with GCP16, but impair its catalytic activity by decreasing the stability of the zDHHC9 autoacylated intermediate, albeit via different mechanisms. The initial burst kinetics forming the autoacylated intermediate of the zDHHC9 P150S mutant is reduced by 50%, whereas the zDHHC9 R148W mutant exhibited a significantly increased intrinsic hydrolysis rate of the autoacylated intermediate instead. Both mechanisms can lead to decreased zDHHC9-mediated S-acylation of substrate proteins, including those involved in intellectual development (Mitchell *et al.*, 2014). Further analysis of the interaction between the XLID-associated zDHHC9 mutants and GCP16 exhibited reduced complex formation (Nguyen *et al.*, 2023), while the cryo-EM structure of the zDHHC9/GCP16 complex revealed that mutation of R148 to a larger amino acid could disrupt the CCHC-coordinated zinc finger formed by Cys-141, Cys-144, His-154 and Cys-161 (Yang *et al.*, 2024), providing more detail into the disruptive zDHHC9 catalytic activity in affected individuals.

Indeed, a later study by the Bamji group characterised the involvement of zDHHC9 in intellectual disability and epilepsy through the S-acylation of two distinct GTPases, N-Ras and TC10. The authors found that zDHHC9 knockdown in rat hippocampal neuronal cultures altered dendritic morphology, decreasing dendrite length and complexity, a feature that is prevalent in intellectual disabilities. The knockdown phenotype was rescued by expressing wild-type zDHHC9 but not the XLID-associated zDHHC9 mutants R148W or P150S. Additionally, a similar decrease in dendrite length was seen after knocking down Ras, and this phenotype was only rescued by the expression of wild-type N-Ras and not by the S-acylation-deficient mutant of N-Ras. These results suggested that S-acylation of N-Ras by zDHHC9 regulates dendrite length. This is mediated by promoting the plasma membrane localisation of N-Ras and the activation of its downstream signalling activity (Shimell *et al.*, 2019).

zDHHC9 knockdown also demonstrated a significant reduction of inhibitory synapses, resulting in an increased ratio of excitatory to inhibitory synapses that also could not be rescued by zDHHC9 mutants R148W and P150S. This effect was later attributed to the S-acylation of TC10 via more knockdown and rescue experiments in hippocampal neurons. Specifically, zDHHC9-mediated S-acylation of TC10 facilitates its plasma membrane association, where it promotes gephyrin clustering, critical to the formation and stability of inhibitory synapses. *In vivo* experiments further verified the role of zDHHC9 in the balance of excitatory and inhibitory synapses, as *Zdhhc9* knockout mice demonstrated increased spontaneous activity similar to epileptic seizures (Shimell *et al.*, 2019).

Individuals with XLID caused by mutations in *ZDHHC9* also demonstrated hypoplasia of the corpus callosum, the tract connecting the two brain hemispheres (Baker *et al.*, 2015). Another study by the Bamji group demonstrated that *Zdhhc9* knockout mice had decreased corpus callosum width and impaired myelinogenesis. The group observed impaired oligodendrocyte maturation and formation of the myelin sheath, with decreased expression of genes involved in myelin production. These results align with the white matter deficits seen in XLID patients with zDHHC9 loss-of-function mutations (White *et al.*, 2025). These studies suggest that the phenotype seen in XLID patients with mutations in zDHHC9 is a result of impaired Ras and TC10 S-acylation, disrupting dendrite growth and inhibitory synapse formation respectively, along with altered gene expression and myelin protein levels, disrupting oligodendrocyte maturation and axon myelination (Shimell *et al.*, 2019, White *et al.*, 2025).

1.14 Therapeutic approaches and development of peptide inhibitors

Research in the field of S-acylation is hindered by the lack of chemical inhibitors that can selectively disrupt the activity of zDHHC isoforms. As a result, the benefits of therapeutically targeting zDHHC enzymes in disease states cannot be explored. The significance of zDHHC enzymes in normal cell physiology and their involvement in a number of diseases highlights the need for the development of novel and specific chemical modulators of S-acylation enzymes.

The palmitate analogue 2-BP is the most widely used S-acylation inhibitor *in vitro*, but since it covalently binds to the highly conserved acyl chain-binding pocket of zDHHC

enzymes, irreversibly inhibiting their autoacylation and subsequent catalytic activity, it has broad effects and no specificity, limiting its therapeutic potential (Jennings *et al.*, 2009, Lan *et al.*, 2021). Another major drawback of 2-BP is its ability to disrupt the activity of thioesterases that facilitate protein deacylation, therefore limiting its use in the study of S-acylation and deacylation cycles (Lan *et al.*, 2021). Cyano-myracrylamide (CMA) is a more recently synthesised potent inhibitor of S-acylation with a similar inhibition mechanism as 2-BP. Even though CMA displayed reduced toxicity and was able to only disrupt the activity of zDHHC enzymes and not thioesterases, this compound is also a broad-spectrum inhibitor, which lacks enzyme selectivity (Azizi *et al.*, 2021, Lan *et al.*, 2021).

Since some substrate-enzyme pairs have been identified in the zDHHC family, the possibility of disrupting the recruitment of substrates to their respective zDHHC enzyme partners was explored as a method of specific inhibition of their S-acylation. Phospholemman (PLM) is a small accessory subunit of the Na-pump, known to be S-acylated by zDHHC5. PLM can regulate the activity of the Na-pump in cardiac muscle through post-translational modifications taking place in its cytosolic C-terminal tail. Specifically, PLM activates and inhibits the activity of the Na-pump via phosphorylation and S-acylation, respectively (Plain *et al.*, 2020).

PLM and zDHHC5 do not interact directly; instead, zDHHC5 interacts with the α subunit of the Na-pump, via a region containing three C-terminal cysteine residues at positions 236, 237, and 245, located away from the enzyme's active site. This interaction provides the optimal positioning of PLM within the zDHHC5 active site. A zDHHC5 catalytic mutant, zDHHS5 exhibits robust S-acylation that is almost abolished after alanine substitution of cysteine-236 and cysteine-237. Alanine substitution of cysteine-236 and cysteine-237 also disrupted the interaction between zDHHC5 and the Na-pump in co-immunoprecipitation experiments, highlighting the importance of the S-acylation of these cysteines for the interaction. In the same study, the authors discovered that the S-acylation of the C-terminal tail of zDHHC5 is mediated by zDHHC20. Additionally, the attachment of sugar groups at serine-241 found near the Na-pump binding site of zDHHC5 via O-GlcNAcylation also increases binding of the Na-pump and presents another PTM that can regulate the subsequent PLM S-acylation (Plain *et al.*, 2020).

The most significant finding of this study is that S-acylation of PLM was significantly reduced after incubation with a cell-penetrating stearate-tagged version of the Na-

pump binding site peptide in HEK293 cells, as a result of disrupting the interaction of zDHHC5 with the Na-pump. Moreover, the peptide inhibitor had no effect on the S-acylation of H-Ras, used as a substrate example of a different zDHHC enzyme, exhibiting selective substrate-enzyme pair inhibition. The importance of this observation lies in the fact that inhibiting the S-acylation of PLM disrupts its effect on the Na-pump, therefore increasing its activity and marking it as a promising tool for treating heart failure (Plain *et al.*, 2020).

Another key study has recently identified the first selective zDHHC enzyme inhibitor, named SD-066-4. The authors reported that SD-066-4 is successful in decreasing the S-acylation of EGFR by zDHHC20 in K-Ras mutant cells, even when used at low concentrations (Lee *et al.*, 2024). In mutant K-Ras settings, zDHHC20-mediated S-acylation of EGFR is dramatically increased, leading to tumorigenesis. zDHHC20 knockout experiments revealed decreased downstream signalling and cell proliferation and also suppressed the growth of mutant K-Ras-dependent lung adenocarcinoma tumours *in vivo*, highlighting the potential therapeutic benefits of a zDHHC20 inhibitor (Kharbanda *et al.*, 2020). The identified SD-066-4 inhibitor seems to interact with zDHHC20 directly, and docking studies revealed that the potential binding site on zDHHC20 for SD-066-4 lies between the acyl-chain binding pocket and the nucleotide-binding site. SD-066-4 exhibits zDHHC isoform selectivity for zDHHC1, zDHHC11, zDHHC20 and zDHHC24 facilitated by the presence of an amino acid with a small side chain at the spatial position of alanine-144 found in the DHHC-CRD of zDHHC20 which can accommodate the methyl group of SD-066-4. Amino acid residues with bulky side chains at that position restrict the interaction with SD-066-4. These findings were validated in experiments in which zDHHC11 or zDHHC23 were overexpressed in NCI-H1975 lung cancer cells and even though both enzymes increased EGFR S-acylation, only zDHHC11, in which the alanine residue is conserved, was susceptible to SD-066-4, while the bulky isoleucine present in zDHHC23 protected the enzyme from inhibition (Lee *et al.*, 2024).

The pharmacological benefits of the compound were underscored in experiments demonstrating low non-specific toxicity, as it inhibited the proliferation of lung cancer cell lines but had no effect on a lung fibroblast cell line. Most importantly, SD-066-4 successfully increased the overall survival of mice with mutant K-Ras lung adenocarcinoma when administered orally, exhibiting tumour growth inhibition mediated by a decrease in EGFR S-acylation. This small molecule inhibitor and its

unique selectivity for a region outside of the usually targeted acyl-chain binding pocket of zDHHC enzymes, can be used as a template to achieve zDHHC isoform specificity and provide a therapeutic approach in other disease settings (Lee *et al.*, 2024).

Two promising inhibitors of zDHHC9 activity were also recently characterised: Treprostinil, an FDA-approved drug for the treatment of pulmonary arterial high blood pressure, and 10-Hydroxycamptothecin (10-HCPT). The oncogenic role of zDHHC9 in the progression of adenocarcinoma was identified, with zDHHC9 knockout experiments resulting in inhibited cell migration *in vitro* and tumour metastasis *in vivo* without affecting the subjects' overall health. The effects of zDHHC9 are mediated through the S-acylation of striatin-4 (STRN4), a scaffolding protein component of striatin-interacting phosphatase and kinase (STRIPAK) complexes organising signalling pathways affecting cell growth. S-Acylation of STRN4 promotes the recruitment of proteins involved in the Hippo/YAP pathway that lead to the transcriptional activation of genes associated with cell metastasis. Blocking STRN4 S-acylation inhibits the nuclear trafficking of YAP and the following gene expression (Tian *et al.*, 2025).

Multiple effectors linked to different oncogenic pathways can be modified by zDHHC9. Hence, the identification of potent zDHHC9 inhibitors Treprostinil and 10-HCPT could present a broad-based therapeutic strategy. The inhibitors were identified in small molecule virtual screening assays, and their ability to inhibit zDHHC9-dependent STRN4 S-acylation was further validated experimentally. Treatment with either Treprostinil or 10-HCPT reverted the increased cell migration seen with zDHHC9 and STRN4 overexpression in the HCT116 human colon cancer cell line. Furthermore, experiments performed *in vivo* on colon cancer spleen-to-liver metastasis mouse models demonstrated decreased metastasis to the liver for both inhibitors. Even though the off-target effects of the inhibitors were not assessed in this study, these findings highlight the potential of targeting zDHHC9 to tackle cancer progression and could pave the way for the development of zDHHC9-targeted cancer therapies (Tian *et al.*, 2025).

The development of zDHHC enzyme inhibitors, however, comes with a number of challenges, reflected in the limited advancements of this field. Isoform-specific inhibitors of zDHHC enzyme activity would impair the S-acylation of all substrates and not just the protein of interest. On the other hand, targeting specific substrate-binding sites on zDHHC enzymes can disrupt the S-acylation of other substrates interacting

via the same binding site. Therefore, the role of zDHHCs in the whole needs to be accounted for before advancing the clinical application of zDHHC inhibitors.

1.15 Aims and hypothesis

The main overarching hypothesis at the outset of this project was that targeting the zDHHC9/GCP16 complex would provide a novel mechanism to mediate inhibition of zDHHC9 (but not other zDHHC enzymes). Therefore, it was essential to understand how GCP16 interacts with zDHHC9 and the functional effects of this interaction in a cellular environment. By understanding these points, we proposed that it would be possible to use peptides mimicking the interaction sites to disrupt the zDHHC9/GCP16 complex. It is important to note that the cryo-EM structure of the zDHHC9/GCP16 complex (Yang *et al.*, 2024) was only reported after the initiation of this project, and so initial analysis of the protein complex involved screening for interaction sites. The specific aims of the project were to:

(i) Identify key regions within GCP16 for its S-acylation, membrane attachment and interaction with zDHHC9

(ii) Characterise the mechanism of interaction of the zDHHC9/GCP16 protein complex and how interaction affects the S-acylation and stability of each protein

(iii) Examine the importance of different binding interfaces identified in the cryo-EM structure of zDHHC9/GCP16 for the S-acylation and stability of each protein

(iv) Investigate the importance of the formation of a functional zDHHC9/GCP16 protein complex in dendritic growth experiments in neurons

(v) Analyse the broader interactions of GCP16 with other zDHHC family members

(vi) Explore the potential use of GCP16-based peptides in the inhibition of zDHHC9/GCP16 complex formation

CHAPTER 2

MATERIALS AND METHODS

Chapter 2 – Materials and methods

Materials

Product Name	Product ID	Provider
1 kb DNA ladder	G571A	Promega, WI, USA
10x FastDigest Green buffer	LT-02241	Thermo Fisher Scientific, Loughborough, UK
5 kDa monomethoxy polyethylene glycol (alkyne-mPEG)	JKA3177-1G	Sigma-Aldrich, Poole, UK
Acrylamide	J60868	Alfa Aesar®, Heysham, UK
Agar powder	LP0011	Oxoid, Hampshire, UK
Agarose powder	BIO-41025	Bioline, London, UK
Amersham™ Protran™ Premium 0.45 µm nitrocellulose membrane	GE10600003	Merck, Poole, UK
Ammonium persulfate (APS)	A3678	Sigma-Aldrich, Poole, UK
Ampicillin	A9518-25G	Sigma-Aldrich, Poole, UK
Ascorbic acid	A15613	Alfa Aesar®, Heysham, UK
Biotin	B4501-1G	Sigma-Aldrich, Poole, UK
Broad Range Prestained Protein Marker	PL00002	Proteintech, Manchester, UK
Bromophenol blue sotdium salt	A16899	Alfa Aesar®, Heysham, UK
BSA	BP9701-100	Thermo Fisher Scientific, Loughborough, UK
$CaCl_2$	10070	BDH Laboratory Supplies, Poole, UK
Chloramphenicol	C0378-5G	Sigma-Aldrich, Poole, UK
ChromoTek GFP-Trap® agarose immunoprecipitation beads (anti-GFP)	GTA	Proteintech, Manchester, UK
Corning® BioCoat™ Poly-D-Lysine 24-well plates	356414	Thermo Fisher Scientific, Loughborough, UK
Corning® BioCoat™ Poly-D-Lysine 6-well plates	356413	Thermo Fisher Scientific, Loughborough, UK
Corning® BioCoat™ Poly-D-Lysine coverslips	354086	Thermo Fisher Scientific, Loughborough, UK
Corning® T75 cm^2 Cell Culture Flask with Vent Cap	430641U	Thermo Fisher Scientific, Loughborough, UK
$CuSO_4$	451657-10G	Sigma-Aldrich, Poole, UK
Cycloheximide (CHX)	C-7698-5G	Sigma-Aldrich, Poole, UK
Cytiva Whatman™ 3MM Chr Chromatography Paper	3030-681	Thermo Fisher Scientific, Loughborough, UK
DAPI	D9542	Sigma-Aldrich, Poole, UK
Digitonin	D141-100MG	Sigma-Aldrich, Poole, UK
Dithiothreitol (DTT)	R0861	Thermo Fisher Scientific, Loughborough, UK
DMSO	D5879	Sigma-Aldrich, Poole, UK
Dulbecco's Modified Eagle Medium (DMEM) + GlutaMAX™ media	31966-021	Gibco, LifeTechnologies™ Ltd., Paisley, UK
EDTA	E6758-100G	Sigma-Aldrich, Poole, UK
EZ-Run™ Pre-Stained Protein Marker	BP3601-500	Thermo Fisher Scientific, Loughborough, UK
FastAP Thermosensitive Alkaline Phosphatase	EF0651	Thermo Fisher Scientific, Loughborough, UK
FastDigest DpnI	FD1704	Thermo Fisher Scientific, Loughborough, UK
Fatty acid-free Bovine Serum Albumin (BSA)	A7030-100G	Sigma-Aldrich, Poole, UK
Foetal Bovine Serum (FBS)	A5256801	Gibco, LifeTechnologies™ Ltd., Paisley, UK
Glacial acetic acid	036289.K3	Thermo Fisher Scientific, Loughborough, UK
Glycerol	A16205	Alfa Aesar®, Heysham, UK

Glycine	101196X	VWR International, Leicestershire, UK
HEPES	391333	Merck, Poole, UK
Hexylene glycol	112100-500G	Sigma-Aldrich, Poole, UK
Human Embryonic Kidney 293T cells (HEK293T)	CRL-3216	ATCC, VA, USA
Invitrogen™ PureLink™ Quick Gel Extraction Kit	K210012	Thermo Fisher Scientific, Loughborough, UK
Invitrogen™ PureLink™ Quick Plasmid Miniprep Kit	K210011	Thermo Fisher Scientific, Loughborough, UK
Invitrogen™ SYBR™ Safe DNA gel stain	S33102	Thermo Fisher Scientific, Loughborough, UK
Kanamycin	K4000-5G	Sigma-Aldrich, Poole, UK
KCl	P/4240/53	Thermo Fisher Scientific, Loughborough, UK
KH_2PO_4	P0662-500G	Sigma-Aldrich, Poole, UK
LI-COR REVERT™ 700 Total Protein Stain kit	926-11021	LI-COR Biosciences Ltd, Cambridge, UK
Lipofectamine® 2000 Reagent	11668019	Thermo Fisher Scientific, Loughborough, UK
MeOH	34860-2.5L-R	Merck, Poole, UK
MG132	M7449	Sigma-Aldrich, Poole, UK
Microscope slides	13192131	Scientific Glass Laboratories Ltd, Stoke-on-Trent, UK
Mowiol® 4-88 Reagent	475904	Merck, Poole, UK
Na_2HPO_4	013437.A1	Thermo Fisher Scientific, Loughborough, UK
NaCl	S/3160/60	Thermo Fisher Scientific, Loughborough, UK
NaOH	S/4800/60	Thermo Fisher Scientific, Loughborough, UK
NucleoBond Xtra Midi kit	740410.100	Macherey-Nagel GmbH & Co. KG, Düren, Germany
Palmitic acid	506345	Sigma-Aldrich, Poole, UK
Pfu 10x reaction buffer	M776A	Promega, WI, USA
Pfu DNA Polymerase enzyme	M774A	Promega, WI, USA
Pierce™ 16% Formaldehyde (w/v)	#28908	Thermo Fisher Scientific, Loughborough, UK
Polyethylenimine (PEI)	43896	Alfa Aesar®, Heysham, UK
Protease inhibitor cocktail	P8340-5ML	Sigma-Aldrich, Poole, UK
SDS	S/P530/53	Thermo Fisher Scientific, Loughborough, UK
Sterilin™ Standard 90mm Petri Dishes	11309283	Thermo Fisher Scientific, Loughborough, UK
T4 DNA Ligase 10x buffer	C126B	Promega, WI, USA
T4 DNA Ligase enzyme	M1801	Promega, WI, USA
TBTA	H66485.03	Thermo Fisher Scientific, Loughborough, UK
TEMED	T9281	Sigma-Aldrich, Poole, UK
TPP® tissue culture plates - uncoated	92024	Merck, Poole, UK
Tris base	BP152-1	Thermo Fisher Scientific, Loughborough, UK
Triton X-100	T8787	Sigma-Aldrich, Poole, UK
TrypLE™ Express	12604-013	Gibco, LifeTechnologies™ Ltd., Paisley, UK
Tryptone	LP0042B	Oxoid, Hampshire, UK
Tween®20	P1379-1L	Sigma-Aldrich, Poole, UK
Yeast extract	LP0021	Oxoid, Hampshire, UK

2.1 Cell culture

Human Embryonic Kidney 293T (HEK293T) cells were cultured in T75 cm^2 flasks with Dulbecco's Modified Eagle Medium (DMEM) + GlutaMAX™ media, supplemented with 10% Foetal Bovine Serum (FBS) and incubated in a Thermo BB15 incubator (Thermo Fisher Scientific, Loughborough, UK), set at 37°C / 5% CO_2. After 7 days, the media was discarded, and cells were briefly washed with 10 mL of warm phosphate-buffered saline (PBS; Stock at 10x: 1.54 M NaCl, 53.6 mM KCl, 80 mM Na_2HPO_4, and 14.6 mM KH_2PO_4 in dH_2O). To dissociate adherent cells, 2.5 mL of TrypLE™ Express was added and incubated for 3 minutes at 37°C. After the incubation period, cells were detached from the flask surface by gently tapping the flask, and then 7.5 mL of DMEM + GlutaMAX™ media, supplemented with 10% FBS was added to inactivate the TrypLE™ Express. Cells were then collected into a 15 mL Falcon tube and pelleted by centrifugation (Heraeus Multifuge 3 S-R, Thermo Fisher Scientific, Loughborough, UK) at 150 x*g* for 3 minutes. The supernatant was removed, and cells were resuspended in 10 mL of DMEM + GlutaMAX™ media, supplemented with 10% FBS. Cells were then seeded into a new T75 cm^2 flask at a 1 : 20 dilution, with a final volume of 10 mL. For experimental analysis, cells were diluted to 1 : 50 using DMEM + GlutaMAX™ media, supplemented with 10% FBS, and plated on poly-D-Lysine-coated 24-well plates, at a volume of 0.5 mL of cells per well, or on poly-D-Lysine-coated 6-well plates, at a volume of 2 mL of cells per well.

2.2 Transfection of HEK293T cells

Plasmid DNA was introduced into the HEK293T cells by transfection with polyethylenimine (PEI) (Stock solution at 1 mg/mL in water, pH 7, sterile filtered, aliquoted, and stored at -20°C), 24 hours after seeding onto plates. 1 µg of plasmid per well was used in single transfections, while 0.6 µg of plasmid encoding zDHHC enzyme was mixed with 0.4 µg of plasmid encoding substrate protein / accessory protein for co-transfections. The plasmid mix was added to a final volume of 50 µL serum-free DMEM + GlutaMAX™ and PEI was added at a ratio of 2 µL PEI : 1 µg total plasmid DNA. The mixture was then vortexed and incubated at room temperature for 20 minutes, before being added to each well of a 24-well plate. When using 6-well

plates, 4 µg of total plasmid DNA (2.4 µg of plasmid encoding zDHHC enzyme and 1.6 µg of plasmid encoding substrate protein / accessory protein for co-transfections) were added to 200 µL serum-free DMEM + GlutaMAX™ and mixed with PEI at a ratio of 2 µL PEI : 1 µg total plasmid DNA. The mixture was treated as above before being added to each well. Cells were incubated at 37°C for 24 hours prior to experimental analysis.

2.3 Plasmid construct design

All zDHHC enzyme constructs (mouse) cloned in pEF-BOS-HA vectors were provided by Professor Masaki Fukata (Fukata *et al*., 2004). The plasmid pcDNA3.1(+)-N-eGFP-zDHHC9 (human) was synthesised by GenScript (GenScript Biotech Ltd, Oxford, UK), and was subsequently subcloned into the pEF-BOS-HA vector. For this, the plasmid was digested with *BamHI*, and the zDHHC9 insert and pEF-BOS-HA vector were then purified and ligated, as described in sections 2.7 - 2.9. The mutant construct pEF-BOS-HA-zDHHA9 (mouse) was previously made by Dr. Jennifer Greaves (Coventry University). All other zDHHC9 mutant constructs (mouse) were synthesised and cloned into pEF-BOS-HA by GenScript (GenScript Biotech Ltd, Oxford, UK) (Table 2.1).

GCP16 WT (human) was synthesised and cloned into the pcDNA3.1(+)-N-eGFP vector by GenScript (GenScript Biotech Ltd, Oxford, UK). This plasmid encodes GCP16 with the GFP tag at the N-terminus. The GCP16 1-30 aa C-terminal mutant was generated via the insertion of a premature stop codon by site-directed mutagenesis of pcDNA3.1(+)-N-eGFP-GCP16, using the primers GCP16 1-30 P1 and P2 (Table 2.2). All other GCP16 mutant constructs (human) were synthesised and cloned into the pcDNA3.1(+)-N-eGFP vector by GenScript (GenScript Biotech Ltd, Oxford, UK) (Table 2.1).

GCP16 WT and GCP16 binding interface mutant constructs 1, 2, 3, and 4a/b were also cloned in pcDNA3.1(+)-N-3xFLAG by GenScript (GenScript Biotech Ltd, Oxford, UK). PEF-BOS-HA-GCP16 (mouse) was previously made by Dr. Jennifer Greaves (Coventry University). GCP16 truncated mutant constructs fused to an N-terminal Golgi localisation sequence, FLWRIFCFRK (Navarro and Cheeseman, 2022), followed by two poly-Glycine-Serine (G_4S) linkers (referred to as GLS-GCP16) were

synthesised by Genscript (GenScript Biotech Ltd, Oxford, UK) and cloned into the mCherry-C1 vector (N-terminally tagged) (the mCherry-C1 plasmid was generated by tag exchange of pEGFP-C1, by Dr. Christine Salaun, University of Strathclyde) (Table 2.1). mCherry-FLWRIFCFRKGGGGSGGGGS-C1 (referred to as GLS) was also synthesised by GenScript (GenScript Biotech Ltd, Oxford, UK).

The sequence of plasmid DNA was confirmed by sequencing performed by GATC Eurofins genetic sequencing service (GATC service by Eurofins Genomics, Wolverhampton, UK, https://eurofinsgenomics.eu/en/custom-dna-sequencing/) or by DNA Sequencing & Services (MRC PPU, School of Life Sciences, University of Dundee, Dundee, UK, www.dnaseq.co.uk).

GCP16			
C-terminal truncation mutants	**N-terminal truncation mutants**	**Alanine scanning mutants**	**Golgi localisation sequence (GLS) mutants**
1-60	11-137	61-65A	**1:** 1-60 C24A
1-90	21-137	66-70A	**2:** 91-124
1-120	31-137	71-75A	**3:** 91-137
1-122	61-137	76-80A	
1-124	91-120	81-85A	
1-126	91-124	86-90A	
1-128	91-128	122-125A	
1-130	91-137	126-130A	
Cysteine mutants		**Mutants based on AlphaFold structure prediction**	
C69A		Y76A/R121A	
C72A		Y76A/R121E	
C69A/C72A		Y76A/F79A/R121A	
C24A/C69A/C72A			
C69A/C72A/C81A			
Interface mutants			
1: Y76A			
2: Y86A			
3: R16A/Y18A			
4a/b: K11A/F13A/R118A/R121A/E124A			
4b: R118A/R121A/E124A			
1-4a/b: K11A/F13A/R16A/Y18A/Y76A/Y86A/R118A/R121A/E124A			
4a/b (D): K11D/F13D/R118D/R121D/E124A			
1-4a/b (D/K): K11D/F13D/R16D/Y18D/Y76K/Y86K/R118D/R121D/E124A			
zDHHC9			
Interface mutant			
1-4a/b: R85A/D100A/E101A/F104A/F129A/P150A/E163A/Y183A/P292A			
DHHC domain mutants			
3.1: K139Y/Y140K/Y142P/T143K			
3.2: K145C/I146S/F147I/R148K			
3.3: I157V/D159K/N160R			
3.4: V162I/E163R/R164K/F165M			
3.5: K178E/R179N/Y181Q/R182K			

Table 2.1 GCP16 and zDHHC9 mutant constructs synthesised by GenScript.

2.4 Primer design

For sub-cloning experiments, primers were designed using the ApE software (A plasmid Editor, https://jorgensen.biology.utah.edu/wayned/ape/) for the identification of the appropriate restriction sites and the online software Primer3Plus (https://dev.primer3plus.com/index.html) for the identification of the hybridisation sequence. For site-directed mutagenesis experiments, primers were designed using the online QuikChange® Primer Design Program by Agilent (https://www.agilent.com/store/primerDesignProgram.jsp). Primers were manufactured by Merck (Darmstadt, Germany) and resuspended in the appropriate volume of dH_2O to give a stock concentration of 100 µM. Resuspended primers were stored at -20°C.

Primer name	Primer sequence (5' - 3')
Site-directed mutagenesis	
GCP16 1-30 P1	CCTGTTCTCCAGCTCGGCCTAGAACTTGGTCTGGAACTG
GCP16 1-30 P2	CAGTTCCAGACCAAGTTCTAGGCCGAGCTGGAGAACAGG
Sub-cloning	
zDHHC9 Forward	AATGAGGCGCGCCATGTCTGTGATGGTGGTG
zDHHC9 Reverse	AGCTGAAGCTGAGAAGACGAATTCAATGA

Table 2.2 Sequence of oligonucleotide primers used for plasmid construct design.

2.5 Polymerase Chain Reaction

Polymerase Chain Reaction (PCR) was used for the amplification of a DNA region of interest, using a hermal cycler (Applied Biosystems™ Veriti™ 96-Well Thermal Cycler, Thermo Fisher Scientific, Loughborough, UK). The appropriate forward and reverse primer stocks were diluted to a final concentration of 10 µM in a primer mix. For the PCR reaction, 2 µL of primer mix, 1.5 µL of 50 ng / µL plasmid DNA, 1 µL of 10 mM dNTPs, 5 µL of Pfu 10x reaction buffer, and 1 µL of Pfu DNA Polymerase enzyme were added to a thin-walled PCR tube and were made up to a final volume of 50 µL with dH_2O. The PCR cycle used consisted of an initial denaturation step of 2

minutes at 95°C, followed by 30 cycles of: denaturation at 95ºC for 30 seconds, annealing at 54°C for 30 seconds and elongation at 72°C for 2 minutes per kb of DNA template. The 30 cycles were followed by a 5-minute incubation at 72°C, with a final hold at 4°C. Agarose gel electrophoresis (section 2.6) was used to confirm the amplification of the PCR product.

2.6 Agarose gel electrophoresis

Agarose gel electrophoresis was used for the identification of PCR products or DNA fragments. Samples were loaded into lanes in an agarose gel submerged in buffer and were resolved by applying an electric current. The intrinsically negative phosphate backbone of DNA, along with its uniform mass to charge ratio, results in its migration through the agarose gel matrix, toward the positively charged anode. The migration speed depends on the size of the DNA fragments, with smaller DNA fragments migrating faster.

The gel was prepared using 1% (w/v) of agarose powder, dissolved in 50 mL of TAE buffer (Stock at 50x: 2 M Tris base, 50 mM EDTA, and glacial acetic acid to pH 8) and by adding Invitrogen™ SYBR™ Safe DNA gel stain at a dilution of 1 : 10,000. The gel was immersed in TAE buffer. Samples were prepared using 5 µL of the amplified PCR product / DNA, 2 µL of 10x FastDigest Green buffer and 13 µL of dH_2O and were then loaded alongside 5 µL of 1 kb DNA ladder. The gel was run at 120V (PowerPac™ Basic, BioRad, CA, USA) for 30 minutes and the DNA was then visualised under UV light by an Ingenius-Syngene Bio UV illuminator and associated camera (Synoptics Syngene GelVue GVM30, Syngene, Cambridge, UK).

2.7 Restriction digestion of DNA

For sub-cloning of plasmids, PCR products were digested for 1 hour at 37°C using 40 µL of the PCR product, 2 µL of each of the appropriate restriction enzymes, 6 µL of 10x FastDigest Green buffer and 10 µL of dH_2O for a total volume of 60 µL. The desired vector for sub-cloning was also digested for 1 hour at 37°C, using 1 µL of the vector (~1 µg / µL), 1 µL of each of the restriction enzymes, 2 µL of 10x FastDigest

Green buffer and by making up to 20 µL with dH_2O. The digested backbone vector was dephosphorylated for 10 minutes at 37°C, using 1 µL of FastAP Thermosensitive Alkaline Phosphatase, to prevent self-annealing.

2.7.1 DpnI treatment of site-directed mutant PCR products

For the generation of the site-directed mutants, the restriction enzyme *DpnI* was used for cleaving methylated adenine (^{m}A) in the recognition sequence G^{m}ATC of the target DNA. After the PCR reaction for the site-directed mutant generation, *DpnI* digestion cleaves any plasmids with methylated sites corresponding to the parental cDNA template, therefore leaving the amplified unmethylated plasmid intact. PCR products were digested by adding 1 µl of *DpnI* to 9 µl of the PCR product and incubating at 37°C for 1 hour in a Clifton water bath (Clifton, Nickel-Electro Ltd., UK). The *DpnI*-treated products were then transformed into competent TOP10 *E. coli* cells (100 µL).

2.8 Agarose gel extraction and purification

Agarose gel electrophoresis was used to resolve the digested products (120V for 45 minutes). The DNA fragments were then visualised by UV illumination (Transilluminator 4000, Stratagene, CA, USA), cut from the gel using a scalpel and placed into 1.5 mL Eppendorf tubes. The DNA was purified from the agarose gel using the Invitrogen™ PureLink™ Quick Gel Extraction Kit as per manufacturer's protocol: 500 µL of gel solubilisation buffer (L3) was added to the tubes containing the DNA agarose gel slices and placed into a 50°C heat block (FB15101, Digital Dry Bath, Thermo Fisher Scientific, Loughborough, UK) until gel dissolution. The dissolved gels containing the DNA were then loaded onto Quick Gel Extraction Columns and centrifuged at 12,000 x*g* for 1 minute. After discarding the flow-through, 500 µL of Wash Buffer (W1) was added, followed by two centrifugations at 16,000 x*g* for 1.5 minutes. For DNA elution, 30 µL of dH_2O was added, followed by centrifugation at 16,000 x*g* for 1 minute. Eluted DNA was kept at -20°C long-term.

2.9 Ligation

The digested and purified PCR products and vector DNAs were ligated overnight at room temperature, using 2 µL of vector DNA, 10 µL of insert DNA, 1.4 µL of T4 DNA ligase 10x buffer and 1 µL of T4 DNA Ligase enzyme. The ligated construct (14 µL) was then transformed into competent TOP10 *E. coli* cells and cultured for DNA amplification (section 2.11). Ligated plasmid constructs were confirmed by restriction enzyme digestion and agarose gel electrophoresis.

2.10 Preparation of competent TOP10 *E. coli* cells

A 100 µL aliquot of competent TOP10 *E. coli* cells stored at -80°C was thawed on ice for 10 minutes, before adding 200 µL of sterile Luria Broth (LB; 1% Tryptone, 1% NaCl, 0.5% Yeast extract). The bacteria were then incubated in a shaking incubator (250 rpm) for 45 minutes, at 37°C. After incubation, bacteria were spread on LB agar Sterilin™ standard 90mm petri dishes containing no antibiotics (10 mL LB broth with 1.5% agar powder) and incubated overnight at 37°C. A single colony was then picked and inoculated in 2 mL of LB containing no antibiotics, which was then incubated overnight in a shaking incubator (250 rpm), at 37°C. 1 mL of the overnight culture was used to inoculate 100 mL of LB and was further incubated at 37°C for 2 - 3 hours, until OD_{600} reached a value of 0.2 - 0.7 (POLARstar Omega, BMG Labtech, Aylesbury, UK). The culture was then chilled on ice for 15 minutes, before being aliquoted into two 50 mL tubes and pelleted by centrifugation at 3,300 x*g* for 10 minutes at 4°C. The supernatant was discarded, and each pellet was resuspended in 10 mL of ice-cold, sterile 0.1 M $CaCl_2$. Cells were then incubated on ice for 30 minutes before being centrifuged at 3,300 x*g* for 10 minutes, at 4°C. After the supernatant was discarded, each pellet was resuspended in 3 mL of ice cold, sterile 0.1 M $CaCl_2$ containing 15% glycerol. The total 6 mL of bacterial culture obtained was snap-frozen into 100 µL aliquots and stored at -80°C.

2.11 Transformation of TOP10 *E. coli* competent cells

An aliquot of competent TOP10 *E. coli* cells was defrosted on ice for 10 minutes. For the transformation of established constructs, 0.2 µL of ~1 µg / µL DNA was added to 35 µL of competent cells in a 1.5 mL Eppendorf tube, while for the transformation of sub-cloned plasmids, 10 µL of the ligation reaction was added to 100 µL of competent cells. After 20 minutes of incubation on ice, the samples were heat shocked at 42°C for 45 seconds and were then placed on ice. Subsequently, 100 µL of sterile LB was added to the Eppendorf tubes, followed by a 1-hour incubation in a shaking incubator (C24 Incubator Shaker, New Brunswick Scientific, NJ, USA) set at 220 rpm, at 37°C. The transformation mix was then spread onto LB agar Sterilin™ standard 90mm petri dishes (10 mL LB broth with 1.5% agar powder), supplemented with either 30 µg / mL Kanamycin, or 100 µg / mL Ampicillin, and incubated overnight at 37°C in a Heraeus B6060 Incubator (Thermo Fisher Scientific, Loughborough, UK). Isolated, single colonies were picked from the plates the next day, using a sterile pipette tip. The selected colonies were incubated overnight at 37°C in either 3 mL of LB media plus antibiotic for Mini preps or in 150 mL of LB media plus antibiotic for Midi preps. The shaking incubator was set at 200 rpm or 250 rpm, respectively. After the incubation period, the Invitrogen™ PureLink™ Quick Plasmid Miniprep Kit or the NucleoBond Xtra Midi kit was used as per the manufacturer's instructions to obtain the purified DNA. The concentration of the purified DNA product was measured using a Nanodrop 2000/2000c Spectrophotometer (Thermo Fisher Scientific, Loughborough, UK). The GATC Eurofins genetic sequencing service (GATC service by Eurofins Genomics, Wolverhampton, UK, https://eurofinsgenomics.eu/en/custom-dna-sequencing/) or the DNA Sequencing & Services (MRC PPU, School of Life Sciences, University of Dundee, Dundee, UK, www.dnaseq.co.uk) were used to confirm the sequence of plasmid DNA. The sequencing outputs were then aligned with the corresponding reference DNA for analysis using the ApE software (A plasmid Editor, https://jorgensen.biology.utah.edu/wayned/ape/).

2.12 Analysis of protein expression

Approximately 24 hours after transfection, cells were washed briefly in PBS and lysed in 100 µL of SDS sample buffer (Stock at 4x: 0.4% bromophenol blue sodium salt, 200 mM Tris base pH 6.8, 40% glycerol, 8% SDS) supplemented with 25 mM dithiothreitol (DTT). Lysates were scraped from the wells using wide-bore tips and transferred to 1.5 mL Eppendorf tubes. The samples were then heated to 95°C for 5 minutes, before being resolved through SDS-PAGE and analysed by immunoblotting (see sections 2.19 and 2.20).

2.13 Fatty acid azide labelling and click chemistry

Click-PEGylation

Cells were plated on 24-well plates (three wells per transfection condition), as described in section 2.1. Approximately 24 hours after transfection of HEK293T cells, the cell media was aspirated, and cells were washed with 0.5 mL of PBS per well. PBS was then aspirated, and 500 µL of labelling mix was added to each well. The labelling mix consisted of 500 µL of warm serum-free DMEM + GlutaMAX™, containing 1 mg / mL fatty acid-free Bovine Serum Albumin and either 100 µM of “cold” palmitic acid (Stock at 50 mM 500x, dissolved in DMSO) used as a negative control (one well per sample), or 100 µM of palmitic acid azide (C16-azide, Stock at 50 mM 500x, dissolved in DMSO, synthesised by Professor Nicholas Tomkinson, University of Strathclyde) (two wells per sample). Cells were then incubated for 4 hours at 37°C. After incubation, the labelling media was aspirated, and cells were washed with 0.5 mL PBS per well. Cells in each well were then lysed, using 100 µL of lysis buffer (50 mM Tris pH 8.0, 0.5% SDS) containing protease inhibitor cocktail at a dilution of 1 : 100. The cells were then scraped off the wells and added into Eppendorf tubes placed on ice.

For the click chemistry reaction and the detection of S-acylation, an alkyne-conjugated 5 kDa monomethoxy polyethylene glycol (mPEG) reporter was used in a click chemistry reaction mix. 80 µL of click chemistry reaction mix (2 mM $CuSO_4$, 0.2 mM TBTA and 200 µM alkyne-mPEG reporter dissolved in DMSO) was added to each

lysate, followed by the addition of 20 µL of 40 mM ascorbic acid. Samples were incubated at room temperature for 1 hour with end-over-end rotation. After the incubation step, 67 µL of 4x SDS sample buffer containing 100 mM DTT was added to the samples, reaching a final concentration of 1x SDS sample buffer containing 25 mM DTT. Samples were then heated to 95°C for 5 minutes before being resolved using SDS-PAGE for further analysis.

The alkyne-mPEG reporter molecule “clicks” with the azide group of the palmitic acid azide in the labelling mix. This results in a 5 kDa band shift for every S-acylated cysteine in a protein, which is visualised by immunoblotting analysis. This band shift is not seen with the palmitic acid used as a control as it lacks the azide group. For quantification, the sum of all S-acylated bands observed was calculated as a percentage of the total protein signal (non-acylated + S-acylated) and a mean value was obtained from the two palmitic acid azide samples for each condition. The data was then normalised to the highest value of each experiment which was set to 1.

2.14 GFP-Trap® agarose bead co-immunoprecipitation

Transfected HEK293T cells plated on 6-well plates were aspirated and washed in 2 mL PBS before being lysed in 280 µL lysis buffer (PBS, 1% Triton X-100 with added protease inhibitor cocktail at a dilution of 1 : 100). Cells were then scraped from the wells and placed into 1.5 mL Eppendorfs. The lysed samples were incubated on ice for 30 minutes, with gentle inversion every 5 minutes. In parallel, ChromoTek GFP-Trap® agarose immunoprecipitation beads (anti-GFP) were briefly vortexed to be resuspended in the stock tube. The beads were washed by taking 12 µL of the anti-GFP bead slurry per immunoprecipitation (IP) sample and adding it to an Eppendorf containing 1 mL of ice-cold PBS, using a cut yellow pipette tip. The beads were then collected by centrifugation at 3,000 x*g* for 3 minutes, at 4°C. PBS was aspirated carefully, and the beads were resuspended in cold PBS (200 µL per IP sample) and vortexed. 200 µL per IP sample were added into new Eppendorf tubes using a cut yellow pipette tip. All the samples were then spun down by centrifugation at 3,000 x*g* for 3 minutes, at 4°C. PBS was then aspirated carefully, and the beads were placed on ice.

After the 30-minute incubation of lysates on ice, 300 µL of cold PBS was added to each lysate to give a final Triton X-100 concentration of 0.5% v/v. The lysates were then centrifuged at 14,000 x*g* for 5 minutes, at 4°C. 45 µL of the supernatant of each sample was retained in a new Eppendorf tube as a "Lysate" sample and stored at -20°C. The remaining 455 µL of the supernatant of each sample was added to the washed GFP Trap® agarose immunoprecipitation beads and incubated for 1 hour at 4°C, with end-over-end rotation.

The agarose beads were then centrifuged at 3,000 x*g* for 3 minutes at 4°C, to get a pellet. The supernatant was aspirated, and the beads were washed twice by adding 1 mL cold PBS in each sample. Samples were centrifuged at 3,000 x*g* for 3 minutes at 4°C and the PBS was aspirated. Proteins were then eluted by adding 50 µL of 2x SDS sample buffer containing 100 mM DTT and heating the samples for 10 minutes at 95°C. Beads were then pelleted by centrifugation at 3,000 x*g* for 3 minutes at 4°C, and the supernatant (approximately 50 µL) was collected for further analysis by SDS-PAGE and immunoblotting. For loading the lysate samples onto gels,15 µL of warm 4x SDS sample buffer containing 100 mM DTT was added to each defrosted lysate sample. Lysates were then heated for 5 minutes at 95°C, before being loaded on the gel. Protein co-immunoprecipitation was calculated by dividing the HA intensity value (IR680) by the corresponding intensity value of the EGFP signal (IR800) in each IP sample. The data was then normalised to the highest value of each experiment which was set to 1.

2.15 Cycloheximide chase

Approximately 24 hours after HEK293T cell transfection, the media was aspirated and cells were either washed and lysed (0-hour samples) or incubated with 0.5 mL of warm DMEM + GlutaMAX™ media supplemented with 10% FBS, containing 50 µg / mL of cycloheximide (CHX) (Stock at 50 mg / mL dissolved in DMSO) for 8 hours. Cells were washed once with 0.5 mL PBS and lysed in 100 µL of SDS sample buffer containing 25 mM DTT. Lysed cells were scraped from the wells and transferred to Eppendorf tubes. Samples were then heated to 95°C for 5 minutes, before being analysed by SDS-PAGE and immunoblotting. For quantification, the signal for each sample was normalised to the corresponding total protein stain levels, and a mean value was calculated from the two samples for each condition. The 8-hour time points

were then expressed as percentage remaining protein relative to the 0-hour time points.

2.16 Cell fractionation

Cells were plated on 6-well plates and transfected as described above. Approximately 24 hours after transfection, the media was aspirated, and the cells were washed in 1.2 mL of PBS. Cells were then scraped and placed into Eppendorf tubes. Samples were centrifuged at 500 x*g* for 3 minutes at 4°C to produce a cell pellet. The supernatant was aspirated, and the cell pellet was resuspended in 1 mL of cold PBS and centrifuged at 500 x*g* for 3 minutes at 4°C. The supernatant was aspirated again, and the cell pellet was resuspended in 200 µL of cold lysis buffer A (150 mM NaCl, 50 mM HEPES, 1 M hexylene glycol and 25 µg / mL digitonin, pH 7.4) containing protease inhibitor cocktail at a dilution of 1 : 100. Samples were then incubated at 4°C for 10 minutes, with end-over-end rotation. After the 10-minute incubation, samples were centrifuged at 2,000 x*g* for 10 minutes, at 4°C. The supernatant was collected in a fresh Eppendorf tube as the cytosol fraction. Then, 67 µL of 4x SDS sample buffer containing 100 mM DTT was added to the cytosol fraction samples, before they were heated to 95°C for 5 minutes. The remaining pellets were dissolved in 267 µL of SDS sample buffer containing 25 mM DTT, these contain the membrane fraction samples. Samples were then analysed using SDS-PAGE, followed by immunoblotting (see sections 2.18 and 2.19). Membrane association was calculated as a percentage of the sum of the corresponding intensity values of the cytosolic and membrane fractions in each sample. The data was then normalised to the highest value of each experiment which was set to 1.

2.17 MG132 proteasomal inhibition

Cells were plated on 24-well plates and transfected as described above. Approximately 8 hours after transfection, MG132 was added to the cells, at a concentration of 10 µM (Stock at 10 mM, dissolved in DMSO). The same volume of DMSO was used as a vehicle control. Around 16 hours later, the media was aspirated, and cells were washed once with 0.5 mL PBS and lysed in 100 µL of SDS sample

buffer containing 25 mM DTT. Lysed cells were scraped from the wells and transferred to Eppendorf tubes. Samples were then heated to 95°C for 5 minutes, before being resolved by SDS-PAGE and analysed by immunoblotting. Protein expression was normalised to the total protein stain levels of each sample and expression levels after 16 hours of MG132 treatment were quantified relative to the corresponding control values. The data was then normalised to the highest value of each experiment which was set to 1.

2.18 Sodium Dodecyl Sulphate-Polyacrylamide Gel Electrophoresis

Glass plates were clamped together in a Bio-Rad casting stand, and gels were cast by pouring two gel solutions: a resolving polyacrylamide mix at the bottom, and a stacking polyacrylamide mix at the top. Resolving gels of 8 - 15% acrylamide were typically used [40% Acrylamide, 5 mL of 2x resolving buffer (0.2% SDS, 4 mM EDTA, 750 mM Tris base, pH 8.9), 100 µL of 438 mM ammonium persulfate (APS, 10%), and 10 µL of TEMED], according to the molecular weights of the proteins being studied to allow for optimal protein separation. After the resolving gel had set, the stacking polyacrylamide mix was added [0.9 mL of 40% Acrylamide, 3.1 mL of dH_2O, 4 mL of 2x stacking buffer (0.2% SDS, 4 mM EDTA, 250 mM Tris base, pH 6.8), 100 µL of 438 mM APS (10%), and 10 µL of TEMED], and a 1.0 mm gel comb inserted to form the wells. Prepared and boiled samples were loaded onto gels placed in a running tank filled with SDS running buffer [Stock at 10x: 250 mM Tris base, 1.92 M Glycine, and 1% SDS], alongside 0.5 µL of a molecular weight marker (either EZ-Run™ Pre-Stained Protein Marker, with a separation range of 20 - 118 kDa, or Broad Range Prestained Protein Marker, with a separation range of 3 - 245 kDa) to be analysed by SDS-PAGE. Gels were run at a constant voltage of 80 V for 20 minutes to allow migration through the stacking gel, followed by 150 V for 60 minutes, or until the bromophenol blue dye in the samples was released into the running buffer.

2.19 Immunoblotting

After analysis by SDS-PAGE, proteins were transferred onto a nitrocellulose membrane (6 x 9 cm), using a Bio-Rad Trans-Blot® SD cell (Bio-Rad Laboratories Ltd, Watford, UK). Whatman™ chromatography paper (3MM CHR) was placed on the anode part of the transfer cassette, followed by the gel and a nitrocellulose membrane placed on top of the gel. Another sheet of Whatman™ 3MM CHR paper was placed on top of the nitrocellulose membrane. Whatman™ 3MM CHR papers and nitrocellulose membranes were pre-soaked in transfer buffer [Stock at 10x: 480 mM Tris base, 390 mM Glycine, 0.06% SDS; for 1x add 20% (v/v) MeOH]. Transfer was carried out overnight (for approximately 16 hours) in transfer buffer, at 120 mA, to allow protein migration from the gel to the membrane.

The next day, nitrocellulose membranes were removed from the cassette and briefly washed in dH_2O. Nitrocellulose membranes were then stained using the LI-COR REVERT™ 700 Total Protein Stain kit on a shaker, at room temperature, for 5 minutes. Membranes were then washed twice in wash buffer (6.6% glacial acetic acid in 30% MeOH in dH_2O) for 30 seconds, on a shaking plate. After washing away the excess stain, membranes were scanned using the 700 nm channel of a LI-COR Odyssey 9120 IR Imager (LI-COR Biosciences Ltd, Cambridge, UK) and the Image Studio software. After scanning, membranes were incubated with REVERT reversal solution (0.1% sodium hydroxide in 30% MeOH in dH_2O) for no longer than 10 minutes on a shaking plate, to completely remove the stain. Membranes were then briefly rinsed in dH_2O before further use.

To perform an immunoblotting analysis, membranes were blocked in 5% (w/v) dried skimmed milk (Tesco, UK), diluted in PBS-T (PBS containing 0.1% Tween®20) for 45 minutes on a shaking plate, to prevent non-specific binding of antibodies. After the blocking step, membranes were washed three times with PBS-T, for 5 minutes per wash, with shaking. The final wash was discarded, and membranes were incubated with the appropriate primary antibody mix diluted in PBS-T (Table 2.3) for at least 2 hours, with shaking. Membranes were washed in PBS-T three more times and were then incubated in PBS-T containing the appropriate secondary antibody (Table 2.3) for 1 hour, with shaking. Membranes were washed in PBS-T for three more times, as described above, before being scanned using the appropriate channels (700 nm and

800 nm) of the LI-COR Odyssey 9120 IR Imager (LI-COR Biosciences Ltd, Cambridge, UK).

Antibody	Species	Clonality	Source	Cat. Code	Dilution
Primary antibodies					
α-Calnexin	Mouse	Monoclonal	BD Transduction Laboratories, NJ, USA	610524	1:1,000
α-GAPDH	Rabbit	Polyclonal	Proteintech, Manchester, UK	10494-1-AP	1:15,000
α-GFP (JL8)	Mouse	Monoclonal, IgG	Takara Bio, CA, USA	632381	1:4,000
α-HA (3F10)	Rat	Monoclonal, IgG	Roche Diagnostics Ltd., Burgess Hill, UK	11867423001	1:1,000
α-RFP	Sheep	Monoclonal, IgG	Ian Prior, Liverpool, UK	N/A	1:2,000
α-FLAG	Mouse	Monoclonal, IgG	GenScript Biotech Ltd, Oxford, UK	A00187	1:2,000
α-FLAG	Rabbit	Polyclonal, IgG	Proteintech, Manchester, UK	20543-1-AP	1:1,000
Secondary antibodies					
IRDye® 680RD anti-Mouse	Donkey	IgG	LI-COR Biosciences, NE, USA	926-68072	1:20,000
IRDye® 680RD anti-Rabbit	Donkey	IgG	LI-COR Biosciences, NE, USA	926-68073	1:20,000
IRDye® 680RD anti-Rat	Goat	IgG	LI-COR Biosciences, NE, USA	926-68076	1:20,000
DyLight™ 680 anti-Goat	Donkey	IgG	Thermo Fisher Scientific, Loughborough, UK	SA5-10090	1:20,000
IRDye® 800CW anti-Mouse	Donkey	IgG	LI-COR Biosciences, NE, USA	926-32212	1:20,000
IRDye® 800CW anti-Rabbit	Donkey	IgG	LI-COR Biosciences, NE, USA	926-32213	1:20,000
IRDye® 800CW anti-Rat	Goat	IgG	LI-COR Biosciences, NE, USA	926-32219	1:20,000
IRDye® 800CW anti-Goat	Donkey	IgG	LI-COR Biosciences, NE, USA	926-32214	1:20,000

Table 2.3 Primary and secondary antibodies used in immunoblotting for the detection of proteins.

2.20 Bioinformatics

2.20.1 Plasmid design

The National Centre for Biotechnology Information (NCBI) database (National Library of Medicine; National Institutes of Health; U.S. Department of Health and Human Services, https://www.ncbi.nlm.nih.gov/) was used to obtain reference DNA sequences. To visualise, design, and present relevant DNA sequences, the ApE software (A plasmid Editor, https://jorgensen.biology.utah.edu/wayned/ape/) was used (Davis and Jorgensen, 2022).

2.20.2 Multiple sequence alignment

For the alignment of multiple protein sequences, the Clustal Omega multiple sequence alignment program was used, through the align tool from UniProt (https://www.uniprot.org/align) (UniProt, 2025), while images generated were annotated using Microsoft PowerPoint.

2.20.3 AlphaFold

The AlphaFold Protein Structure Database developed by DeepMind and the European Molecular Biology Laboratory-European Bioinformatics Institute (EMBL-EBI) (Jumper *et al*., 2021, Varadi *et al*., 2022, Varadi *et al*., 2024) was used to obtain 3D protein structure predictions. Outputs were saved as PDB files and visualised using the RCSB Protein Data Bank 3D Mol* Viewer, a modern web app for 3D visualisation and analysis of large biomolecular structures (Sehnal *et al*., 2021). The obtained images were then edited in Microsoft PowerPoint.

2.20.4 Kyte-Doolittle hydropathy profiling

The Kyte-Doolittle scale was used to examine the relative hydrophobicity and hydrophilicity of amino acid residues along the polypeptide chain of GCP16. As part of the hydropathy profiling, each residue was assigned a hydropathy index based on the Kyte-Doolittle scale, and average scores were calculated using a sliding window of nine residues to smooth local fluctuations and identify broader hydropathy trends (Kyte and Doolittle, 1982).

2.21 Quantification and statistical analysis

Quantification of band intensities obtained from all immunoblot experiments was carried out using the Licor® Image Studio™ Lite Software (LI-COR Biosciences, NE, USA), and all figures were created using Microsoft PowerPoint. Statistical analysis was performed using GraphPad Prism version 8.0.2 (263) for Windows (GraphPad Software, Boston, Massachusetts USA). Statistical significance was determined using either one-way ANOVA followed by Dunnett's or Tukey's multiple comparisons test, or an unpaired t-test where appropriate. Mean values ± standard error of the mean (SEM) were plotted, and the number of replicates was specified in the figure legends. Significant difference was indicated with the use of asterisks (*), where * $p < 0.05$, ** $p < 0.01$, *** $p < 0.001$, while ns indicates non-significance.

Materials and methods for work on neuronal cultures

For work performed on neuronal cultures at Prof. Shernaz Bamji's lab at the Life Sciences Institute of the University of British Columbia, Canada, USA, the following materials and methods were used.

All procedures involving animals were in accordance with the Canadian Council of Animal Care (CCAC) and approved by the University of British Columbia Animal Care Committee.

Materials

Product Name	Product ID	Provider
18 mm coverslips	0111580	Marienfeld, Lauda-Königshofen, Germany
Poly-L-lysine hydrobromide	P9155-5MG	Sigma-Aldrich, St. Louis, MO
Minimum Essential Medium (MEM) plating media	11090-081	GIBCO, Thermo Fisher Scientific, Waltham, MA
Sodium pyruvate	11360-070	GIBCO, Thermo Fisher Scientific, Waltham, MA
GlutaMAX™	35050-161	Invitrogen, Thermo Fisher Scientific, Waltham, MA
Pen/Strep	15140-148	Invitrogen, Thermo Fisher Scientific, Waltham, MA
Hanks' Balanced Salt Solution (HBSS)	14170-112	GIBCO, Thermo Fisher Scientific, Waltham, MA
Trypsin	LS003667	Worthington Biochemical, Lakewood, NJ
DNase I	DN25	Sigma-Aldrich, St. Louis, MO
Neurobasal medium	21103-049	GIBCO, Thermo Fisher Scientific, Waltham, MA
Neurocult SM1 Neuronal Supplement	05711	STEMCELL technologies, Canada
Lipofectamine® 2000 Reagent	11668019	Invitrogen, Thermo Fisher Scientific, Waltham, MA
Opti-MEM™	31985-062	GIBCO, Thermo Fisher Scientific, Waltham, MA
Paraformaldehyde (PFA) 16%	15710	Electron Microscopy Sciences, Hatfield, PA
Triton X-100	T8787	Sigma-Aldrich, St.Louis, MO
Goat serum (GS)	AB7481	Abcam, USA
ProLong™ Gold Antifade Mountant with DNA Stain DAPI	P36941	Invitrogen, Thermo Fisher Scientific, Waltham, MA
ProLong™ Gold Antifade Mountant	P36934	Invitrogen, Thermo Fisher Scientific, Waltham, MA
Primary antibodies		
FLAG-tag Mouse mAb	9A3	Cell Signaling Technology, Danvers, MA
HA-tag Rabbit mAb	C29F4	Cell Signaling Technology, Danvers, MA
Secondary antibodies		
Alexa Fluor™ Plus 647 Goat anti-Rabbit IgG pAb	A32733	Invitrogen, Thermo Fisher Scientific, Waltham, MA
Alexa Fluor™ 568 Goat anti-Mouse IgG pAb	A11031	Invitrogen, Thermo Fisher Scientific, Waltham, MA
Plasmid constructs		
pcDNA3.1(+)-N-3xFLAG-GCP16	N/A	GenScript Biotech Ltd, Oxford, UK
pcDNA3.1(+)-N-3xFLAG-GCP16 3	N/A	GenScript Biotech Ltd, Oxford, UK
pcDNA3.1(+)-N-3xFLAG-GCP16 4a/b	N/A	GenScript Biotech Ltd, Oxford, UK
pAAV-Camk2a-EGFP	VB230707-1353nff	VectorBuilder Inc., Chicago, IL
HA-zDHHC9	N/A	(Shimell *et al.*, 2019)

2.22 Plate preparation

Hippocampal neurons from male or female Sprague-Dawley rats (Charles River, Sherbrooke, Canada) were prepared as described below and plated on 18 mm coverslips placed in 12-well dishes, at a density of approximately 470 cells / mm². Coverslips were sterilised by dipping in 70% ethanol before being exposed to UV light for 30 minutes. Each coverslip was then coated overnight with 500 µl of 0.4 mg / mL poly-L-lysine hydrobromide in 0.1 M borate buffer pH 8.5. Plates were covered and left overnight in the biosafety cabinet. The next day, the wells were rinsed three times with sterile distilled water and 1 mL of Minimum Essential Medium (MEM) plating media (500 mL MEM with Earle's Salts, 50 mL FBS, 11.25 mL of 20% glucose, 5 mL sodium pyruvate, 5 mL 100X GlutaMAX™, 5 mL 100X Pen/Strep) was added in each well. The plates were stored in a 5% CO_2 incubator at 37°C for 4 hours.

2.23 Preparation of hippocampal neurons from Sprague-Dawley rats

Embryonic day 18 (E18) pups were harvested from euthanised timed-pregnant Sprague-Dawley rats (Charles River, Sherbrooke, Canada) and placed in cold HBSS on ice. Hippocampi were carefully dissected out and placed in 10 mL of fresh, warm HBSS (37°C) and were then washed twice with 10 mL of warm HBSS, before being incubated with 5 mL of 0.25% Trypsin for 20 minutes with gentle agitation every 5 minutes, in a water bath set at 37°C. After the 20-minute incubation, 4 mL of Trypsin was removed and 1% DNase I was added to the remaining 1 mL. Hippocampi were washed three times with fresh, warm HBSS and were then resuspended in 1 mL of HBSS. Cell density was determined using a haemocytometer, before the cells were seeded. The plating media was replaced 3 - 4 hours later with prewarmed maintenance media (500 mL Neurobasal medium, 10 mL Neurocult SM1 Neuronal Supplement, 5 mL 100X GlutaMAX™, 5 mL 100X Pen/Strep). Two to three days later, the maintenance media was replaced.

2.24 Transfection of primary hippocampal cultures

Primary rat hippocampal cultures were transfected at DIV 9 using Lipofectamine, as per the manufacturer's protocol. Two aliquots of 25 µL of Opti-Mem™ were prepared per well of a 12-well plate. For the overexpression of zDHHC9 and GCP16 WT or mutant constructs, 1.5 µg of DNA of each plasmid was added to one Opti-Mem™ aliquot, while for the overexpression of GCP16 WT or mutant constructs alone, 3 µg of DNA of each plasmid were added. 1.5 µg of the Camk2a plasmid was used in both experiments as a control (1.5 - 4.5 µg of total plasmid DNA / well). 1 µL of Lipofectamine was added to the other Opti-Mem™ aliquot and allowed to mix for 5 minutes. Aliquots were then combined to a final volume of 50 µL and incubated for 20 minutes, before being added to each well. Cells were then fixed (DIV 14) for subsequent experiments.

2.25 Immunocytochemistry

For immunocytochemistry experiments, cells were fixed for 10 min in 0.5 mL of warm fixing solution (4% PFA, 50mM HEPES, 4% sucrose in PBS) per well. Cells were then washed three times with 1 mL / well of PBS for 10 minutes and were subsequently permeabilised using 0.5 mL / well of 0.1% Triton X-100 in PBS for 10 minutes at room temperature. Cells were washed for three times as above and blocked with 0.5 mL of 10% goat serum (GS) in PBS per well, for 1 hour at room temperature, in the dark. Coverslips were then placed on parafilm, and each was incubated with 120 µL of primary antibody (1 : 500) dissolved in 1% GS in PBS overnight at 4°C, in the dark. The next day, coverslips were placed back into the wells to be washed three times as above and were then placed on parafilm to be incubated in secondary antibodies prepared in 1% GS in PBS, for 1 hour at room temperature, in the dark. During the secondary antibody incubation, 30 µL of ProLong™ Gold Antifade Mountant with DNA Stain DAPI was added to each coverslip, for 30 minutes. Coverslips were then washed for three more times and were finally mounted on microscope slides using one drop of ProLong™ Gold Antifade Mountant.

2.26 Imaging

Fixed neurons were imaged on an Evident IX83 inverted microscope equipped with a Hamamatsu Orca Flash sCMOS camera and a X-Cite white light LED. Dendritic morphology was visualised using single 16-bit snaps using a 20x / 0.8 NA UPLANAPO air objective with the camera in a 23 MHz readout mode. All images were acquired with equal LED settings and exposure times.

2.27 Total dendritic length and mean protein intensity

To measure total dendritic length, .vsi files of imaged neurons at 20X magnification were imported into Image J software (version v1.54p) (Schneider *et al*., 2012) using the Bio-Formats Importer. The EGFP channel was manually thresholded and binarised into a mask. The mask was then imported into the SimpleNeuriteTracer (SNT) plugin (Arshadi *et al*., 2021) and dendritic arbors were manually traced. The total dendritic length was then measured in SNT. The scales for the distance were automatically calibrated based on the metadata for each image. The mean grey value for the FLAG-GCP16 WT and mutant constructs and HA-ZDHHC9 channels was also measured within the EGFP mask in ImageJ as an indication of protein intensity.

2.28 Quantification and statistical analysis

All data values were imported on GraphPad Prism version 8.0.2 (263) for Windows (GraphPad Software, Boston, Massachusetts USA) and plotted as mean ± standard error of the mean (SEM). Statistical significance was determined using either one-way ANOVA followed by a Tukey's multiple comparisons test, or an unpaired t-test where appropriate. Significant difference was indicated with the use of asterisks (*), where * $p < 0.05$, ** $p < 0.01$, *** $p < 0.001$, while ns indicates non-significance. The value of ''n'' represents the number of cells used per condition, from three separate cultures, or as stated in the figure legend.

CHAPTER 3

MOLECULAR CHARACTERISATION OF GCP16: IDENTIFICATION OF KEY REGIONS REQUIRED FOR S-ACYLATION, MEMBRANE ASSOCIATION, AND REGULATION OF ZDHHC9

Chapter 3 - Molecular characterisation of GCP16: Identification of key regions required for S-acylation, membrane association, and regulation of zDHHC9

Introduction

The Golgi-associated protein GCP16 is an evolutionarily conserved membrane protein that was initially characterised as a protein involved in vesicular trafficking from the Golgi to the plasma membrane (Ohta *et al.*, 2003). Sequence homology analysis subsequently identified GCP16 as the orthologue of *Saccharomyces cerevisiae* Erf4, which is an essential accessory protein of the zDHHC9 orthologue, Erf2. The same study also used co-immunoprecipitation experiments to show that GCP16 forms a protein complex with zDHHC9, similarly to Erf2 and Erf4 (Swarthout *et al.*, 2005).

To confirm whether the zDHHC9/GCP16 complex has acyltransferase activity like that of the Erf2/Erf4 yeast orthologue, Swarthout *et al.* (2005) purified the zDHHC9/GCP16 complex from insect cells and assessed its enzymatic activity using H-Ras as a substrate. The purified zDHHC9/GCP16 protein complex was shown to mediate the S-acylation of H-Ras, and GCP16 was found to be essential for the acyltransferase activity of zDHHC9. Interestingly, proteolysis of zDHHC9 was observed when expressed in the absence of GCP16, suggesting that GCP16 may enhance the stability of zDHHC9 (Swarthout *et al.*, 2005). This idea was supported by a later study, which showed that zDHHC9 aggregates in the absence of GCP16 (Nguyen *et al.*, 2023). However, the role of GCP16 in regulating the activity of zDHHC9 in mammalian cells has not been examined, and its effect on zDHHC9 stability was not investigated directly through protein stability analysis.

Ohta *et al.* (2003) demonstrated that GCP16 behaves like an integral membrane protein in HeLa cells, although hydropathy analysis showed that it lacks a hydrophobic transmembrane domain. Instead, they proposed that the tight membrane association of GCP16 is driven by the S-acylation of cysteine-69 and cysteine-72 (Ohta *et al.*, 2003). Swarthout *et al.* (2005) also assessed the membrane association of zDHHC9 and GCP16 co-expressed in HEK293 cells and found that the proteins were resistant to extraction using high salt or high pH conditions and were only extracted by the detergent dodecyl maltoside, similarly to other integral membrane proteins and the yeast Erf2/Erf4 protein complex (Swarthout *et al.*, 2005). Both studies underlined the

importance of S-acylation for the integral membrane behavior and membrane association of GCP16.

The majority of zDHHC enzymes are believed to function without the need for an accessory protein, and therefore, understanding how GCP16 regulates zDHHC9 is of particular interest (Salaun *et al.*, 2020). When the work in this chapter was initiated, there was no published information available on the mechanism of zDHHC9/GCP16 interaction, and little was known about the reciprocal effects of this interaction on both proteins in mammalian cells. The main aims of this chapter were: (i) to elucidate the effects of complex formation on the S-acylation and stability of both zDHHC9 and GCP16 in mammalian cells; (ii) to generate GCP16 truncation mutants and use these to identify key regions required for zDHHC9 interaction; (iii) to examine how specific truncations of GCP16 affect the S-acylation and stability of both GCP16 and zDHHC9, and (iv) to further investigate the role of the cysteine residues within GCP16 for protein S-acylation and membrane association.

Results

3.1 Analysis of the reciprocal regulatory effects of zDHHC9 and GCP16 when co-expressed in mammalian cells

The effects of GCP16 on zDHHC9 have been examined in several studies. Swarthout *et al.* (2005) observed that the autoacylation of zDHHC9, along with its enzymatic activity against Ras proteins are dependent upon GCP16 association, using proteins purified from baculovirus-infected Sf9 insect cells. In addition, when expressed alone, purified zDHHC9 from insect cells is more susceptible to proteolysis, compared to the purified zDHHC9/GCP16 complex (Swarthout *et al.*, 2005). Furthermore, zDHHC9 is prone to aggregation in cell extracts when not co-expressed with GCP16, in FSEC analyses (Nguyen *et al.*, 2023). However, it is less clear how GCP16 affects zDHHC9 activity and stability in intact mammalian cells, and there is very little known about the reciprocal effects of zDHHC9 on GCP16. Therefore, as a first step, we investigated the bidirectional effects on both zDHHC9 and GCP16 proteins after co-expression in HEK293T cells.

To investigate the effects on their S-acylation status, HEK293T cells were co-transfected with EGFP-GCP16 or EGFP (control), together with HA-zDHHC9 or PEF-BOS-HA (empty control plasmid). Cells were then labelled using either palmitic acid as a control or palmitic acid azide and processed for click chemistry detection of S-acylation using alkyne mPEG (5 kDa). Samples were then resolved by SDS-PAGE and visualised by immunoblotting (Figure 3.1A). S-acylation is indicated by band shifts on the immunoblot, caused by the addition of the 5 kDa mPEG molecule after the alkyne and azide groups “click” together. For each substrate incubated with palmitic acid azide, S-acylation levels were calculated as a percentage of total expression and normalised to the highest value of each experiment. Quantified data and statistical analysis confirmed that GCP16 co-expression significantly increased the S-acylation levels of zDHHC9, when compared to the EGFP control. The experiment also revealed that although GCP16 is partially S-acylated when co-expressed with the PEF-BOS control, its S-acylation levels are significantly increased upon zDHHC9 co-expression.

The effects of zDHHC9/GCP16 complex formation on the protein stability of both zDHHC9 and GCP16 were also investigated in a cycloheximide assay. HEK293T cells were co-transfected as described above, and cells were either lysed at 0 hours or incubated with cycloheximide, a protein synthesis inhibitor, for 8 hours. The 8-hour samples were then lysed, and all proteins were resolved by SDS-PAGE and detected by immunoblotting (Figure 3.1B). Protein expression after 8 hours of protein synthesis inhibition by cycloheximide was quantified as a percentage of the initial 0-hour expression point. The results demonstrated that the protein stability of zDHHC9 is significantly increased when GCP16 is co-expressed, with the percentage of protein remaining after 8 hours of cycloheximide treatment being more than two times higher than those seen with the EGFP control. Additionally, the protein stability of GCP16 was also significantly increased when co-expressed with zDHHC9, albeit to a lesser extent than the increased stability seen for zDHHC9.

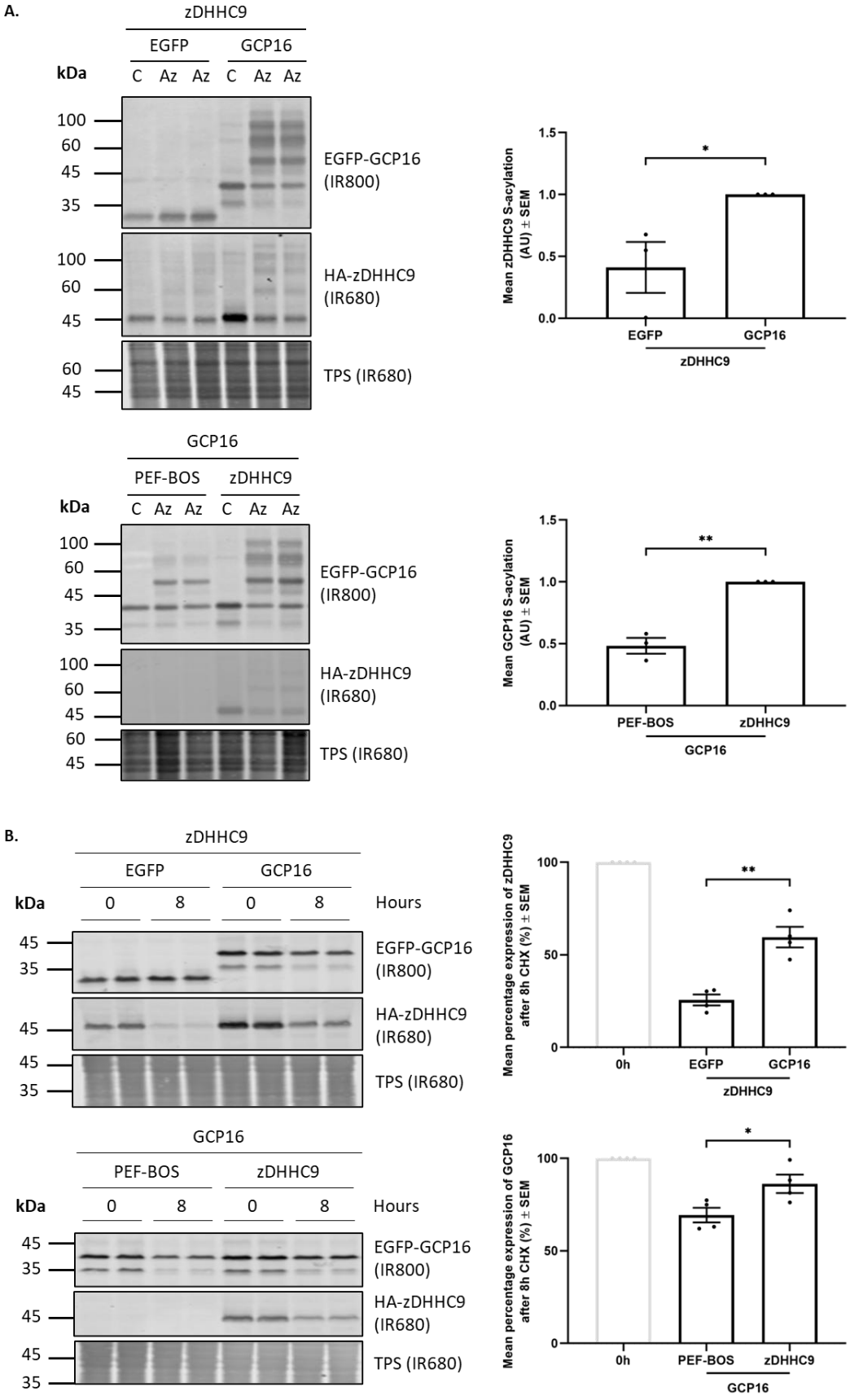
A.
zDHHC9
EGFP
GCP16
kDa
C Az Az C Az Az
100
60
45
35
EGFP-GCP16
(IR800)
HA-zDHHC9
(IR680)
TPS (IR680)
Mean zDHHC9 S-acylation
(AU) ± SEM
1.5
1.0
0.5
0.0
*
EGFP
GCP16
zDHHC9
GCP16
PEF-BOS
zDHHC9
Mean GCP16 S-acylation
(AU) ± SEM
**
PEF-BOS
zDHHC9
GCP16
B.
zDHHC9
EGFP
GCP16
kDa
0 8 0 8
Hours
EGFP-GCP16
(IR800)
HA-zDHHC9
(IR680)
TPS (IR680)
Mean percentage expression of zDHHC9
after 8h CHX (%) ± SEM
100
50
0
**
0h
EGFP
GCP16
zDHHC9
GCP16
PEF-BOS
zDHHC9
Mean percentage expression of GCP16
after 8h CHX (%) ± SEM
*
0h
PEF-BOS
zDHHC9
GCP16

Figure 3.1 The bidirectional effects of zDHHC9 and GCP16 when co-expressed in HEK293T cells.

HEK293T cells were co-transfected with EGFP-GCP16, or EGFP, together with HA-zDHHC9, or PEF-BOS-HA (empty plasmid control). ***(A)*** *Cells were labelled with palmitic acid (C16:0) as a control (C) or palmitic acid azide (Az-C16:0) for 4 hours and were then lysed and clicked using alkyne mPEG (kDa). S-acylation is indicated by band-shifts in Az samples. Quantified data show mean protein S-acylation (± SEM). The S-acylated bands were quantified as a percentage of total expression (non-acylated + S-acylated bands) for each substrate incubated with the palmitic acid azide. The data have been normalised to the highest value of each experiment, which was set to 1.* ***(B)*** *Cell lysates were collected at 0 hours or after 8 hours of incubation with 50 µg/ml cycloheximide (CHX). Protein expression levels were detected by immunoblotting. Quantified data show mean percentage protein expression (± SEM) after 8 hours of CHX treatment, quantified relative to the corresponding 0-hour value and normalised to the total protein stain levels of each sample. Statistical significance was analysed using an unpaired t-test. *p<0.05, **p<0.01 and ***p<0.001, while ns denotes non-significance, where p>0.05. (A) n = 3, from two independent experiments, (B) n = 4, from three independent experiments. The position of molecular weight markers (kDa) is shown on the left. The data shown in this figure were part of larger experiments, and as a result, the immunoblots in panel A are also presented in Figures 5.4 and 4.8, respectively, and the immunoblots in panel B are also shown in Figure 4.9*

3.2 The amino acid region 60-90 of GCP16 is involved in the interaction with zDHHC9

When this project was started, there was no information on the regions involved in the interaction between zDHHC9 and GCP16. To identify regions in GCP16 that are important for the association with zDHHC9, truncation mutants of GCP16 were designed to be used in co-immunoprecipitation experiments, as shown in Figure 3.2A. To investigate protein binding, HEK293T cells were co-transfected with HA-tagged zDHHC9 and either EGFP-tagged GCP16 WT, 1-30, 1-60, 1-90, 1-120, or EGFP as a negative control. Cell lysates were incubated with GFP-Trap® Agarose beads, and captured EGFP-tagged proteins together with any co-immunoprecipitated HA-zDHHC9 were examined by immunoblotting (Figure 3.2B). The co-immunoprecipitated levels of HA-tagged zDHHC9 were calculated relative to the levels of the corresponding immunoprecipitated EGFP-tagged proteins and normalised to the highest value of each experiment.

The quantified data in Figure 3.2C shows that, except for full-length WT GCP16, which is known to interact with zDHHC9 (positive control), only GCP16 truncation mutants 1-90 and 1-120 were able to co-immunoprecipitate zDHHC9 when compared statistically to the EGFP negative control.

Although the quantified data suggests that both mutants have increased co-immunoprecipitation levels of zDHHC9 compared to GCP16 WT, this result is potentially influenced by the lower expression of these proteins (Figure 3.2B, EGFP panel), as co-immunoprecipitation levels for HA-tagged zDHHC9 are quantified as a fraction of the EGFP-tagged proteins.

A.

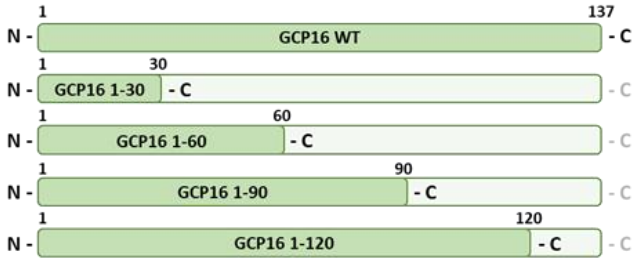
1
137
N -
GCP16 WT
- C
1
30
N -
GCP16 1-30
- C
- C
1
60
N -
GCP16 1-60
- C
- C
1
90
N -
GCP16 1-90
- C
- C
1
120
N -
GCP16 1-120
- C
- C

B.

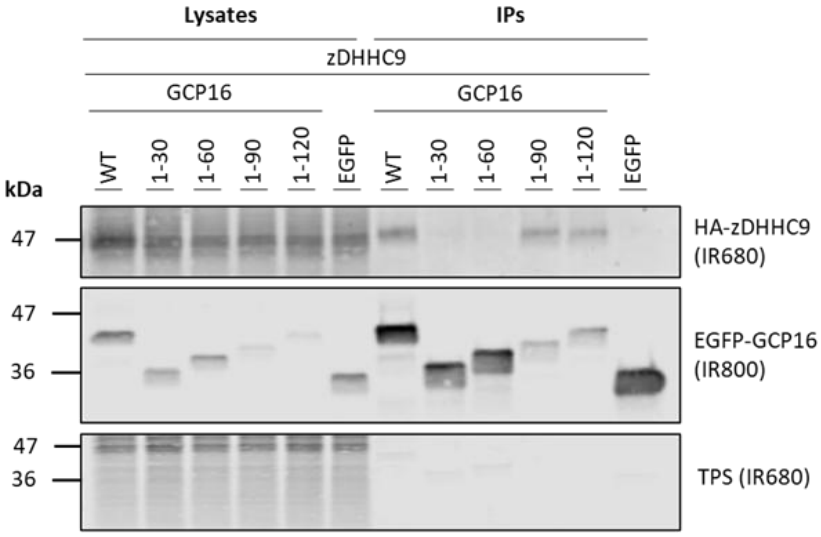
Lysates
IPs
zDHHC9
GCP16
GCP16
WT
1-30
1-60
1-90
1-120
EGFP
WT
1-30
1-60
1-90
1-120
EGFP
kDa
47
HA-zDHHC9
(IR680)
47
36
EGFP-GCP16
(IR800)
47
36
TPS (IR680)

C.

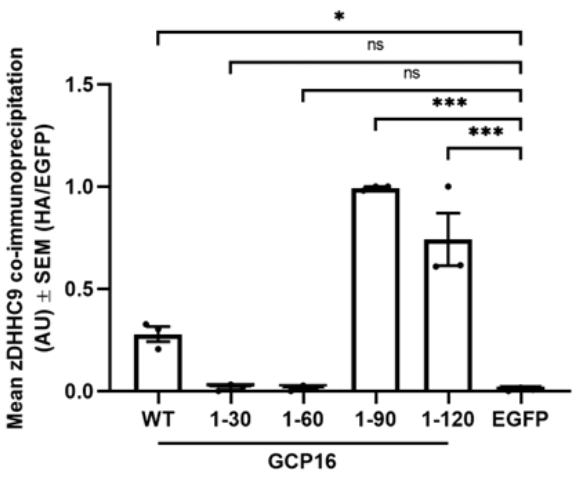
*
ns
ns
***
***
Mean zDHHC9 co-immunoprecipitation
(AU) ± SEM (HA/EGFP)
1.5
1.0
0.5
0.0
WT
1-30
1-60
1-90
1-120
EGFP
GCP16

Figure 3.2 Amino acid residues 60-90 of GCP16 are important for the co-immunoprecipitation of zDHHC9.

(A) *Schematic of GCP16 WT, 1-30, 1-60, 1-90, and 1-120.* ***(B)*** *HEK293T cells were co-transfected with HA-tagged zDHHC9, along with EGFP-tagged GCP16 WT, 1-30, 1-60, 1-90, or 1-120. The EGFP plasmid was used as a negative control. The EGFP-tagged proteins (IR800) were immunoprecipitated using anti-EGFP beads and detected by immunoblotting, along with co-immunoprecipitated HA-tagged proteins (IR680). The position of molecular weight markers (kDa) is shown on the left.* ***(C)*** *Quantified data show the mean (± SEM) of the HA-zDHHC9 (IR680) intensity value divided by the corresponding intensity value of the EGFP signal (IR800) in each IP sample. The data has been normalised to the highest value of each experiment, which was set to 1. Statistical significance was analysed using an ordinary one-way ANOVA, followed by a Dunnett's multiple comparisons test. *p<0.05, **p<0.01 and ***p<0.001, while ns denotes non-significance, where p>0.05. n = 3, from two independent experiments.*

3.3 Alanine scanning mutagenesis of the 60-90 amino acid region of GCP16

The results in Figure 3.2 indicated that the amino acid region 60-90 of GCP16 is involved in binding to zDHHC9. To further analyse this region and highlight important amino acids, alanine scanning mutagenesis was undertaken. Six EGFP-tagged GCP16 mutants were generated in which blocks of five amino acid residues were substituted with alanine (Figure 3.3A). HA-tagged zDHHC9 was co-transfected with EGFP, EGFP-GCP16 WT, or the GCP16 alanine mutant constructs into HEK293T cells. The cells were then lysed and EGFP-tagged proteins captured by immunoprecipitation, and the samples analysed by immunoblotting (Figure 3.3B).

All of the mutant constructs were able to co-immunoprecipitate zDHHC9 (Figure 3.3B), and when analysed using a one-way ANOVA followed by a Dunnett's multiple comparisons test, the levels of co-immunoprecipitated zDHHC9 were not significantly different with any of the mutants *versus* WT GCP16 (Figure 3.3C). GCP16 mutant constructs 71-75A and 81-85A did show a significant *increase* in co-immunoprecipitation of zDHHC9, but as discussed above, this likely reflects the lower

expression of these proteins (as quantification takes into account both the HA and EGFP signal in the IP samples).

A.

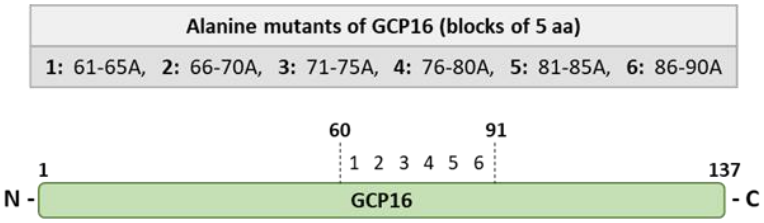
Alanine mutants of GCP16 (blocks of 5 aa)
1: 61-65A, 2: 66-70A, 3: 71-75A, 4: 76-80A, 5: 81-85A, 6: 86-90A
60
91
1 2 3 4 5 6
1
137
N -
GCP16
- C

B.

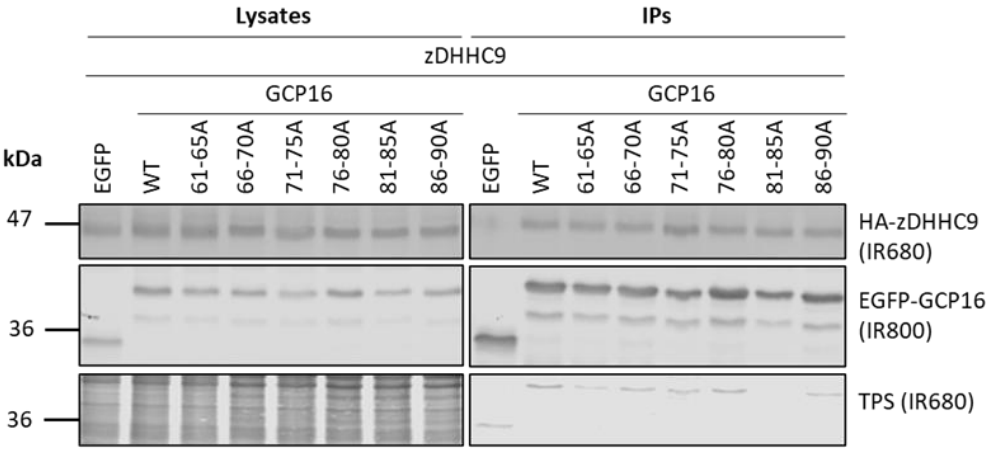
Lysates
IPs
zDHHC9
GCP16
GCP16
kDa
EGFP
WT
61-65A
66-70A
71-75A
76-80A
81-85A
86-90A
47
36
36
HA-zDHHC9 (IR680)
EGFP-GCP16 (IR800)
TPS (IR680)

C.

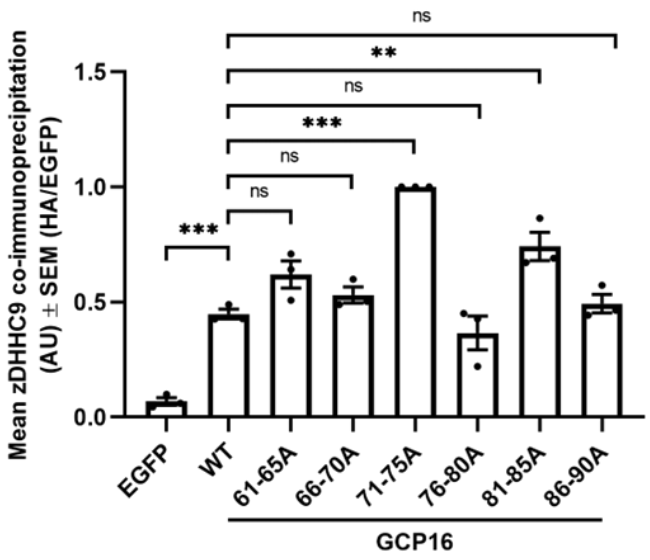
Mean zDHHC9 co-immunoprecipitation (AU) ± SEM (HA/EGFP)
1.5
1.0
0.5
0.0
ns
**
ns
***
ns
ns
***
EGFP
WT
61-65A
66-70A
71-75A
76-80A
81-85A
86-90A
GCP16

Figure 3.3 Alanine scanning mutagenesis of the 60-90 amino acid region of GCP16.

(A) *GCP16 alanine mutants.* ***(B)*** *HEK293T cells were co-transfected with EGFP-tagged GCP16 WT, 61-65A, 66-70A, 71-75A, 76-80A, 81-85A, or 86-90A and HA-tagged zDHHC9. The EGFP plasmid was used as a negative control. The EGFP-tagged proteins (IR800) were immunoprecipitated using anti-EGFP beads and detected by immunoblotting, along with co-immunoprecipitated HA-tagged proteins (IR680). The position of molecular weight markers (kDa) is shown on the left.* ***(C)*** *Quantified data show the mean (± SEM) of the HA-zDHHC9 (IR680) intensity value divided by the corresponding intensity value of the EGFP signal (IR800) in each IP sample. The data has been normalised to the highest value of each experiment, which was set to 1. Statistical significance was analysed using an ordinary one-way ANOVA, followed by a Dunnett's multiple comparisons test. *p<0.05, **p<0.01 and ***p<0.001, while ns denotes non-significance, where p>0.05. n = 3, from three independent experiments.*

3.4 The C-terminal region of GCP16 is important for its S-acylation and for stabilising zDHHC9 S-acylation

In Figure 3.1A, we confirmed that GCP16 co-expression results in increased zDHHC9 autoacylation, in agreement with results from previous studies (Swarthout *et al.*, 2005, Mitchell *et al.*, 2012). Therefore, after identifying that GCP16 truncation mutants 1-90 and 1-120 can interact with zDHHC9, both their S-acylation status and their ability to stabilise zDHHC9 S-acylation were examined.

HEK293T cells were co-transfected with EGFP-GCP16 WT, 1-90, or 1-120, together with PEF-BOS-HA (control) or HA-tagged zDHHC9. Transfected cells were then labelled and processed for click chemistry detection of S-acylation using alkyne mPEG (5 kDa). Samples were then resolved by SDS-PAGE and visualised by immunoblotting (Figure 3.4).

Even though both 1-90 and 1-120 mutant constructs include all cysteine residues found in GCP16 (C24, C69, C72, and C81) (Figure 3.4A), no S-acylation was detected for either mutant, whereas wild-type GCP16 S-acylation was clearly visible when co-

expressed with the PEF-BOS control plasmid (Figure 3.4B). Furthermore, co-expression with zDHHC9 did not rescue the S-acylation of GCP16 mutant constructs (Figure 3.4C). Moreover, the S-acylation of zDHHC9 was significantly lower when expressed with either of the truncation mutants compared to GCP16 WT, suggesting that the mutants cannot stabilise the S-acylated state of this enzyme (Figure 3.4C).

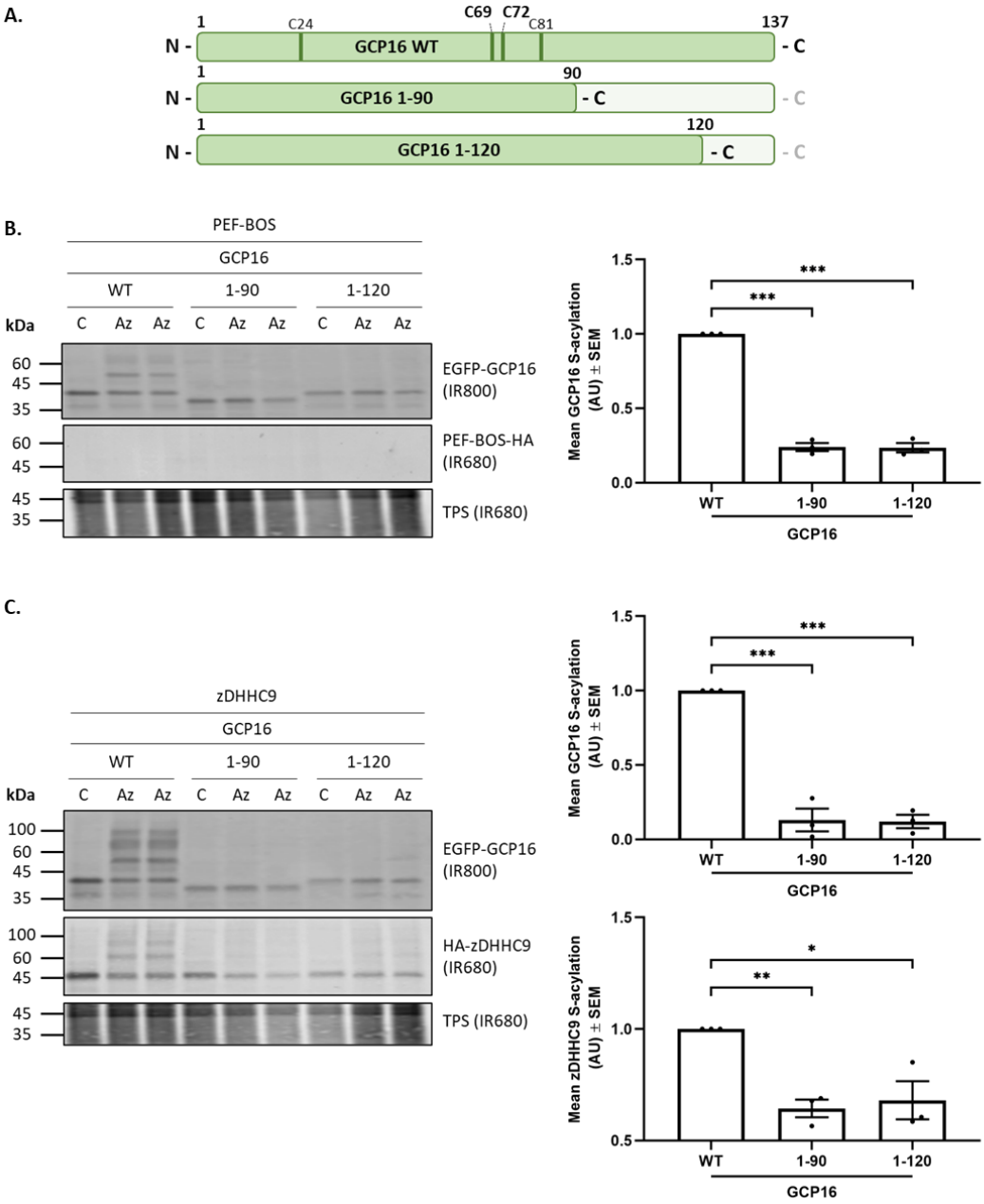
A.
1
C24
C69
C72
C81
137
N -
GCP16 WT
- C
1
90
N -
GCP16 1-90
- C
- C
1
120
N -
GCP16 1-120
- C
- C
B.
PEF-BOS
GCP16
WT
1-90
1-120
kDa
C Az Az C Az Az C Az Az
60
45
35
EGFP-GCP16
(IR800)
60
45
PEF-BOS-HA
(IR680)
45
35
TPS (IR680)
Mean GCP16 S-acylation
(AU) ± SEM
1.5
1.0
0.5
0.0
***
***
WT
1-90
1-120
GCP16
C.
zDHHC9
GCP16
WT
1-90
1-120
kDa
C Az Az C Az Az C Az Az
100
60
45
35
EGFP-GCP16
(IR800)
100
60
45
HA-zDHHC9
(IR680)
45
35
TPS (IR680)
Mean GCP16 S-acylation
(AU) ± SEM
1.5
1.0
0.5
0.0
***
***
WT
1-90
1-120
GCP16
Mean zDHHC9 S-acylation
(AU) ± SEM
1.5
1.0
0.5
*
**
WT
1-90
1-120
GCP16

Figure 3.4 GCP16 truncation mutants 1-90 and 1-120 are not S-acylated and fail to stabilise zDHHC9 S-acylation.

(A) *Schematic showing the position of the S-acylated cysteine residues within GCP16. For the investigation of protein S-acylation, HEK293T cells were co-transfected with* ***(B)*** *PEF-BOS-HA (empty plasmid control), or* ***(C)*** *HA-zDHHC9, along with EGFP-tagged GCP16 WT, 1-90, or 1-120. Cells were labelled with palmitic acid (C16:0) as a control (C) or palmitic acid azide (Az-C16:0) for 4 hours and were then lysed and clicked using alkyne mPEG (kDa). S-acylation is indicated by band-shifts in Az samples. The position of molecular weight markers (kDa) is shown on the left. Quantified data show mean protein S-acylation (± SEM). The S-acylated bands were quantified as a percentage of total expression (non-acylated + S-acylated bands) for each substrate incubated with the palmitic acid azide. The data has been normalised to the highest value of each experiment, which was set to 1. Statistical significance was analysed using an ordinary one-way ANOVA, followed by a Dunnett's multiple comparisons test. *p<0.05, **p<0.01 and ***p<0.001, while ns denotes non-significance, where p>0.05. n = 3, from two independent experiments.*

To confirm the role of the C-terminal domain of GCP16 for the protein's S-acylation, shorter C-terminal truncation mutants were designed and analysed. These mutants had the successive addition of 2 amino acid blocks onto the 1-120 region (Figure 3.5A). HEK293T cells were transfected with EGFP-GCP16 WT, 1-120, 1-122, 1-124, 1-126, 1-128, or 1-130, and their S-acylation was examined by click chemistry. The results in Figure 3.5 show that S-acylation was only observed for the 1-128 and 1-130 truncation mutants, and indeed statistical analysis showed that the S-acylation levels of these mutants were not significantly different to the GCP16 WT protein.

To complement the experiments using C-terminal truncation mutants, two alanine mutant constructs of the C-terminal region of full-length GCP16 were also generated: 122-125A and 126-130A. These mutants were used to determine if there are specific residues in this region that are essential for GCP16 S-acylation. Click chemistry analysis of the S-acylation of these mutants showed that these alanine substitutions led to a complete loss of GCP16 S-acylation (Figure 3.5B), confirming the importance of this region for effective modification of the full-length GCP16 protein.

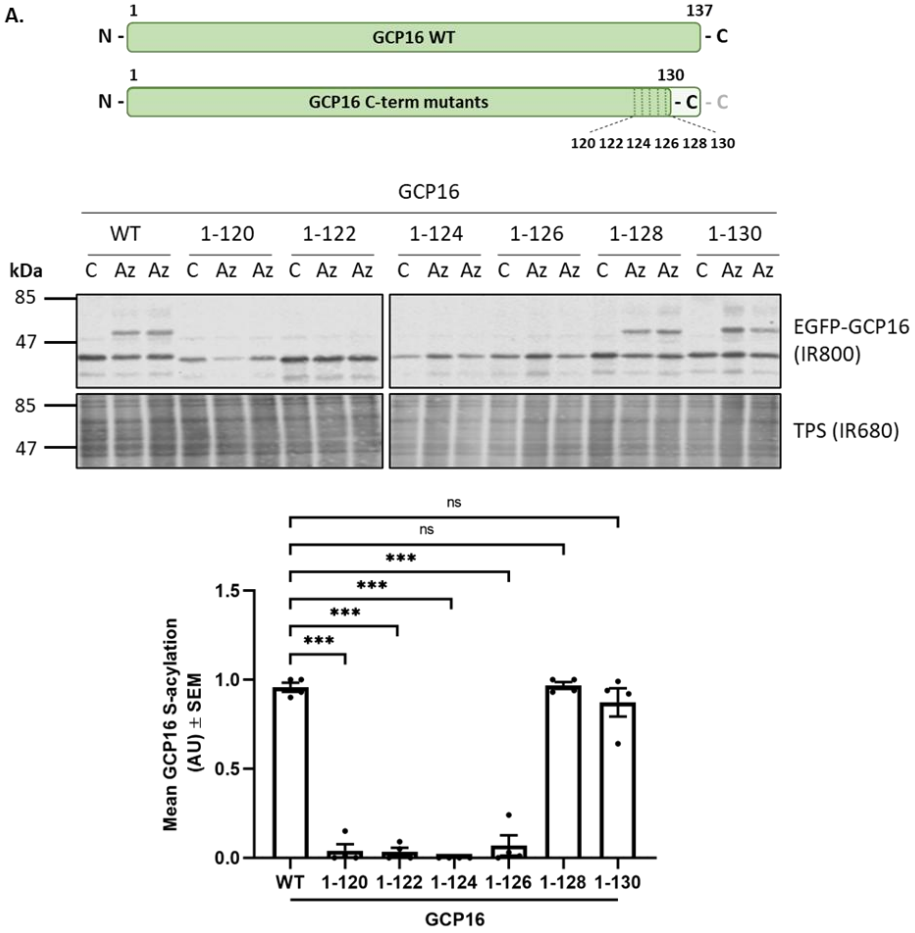
A.
1
137
N -
GCP16 WT
- C
1
130
N -
GCP16 C-term mutants
- C
- C
120 122 124 126 128 130
GCP16
WT
1-120
1-122
1-124
1-126
1-128
1-130
kDa
C Az Az C Az Az C Az Az C Az Az C Az Az C Az Az C Az Az
85
47
85
47
EGFP-GCP16
(IR800)
TPS (IR680)
ns
ns
***
***
***
***
Mean GCP16 S-acylation
(AU) ± SEM
1.5
1.0
0.5
0.0
WT
1-120
1-122
1-124
1-126
1-128
1-130
GCP16

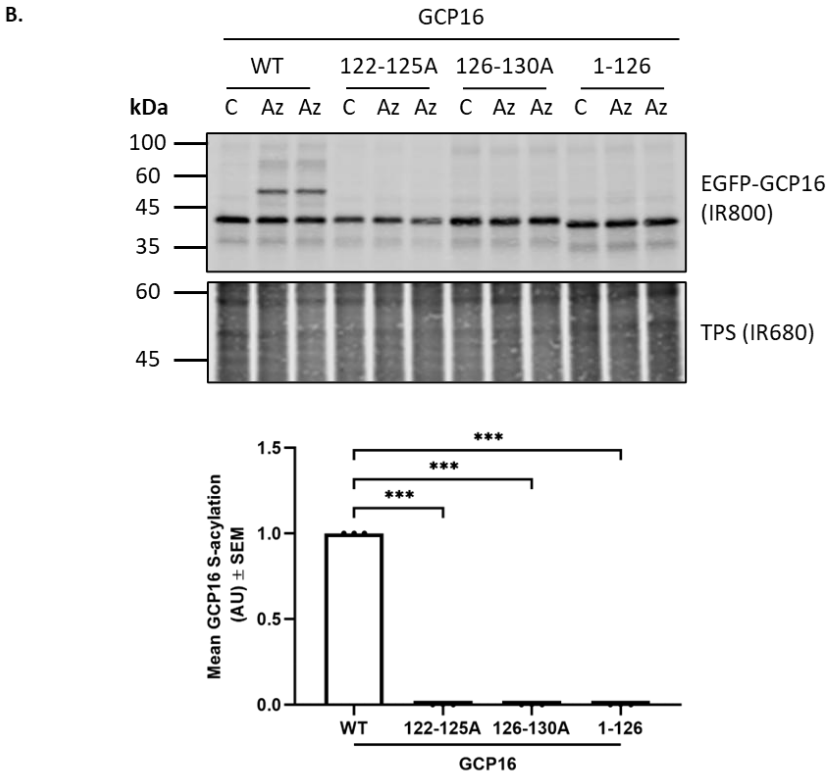
B.
GCP16
WT
122-125A
126-130A
1-126
kDa
C Az Az C Az Az C Az Az C Az Az
100
60
45
35
60
45
EGFP-GCP16
(IR800)
TPS (IR680)
***
***
***
Mean GCP16 S-acylation
(AU) ± SEM
1.5
1.0
0.5
0.0
WT
122-125A
126-130A
1-126
GCP16

Figure 3.5 The C-terminal region of GCP16 is important for its S-acylation.

(A) *Schematic showing the C-terminal truncation mutants of GCP16. For the investigation of protein S-acylation, HEK293T cells were transfected with EGFP-tagged GCP16 WT, 1-120, 1-122, 1-124, 1-126, 1-128, or 1-130.* ***(B)*** *HEK293T cells were transfected with EGFP-tagged GCP16 WT, 122-125A, 126-130A, or 1-126. In both (A) and (B), cells were labelled with palmitic acid (C16:0) as a control (C) or palmitic acid azide (Az-C16:0) for 4 hours and were then lysed and clicked using alkyne mPEG (kDa). S-acylation is indicated by band-shifts in Az samples. The position of molecular weight markers (kDa) is shown on the left. Quantified data show mean protein S-acylation (± SEM). The S-acylated bands were quantified as a percentage of total expression (non-acylated + S-acylated bands) for each substrate incubated with the palmitic acid azide. The data has been normalised to the highest value of each experiment, which was set to 1. Statistical significance was analysed using an ordinary one-way ANOVA, followed by a Dunnett's multiple comparisons test. *p<0.05, **p<0.01 and ***p<0.001, while ns denotes non-significance, where p>0.05. (A) n = 4, from two independent experiments and (B) n = 3, from two independent experiments.*

3.5 GCP16 truncation mutants 1-90 and 1-120 show decreased stability that is not recovered by zDHHC9 interaction

After observing that the C-terminal region of GCP16 is important for the S-acylation of both GCP16 and zDHHC9 (Figure 3.4 and Figure 3.5), the stability of the GCP16 1-90 and 1-120 truncation mutants and their ability to stabilise zDHHC9 was also examined, to determine if the C-terminus is also important for the stabilisation effects.

For this, HEK293T cells were co-transfected with PEF-BOS-HA (control) or HA-zDHHC9, along with either EGFP-GCP16 WT, 1-90, or 1-120. Cells were either lysed at 0 hours or incubated with cycloheximide for 8 hours. The 8-hour samples were then lysed, and all proteins were resolved by SDS-PAGE and detected by immunoblotting (Figure 3.6). The quantified results indicated that GCP16 C-terminal truncated mutants 1-90 and 1-120 are significantly less stable than GCP16 WT, when co-expressed with the PEF-BOS control, and co-expression with zDHHC9 had no effect on their stability. In addition, the protein stability of zDHHC9 was also significantly

lower when co-expressed with either 1-90 or 1-120, compared to co-expression with GCP16 WT (Figure 3.6C).

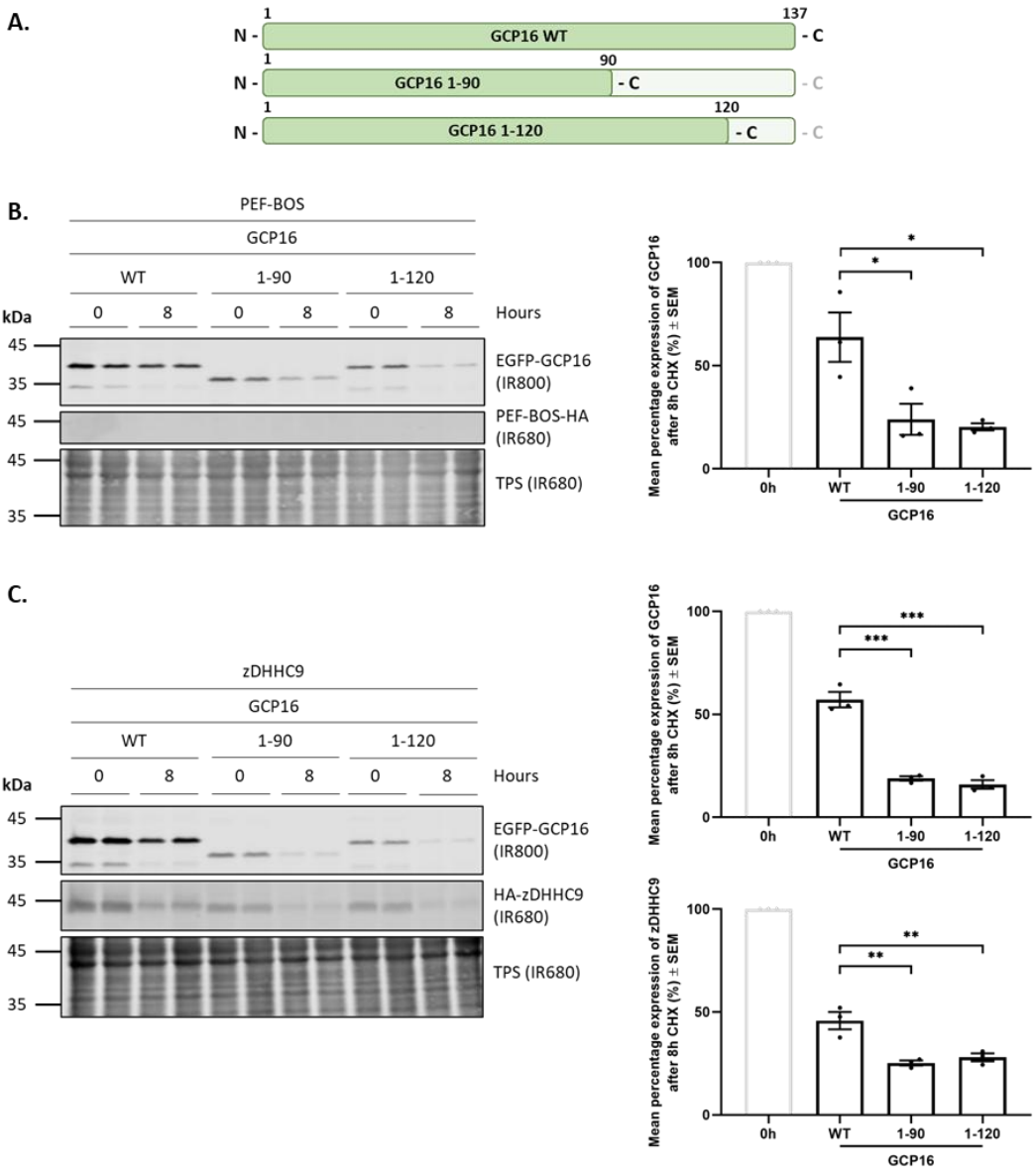
A.
1
137
N -
GCP16 WT
- C
1
90
N -
GCP16 1-90
- C
- C
1
120
N -
GCP16 1-120
- C
- C
B.
PEF-BOS
GCP16
WT
1-90
1-120
kDa
0
8
0
8
0
8
Hours
45
35
EGFP-GCP16
(IR800)
45
PEF-BOS-HA
(IR680)
45
TPS (IR680)
35
Mean percentage expression of GCP16
after 8h CHX (%) ± SEM
100
50
0
*
*
0h
WT
1-90
1-120
GCP16
C.
zDHHC9
GCP16
WT
1-90
1-120
kDa
0
8
0
8
0
8
Hours
45
35
EGFP-GCP16
(IR800)
45
HA-zDHHC9
(IR680)
45
TPS (IR680)
35
Mean percentage expression of GCP16
after 8h CHX (%) ± SEM
100
50
0
***
***
0h
WT
1-90
1-120
GCP16
Mean percentage expression of zDHHC9
after 8h CHX (%) ± SEM
100
50
0
**
**
0h
WT
1-90
1-120
GCP16

Figure 3.6 GCP16 truncation mutants 1-90 and 1-120 show decreased stability and reduced ability to stabilise zDHHC9.

(A) *Schematic of GCP16 WT, 1-90, and 1-120. To investigate protein stability, HEK293T cells were co-transfected with EGFP-tagged GCP16 WT, 1-90, or 1-120 and* ***(B)*** *PEF-BOS-HA (empty plasmid control) or* ***(C)*** *HA-zDHHC9. Lysates were collected at 0 hours or after 8 hours of incubation with 50 µg/ml cycloheximide (CHX). Protein expression levels were detected by immunoblotting. The position of molecular weight markers (kDa) is shown on the left. Quantified data show the mean percentage protein expression (± SEM) after 8 hours of CHX treatment, quantified relative to the corresponding 0-hour value and normalised to the total protein stain levels of each sample. Statistical significance was analysed using an ordinary one-way ANOVA, followed by a Dunnett's multiple comparisons test. *p<0.05, **p<0.01 and ***p<0.001, while ns denotes non-significance, where p>0.05. n = 3, from three independent experiments.*

3.6 Identification of a second zDHHC9-binding region within GCP16 amino acid region 91-137

After identifying that the amino acid region 60-90 of GCP16 is important for the interaction with zDHHC9, N-terminal truncation mutants of GCP16 were also generated to further confirm this finding, as seen in Figure 3.7A. HEK293T cells were co-transfected with HA-zDHHC9 and EGFP (control), EGFP-GCP16 WT, or 31-137 and 61-137 truncation mutants. Samples were then lysed and immunoprecipitated, before being resolved by SDS-PAGE and analysed by immunoblotting. Quantified data in Figure 3.7B showed that zDHHC9 was co-immunoprecipitated with both GCP16 truncated mutants 31-137 and 61-137. This is consistent with the previous finding that the 60-90 region is important for zDHHC9 interaction. It should be noted that both mutants displayed a lower expression compared to that of GCP16 WT, which may explain why the quantified data indicate increased binding to HA-zDHHC9 (as data is quantified as HA/EGFP signal intensity in the IP samples).

To further confirm the importance of the 60-90 region of GCP16 for zDHHC9 binding, a 91-137 GCP16 truncation mutant was also examined in co-immunoprecipitation experiments. Unexpectedly, zDHHC9 was also successfully co-immunoprecipitated

with this GCP16 mutant at levels similar to the WT protein (Figure 3.7C). This finding may suggest that GCP16 interaction with zDHHC9 involves residues in both the 60-90 region of GCP16 and also residues downstream of this region (amino acids 91-137).

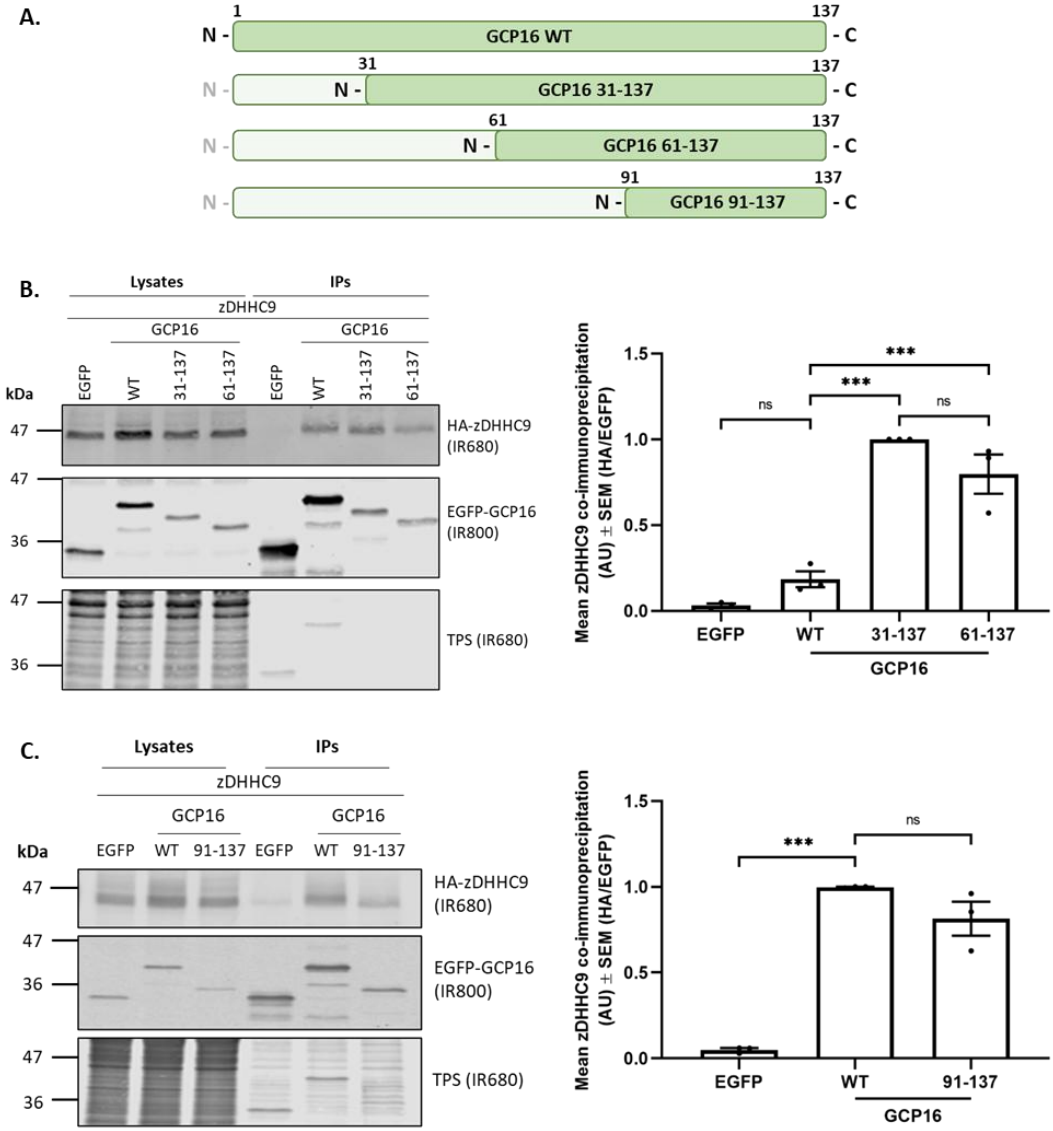
A.
1
137
N -
GCP16 WT
- C
31
137
N -
N -
GCP16 31-137
- C
61
137
N -
N -
GCP16 61-137
- C
91
137
N -
N -
GCP16 91-137
- C
B.
Lysates
IPs
zDHHC9
GCP16
GCP16
kDa
EGFP
WT
31-137
61-137
EGFP
WT
31-137
61-137
47
HA-zDHHC9
(IR680)
47
36
EGFP-GCP16
(IR800)
47
36
TPS (IR680)
Mean zDHHC9 co-immunoprecipitation
(AU) ± SEM (HA/EGFP)
1.5
1.0
0.5
0.0
***
***
ns
ns
EGFP
WT
31-137
61-137
GCP16
C.
Lysates
IPs
zDHHC9
GCP16
GCP16
kDa
EGFP
WT
91-137
EGFP
WT
91-137
47
HA-zDHHC9
(IR680)
47
36
EGFP-GCP16
(IR800)
47
36
TPS (IR680)
Mean zDHHC9 co-immunoprecipitation
(AU) ± SEM (HA/EGFP)
1.5
1.0
0.5
0.0
***
ns
EGFP
WT
91-137
GCP16

Figure 3.7 The 91-137 region of GCP16 co-immunoprecipitates zDHHC9.

(A) *Schematic of GCP16 WT, 31-137, 61-137, and 91-137. HEK293T cells were co-transfected with HA-tagged zDHHC9 and* ***(B)*** *EGFP-tagged GCP16 WT, 31-137, or 61-137, or* ***(C)*** *EGFP-tagged GCP16 WT, or 91-137. The EGFP plasmid was used as a negative control. The EGFP-tagged proteins (IR800) were immunoprecipitated using anti-EGFP beads and detected by immunoblotting, along with co-immunoprecipitated HA-tagged proteins (IR680). The position of molecular weight markers (kDa) is shown on the left. Quantified data show the mean (± SEM) of the HA-zDHHC9 (IR680) intensity value divided by the corresponding intensity value of the EGFP signal (IR800) in each IP sample. The data has been normalised to the highest value of each experiment, which was set to 1. Statistical significance was analysed using an ordinary one-way ANOVA, followed by a Tukey's multiple comparisons test. *p<0.05, **p<0.01 and ***p<0.001, while ns denotes non-significance, where p>0.05. n = 3, from (B) three independent experiments, or (C) from two independent experiments.*

To examine the regions in the C-terminus of GCP16 that are important for the co-immunoprecipitation of zDHHC9 in more detail, a further set of truncation mutants was analysed. GCP16 91-120, 91-124, and 91-128 were co-transfected together with HA-zDHHC9. Cell lysates were then incubated with GFP-Trap® Agarose beads, and immunoprecipitated proteins were examined by immunoblotting (Figure 3.8).

Quantified results in Figure 3.8B show that GCP16 mutant 91-128 was able to interact with zDHHC9 as its zDHHC9 co-immunoprecipitation levels were significantly higher than the EGFP negative control. In addition, the co-immunoprecipitated zDHHC9 levels with the GCP16 mutant 91-128 were not significantly different from those with GCP16 mutant 91-137. In contrast, both the 91-120 and 91-124 mutants did not show any significant increase in zDHHC9 co-immunoprecipitation compared to the EGFP negative control. These data suggest that there is a binding site for zDHHC9 in the C-terminal region of GCP16 between residues 91-128. Interestingly, this finding is consistent with the observation that the 1-128 truncation mutant of GCP16 was S-acylated efficiently, but the 1-126 mutant was not (Figure 3.5).

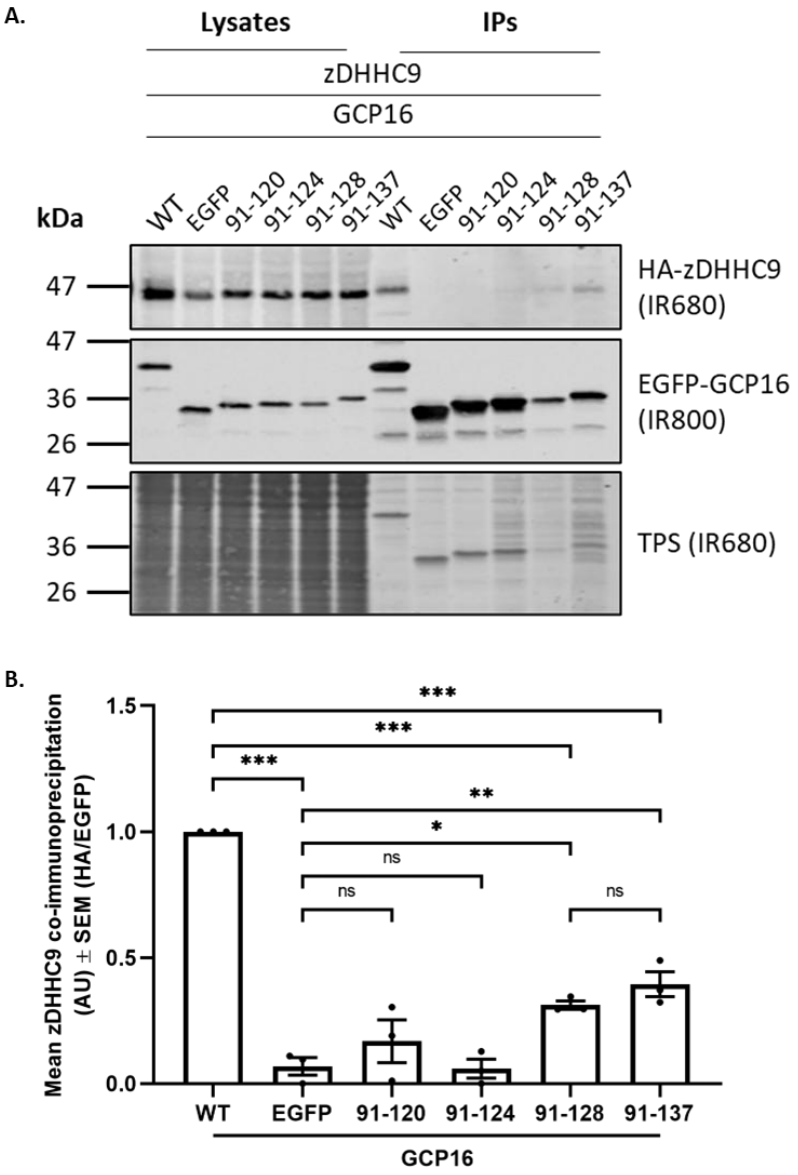
A.
Lysates
IPs
zDHHC9
GCP16
kDa
WT
EGFP
91-120
91-124
91-128
91-137
47
47
36
26
47
36
26
HA-zDHHC9
(IR680)
EGFP-GCP16
(IR800)
TPS (IR680)
B.
Mean zDHHC9 co-immunoprecipitation
(AU) ± SEM (HA/EGFP)
1.5
1.0
0.5
0.0
***
***
***
**
*
ns
ns
ns
WT
EGFP
91-120
91-124
91-128
91-137
GCP16

Figure 3.8 The C-terminal region of GCP16 interacts with zDHHC9.

(A) *HEK293T cells were co-transfected with HA-tagged zDHHC9 and EGFP-tagged GCP16 WT, 91-120, 91-124, 91-128, or 91-137. The EGFP plasmid was used as a negative control. The EGFP-tagged proteins (IR800) were immunoprecipitated using anti-EGFP beads and detected by immunoblotting, along with co-immunoprecipitated HA-tagged proteins (IR680). The position of molecular weight markers (kDa) is shown on the left.* ***(B)*** *Quantified data show the mean (± SEM) of the HA-zDHHC9 (IR680) intensity value divided by the corresponding intensity value of the EGFP signal (IR800) in each IP sample. The data has been normalised to the highest value of each experiment, which was set to 1. Statistical significance was analysed using an ordinary one-way ANOVA, followed by a Tukey's multiple comparisons test. *p<0.05, **p<0.01 and ***p<0.001, while ns denotes non-significance, where p>0.05. n = 3, from three independent experiments.*

3.7 The C-terminal 91-137 region of GCP16 does not stabilise the S-acylated state of zDHHC9

The previous results suggest that there are possible binding sites for zDHHC9 in the 60-90 and 91-128 amino acid regions of GCP16. The results in Figures 3.4 and 3.6 showed that the 1-90 truncation mutant, despite interacting with zDHHC9 and containing the main S-acylated cysteines, did not stabilise the zDHHC9 protein or its S-acylated state. To determine if binding of the C-terminal region of GCP16 to zDHHC9 had any functional effects, the S-acylation of zDHHC9 in the presence of WT GCP16 and the 91-137 mutant was examined. In addition, the 1-90 mutant was included as a negative control in these experiments. Transfected cells were labelled with either palmitic acid as a control or palmitic acid azide and processed for click chemistry detection of S-acylation using alkyne mPEG (5 kDa).

The results presented in Figure 3.9 confirmed that GCP16 1-90 is not S-acylated, despite all cysteines being located in that region, whereas the absence of S-acylation of the 91-137 mutant was expected as it lacks any cysteine residues. In addition, zDHHC9 S-acylation was significantly lower when expressed with the 91-137 mutant (and the 1-90 mutant) compared to expression with WT GCP16. Thus, despite the C-

terminus of GCP16 interacting with zDHHC9, this interaction had no functional effect on the S-acylation of the enzyme.


A.
1
137
N -
GCP16 WT
- C
1
90
N -
GCP16 1-90
- C
- C
91
137
N -
N -
GCP16 91-137
- C

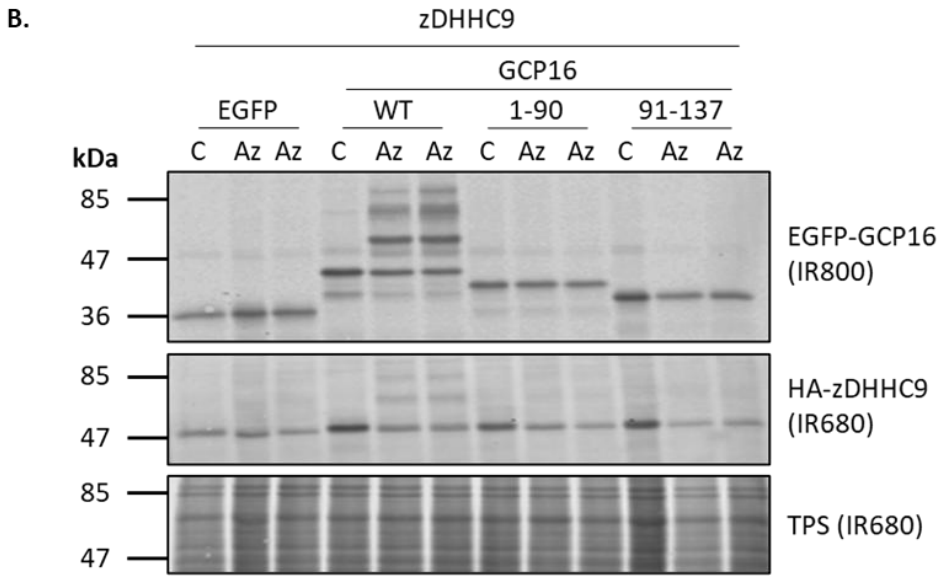
B.
zDHHC9
GCP16
EGFP
WT
1-90
91-137
kDa
C Az Az C Az Az C Az Az C Az Az
85
47
36
EGFP-GCP16
(IR800)
85
47
HA-zDHHC9
(IR680)
85
47
TPS (IR680)

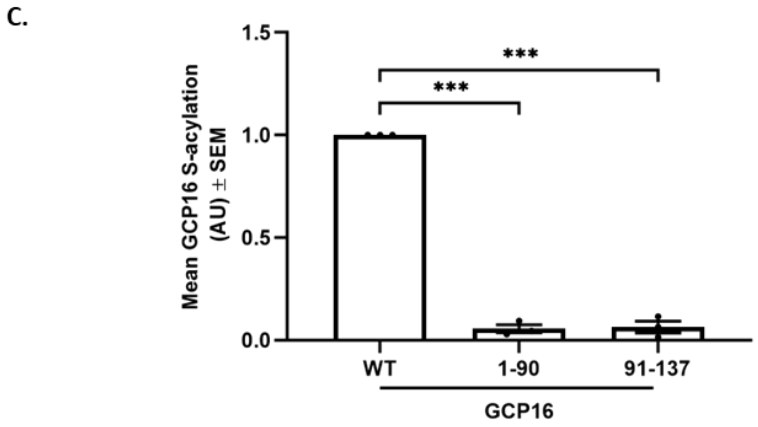
C.
Mean GCP16 S-acylation
(AU) ± SEM
1.5
1.0
0.5
0.0
***
***
WT
1-90
91-137
GCP16

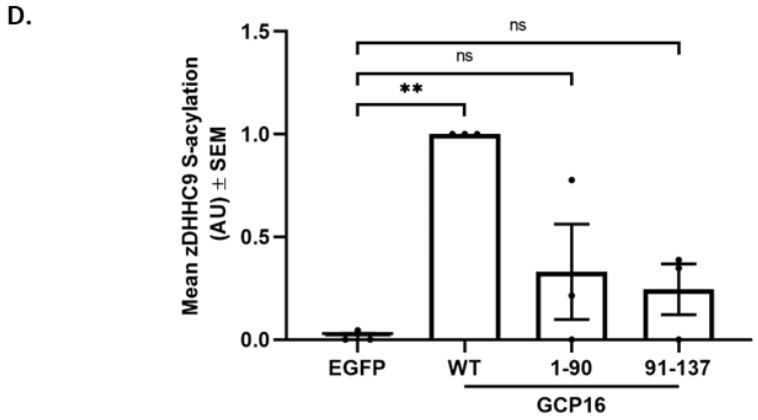
D.
Mean zDHHC9 S-acylation
(AU) ± SEM
1.5
1.0
0.5
0.0
ns
ns
**
EGFP
WT
1-90
91-137
GCP16

Figure 3.9 The C-terminal 91-137 region of GCP16 is not able to stabilise the S-acylated state of zDHHC9.

(A) *Schematic of GCP16 WT, 1-90, and 91-137.* ***(B)*** *HEK293T cells were co-transfected with HA-tagged zDHHC9 and EGFP-tagged GCP16 WT, 1-90, or 91-137. EGFP was used as a control. Cells were labelled with palmitic acid (C16:0) as a control (C) or palmitic acid azide (Az-C16:0) for 4 hours and were then lysed and clicked using alkyne mPEG (kDa). S-acylation is indicated by band-shifts in Az samples. The position of molecular weight markers (kDa) is shown on the left.* ***(C-D)*** *Quantified data showing the mean percentage (± SEM) intensity values of the S-acylated substrates. The S-acylated bands were quantified as a percentage of total expression (non-acylated + S-acylated bands) for each substrate incubated with the palmitic acid azide. The data has been normalised to the highest value of each experiment, which was set to 1. Statistical significance was analysed using an ordinary one-way ANOVA, followed by a Dunnett's multiple comparisons test. *p<0.05, **p<0.01 and ***p<0.001, while ns denotes non-significance, where p>0.05. n = 3, from three independent experiments.*

3.8 The GCP16 N-terminal region is important for GCP16 and zDHHC9 S-acylation

An interesting finding from the previous sections was the importance of the extreme C-terminus of GCP16 for its efficient S-acylation. Specifically, a 1-128 mutant of GCP16 was S-acylated to a similar level as GCP16 WT, but a 1-126 mutant was not (Figure 3.5). This was a surprising observation given that the S-acylated cysteines in GCP16 are present at positions Cys-69 and Cys-72 (Ohta *et al.*, 2003), however the results were consistent with immunoprecipitation experiments, which found that a 91-128 mutant was able to co-immunoprecipitate zDHHC9, but a 91-124 mutant was not (Figure 3.8). Therefore, we also looked more closely at the N-terminus of GCP16 to identify other important regions needed for S-acylation. The mutants used in these experiments are depicted in Figure 3.10A.

Initially, HEK293T cells were co-transfected with HA-zDHHC9 along with EGFP-GCP16 WT, 31-137, or EGFP (control). Cells were labelled with either palmitic acid as a control or palmitic acid azide for 4 hours and were then processed for click

chemistry detection of S-acylation using alkyne mPEG (5 kDa) as above. Immunoblot detection showed that the GCP16 31-137 mutant was not S-acylated, and neither could it stabilise zDHHC9 S-acylation (Figure 3.10B). This experiment was followed by a similar analysis of shorter N-terminal truncation mutants (11-137 and 21-137) of GCP16. Figure 3.10C shows that the GCP16 mutant 11-137 was effectively S-acylated, whereas no S-acylation was detected for mutant 21-137. In addition, the levels of zDHHC9 S-acylation detected with GCP16 mutant 11-137 were not significantly different to those seen with GCP16 WT, whereas no zDHHC9 S-acylation was detected when co-transfected with the GCP16 mutant 21-137. These results highlight the importance of the 11-20 region of GCP16 for efficient S-acylation of the protein and for stabilisation of zDHHC9 S-acylation.

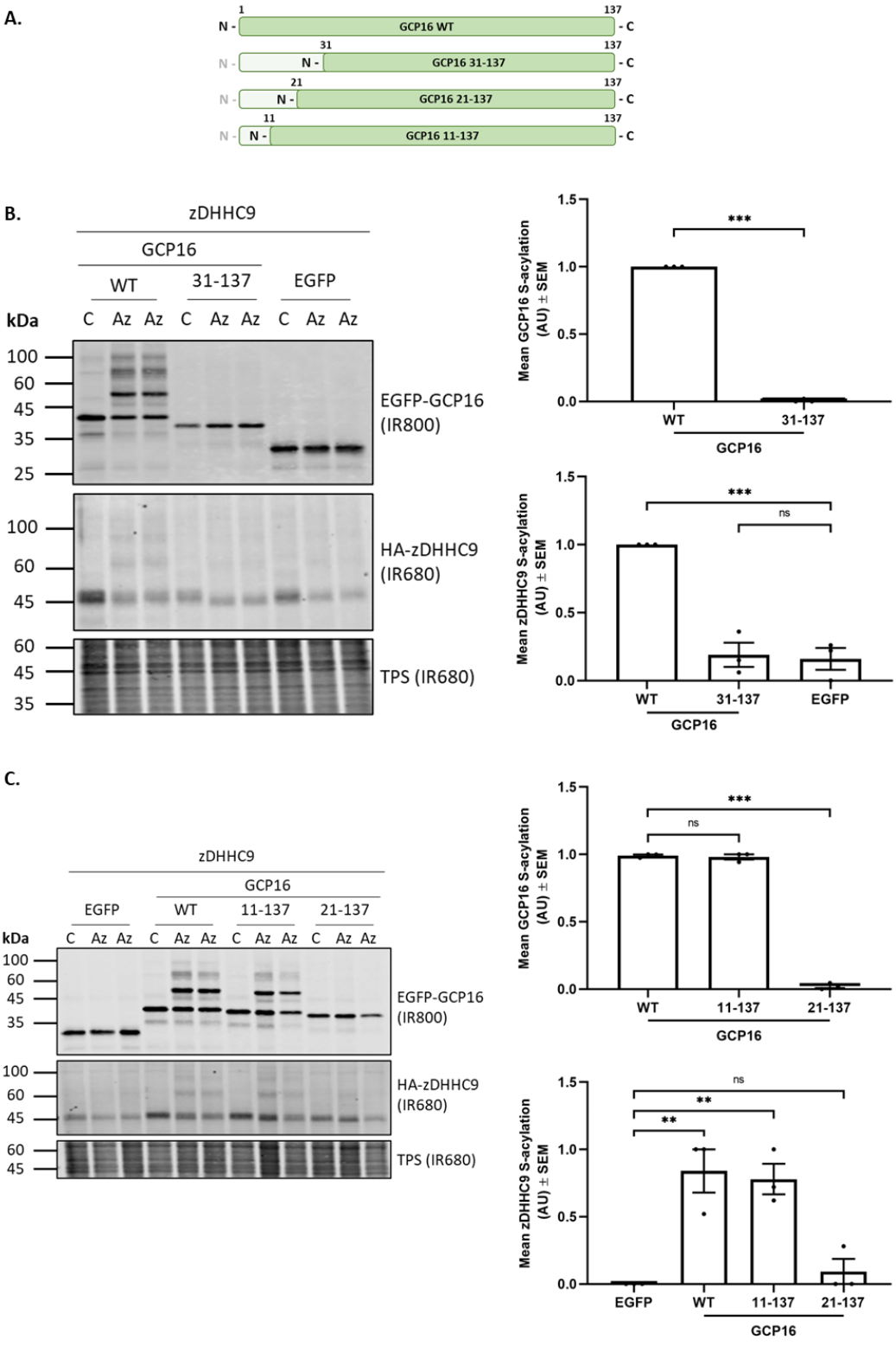
A.
GCP16 WT
GCP16 31-137
GCP16 21-137
GCP16 11-137
B.
zDHHC9
GCP16
WT
31-137
EGFP
kDa
C Az Az C Az Az C Az Az
EGFP-GCP16 (IR800)
HA-zDHHC9 (IR680)
TPS (IR680)
Mean GCP16 S-acylation (AU) ± SEM
Mean zDHHC9 S-acylation (AU) ± SEM
***
ns
C.
EGFP
11-137
21-137
EGFP-GCP16 (IR800)
HA-zDHHC9 (IR680)
TPS (IR680)
**

Figure 3.10 The GCP16 N-terminal region is important for GCP16 and zDHHC9 S-acylation.

(A) *Schematic of GCP16 WT, 31-137, 21-137, and 11-137. HEK293T cells were co-transfected with HA-tagged zDHHC9 and* ***(B)*** *EGFP-tagged GCP16 WT, or 31-137, or with* ***(C)*** *EGFP-tagged GCP16 WT, 11-137, and 21-137. EGFP was used as a control. Cells were labelled with palmitic acid (C16:0) as a control (C) or palmitic acid azide (Az-C16:0) for 4 hours and were then lysed and clicked using alkyne mPEG (kDa). S-acylation is indicated by band-shifts in Az samples. The position of molecular weight markers (kDa) is shown on the left. Quantified data show the mean percentage (± SEM) intensity values of the S-acylated substrates. The S-acylated bands were quantified as a percentage of total expression (non-acylated + S-acylated bands) for each substrate incubated with the palmitic acid azide. The data has been normalised to the highest value of each experiment, which was set to 1. Statistical significance was analysed using an unpaired t-test, or an ordinary one-way ANOVA, followed by a Dunnett's multiple comparisons test where appropriate. (B) n = 3, from two independent experiments, (C) n = 3, from three independent experiments. *p<0.05, **p<0.01 and ***p<0.001, while ns denotes non-significance, where p>0.05.*

3.9 Analysis of the effects of cysteine substitutions on the S-acylation of GCP16

The previous sections highlighted the importance of the extreme N- and C-terminal regions of GCP16 for its S-acylation and ability to stabilise the S-acylation of zDHHC9. GCP16 has four cysteine residues at amino acid positions 24, 69, 72, and 81 (Figure 3.11A). Ohta *et al.* (2003) were the first to demonstrate that GCP16 is S-acylated, using metabolic labelling with [^{3}H] palmitic acid. Through cysteine-to-alanine substitutions, they found that substitution of either of the cysteine residues at position 69 or 72 caused a significant decrease in the incorporation of [^{3}H] palmitic acid, while substitution of both C69 and C72 completely abolished GCP16 S-acylation (Ohta *et al.*, 2003).

As click chemistry-based methods to study S-acylation are more sensitive than the use of radiolabelled palmitate, we sought to confirm the results of Ohta *et al.* (2003). Double and triple cysteine-to-alanine substitutions were introduced into GCP16. HEK293T cells were co-transfected with HA-zDHHC9 and either EGFP (control),

EGFP-GCP16 WT, C69A/C72A, C24A/C69A/C72A or C69A/C72A/C81A. Cells were labelled with either palmitic acid as a control or palmitic acid azide and processed for click chemistry detection of S-acylation using alkyne mPEG (5 kDa).

The immunoblot results in Figure 3.11B and the quantified data in Figure 3.11C show that although S-acylation of the double cysteine-to-alanine GCP16 mutant C69A/C72A is substantially reduced compared to WT GCP16, S-acylation is nevertheless still detected. However, introducing an additional C24A (C24A/C69A/C72A) or C81A (C69A/C72A/C81A) substitution led to a complete loss of GCP16 S-acylation (Figure 3.11B and C). These results suggest that Cys-69 and Cys-72 are the major sites of S-acylation in GCP16 (in agreement with Ohta *et al.*) but that S-acylation can also occur to a minor level at Cys-24 or Cys-81.

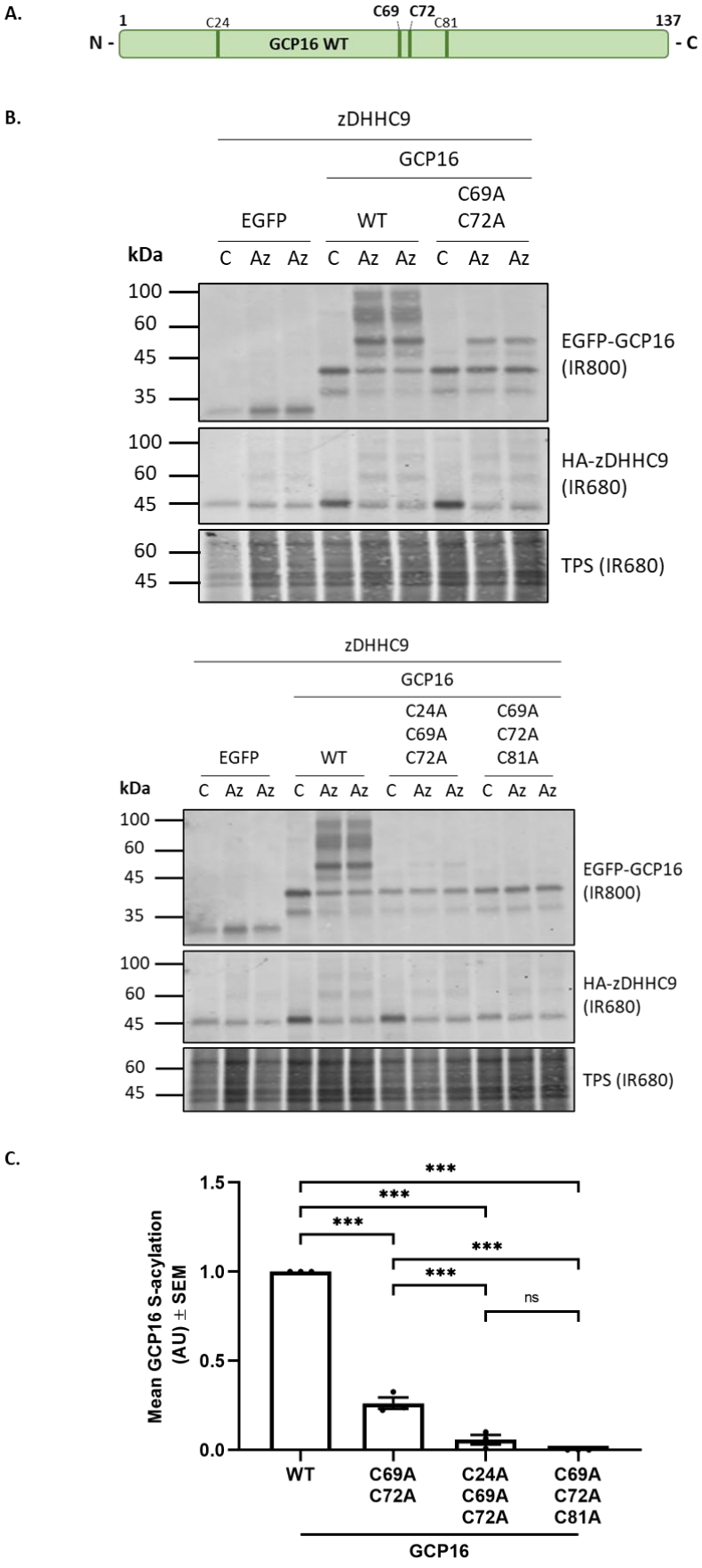
A.
1
C24
C69
C72
C81
137
N -
GCP16 WT
- C
B.
zDHHC9
GCP16
EGFP
WT
C69A
C72A
kDa
C Az Az C Az Az C Az Az
100
60
45
35
EGFP-GCP16
(IR800)
HA-zDHHC9
(IR680)
TPS (IR680)
zDHHC9
GCP16
EGFP
WT
C24A
C69A
C72A
C69A
C72A
C81A
C Az Az C Az Az C Az Az C Az Az
C.
Mean GCP16 S-acylation
(AU) ± SEM
1.5
1.0
0.5
0.0
***
***
***
***
***
ns
WT
C69A
C72A
C24A
C69A
C72A
C69A
C72A
C81A
GCP16

Figure 3.11 Analysis of the effects of cysteine substitutions on the S-acylation of GCP16.

(A) *Schematic showing the position of the cysteine residues within GCP16.* ***(B)*** *HEK293T cells were co-transfected with HA-tagged zDHHC9 and EGFP-tagged GCP16 WT, C69A/C72A, C24A/C69A/C72A, or C69A/C72A/C81A. Cells were labelled with palmitic acid (C16:0) as a control (C) or palmitic acid azide (Az-C16:0) for 4 hours and were then lysed and clicked using alkyne mPEG (kDa). S-acylation is indicated by band-shifts in Az samples. The position of molecular weight markers (kDa) is shown on the left.* ***(C)*** *Quantified data show mean GCP16 S-acylation (± SEM). The S-acylated bands were quantified as a percentage of total expression (non-acylated + S-acylated bands) for each substrate incubated with the palmitic acid azide. The data has been normalised to the highest value of each experiment, which was set to 1. Statistical significance was analysed using an ordinary one-way ANOVA, followed by a Tukey's multiple comparisons test. *p<0.05, **p<0.01 and ***p<0.001, while ns denotes non-significance, where p>0.05. n = 3, from three independent experiments.*

3.10 Cysteine-69 and cysteine-72 may have a direct role in GCP16 membrane association and binding to zDHHC9

Ohta *et al.* (2003) showed that GCP16 was present in the total membrane, Golgi, and post-nuclear fractions following cell fractionation, but not in the cytosol fraction, suggesting that the protein is tightly associated with membranes. As previously mentioned, the authors proposed that S-acylation of C69 and C72 anchors GCP16 to the membrane, accounting for its Golgi localisation. Hence, they examined the intracellular localisation of a double cysteine GCP16 mutant C69A/C72A by immunofluorescence microscopy and cell fractionation and observed that it was enriched in the cytosol (Ohta *et al.*, 2003).

Previous work has shown that cysteine residues can directly contribute to membrane association independently of their S-acylation (Greaves *et al.*, 2008, Greaves *et al.*, 2009), therefore, as previous work in this chapter identified truncation mutants of GCP16 that are defective for S-acylation but retain all cysteine residues (e.g.

truncation mutant 1-126), we decided to examine more closely the role of the cysteines and S-acylation in the membrane association of GCP16.

HEK293T cells were initially co-transfected with either PEF-BOS-HA (control) (Figure 3.12B) or HA-zDHHC9 (Figure 3.12C), along with EGFP-tagged GCP16 WT, C69A, C72A, or C69A/C72A. Cells were then lysed and fractionated using appropriate buffers to separate cytosolic fractions from membrane fractions.

Analysis of the samples by immunoblotting and subsequent statistical analysis showed that neither of the GCP16 single cysteine substitutions affected membrane association, whereas the double cysteine mutant C69A/C72A showed a significant decrease in membrane association compared to the WT protein. This decrease in membrane association of the double cysteine mutant was seen both with PEF-BOS-HA and HA-zDHHC9 co-transfection (Figure 3.12B and Figure 3.12C). This data is consistent with the previous findings of Ohta *et al.* (2003).

As the double cysteine-to-alanine mutant of GCP16 had a loss of membrane association, its interaction with zDHHC9 was also investigated. HEK293T cells were co-transfected with HA-zDHHC9 and either EGFP, EGFP-tagged GCP16 WT, C69A, C72A, or C69A/C72A. Cell lysates were incubated with GFP-Trap® Agarose beads, and immunoprecipitated proteins were examined by immunoblotting. The results in Figure 3.12D show that zDHHC9 was co-immunoprecipitated with all GCP16 cysteine mutants, but binding to the C69A/C72A mutant was significantly less than for the other GCP16 proteins.

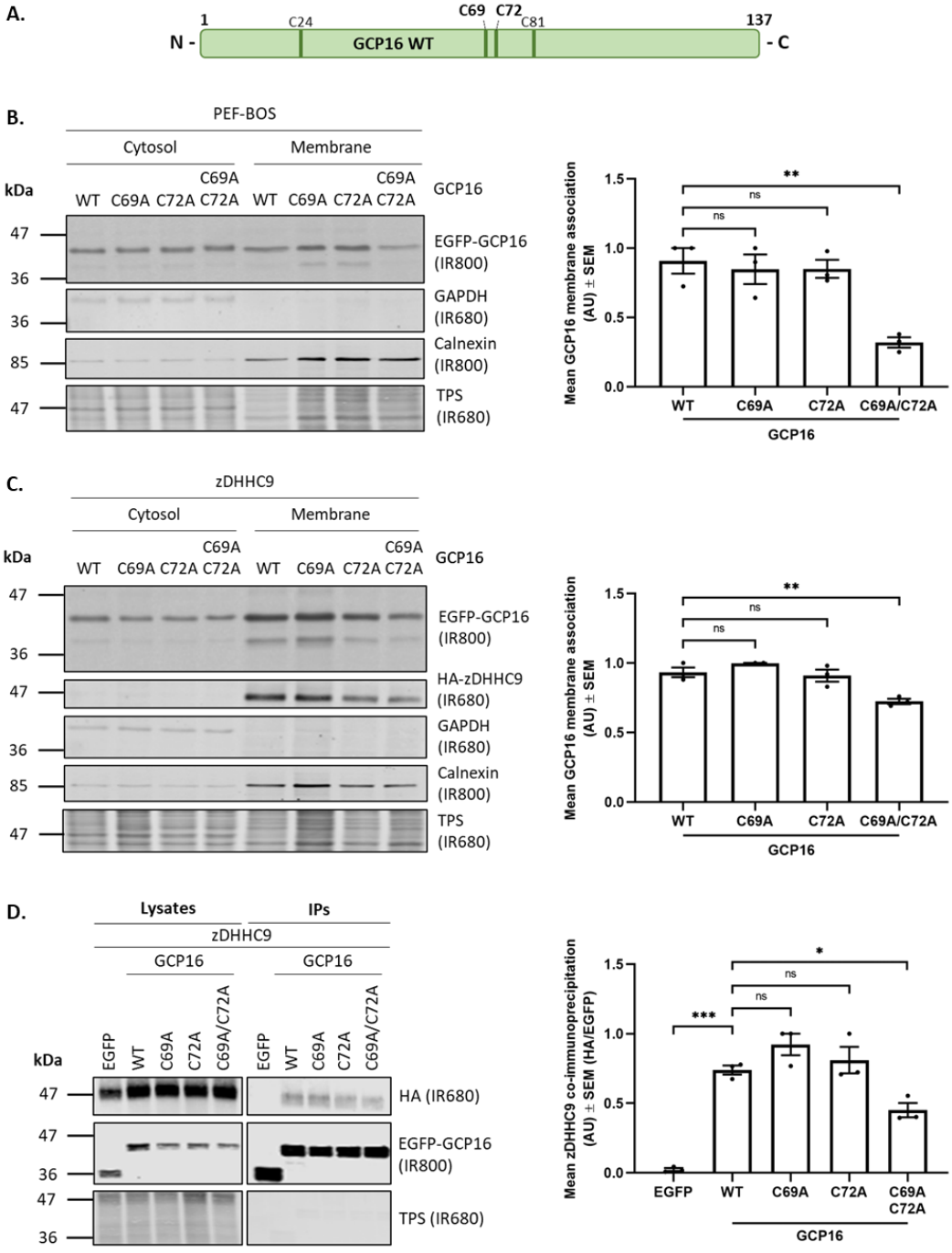
A.
1
C24
C69
C72
C81
137
N -
GCP16 WT
- C
B.
PEF-BOS
Cytosol
Membrane
kDa
WT C69A C72A C69A C72A WT C69A C72A C69A C72A
GCP16
47
36
36
85
47
EGFP-GCP16 (IR800)
GAPDH (IR680)
Calnexin (IR800)
TPS (IR680)
Mean GCP16 membrane association (AU) ± SEM
**
ns
ns
WT
C69A
C72A
C69A/C72A
GCP16
C.
zDHHC9
Cytosol
Membrane
kDa
WT C69A C72A C69A C72A WT C69A C72A C69A C72A
GCP16
47
36
47
36
85
47
EGFP-GCP16 (IR800)
HA-zDHHC9 (IR680)
GAPDH (IR680)
Calnexin (IR800)
TPS (IR680)
Mean GCP16 membrane association (AU) ± SEM
**
ns
ns
WT
C69A
C72A
C69A/C72A
GCP16
D.
Lysates
IPs
zDHHC9
GCP16
GCP16
kDa
EGFP
WT
C69A
C72A
C69A/C72A
EGFP
WT
C69A
C72A
C69A/C72A
47
47
36
47
36
HA (IR680)
EGFP-GCP16 (IR800)
TPS (IR680)
Mean zDHHC9 co-immunoprecipitation (AU) ± SEM (HA/EGFP)
*
ns
ns
***
EGFP
WT
C69A
C72A
C69A C72A
GCP16

Figure 3.12 GCP16 cysteine residues at positions 69 and 72 are important for GCP16 membrane association and interaction with zDHHC9.

(A) *Schematic showing the position of the cysteine residues within GCP16. For investigating membrane association, HEK293T cells were co-transfected with EGFP-tagged GCP16 WT, C69A, C72A, or C69A/C72A and* ***(B)*** *PEF-BOS-HA (empty plasmid control) or* ***(C)*** *HA-zDHHC9. Cells were fractionated using differential detergent extraction to separate the cytosolic and membrane proteins. Protein distribution in the recovered samples was assessed by immunoblotting. GAPDH was used as a cytosolic marker, while calnexin was used as a membrane marker. Quantified data show the mean membrane association (± SEM) of GCP16 WT, C69A, C72A, and C69A/C72A with PEF-BOS or HA-zDHHC9 co-expression. The intensity value for the membrane fraction of GCP16 proteins (IR800) was calculated as a percentage of the sum of the corresponding intensity values of the cytosolic and membrane fractions in each sample. Data has been normalised to the highest value of each experiment, which was set to 1. Statistical significance was analysed using an ordinary one-way ANOVA, followed by a Dunnett's multiple comparisons test. n = 3, from two independent experiments.* ***(D)*** *HEK293T cells were co-transfected with EGFP-tagged GCP16 WT, C69A, C72A, or C69A/C72A and HA-tagged zDHHC9. The EGFP plasmid was used as a negative control. The EGFP-tagged proteins (IR800) were immunoprecipitated using anti-EGFP beads and detected by immunoblotting, along with co-immunoprecipitated HA-tagged proteins (IR680). Quantified data show the mean (± SEM) of the HA-zDHHC9 (IR680) intensity value divided by the corresponding intensity value of the EGFP signal (IR800) in each IP sample. The data has been normalised to the highest value of each experiment, which was set to 1. Statistical significance was analysed using an ordinary one-way ANOVA, followed by a Dunnett's multiple comparisons test. n = 3, from two independent experiments. *p<0.05, **p<0.01 and ***p<0.001, while ns denotes non-significance, where p>0.05. The position of molecular weight markers (kDa) is shown on the left.*

Although the C69A/C72A mutant of GCP16 showed a loss of membrane binding in fractionation experiments, this may reflect a loss of the hydrophobic cysteine residues rather than being due to a loss of S-acylation. To examine this more closely, the non-acylated 1-126 and the S-acylated 1-128 GCP16 mutants were compared to the double cysteine mutant C69A/C72A, and also to the triple cysteine mutants

C24A/C69A/C72A and C69A/C72A/C81A, which we showed previously to have a complete loss of S-acylation.

HEK293T cells were transfected with these constructs and then separated into cytosolic and membrane fractions (Figure 3.13B). Quantification and statistical analysis showed that the membrane association of the 1-126 and 1-128 truncation mutants was not significantly different from the wild-type protein. In contrast, all the cysteine mutants displayed a significant decrease in membrane association, as shown previously (Figure 3.13C).

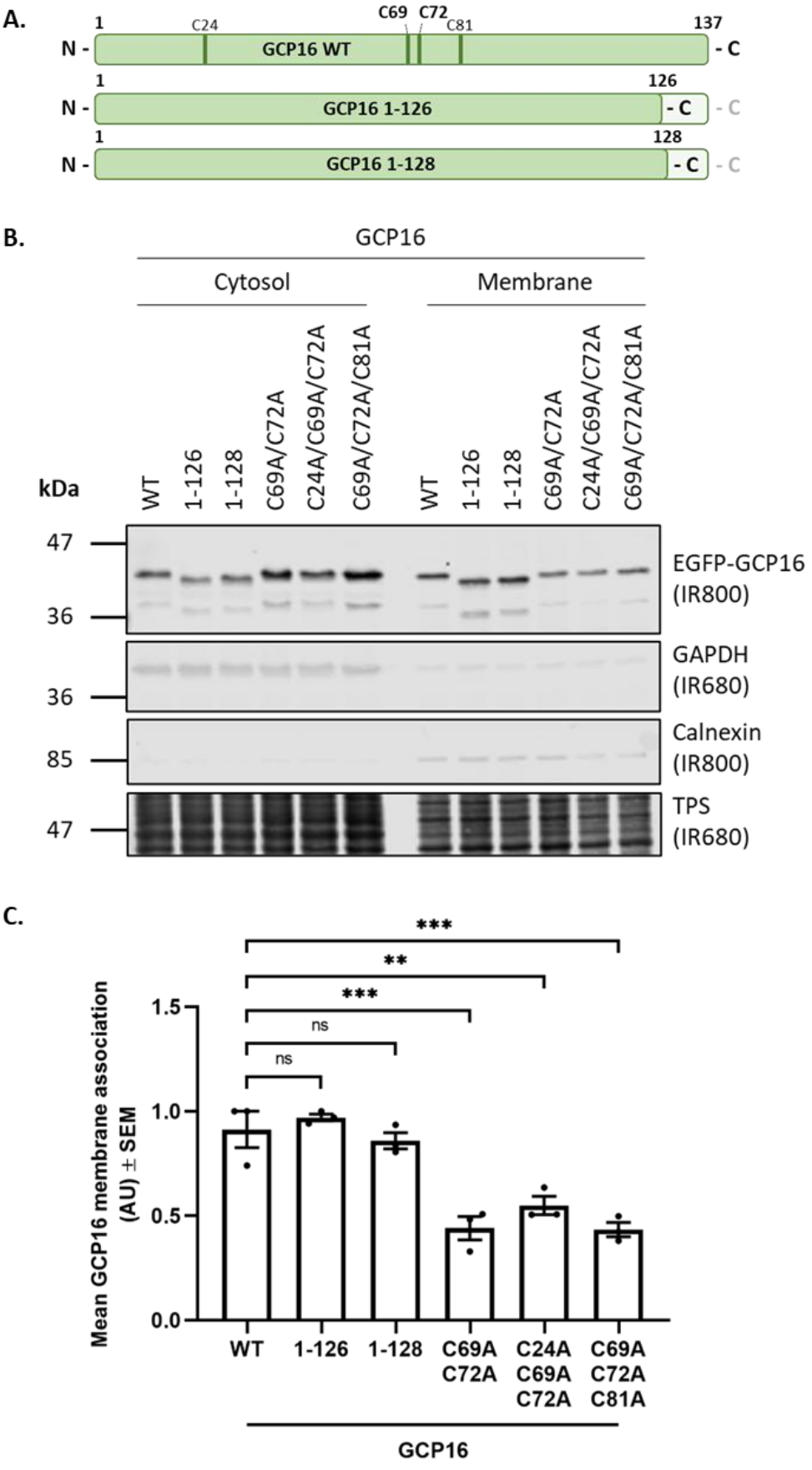
A.
1
C24
C69
C72
C81
137
N -
GCP16 WT
- C
1
126
GCP16 1-126
1
128
GCP16 1-128
B.
GCP16
Cytosol
Membrane
kDa
WT
1-126
1-128
C69A/C72A
C24A/C69A/C72A
C69A/C72A/C81A
47
36
EGFP-GCP16
(IR800)
GAPDH
(IR680)
85
Calnexin
(IR800)
TPS
(IR680)
C.
Mean GCP16 membrane association
(AU) ± SEM
1.5
1.0
0.5
0.0
***
**
ns
WT
1-126
1-128
C69A
C72A
C24A
C69A
C72A
C69A
C72A
C81A
GCP16

Figure 3.13 GCP16 cysteine residues facilitate membrane association independently of S-acylation.

(A) *Schematic showing the position of the S-acylated cysteine residues within GCP16 and the GCP16 C-terminal truncation mutants used.* ***(B)*** *HEK293T cells were co-transfected with EGFP-tagged GCP16 WT, 1-126, 1-128, C69A/C72A, C24A/C69A/C72A, or C69A/C72A/C81A. Cells were fractionated by differential detergent solubility to separate the cytosolic from the membrane proteins, and then proteins were detected by immunoblotting. GAPDH was used as a cytosolic marker, while calnexin was used as a membrane marker. The position of molecular weight markers (kDa) is shown on the left.* ***(C)*** *Quantified data show the mean membrane association (± SEM) of each protein. The intensity value for the membrane fraction of GCP16 proteins (IR800) was calculated as a percentage of the sum of the corresponding intensity values of the cytosolic and membrane fractions in each sample. Data has been normalised to the highest value of each experiment, which was set to 1. Statistical significance was analysed using an ordinary one-way ANOVA, followed by a Dunnett's multiple comparisons test. *p<0.05, **p<0.01 and ***p<0.001, while ns denotes non-significance, where p>0.05. n = 3, from three independent experiments.*

Discussion

In humans, zDHHC9 was the first zDHHC enzyme known to have an obligatory accessory partner required for its S-acylation activity (Swarthout *et al.*, 2005). Analysis of the mechanisms through which GCP16 interacts with and stabilises zDHHC9 expression and activity is important to understand the basis of zDHHC9 regulation. The results presented in this chapter provide several novel findings. Regarding S-acylation, the data suggest that: (i) GCP16 stabilises the S-acylated state of zDHHC9; (ii) zDHHC9 S-acylates GCP16; (iii) S-acylation of GCP16 occurs mainly at Cys-69 and Cys-72, but lower levels of S-acylation are likely to occur on Cys-24 or Cys-81; (iv) S-acylation of GCP16 is dependent on both the N-terminal and C-terminal regions of the protein and these regions are also important for stabilising zDHHC9 S-acylation; and (v) S-acylation is not essential for membrane interaction of GCP16, but Cys-69 and Cys-72 are important for membrane association. In addition, the results in this

chapter have also uncovered new information about the interaction of GCP16 and zDHHC9, with regions 60-90 and 91-128 identified as being important for binding. Finally, GCP16 and zDHHC9 also have a bidirectional effect on each other's protein stability, and this seems to require multiple regions of GCP16 as neither the 1-90 nor the 1-120 truncation mutants of GCP16 could stabilise zDHHC9, despite showing an interaction in co-immunoprecipitation experiments.

Interactions between zDHHC9 and GCP16

Despite the importance of GCP16 as an accessory protein, when this project was initiated, there was no published information on how the zDHHC9/GCP16 complex forms, and which residues are involved in the interaction. Hence, our initial approach was to break down GCP16 into several truncation mutants to pinpoint any interacting regions. One of the main findings of this chapter was the identification of a potential zDHHC9-binding region within GCP16 between amino acid residues 60-90 (Figure 3.2). Interestingly, work from Yang *et al.* (2024) has since identified the cryo-EM structure of the zDHHC9/GCP16 complex. This study identified four binding interfaces, and two of these binding interfaces involve amino acids in the 60-90 amino acid region of GCP16. In one interface, Arginine-85 in the second TMD of zDHHC9 donates a hydrogen bond to the Tyrosine-76 on the main chain of GCP16, and Tyrosine-183 in TMD3 of zDHHC9 interacts with Tyrosine-76 in GCP16 through π–π stacking. In another binding interface, there are interactions between a type II polyproline (PPII) helix in zDHHC9 with α-helices in GCP16, and these interactions include a CH-π hydrogen bond between Proline-292 of zDHHC9 and Tyrosine-86 in GCP16 (Yang *et al.*, 2024). In this chapter, site-directed mutagenesis of these amino acids in GCP16 did not lead to a significant reduction in co-immunoprecipitation of zDHHC9. However, there was a modest but non-significant decrease in binding to the 76-80A mutant of GCP16, which removes Tyr-76 (Figure 3.3). In future experiments, it would be interesting to undertake a combined substitution of Tyr-76 and Tyr-86 to determine if this leads to a loss of binding to the 1-90 region. Interestingly, the work of Yang *et al.* (2024) also identified interactions of N-terminal residues of GCP16 with zDHHC9 (discussed later), but these were not sufficient to co-immunoprecipitate zDHHC9 in the absence of the 60-90 region (i.e. the 1-60 GCP16 mutant) (Figure 3.2). Further analysis of the 60-90 region in full-length GCP16 via alanine scanning mutagenesis to identify specific amino acid residues involved in the interaction was

not successful, which led us to believe that there might be another interaction site present in GCP16 (Figure 3.3).

Indeed, we found that the region 91-137 of GCP16 also co-immunoprecipitated zDHHC9 (Figure 3.7), and further mutagenesis showed that amino acids 91-128 in this region were sufficient for zDHHC9 interaction (Figure 3.8). The work of Yang *et al.* (2024) showed that amino acids in this region of GCP16 are involved in the interaction with zDHHC9. Specifically, one binding interface in the zDHHC9/GCP16 cryo-EM structure involves interactions between Glu-101 in zDHHC9 with both Arg-118 and Arg-121 in GCP16 (Yang *et al.*, 2024). It will be interesting in future work to test if the substitution of these arginine residues in the 91-128 GCP16 construct ablates its interaction with zDHHC9.

Reciprocal effects of GCP16 and zDHHC9 on S-acylation

It was reported that GCP16 is S-acylated at Cys-69 and Cys-72 (Ohta *et al.*, 2003), but the enzymes that mediate this modification have not previously been reported. By undertaking click chemistry experiments with palmitic acid azide, the work in this chapter clearly showed that zDHHC9 can mediate the S-acylation of GCP16 (Figure 3.1). Although Cys-69 and Cys-72 were previously identified as the major sites of GCP16 S-acylation (Ohta *et al.*, 2003), the work in this chapter also showed that S-acylation can occur to a minor extent at Cys-24 or Cys-81 (Figure 3.11). This is an interesting observation, as both of these cysteines are in proximity to regions of GCP16 involved in zDHHC9 interaction (Yang *et al.*, 2024), and so S-acylation at these sites could potentially modify or regulate the zDHHC9/GCP16 complex.

zDHHC9 is S-acylated at its active site, an essential step in substrate S-acylation, and also at positions Cys-24, Cys-25, and Cys-288, and these cysteines (especially C288) are also important for the catalytic activity of the enzyme (Yang *et al.*, 2024). S-acylation of the cysteine in the DHHC motif of zDHHC enzymes is referred to as autoacylation, and this enzyme-acyl complex is a key intermediate in the S-acylation reaction (Mitchell *et al.*, 2010, Jennings and Linder, 2012). Therefore, zDHHC enzyme acylation status is often used as a proxy for enzyme “activity”. Swarthout *et al.* (2005) have demonstrated that this active site autoacylation of zDHHC9 and subsequent transfer of the acyl chain to H-Ras require the presence of GCP16, using purified proteins (Swarthout *et al.*, 2005). Mitchell *et al.* (2014) expanded on these findings by

showing that without GCP16, partially purified zDHHC9 can still undergo autoacylation, but the acyl group is more susceptible to hydrolysis (Mitchell *et al.*, 2014). Therefore, GCP16 is not only a substrate of zDHHC9, but it also regulates the autoacylation of the enzyme. However, the regulation of zDHHC9 acylation status by GCP16 has never been reported in cells and has only been shown for purified proteins. In this chapter, we showed that GCP16 co-expression indeed leads to an increase in the S-acylation status of zDHHC9 (Figure 3.1), supporting its role as a key regulator of enzyme activity. We suggest that the GCP16-mediated increase in zDHHC9 S-acylation is a result of stabilising the active site autoacylation, as shown for recombinant purified ERF2/ERF4 (Mitchell *et al.*, 2012) and zDHHC9/GCP16 (Mitchell *et al.*, 2014) protein complexes. In addition, GCP16 may also stabilise other S-acylated cysteines, such as C288 (Yang *et al.*, 2024), as we can identify multiple zDHHC9 band shifts in the samples incubated with palmitic acid azide on the immunoblot following GCP16 co-expression (Figure 3.1). It will be interesting in future work to explore if GCP16 also stabilises the S-acylation of other enzymes that are regulated by this accessory protein, including zDHHC14 and zDHHC18 (Yang *et al.*, 2024).

Interestingly, the analysis of GCP16 truncation mutants showed that both the N- and the C-terminal regions of GCP16 were essential for GCP16 S-acylation and for the ability of this protein to stabilise zDHHC9 acylation. Although GCP16 mutants 1-90 and 1-120 included all four cysteines and were shown to co-immunoprecipitate zDHHC9 (Figure 3.2), these truncation mutants were unable to be S-acylated by zDHHC9 or to stabilise the acylation of this enzyme (Figure 3.4).

The lack of S-acylation for GCP16 1-90 and 1-120 indicated that the C-terminal region of GCP16 might be important for the S-acylation of the protein. Indeed, GCP16 C-terminal truncation mutant analysis demonstrated that S-acylation can only be recovered with mutant 1-128, proving the requirement of the C-terminal region for this post-translational modification (Figure 3.5). When trying to pinpoint the specific amino acids responsible using alanine substitutions, S-acylation was completely abolished for both 122-125A and 126-130A GCP16 mutants (Figure 3.5). The most likely explanation for these findings is that this region of GCP16 is important for the correct structural folding of the protein and to ensure efficient interaction of Arg-118 and Arg-121 with zDHHC9.

The results presented in Figure 3.10 also showed that the N-terminal region of GCP16 is important for S-acylation of both GCP16 and zDHHC9. Amino acids 11-20 of GCP16 appear to be critical for S-acylation, and interestingly, this region of GCP16 is known to form contacts with zDHHC9 in the cryo-EM structure (Yang *et al.*, 2024). Specifically, Lys-11, Phe-13, Arg-16 and Tyr-18 have all been shown to form contacts with zDHHC9, likely explaining the importance of the 11-20 region for effective S-acylation of both proteins.

It is interesting to note that the reported cryo-EM structure of the zDHHC9/GCP16 complex revealed that Cys-69 and Cys-72 of GCP16 are part of a cysteine cluster that includes the three C-terminal cysteines of zDHHC9: Cys-283, Cys-284, Cys-288. The cysteine cluster is important for mediating the correct folding of the complex, while the S-acylation of the cysteine cluster, especially Cys-288 of zDHHC9, is also important for catalytic activity, reinforcing intrinsic stability and membrane association (Yang *et al.*, 2024). It would be interesting to use the triple GCP16 cysteine-to-alanine mutant, along with 1-126 (unable to S-acylate) and 1-128 (able to S-acylate) mutants with intact cysteines to investigate the role of GCP16 S-acylation or the immediate involvement of the cysteine residues in stabilising the S-acylation of zDHHC9 and the overall stability of the complex.

Reciprocal effects of GCP16 and zDHHC9 on protein stability

In addition to regulating zDHHC9 S-acylation, there is evidence suggesting that GCP16 may also regulate the stability of zDHHC9. For the yeast orthologues of these proteins, Erf2 and Erf4, it has been shown that expression levels of Erf2 are significantly reduced in Erf4 mutant cells (Lobo *et al.*, 2002). Additionally, the stability of Erf2 in Erf4 mutant cells after cycloheximide inhibition of protein synthesis was significantly decreased, and Erf2 showed enhanced levels of ubiquitination in the absence of Erf4 (Mitchell *et al.*, 2012). Regarding GCP16 and zDHHC9, experiments performed using purified proteins from insect cells have shown that zDHHC9 is prone to proteolysis in the absence of GCP16 (Swarthout *et al.*, 2005). Furthermore, it was shown that zDHHC9 forms higher molecular weight oligomers in HEK293 cell lysates in the absence of GCP16, in FSEC experiments (Nguyen *et al.*, 2023). Therefore, there is some evidence that GCP16 may stabilise zDHHC9, but this has not been definitively shown in mammalian cells. The work in this chapter showed for the first time that the stability of zDHHC9 is decreased in the absence of GCP16, and *vice*

versa (Figure 3.1). These effects are dependent on the formation of an intact zDHHC9/GCP16 complex as although the 1-90 and 1-120 GCP16 truncation mutants can co-immunoprecipitate with zDHHC9, they are unable to stabilise the enzyme. These truncated GCP16 mutants were also less stable themselves, and their stability was not recovered by zDHHC9 co-expression (Figure 3.6). These findings highlight that there are reciprocal effects of GCP16 and zDHHC9 on both S-acylation and protein stability and that these effects require almost the full-length GCP16 protein.

S-acylation of GCP16 and membrane binding

Ohta *et al.* (2003) identified the S-acylated cysteines within GCP16 and highlighted that this PTM accounts for the tight membrane association of this protein. This latter finding was through analysis of cysteine-to-alanine mutants of GCP16 and their association with purified membrane fractions. This was confirmed by immunofluorescence microscopy experiments in HeLa cells, which showed that cysteine-to-alanine substitution of C69 and C72 also showed a cytoplasmic localisation instead of Golgi staining (Ohta *et al.*, 2003). To investigate the involvement of C69 and C72 in membrane association, we used single alanine mutants, along with the double alanine mutant in cell fractionation experiments, and the results confirmed that only substitution of both C69 and C72 decreased the membrane association of GCP16 (Figure 3.12). When GCP16 was co-expressed with zDHHC9, this decrease in membrane binding of the cysteine-to-alanine mutants was not as dramatic, suggesting that association with zDHHC9 might partially stabilise the membrane attachment of GCP16 (Figure 3.12C). Co-immunoprecipitation of zDHHC9 confirmed that the C69A/C72A mutant could still interact with zDHHC9, albeit at reduced levels (Figure 3.12D). This observation is in contrast to the findings by Mitchell *et al.* (2014) in which they could not detect any zDHHC9 bound to the GCP16 C69S/C72S mutant (Mitchell *et al.*, 2014).

Interestingly, analysis of the non-acylated GCP16 truncation mutant 1-126 and the S-acylated 1-128 mutant showed that both of these proteins had a similar level of membrane association as wild-type GCP16 (Figure 3.13). For this comparison, the GCP16 constructs were expressed in the absence of zDHHC9 to prevent any effects on the membrane association of the GCP16 constructs through direct association with zDHHC9. The key difference between these truncation mutants and the cysteine-to-alanine substitution mutants is that all cysteine residues are intact in the truncation

mutants. This indicates that membrane association is not dependent on S-acylation, in contrast to previous suggestions. Instead, we propose that the cysteine residues of GCP16 are directly involved in membrane association. A possible explanation is that the cysteine residues provide a strong intrinsic membrane affinity due to their hydrophobicity. There seems to be no difference in the membrane association of mutants 1-126 and 1-128, despite their differences in S-acylation, further suggesting that cysteines have a primary role in membrane attachment. It is interesting to note that Cys-69 and Cys-72 are in fact present in a region of GCP16 that has strong hydrophobicity (Figure 3.14), and hence, this region of the protein could facilitate membrane association prior to the S-acylation of the cysteine residues.

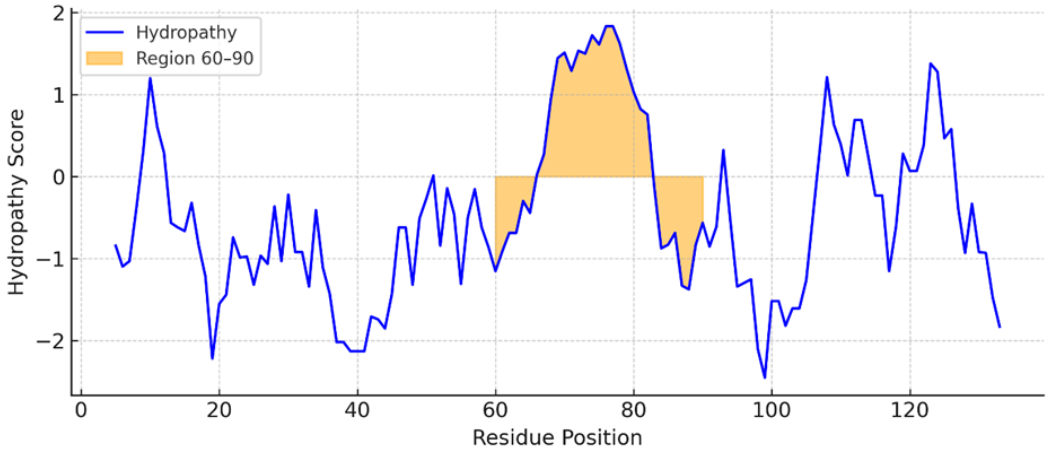

Figure 3.14 Hydropathy profiling of GCP16.

Kyte-Doolittle hydropathy profiling of the protein sequence to assess the relative hydrophobicity and hydrophilicity of amino acid residues along the polypeptide. Each amino acid residue was assigned a hydropathy index based on the Kyte-Doolittle scale, and average scores were calculated using a sliding window of nine residues to smooth local fluctuations and highlight broader hydropathy trends. The amino acid region 60-90 is highlighted.

Limitations and future directions

This study used protein overexpression analysis to investigate binding, S-acylation, stability and membrane association. Although this is a widely used strategy in

molecular biology, and some of our conclusions using this approach have been subsequently validated by the cryo-EM structure of zDHHC9 and GCP16, overexpression has several limitations to consider. Overexpression typically results in much higher protein levels than those produced endogenously, and this can lead to molecular interactions being saturated or to protein mislocalisation, which could also affect S-acylation. Therefore, the findings of this study should be confirmed using knockdown approaches such as CRISPR to engineer or mutate the endogenous *ZDHHC9* and *GCP16* genes (e.g. introducing specific point mutations or knocking down protein expression). Furthermore, a recurring limitation of co-immunoprecipitation experiments was differences in protein expression that affect quantification. It was often seen that lower expression of EGFP-tagged GCP16 mutants gave a higher binding of HA-zDHHC9 when quantification was performed. It is possible that GCP16 is expressed at higher levels than zDHHC9 under the conditions that we have used, and that lowering GCP16 expression may not lead to a corresponding decrease in zDHHC9 co-immunoprecipitation (e.g. if the expressed GCP16 is able to co-precipitate all of the expressed zDHHC9). Therefore, immunoprecipitation experiments could be undertaken using much lower levels of GCP16, which may give a more linear range that is sensitive enough to detect subtle changes in binding even when EGFP-GCP16 proteins are expressed at different levels. At present, the conditions used can clearly detect where there is a loss of binding (e.g. with the 1-30 and 1-60 mutants) but may not be sensitive enough to detect more subtle changes. Studying binding using a different approach such as fluorescence resonance energy transfer (FRET) would also provide insight into real-time interactions and would complement the immunoprecipitation experiments performed here. Overall, the work presented in this chapter has provided new insights into the zDHHC9/GCP16 interaction and its reciprocal effects on S-acylation and protein stability. Importantly, the results are also broadly consistent with the cryo-EM structure of the complex (Yang *et al.*, 2024), which was reported after most of the work in this chapter had been completed.

CHAPTER 4

IDENTIFICATION OF AMINO ACID RESIDUES IMPORTANT FOR THE S-ACYLATION, STABILITY AND FUNCTION OF THE ZDHHC9/GCP16 COMPLEX

Chapter 4 - Identification of amino acid residues important for the S-acylation, stability and function of the zDHHC9/GCP16 complex

Introduction

In mammals, protein S-acylation occurs on an array of proteins, and influences membrane association, protein localisation, interactions, stability and activity (Chamberlain and Shipston, 2015). This regulation is highly dynamic and can affect several physiological cellular pathways. The zDHHC9/GCP16 protein complex has been directly associated with growth factor signalling pathways (Swarthout *et al.*, 2005, Malgapo and Linder, 2021), along with neuronal signalling and plasticity (Raymond *et al.*, 2007, Shimell *et al.*, 2019). Notably, mutations in *ZDHHC9* cause intellectual disability and childhood epilepsy (Baker *et al.*, 2015), and studies in primary rat neurons have linked this to effects of zDHHC9 on dendrite growth and formation of inhibitory synapses (Shimell *et al.*, 2019). The relevance of zDHHC9 in these cell pathways and for human health more generally underscores the importance of elucidating the mechanism through which the enzyme is regulated by GCP16.

The development of AlphaFold protein structure prediction software by DeepMind and EMBL-EBI has been a major breakthrough in computational biology for the prediction of protein structure and protein interaction interfaces (Jumper *et al*., 2021, Varadi *et al*., 2022, Abramson *et al*., 2024, Varadi *et al*., 2024). AlphaFold offers a powerful tool to build on the truncation analyses of GCP16 undertaken in Chapter 3 by identifying specific binding interfaces and key residues in the zDHHC9/GCP16 complex. AlphaFold is especially useful where there is a lack of experimental structural information, such as at the outset of this project, and prior to the reported cryo-EM structure of the zDHHC9/GCP16 complex (Yang *et al.*, 2024).

The study of Yang *et al.* (2024) represented a major breakthrough in our understanding of the molecular interaction between zDHHC9 and GCP16. This work identified four main binding interfaces making up the interaction between the two proteins, which we refer to as interfaces 1, 2, 3, and 4a/b. Interface 1 involves hydrogen-bond interactions between tyrosine-76 in GCP16 and arginine-85 in the second transmembrane helix of zDHHC9 , and π–π stacking interactions between tyrosine 76 in GCP16 and tyrosine-183 in the third transmembrane helix of zDHHC9. Binding interface 2 involves interactions between a type II polyproline (PPII) helix near

the C-terminal region of zDHHC9 with GCP16 α-helices. Three prolines in this region of zDHHC9 are highlighted: proline-290 and proline-293 dock into two pockets formed by α-helices in GCP16 with a weak negative charge, and proline-292 forms a CH-π hydrogen bond with tyrosine-86 in GCP16. Interface 3 involves zinc finger motifs in the DHHC catalytic domain of zDHHC9, where phenylalanine-129 and proline-150 form π–π stacking and CH-π interactions with tyrosine-18 in GCP16 found in the loop after the β1' stand of the protein. Moreover, glutamate-163 in zDHHC9 forms charge-charge interactions with arginine-16 in GCP16. Finally, interface 4a/b is formed by charge-charge and anion-π interactions of aspartate-100 of zDHHC9 with lysine-11 and phenylalanine-13 of GCP16, charge-charge interaction between glutamate-101 in zDHHC9 and arginine-118 in GCP16, and a charge-stabilised H-bond between glutamate-101 in zDHHC9 and arginine-121 in GCP16. Although not directly involved in the binding interfaces of zDHHC9 and GCP16, through AlphaFold analysis of the protein complex, we also noted that glutamate-124 of GCP16 stabilises lysine-11 and arginine-118 through a hydrogen bond interaction (the interaction with R118 was also confirmed by the cryo-EM structure). Interfaces 3 and 4a/b were also proposed to affect the stabilisation of the zinc finger motifs in the DHHC catalytic domain of zDHHC9. Additionally, S-acylation of C288 found at the C-terminal region of zDHHC9 was proposed to promote the membrane association of the α3' helix into a hydrophobic pocket formed by TMD2 and TMD3, resulting in a more compact structural conformation of the enzyme. C288 is found at the centre of a cysteine cluster formed by C283, C284, and C288 in zDHHC9, together with C69 and C72 in GCP16. Substitution of C288 to alanine abolished the catalytic activity of the complex against H-Ras (Yang *et al.*, 2024).

A notable omission from the study of Yang *et al.* (2024) was the lack of a detailed analysis of the effects of substituting the identified interacting residues on the formation of the zDHHC9/GCP16 complex. There was also no analysis of how the disruption of these binding interfaces affected zDHHC9/GCP16 stability and activity in cells (Yang *et al.*, 2024). This chapter sought to build on the reported cryo-EM structure to generate a more detailed understanding of how different interacting residues impact the functional regulation of the zDHHC9/GCP16 complex. The aims were: (i) to build on the knowledge acquired through the analyses of GCP16 truncation mutants in Chapter 3 by using AlphaFold analyses, and subsequently the cryo-EM structure of zDHHC9/GCP16; (ii) to explore the importance of the various interaction interfaces of the cryo-EM structure on the reciprocal S-acylation and stability of

zDHHC9 and GCP16; (iii) to explore the involvement of the identified interaction sites for zDHHC9/GCP16 complex formation; and (iv) to investigate the effects of mutating the identified binding interfaces on zDHHC9 function in neuronal cultures.

Results

4.1 AlphaFold structure prediction of the zDHHC9/GCP16 protein complex

When this project was initiated, there was no published structure of the zDHHC9/GCP16 complex available. Therefore, we initially sought to build on the results of Chapter 3 by using AlphaFold, a protein structure predicition platform (Jumper *et al.*, 2021, Varadi *et al.*, 2022, Varadi *et al.*, 2024). The structure of the zDHHC9/GCP16 complex predicted by AlphaFold was visualised and explored using the RCSB Protein Data Bank 3D Mol* Viewer (Sehnal *et al.*, 2021), allowing the identification of interacting residues and intramolecular interactions.

Figure 4.1 displays the structure prediction of human zDHHC9 (UniProt ID: Q9Y397) shown in green, interacting with human GCP16 (UniProt ID: Q7Z5G4), displayed in orange. The prediction highlighted two interacting residues in each protein chain, which are shown in neon green on the protein complex. These two binding interfaces are shown in enlarged images and include tyrosine-183 of zDHHC9 forming a Pi stack with tyrosine-76 of GCP16, and glutamic acid-101 of zDHHC9 forming a hydrogen bond with arginine-121 of GCP16.

Pi stacking between **TYR 183** of **zDHHC9** and **TYR 76** of **GCP16**

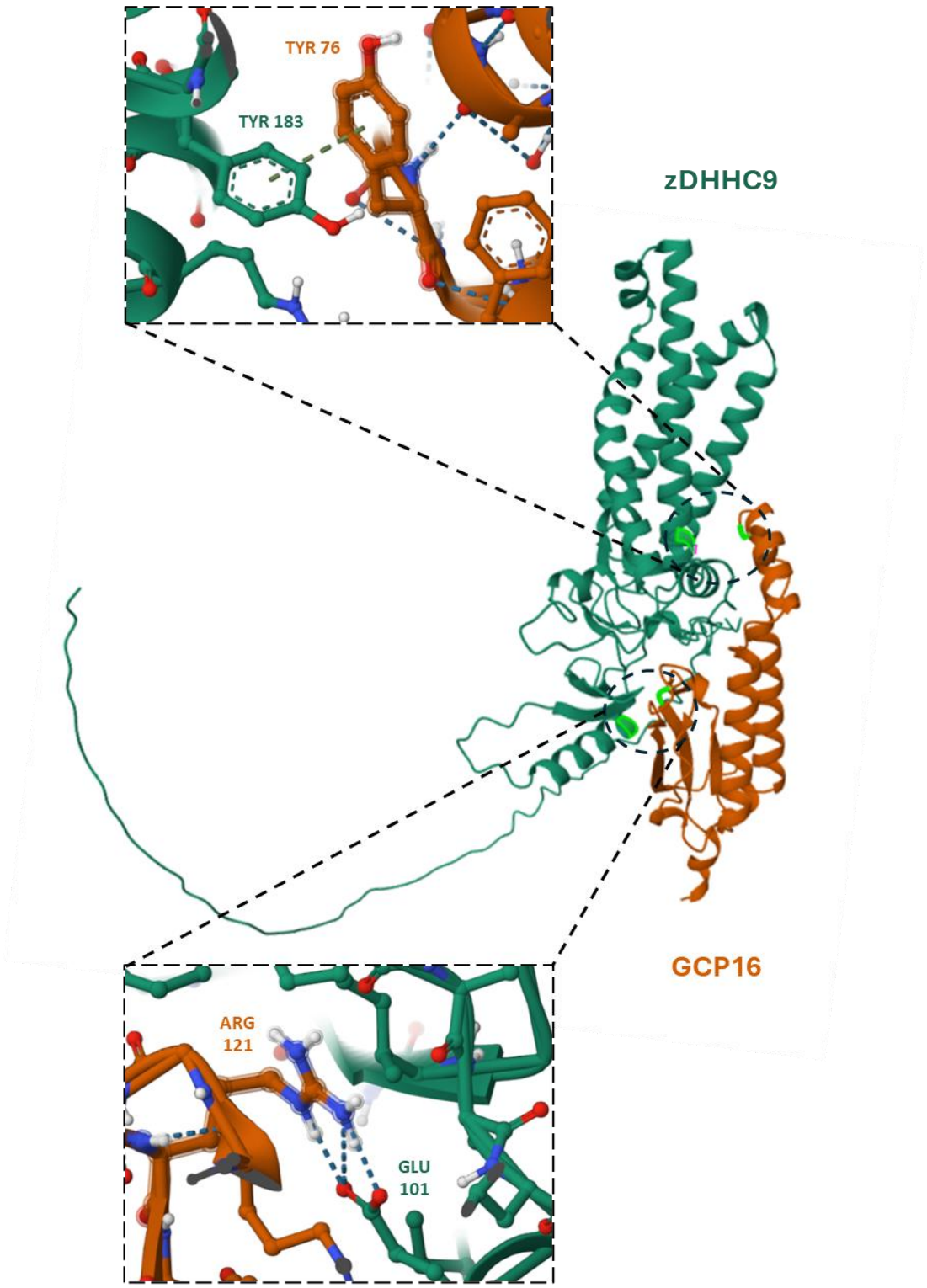

Hydrogen bond between **GLU 101** of **zDHHC9** and **ARG 121** of **GCP16**

Figure 4.1 AlphaFold structure prediction of the zDHHC9/GCP16 protein complex.

Protein structure predictions of human zDHHC9 (UniProt ID: Q9Y397) interacting with human Golgin subfamily A member 7 (UniProt ID: Q7Z5G4). The zDHHC9 protein chain is shown in green and the GCP16 protein chain is shown in orange. Enlarged images show the interactions between the two proteins. TYR 183 of zDHHC9 forms a Pi stack with TYR 76 of GCP16, and GLU 101 of zDHHC9 forms a hydrogen bond with ARG 121 of GCP16. Protein complex prediction was visualised using the RCSB Protein Data Bank 3D Mol Viewer (Sehnal et al., 2021), based on AlphaFold by DeepMind and EMBL-EBI (Jumper et al., 2021, Varadi et al., 2022, Varadi et al., 2024).*

4.2 Investigation of the AlphaFold modelling prediction of the zDHHC9/GCP16 protein complex using GCP16 mutant constructs

The AlphaFold prediction in Figure 4.1 is consistent with the results of Chapter 3, which showed an important role for both the region containing amino acids 60-90 (which includes Tyrosine-76) and the C-terminal region 91-128 (which includes Arginine-121) of GCP16 for the observed interaction with zDHHC9. To further investigate the validity of the AlphaFold prediction for the zDHHC9/GCP16 interaction, GCP16 mutant constructs were synthesised in which the identified interacting residues, Y76 and R121, were substituted with alanine. This construct was then used in co-immunoprecipitation and S-acylation experiments to study the effect on the interaction with zDHHC9. HEK293T cells were transfected with EGFP (control), EGFP-tagged GCP16 WT, or Y76A/R121A, together with HA-zDHHC9. Cell lysates were then incubated with GFP-Trap® Agarose beads, and immunoprecipitated proteins were examined by immunoblotting (Figure 4.2A). Surprisingly, data quantification and statistical analysis showed that there was no change in the ability of this GCP16 Y76A/R121A mutant to co-immunoprecipitate zDHHC9, when compared to wild-type GCP16.

To investigate the effects of these amino acid substitutions on GCP16 and zDHHC9 S-acylation, HEK293T cells were co-transfected with PEF-BOS-HA control or HA-tagged zDHHC9, together with EGFP-tagged GCP16 WT, Y76A/R121A, or EGFP.

Cells were labelled with either palmitic acid as a control or palmitic acid azide to be processed for click chemistry detection of S-acylation using alkyne mPEG (5 kDa) (Figure 4.2B-C). Quantified results showed that GCP16 Y76A/R121A S-acylation was not significantly different to GCP16 WT S-acylation when co-expressed with either PEF-BOS or zDHHC9. However, the Y76A/R121A mutant showed a decreased ability to stabilise zDHHC9 S-acylation compared to GCP16 WT (Figure 4.2C).

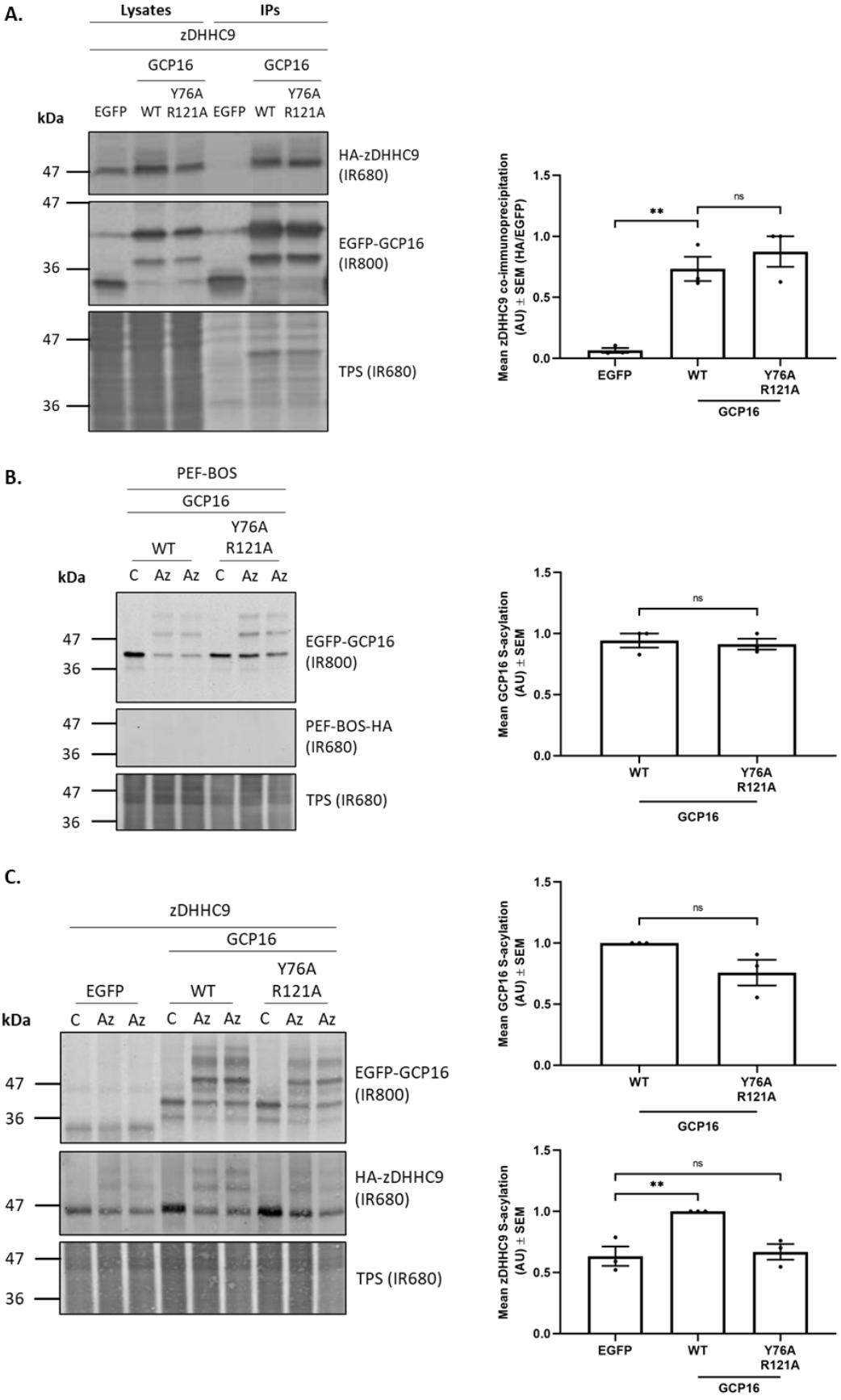
A.
Lysates
IPs
zDHHC9
GCP16
GCP16
Y76A
Y76A
EGFP
WT
R121A
EGFP
WT
R121A
kDa
47
47
36
47
36
HA-zDHHC9
(IR680)
EGFP-GCP16
(IR800)
TPS (IR680)
Mean zDHHC9 co-immunoprecipitation
(AU) ± SEM (HA/EGFP)
1.5
1.0
0.5
0.0
**
ns
EGFP
WT
Y76A
R121A
GCP16
B.
PEF-BOS
GCP16
Y76A
WT
R121A
kDa
C
Az
Az
C
Az
Az
47
36
47
36
47
36
EGFP-GCP16
(IR800)
PEF-BOS-HA
(IR680)
TPS (IR680)
Mean GCP16 S-acylation
(AU) ± SEM
1.5
1.0
0.5
0.0
ns
WT
Y76A
R121A
GCP16
C.
zDHHC9
GCP16
Y76A
EGFP
WT
R121A
kDa
C
Az
Az
C
Az
Az
C
Az
Az
47
36
47
47
36
EGFP-GCP16
(IR800)
HA-zDHHC9
(IR680)
TPS (IR680)
Mean GCP16 S-acylation
(AU) ± SEM
1.5
1.0
0.5
0.0
ns
WT
Y76A
R121A
GCP16
Mean zDHHC9 S-acylation
(AU) ± SEM
1.5
1.0
0.5
0.0
ns
**
EGFP
WT
Y76A
R121A
GCP16

Figure 4.2 Analysis of the effects of Y76A and R121A substitutions in GCP16 on S-acylation and interaction with zDHHC9.

(A) *HEK293T cells were co-transfected with HA-tagged zDHHC9 and EGFP-tagged GCP16 WT, or Y76A/R121A. The EGFP plasmid was used as a negative control. The EGFP-tagged proteins (IR800) were immunoprecipitated using anti-EGFP beads and detected by immunoblotting, along with co-immunoprecipitated HA-tagged proteins (IR680). Quantified data show the mean (± SEM) of the HA-zDHHC9 (IR680) intensity value divided by the corresponding intensity value of the EGFP signal (IR800) in each IP sample. The data has been normalised to the highest value of each experiment, which was set to 1. Statistical significance was analysed using an ordinary one-way ANOVA, followed by a Dunnett's multiple comparisons test. n = 3, from two independent experiments. For investigating protein S-acylation, HEK293T cells were co-transfected with EGFP-tagged GCP16 WT or Y76A/R121A and either* ***(B)*** *PEF-BOS-HA (empty plasmid control), or* ***(C)*** *HA-tagged zDHHC9. EGFP was used as a control. Cells were labelled with palmitic acid (C16:0) as a control (C) or palmitic acid azide (Az-C16:0) for 4 hours and were then lysed and clicked using alkyne-mPEG. S-acylation is indicated by band-shifts in Az samples. Quantified data show mean protein S-acylation (± SEM). The S-acylated bands were quantified as a percentage of total expression for each protein incubated with the palmitic acid azide. The data has been normalised to the highest value of each experiment, which was set to 1. Statistical significance was analysed using an unpaired t-test, or an ordinary one-way ANOVA, followed by a Dunnett's multiple comparisons test where appropriate. *p<0.05, **p<0.01 and ***p<0.001, while ns denotes non-significance, where p>0.05. n = 3, from two independent experiments. The position of molecular weight markers (kDa) is shown on the left.*

4.3 Investigation of the AlphaFold modelling prediction of the zDHHC9/GCP16 protein complex using more disruptive GCP16 mutant constructs

Since the GCP16 mutant Y76A/R121A, designed based on the AlphaFold prediction of the zDHHC9/GCP16 interaction, was still able to interact with zDHHC9, more disruptive amino acid susbtitutions were introduced at these sites. These mutants included Y76A/R121E, in which Y76 was substituted with alanine and R121 was

substituted with glutamic acid. The second construct was Y76A/F79A/R121A, in which Y76 and R121 were substituted with alanine, along with F79, which was shown to form a hydrogen bond with Y76 in the AlphaFold model (Figure 4.3A). Both GCP16 mutant constructs were then used in co-immunoprecipitation and S-acylation experiments to study their effect on the interaction with zDHHC9.

HEK293T cells were transfected with EGFP (control), EGFP-tagged GCP16 WT, Y76A/R121E, or Y76A/F79A/R121A, together with HA-zDHHC9. Cell lysates were incubated with GFP-Trap® Agarose beads for 1 hour, and immunoprecipitated proteins were examined by immunoblotting (Figure 4.3B). Quantified data and statistical analysis showed that both GCP16 mutants Y76A/R121E, or Y76A/F79A/R121A were able to co-immunoprecipitate zDHHC9 at similar levels to the wild-type protein.

To investigate the effects of these mutants on S-acylation activity, click chemistry experiments were carried out as shown in Figure 4.2. The results show that GCP16 Y76A/R121E S-acylation was not significantly different to GCP16 WT S-acylation when co-expressed with either PEF-BOS or zDHHC9. However, the GCP16 Y76A/F79A/R121A showed decreased S-acylation when co-expressed with either PEF-BOS or zDHHC9, compared to GCP16 WT (Figure 4.4A-B). Similar to the results seen for the Y76A/R121A mutant (Figure 4.2), both the Y76A/R121E and Y76A/F79A/R121A mutants showed a decreased ability to stabilise zDHHC9 S-acylation compared to GCP16 WT (Figure 4.4B).

Collectively, the analysis of amino acid substitutions at positions Y76 and R121 showed that disrupting these sites had no effect on co-immunoprecipitation of zDHHC9 but did affect the S-acylation of GCP16 (Y76A/F79A/R121A mutant only) and the stabilisation of zDHHC9 S-acylation (seen for all three mutants tested).

A.

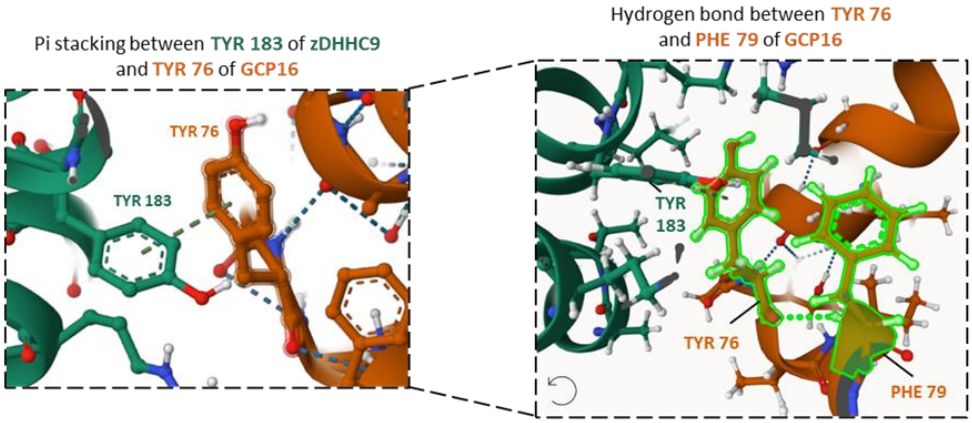
Pi stacking between TYR 183 of zDHHC9
and TYR 76 of GCP16
TYR 76
TYR 183
Hydrogen bond between TYR 76
and PHE 79 of GCP16
TYR
183
TYR 76
PHE 79

B.

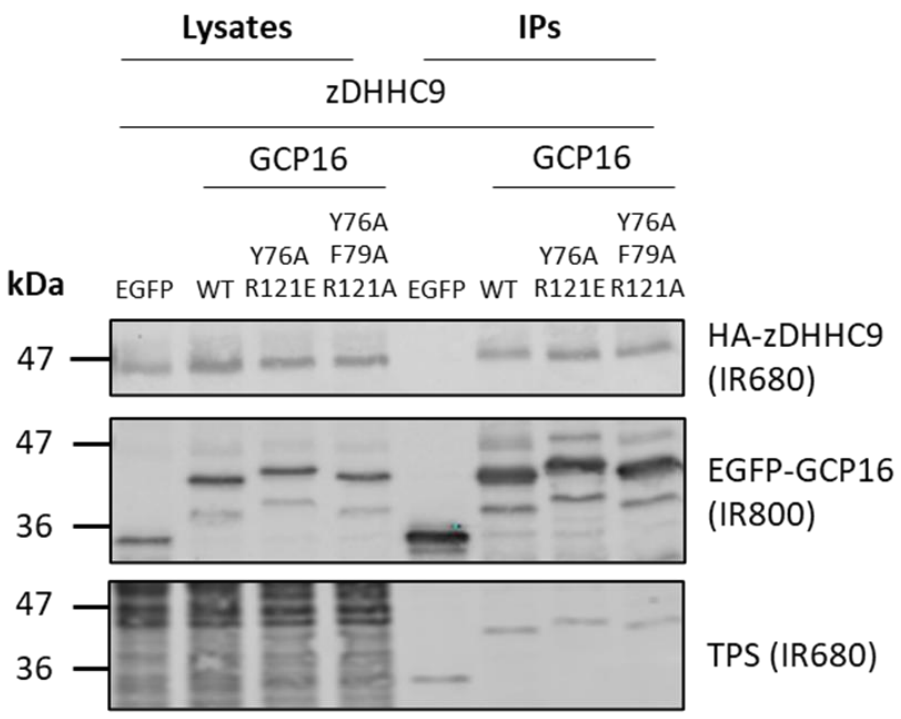
Lysates
IPs
zDHHC9
GCP16
GCP16
kDa
EGFP
WT
Y76A R121E
Y76A F79A R121A
EGFP
WT
Y76A R121E
Y76A F79A R121A
47
HA-zDHHC9 (IR680)
47
36
EGFP-GCP16 (IR800)
47
36
TPS (IR680)

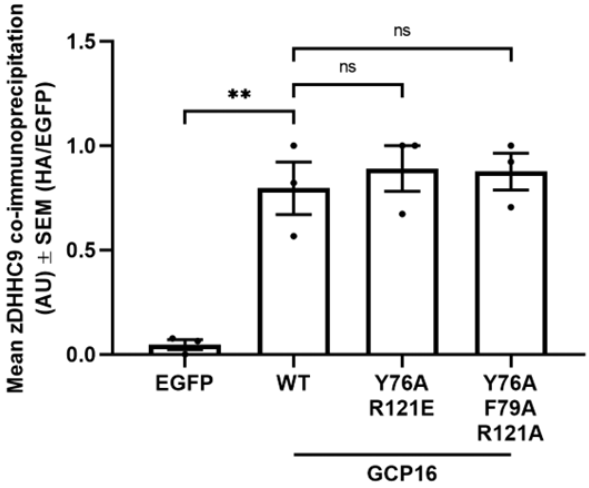
Mean zDHHC9 co-immunoprecipitation (AU) ± SEM (HA/EGFP)
1.5
1.0
0.5
0.0
**
ns
ns
EGFP
WT
Y76A R121E
Y76A F79A R121A
GCP16

Figure 4.3 Effects of Y76A/R121E and Y76A/F79A/R121A amino acid substitutions in GCP16 on the interaction with zDHHC9.

(A) *Enlarged images of the AlphaFold structure prediction of the zDHHC9/GCP16 protein complex showing the intramolecular hydrogen bond between TYR 76 and PHE 79 of GCP16.* ***(B)*** *HEK293T cells were co-transfected with HA-tagged zDHHC9 and EGFP-tagged GCP16 WT, Y76A/R121E, or Y76A/F79A/R121A. The EGFP plasmid was used as a negative control. The EGFP-tagged proteins (IR800) were immunoprecipitated using anti-EGFP beads and detected by immunoblotting, along with co-immunoprecipitated HA-tagged proteins (IR680). The position of molecular weight markers (kDa) is shown on the left. Quantified data show the mean (± SEM) of the HA-zDHHC9 (IR680) intensity value divided by the corresponding intensity value of the EGFP signal (IR800) in each IP sample. The data has been normalised to the highest value of each experiment, which was set to 1. Statistical significance was analysed using an ordinary one-way ANOVA, followed by a Dunnett's multiple comparisons test against GCP16 WT. *p<0.05, **p<0.01 and ***p<0.001, while ns denotes non-significance, where p>0.05. n = 3, from two independent experiments.*

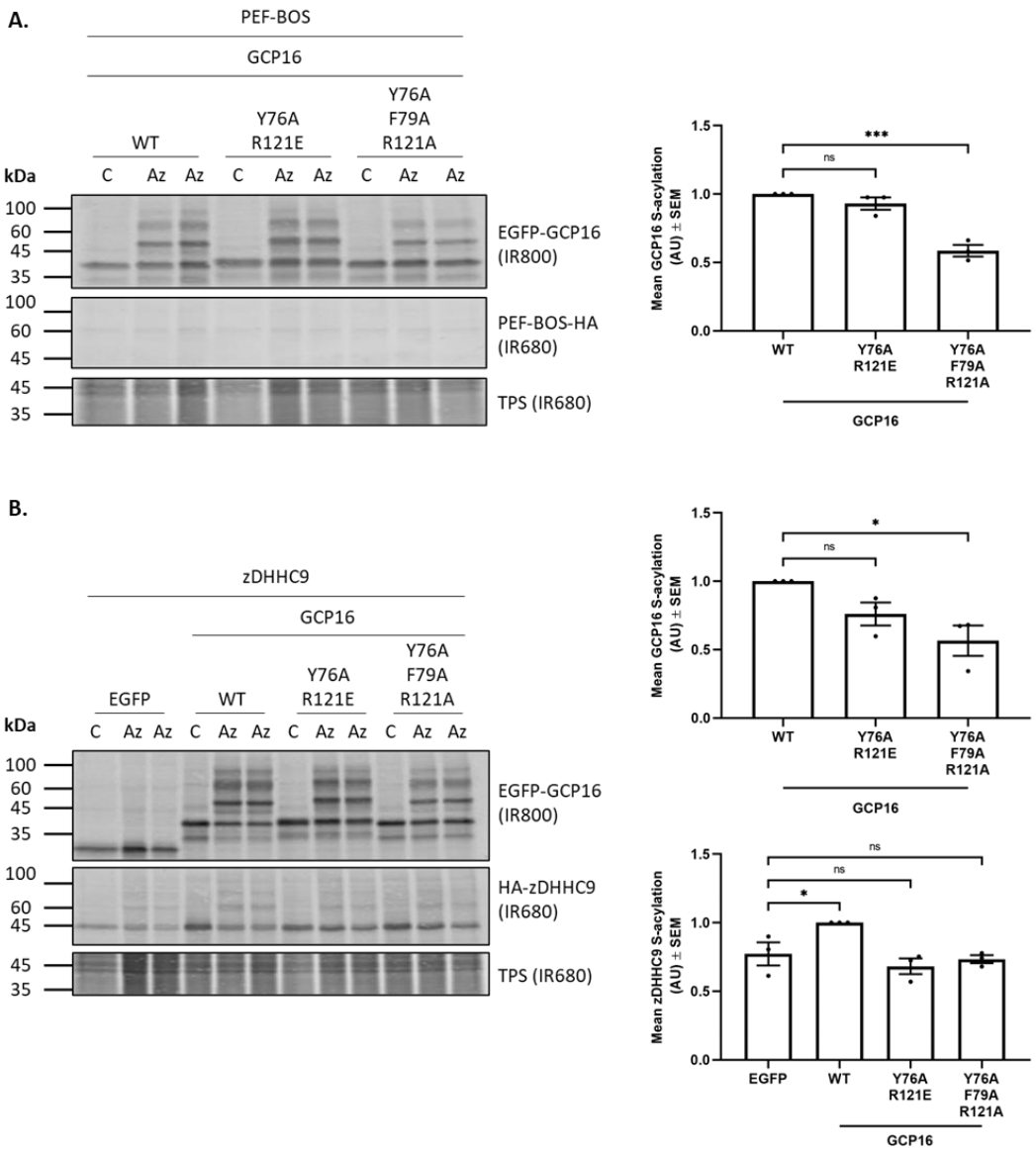
A.
PEF-BOS
GCP16
WT
Y76A R121E
Y76A F79A R121A
kDa
C Az Az C Az Az C Az Az
100
60
45
35
EGFP-GCP16 (IR800)
PEF-BOS-HA (IR680)
TPS (IR680)
Mean GCP16 S-acylation (AU) ± SEM
ns
***
WT
Y76A R121E
Y76A F79A R121A
GCP16
B.
zDHHC9
GCP16
EGFP
WT
Y76A R121E
Y76A F79A R121A
HA-zDHHC9 (IR680)
Mean zDHHC9 S-acylation (AU) ± SEM
*

Figure 4.4 Effects of Y76A/R121E and Y76A/F79A/R121A amino acid substitutions in GCP16 on S-acylation.

HEK293T cells were co-transfected with EGFP-tagged GCP16 WT, Y76A/R121E, or Y76A/F79A/R121A and either ***(A)*** *PEF-BOS-HA or* ***(B)*** *HA-zDHHC9. EGFP was used as a control. Cells were labelled with palmitic acid (C16:0) as a control (C) or palmitic acid azide (Az-C16:0) for 4 hours and were then lysed and clicked using alkyne-mPEG. S-acylation is indicated by band shifts in Az samples. The position of molecular weight markers (kDa) is shown on the left. Quantified data show mean protein S-acylation (± SEM). The S-acylated bands were quantified as a percentage of total expression for each substrate incubated with the palmitic acid azide. The data has been normalised to the highest value of each experiment, which was set to 1. Statistical significance was analysed using an ordinary one-way ANOVA, followed by a Dunnett's multiple comparisons test. *p<0.05, **p<0.01 and ***p<0.001, while ns denotes non-significance, where p>0.05. n = 3, from three independent experiments.*

4.4 S-acylation of GCP16 and zDHHC9 is disrupted by mutations in the N- and C-terminal regions of GCP16

During the course of this work, the cryo-EM structure of the zDHHC9/GCP16 protein complex was reported (Yang *et al.*, 2024). At this point, the focus of the PhD moved away from AlphaFold predictions and onto the published zDHHC9/GCP16 complex. The reported structure identified key residues involved in the zDHHC9/GCP16 interaction, which occur at four main interfaces (Yang *et al.*, 2024). To examine how these interfaces contribute to the reciprocal S-acylation of GCP16 and zDHHC9, alanine substitutions in these regions of GCP16 were generated as shown in Figure 4.5A. HEK293T cells were then co-transfected with HA-zDHHC9, together with EGFP-tagged GCP16 WT, interface mutants 1, 2, 3, 4a/b, 1-4a/b, or EGFP (control). Cells were labelled with either palmitic acid as a control or palmitic acid azide and processed for click chemistry detection of S-acylation using alkyne mPEG (5 kDa). The protein samples were then resolved by SDS-PAGE, while immunoblot analysis allowed for the visualisation of the proteins and the detection of any S-acylation (Figure 4.5B).

Quantified data suggested that alanine substitutions introduced into interface 3 of GCP16 (R16A/Y18A) reduced the S-acylation of GCP16, while S-acylation was completely abolished when alanine substitutions were introduced in interface 4a/b (K11A/F13A/R118A/R121A/E124A). S-acylation of GCP16 was also fully lost when all binding interface regions were mutated in the 1-4a/b construct (K11A/F13A/R16A/Y18A/Y76A/Y86A/R118A/R121A/E124A). Furthermore, none of the binding interface mutants was able to stabilise the S-acylation of zDHHC9 when compared to the EGFP control. In fact, binding interface mutants 4a/b and 1-4a/b appeared to inhibit zDHHC9 basal S-acylation, as the levels detected were significantly lower than those of the EGFP control. Alanine substitutions made in binding interface 1 (Y76A) or interface 2 (Y86A) did not affect the S-acylation of GCP16, but did not significantly increase zDHHC9 S-acylation above the EGFP control levels (Figure 4.5B).

A.

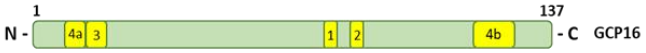

Interface mutants of **GCP16**	
1:	Y76A
2:	Y86A
3:	R16A/Y18A
4a/b:	K11A/F13A/R118A/R121A/E124A
1-4a/b:	K11A/F13A/R16A/Y18A/Y76A/Y86A/R118A/R121A/E124A

B.

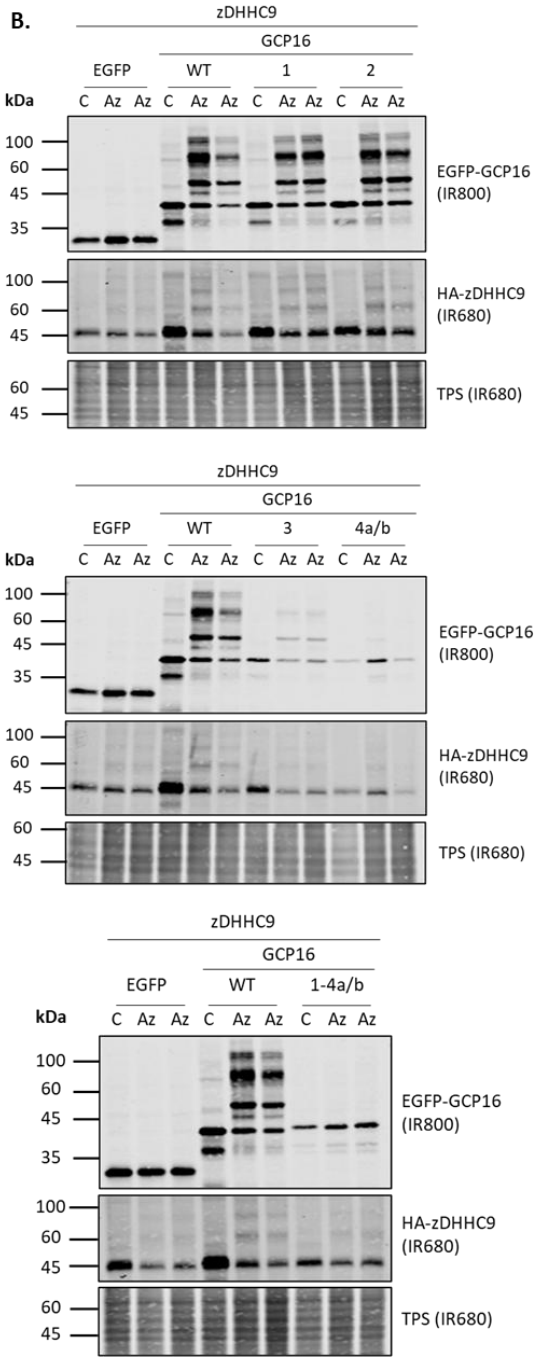

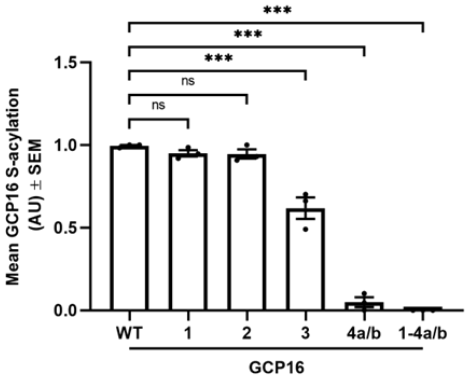

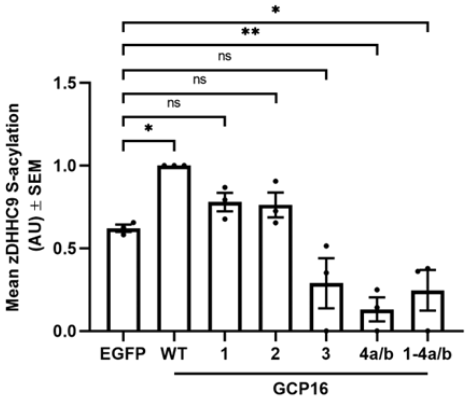

Figure 4.5 S-acylation of GCP16 interface mutant constructs and their effects on stabilising zDHHC9 S-acylation.

(A) *Schematic of the GCP16 interface mutant constructs, designed based on the cryo-EM structure of the zDHHC9/GCP16 protein complex.* ***(B)*** *HEK293T cells were co-transfected with HA-tagged zDHHC9 and EGFP-tagged GCP16 WT, 1, 2, 3, 4a/b, or 1-4a/b. EGFP was used as a control. Cells were labelled with palmitic acid (C16:0) as a control (C) or palmitic acid azide (Az-C16:0) for 4 hours and were then lysed and clicked using alkyne-mPEG. S-acylation is indicated by band shifts in Az samples. The position of molecular weight markers (kDa) is shown on the left. Quantified data show the mean percentage (± SEM) intensity values of the S-acylated proteins. The S-acylated bands were quantified as a percentage of total expression for each protein incubated with the palmitic acid azide. The data has been normalised to the highest value of each experiment, which was set to 1. Statistical significance was analysed using an ordinary one-way ANOVA, followed by a Dunnett's multiple comparisons test. *p<0.05, **p<0.01 and ***p<0.001, while ns denotes non-significance, where p>0.05. n = 3, from three independent experiments.*

4.5 Reciprocal stabilisation of GCP16 and zDHHC9 is disrupted by mutations in the interface binding regions of GCP16

As shown in Chapter 3, there is a reciprocal stabilisation of GCP16 and zDHHC9 when co-expressed in HEK293T cells. To investigate the effects of the binding interface mutations on protein stability, HEK293T cells were co-transfected with PEF-BOS-HA (control) or HA-zDHHC9, along with either EGFP-tagged GCP16 WT, interface mutants 1, 2, 3, 4a/b, 1-4a/b, or EGFP as a control (Figure 4.6A). Cells were then either lysed at 0 hours or incubated with the cycloheximide protein synthesis inhibitor for 8 hours, and protein levels were subsequently examined by immunoblotting (Figure 4.6). Quantified data in Figure 4.6B shows that while interface binding mutants 1, 2, 3, or 4a/b had no significant difference in protein stability compared to GCP16 WT, alanine substitutions of all interfaces in mutant 1-4a/b significantly decreased protein stability with PEF-BOS co-expression.

When GCP16 WT or interface mutants were co-expressed with zDHHC9 (Figure 4.6C), it was evident that GCP16 WT enhanced the stability of zDHHC9, as there was

an increase in the relative percentage expression of zDHHC9 after 8 hours of cycloheximide treatment compared to the EGFP control levels. This stabilisation effect on zDHHC9 was lost with interface mutants 1, 3, 4a/b, and 1-4a/b of GCP16, and these mutants were also less stable than GCP16 WT in the presence of zDHHC9. Interestingly, interface mutant 2 was the only stable GCP16 binding interface mutant, and the only mutant able to stabilise zDHHC9 (Figure 4.6C).

A.

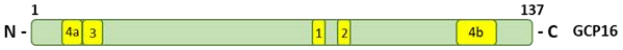

Interface mutants of **GCP16**	
1:	Y76A
2:	Y86A
3:	R16A/Y18A
4a/b:	K11A/F13A/R118A/R121A/E124A
1-4a/b:	K11A/F13A/R16A/Y18A/Y76A/Y86A/R118A/R121A/E124A

B.

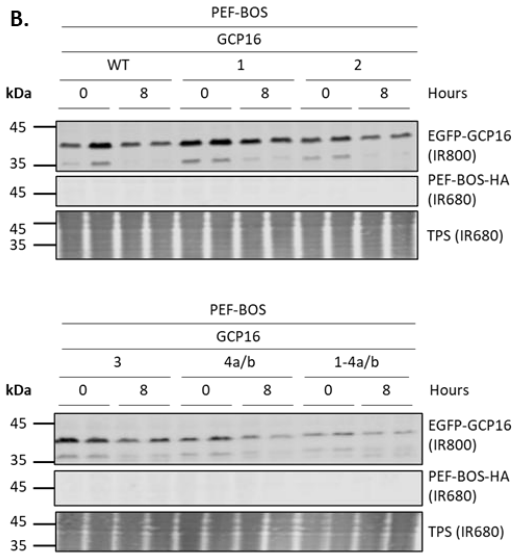

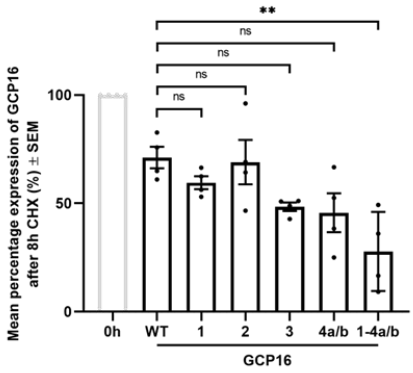

C.

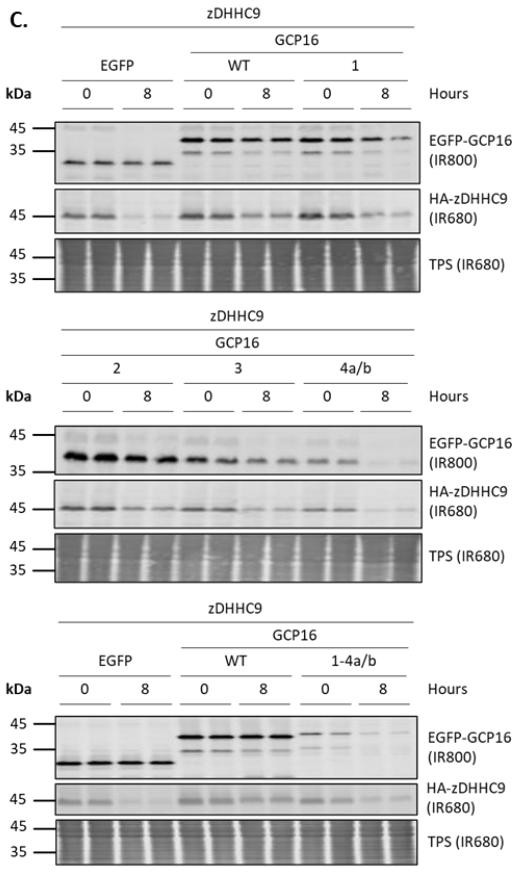

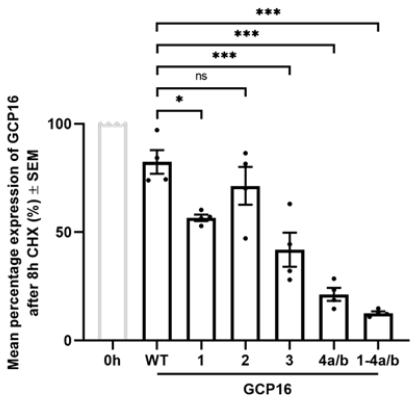

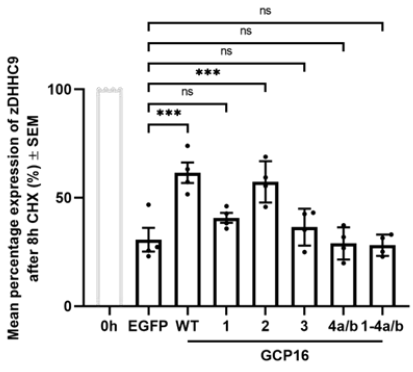

Figure 4.6 Protein stability of GCP16 interface mutant constructs and their effects on stabilising zDHHC9.

(A) *Schematic of the GCP16 interface mutant constructs, designed based on the cryo-EM structure of the zDHHC9/GCP16 protein complex. To investigate protein stability, HEK293T cells were co-transfected with EGFP-tagged GCP16 WT, 1, 2, 3, 4a/b, or 1-4a/b, together with either* ***(B)*** *PEF-BOS HA (empty plasmid control), or* ***(C)*** *HA-tagged zDHHC9. EGFP was used as a control. Lysates were collected at 0 hours or after 8 hours of incubation with 50 µg/ml cycloheximide (CHX). Protein expression levels were detected by immunoblotting. The position of molecular weight markers (kDa) is shown on the left. Quantified data show the mean percentage protein expression (± SEM) after 8 hours of CHX treatment, quantified relative to the corresponding 0-hour value and normalised to the total protein stain levels of each sample. Statistical significance was analysed using an ordinary one-way ANOVA, followed by a Dunnett's multiple comparisons test against GCP16 WT. *p<0.05, **p<0.01 and ***p<0.001, while ns denotes non-significance, where p>0.05. n = 4, from four independent experiments.*

4.6 Further analysis of residues in binding interface 4a/b on the reciprocal S-acylation and stabilisation of GCP16 and zDHHC9

Since we have previously demonstrated the importance of the N- and C-terminal regions of GCP16 in the S-acylation and protein stability of GCP16 and zDHHC9 (Chapter 3), we decided to further examine binding interface 4a/b, which spans both the N- and C-terminal regions of GCP16. Here, an additional mutant construct was generated that contained amino acid substitutions in the C-terminal part of the 4a/b interface (i.e. in region 4b). This mutant was GCP16 R118A/R121A/E124A (Figure 4.7A). Both 4b and 4a/b binding interface mutants of GCP16 were then compared in binding, S-acylation and stabilisation experiments with zDHHC9 to investigate their effects.

To investigate binding to zDHHC9, HEK293T cells were co-transfected with HA-tagged zDHHC9 and either EGFP-tagged GCP16 WT, 4b, 4a/b, or EGFP as a negative control. Cell lysates were incubated with GFP-Trap® Agarose, and immunoprecipitated proteins were examined by immunoblotting (Figure 4.7B). Data

quantification and statistical analysis indicated that GCP16 interface mutant 4b (and 4a/b) did not have any loss in ability to co-immunoprecipitate zDHHC9 compared to WT GCP16 (Figure 4.7B). Although the 4a/b mutant showed enhanced zDHHC9 binding following data quantification, this likely reflects the lower expression levels of this protein (as data is analysed as HA/EGFP signal in IP samples).

To examine the effects on S-acylation, HEK293T cells were co-transfected with HA-zDHHC9, together with EGFP-tagged GCP16 WT, interface mutants 4b, 4a/b, or EGFP as a control. Cells were labelled with either palmitic acid as a control or palmitic acid azide and were then processed for click chemistry detection of S-acylation using alkyne mPEG (5 kDa). Results in Figure 4.7C show that S-acylation of GCP16 was lost when substitutions were introduced in interface mutant 4a/b. In contrast, the amino acid substitutions in mutant 4b did not affect GCP16 S-acylation. Although the 4b interface mutant has no loss of S-acylation, it was nevertheless unable to stabilise the S-acylation of zDHHC9 (Figure 4.7C).

To investigate the effects of the 4b interface mutations on protein stability in mammalian cells, HEK293T cells were co-transfected with PEF-BOS-HA (control) or HA-zDHHC9, along with either EGFP-tagged GCP16 WT, interface mutant 4/b, or EGFP as a control. Cells were then either lysed at 0 hours or incubated with cycloheximide protein synthesis inhibitor for 8 hours, and protein levels were examined by immunoblotting (Figure 4.7D). Quantification of protein expression after 8 hours of protein synthesis inhibition by cycloheximide showed that the stability of binding interface mutant 4b was significantly decreased compared to the wild-type protein when co-expressed with either PEF-BOS or zDHHC9. GCP16 binding interface mutant 4b also failed to stabilise zDHHC9 expression (similarly to mutant 4a/b, as shown in Figure 4.6) (Figure 4.7D).

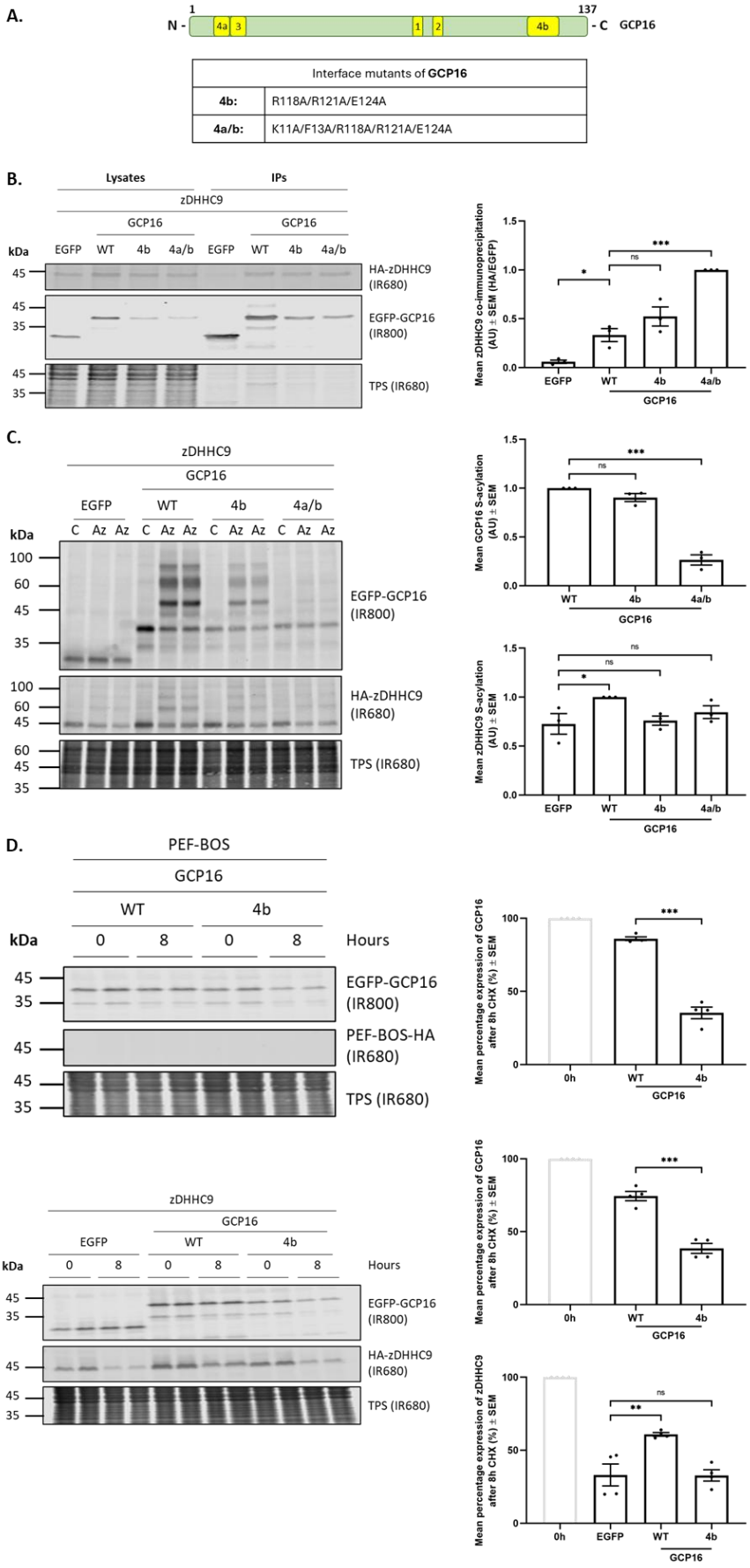
A.
1
137
N -
4a
3
1
2
4b
- C
GCP16
Interface mutants of GCP16
4b:
R118A/R121A/E124A
4a/b:
K11A/F13A/R118A/R121A/E124A
B.
Lysates
IPs
zDHHC9
GCP16
GCP16
kDa
EGFP
WT
4b
4a/b
EGFP
WT
4b
4a/b
HA-zDHHC9 (IR680)
EGFP-GCP16 (IR800)
TPS (IR680)
Mean zDHHC9 co-immunoprecipitation (AU) ± SEM (HA/EGFP)
C.
zDHHC9
GCP16
EGFP
WT
4b
4a/b
C
Az
Az
EGFP-GCP16 (IR800)
HA-zDHHC9 (IR680)
TPS (IR680)
Mean GCP16 S-acylation (AU) ± SEM
Mean zDHHC9 S-acylation (AU) ± SEM
D.
PEF-BOS
GCP16
WT
4b
Hours
PEF-BOS-HA (IR680)
Mean percentage expression of GCP16 after 8h CHX (%) ± SEM
0h
Mean percentage expression of zDHHC9 after 8h CHX (%) ± SEM

Figure 4.7 Effects of a C-terminal binding interface GCP16 mutant on the reciprocal S-acylation and stabilisation of GCP16 and zDHHC9.

(A) *Schematic of the GCP16 interface mutant constructs, designed based on the cryo-EM structure of the zDHHC9/GCP16 protein complex.* ***(B)*** *HEK293T cells were co-transfected with HA-tagged zDHHC9 and EGFP-tagged GCP16 WT, 4b, or 4a/b. The EGFP plasmid was used as a negative control. The EGFP-tagged proteins (IR800) were immunoprecipitated using anti-EGFP beads and detected by immunoblotting, along with co-immunoprecipitated HA-tagged proteins (IR680). Quantified data show the mean (± SEM) of the HA-zDHHC9 (IR680) intensity value divided by the corresponding intensity value of the EGFP signal (IR800) in each IP sample. The data has been normalised to the highest value of each experiment, which was set to 1. Statistical significance was analysed using an ordinary one-way ANOVA, followed by a Dunnett's multiple comparisons test. n = 3, from three independent experiments.* ***(C)*** *To investigate protein S-acylation, HEK293T cells were co-transfected with HA-tagged zDHHC9 and EGFP-tagged GCP16 WT, 4b, or 4a/b. EGFP was used as a control. Cells were labelled with palmitic acid (C16:0) as a control (C) or palmitic acid azide (Az-C16:0) for 4 hours and were then lysed and clicked using alkyne-mPEG. S-acylation is indicated by band shifts in Az samples. Quantified data show the mean percentage (± SEM) intensity values of the S-acylated substrates. The S-acylated bands were quantified as a percentage of total expression for each substrate incubated with the palmitic acid azide. The data has been normalised to the highest value of each experiment, which was set to 1. Statistical significance was analysed using an ordinary one-way ANOVA, followed by a Dunnett's multiple comparisons test. n = 3, from two independent experiments.* ***(D)*** *To investigate protein stability, HEK293T cells were co-transfected with EGFP-tagged GCP16 WT, or 4b and PEF-BOS-HA (empty plasmid control), or HA-tagged zDHHC9. EGFP was used as a control. Lysates were collected at 0 hours or after 8 hours of incubation with 50 µg/ml cycloheximide (CHX). Protein expression levels were detected by immunoblotting. Quantified data show the mean percentage protein expression (± SEM) after 8 hours of CHX treatment, quantified relative to the corresponding 0-hour value and normalised to the total protein stain levels of each sample. Statistical significance was analysed using an unpaired t-test, or an ordinary one-way ANOVA, followed by a Dunnett's multiple comparisons test where appropriate. n = 4, from four independent experiments. *p<0.05, **p<0.01 and ***p<0.001, while ns denotes non-significance, where p>0.05. The position of molecular weight markers (kDa) is shown on the left.*

4.7 A zDHHC9 binding interface mutant disrupts reciprocal S-acylation and stabilisation of GCP16 and zDHHC9

The analyses to this point have all focused on binding interface mutants of GCP16. To confirm the key findings, we also examined a mutant of zDHHC9 that had amino acid substitutions in all four binding interfaces. This mutant (1-4a/b; R85A/D100A/E101A/F104A/F129A/P150A/E163A/Y183A/P292A) is shown in Figure 4.8A. HEK293T cells were co-transfected with EGFP as a control, or EGFP-GCP16, along with either HA-zDHHC9 WT, HA-zDHHC9 1-4a/b, or PEF-BOS-HA as a control. Cells were labelled with either palmitic acid or palmitic acid azide and processed for click chemistry detection of S-acylation using alkyne mPEG (5 kDa). Results in Figure 4.8B show that GCP16 S-acylation by zDHHC9 interface mutant 1-4a/b was significantly reduced compared to that seen with zDHHC9 WT. Moreover, the reciprocal effect of GCP16 on the S-acylation of zDHHC9 was also lost with this zDHHC9 interface mutant 1-4a/b (Figure 4.8C).

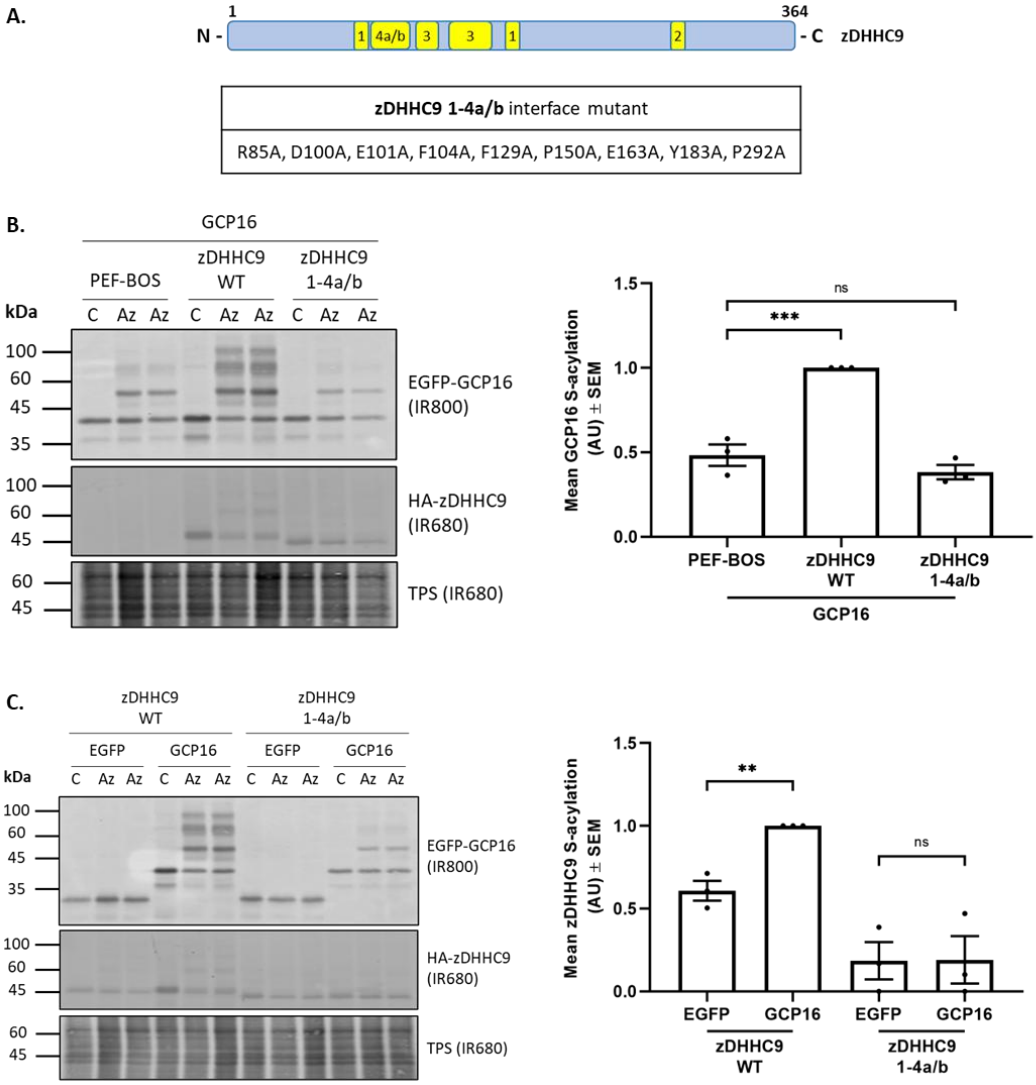
A.
1
364
N -
1
4a/b
3
3
1
2
- C
zDHHC9
zDHHC9 1-4a/b interface mutant
R85A, D100A, E101A, F104A, F129A, P150A, E163A, Y183A, P292A
B.
GCP16
PEF-BOS
zDHHC9 WT
zDHHC9 1-4a/b
kDa
C Az Az C Az Az C Az Az
100
60
45
35
EGFP-GCP16 (IR800)
HA-zDHHC9 (IR680)
TPS (IR680)
Mean GCP16 S-acylation (AU) ± SEM
ns
***
PEF-BOS
zDHHC9 WT
zDHHC9 1-4a/b
GCP16
C.
zDHHC9 WT
zDHHC9 1-4a/b
EGFP
GCP16
Mean zDHHC9 S-acylation (AU) ± SEM
**
ns
EGFP
GCP16
zDHHC9 WT
zDHHC9 1-4a/b

Figure 4.8 Alanine substitutions in the binding interfaces of zDHHC9 disrupt the S-acylation of zDHHC9 and GCP16.

(A) *Schematic of the zDHHC9 interface mutant construct, designed based on the cryo-EM structure of the zDHHC9/GCP16 protein complex.* ***(B)*** *HEK293T cells were co-transfected with HA-zDHHC9 WT or HA-zDHHC9 1-4a/b interface mutant, and EGFP-GCP16. The PEF-BOS-HA and EGFP empty plasmids were used as controls. Cells were labelled with palmitic acid (C16:0) as a control (C) or palmitic acid azide (Az-C16:0) for 4 hours and were then lysed and clicked using alkyne-mPEG. S-acylation is indicated by band shifts in Az samples. The position of molecular weight markers (kDa) is shown on the left. Quantified data show the mean percentage (± SEM) intensity values of the S-acylated substrates. The S-acylated bands were quantified as a percentage of total expression for each substrate incubated with the palmitic acid azide. The data has been normalised to the highest value of each experiment, which was set to 1. Statistical significance was analysed using an ordinary one-way ANOVA, followed by a Dunnett's multiple comparisons test, or an unpaired t-test where appropriate. *p<0.05, **p<0.01 and ***p<0.001, while ns denotes non-significance, where p>0.05. n = 3, from three independent experiments.*

Subsequently, we studied the effect of zDHHC9 interface mutant 1-4a/b (Figure 4.9A) on the reciprocal stabilisation of GCP16 and zDHHC9 in a cycloheximide experiment, in mammalian cells. HEK293T cells were co-transfected with EGFP as a control, or EGFP-GCP16, along with either HA-zDHHC9 WT, HA-zDHHC9 1-4a/b, or PEF-BOS-HA as a control. Cells were then either lysed at 0 hours or incubated with cycloheximide protein synthesis inhibitor for 8 hours and protein expression was examined by immunoblotting (Figure 4.9).

The results showed that GCP16 was significantly less stable in the presence of zDHHC9 1-4a/b, compared to zDHHC9 WT co-expression. In this experiment, although zDHHC9 WT co-expression increased the stability of GCP16, the effect was not statistically different than the control. Finally, the zDHHC9 1-4a/b was not stabilised by co-expression of GCP16, in contrast to zDHHC9 WT, which showed a significant increase in protein stability (Figure 4.9B). Thus, overall, the results with the zDHHC9 1-4a/b mutant confirm the findings with the corresponding GCP16 mutants.

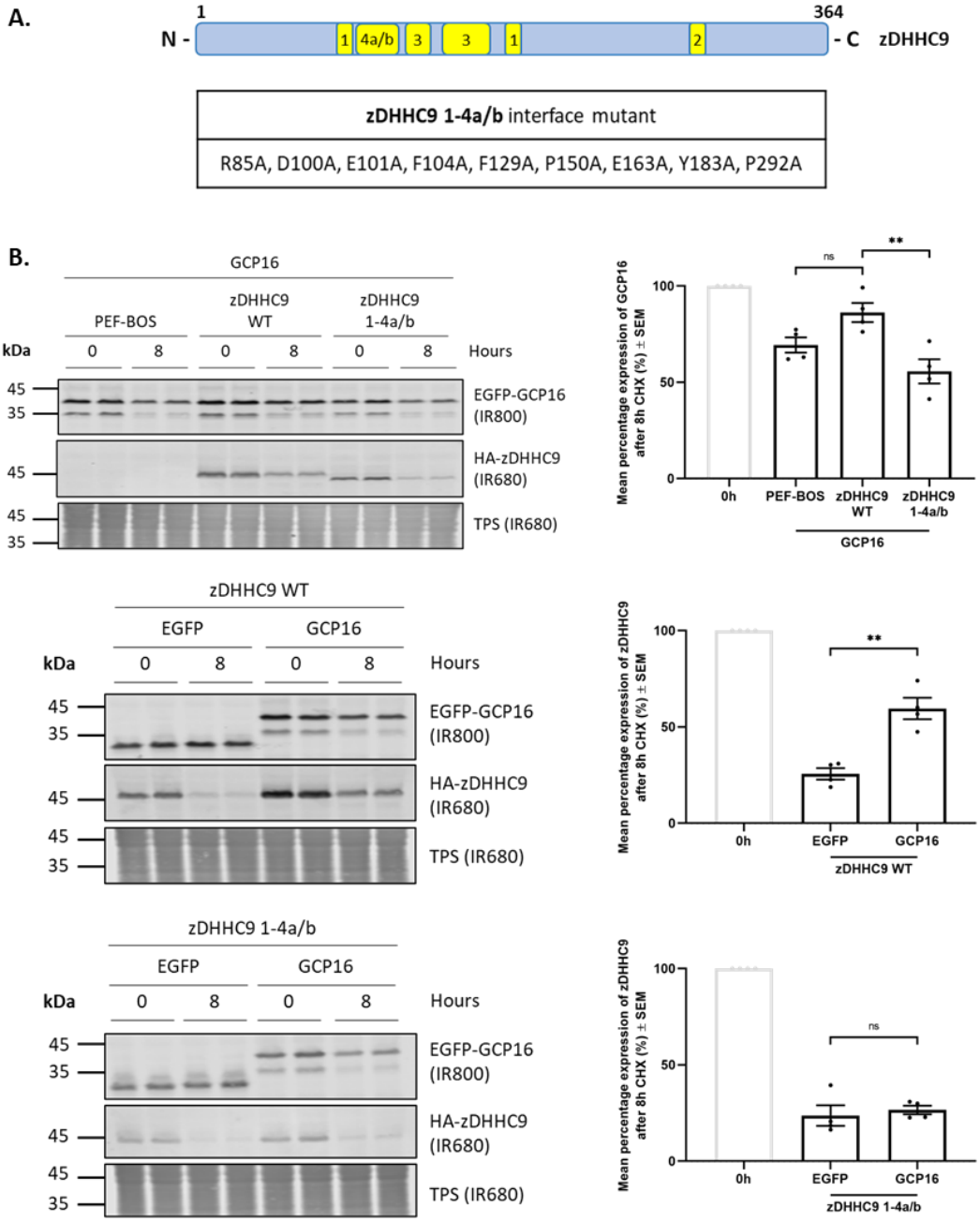
A.
1
364
N -
1
4a/b
3
3
1
2
- C
zDHHC9
zDHHC9 1-4a/b interface mutant
R85A, D100A, E101A, F104A, F129A, P150A, E163A, Y183A, P292A
B.
GCP16
PEF-BOS
zDHHC9 WT
zDHHC9 1-4a/b
kDa
0
8
0
8
0
8
Hours
45
35
EGFP-GCP16 (IR800)
HA-zDHHC9 (IR680)
TPS (IR680)
Mean percentage expression of GCP16 after 8h CHX (%) ± SEM
ns
**
0h
PEF-BOS
zDHHC9 WT
zDHHC9 1-4a/b
GCP16
zDHHC9 WT
EGFP
GCP16
Mean percentage expression of zDHHC9 after 8h CHX (%) ± SEM
zDHHC9 1-4a/b

Figure 4.9 The zDHHC9 interface mutant disrupts the reciprocal stabilisation of GCP16 and zDHHC9.

(A) *Schematic of the zDHHC9 interface mutant construct, designed based on the cryo-EM structure of the zDHHC9/GCP16 protein complex.* ***(B)*** *To investigate protein stability, HEK293T cells were co-transfected with PEF-BOS-HA (empty plasmid control), HA-zDHHC9 WT, or HA-zDHHC9 1-4a/b, along with EGFP-GCP16, or EGFP as a control. Lysates were collected at 0 hours, or after 8 hours of incubation with 50 µg/ml cycloheximide (CHX). Protein expression levels were detected by immunoblotting. The position of molecular weight markers (kDa) is shown on the left. Quantified data show the mean percentage protein expression (± SEM) after 8 hours of CHX treatment, quantified relative to the corresponding 0-hour value and normalised to the total protein stain levels of each sample. Statistical significance was analysed using an ordinary one-way ANOVA, followed by a Dunnett's multiple comparisons test, or an unpaired t-test where appropriate. *p<0.05, **p<0.01 and ***p<0.001, while ns denotes non-significance, where p>0.05. n = 4, from three independent experiments.*

4.8 Stabilisation of GCP16 by zDHHC9 is dependent on the catalytic activity of the enzyme

The data presented above have clearly shown the importance of specific binding interfaces for the reciprocal S-acylation and stabilisation of GCP16 and zDHHC9. However, one aspect that is unclear at this stage is whether the stabilisation of GCP16 by zDHHC9 is due to protein complex formation or linked to the S-acylation of GCP16 by zDHHC9. This is an important point as S-acylation is commonly associated with an increase in protein stability (Chamberlain and Shipston, 2015). To investigate this question, HEK293T cells were co-transfected with EGFP-tagged GCP16, together with either PEF-BOS-HA (control), HA-tagged zDHHC9 (wild-type protein), or the inactive mutant zDHHA9 (in which the catalytic cysteine in the DHHC motif of the enzyme is replaced by an alanine). Cells were then either lysed at 0 hours or incubated with cycloheximide for 8 hours, and protein expression was examined by immunoblotting.

The quantified data in Figure 4.10B demonstrate that, in contrast to the wild-type enzyme, the catalytically inactive mutant zDHHA9 was unable to stabilise GCP16, as the expression levels detected after zDHHA9 co-expression were similar to those seen with the PEF-BOS control. This observation suggests that the increase in stability for GCP16 depends on the catalytic activity of zDHHC9.

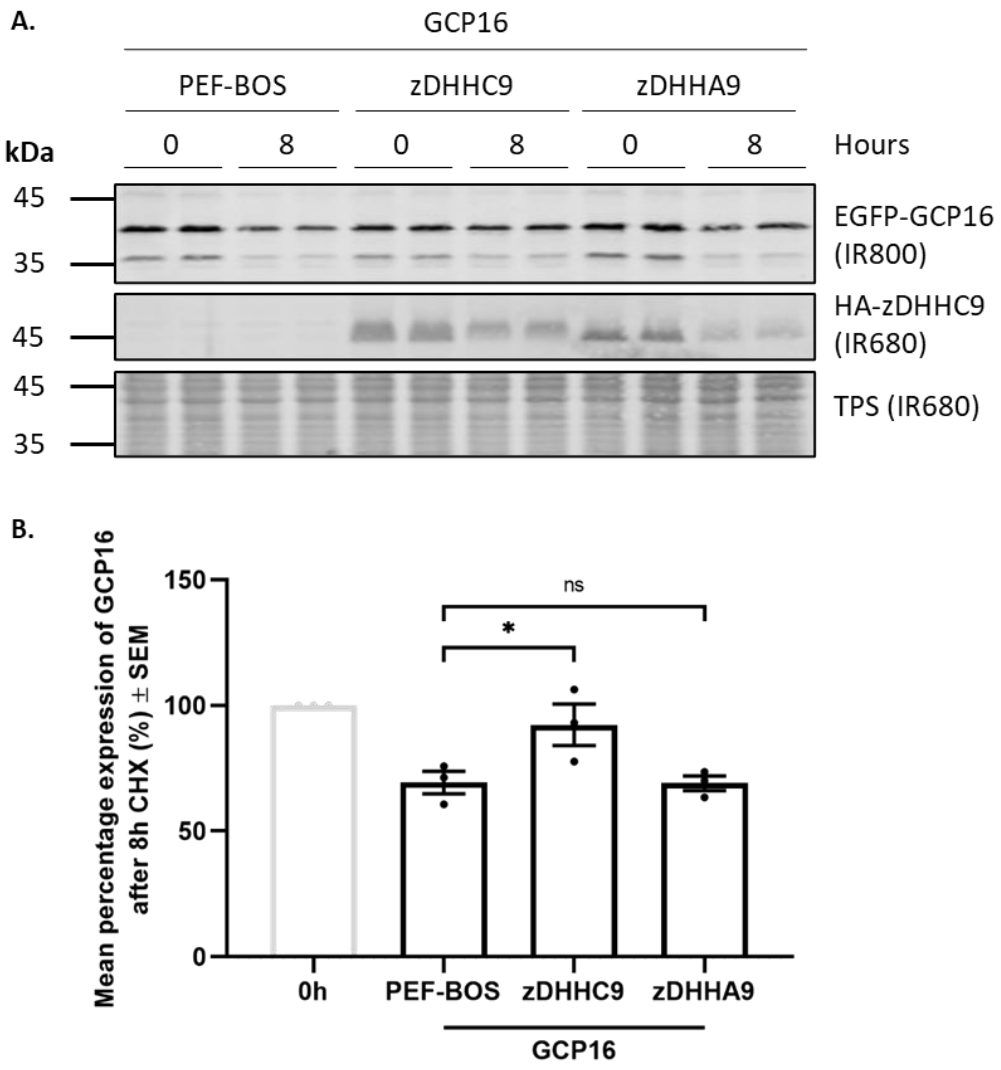

Figure 4.10 The zDHHA9 catalytically inactive mutant cannot stabilise GCP16.

(A) *HEK293T cells were co-transfected with EGFP-tagged GCP16, along with either PEF-BOS-HA (empty plasmid control), HA-zDHHC9, or HA-zDHHA9. Lysates were collected at 0 hours, or after 8 hours of incubation with 50 µg/ml cycloheximide (CHX). Protein expression levels were detected by immunoblotting. The position of molecular weight markers (kDa) is shown on the left. Quantified data show the mean percentage protein expression (± SEM) after 8 hours of CHX treatment, quantified relative to the corresponding 0-hour value and normalised to the total protein stain levels of each sample. Statistical significance was analysed using an ordinary one-way ANOVA, followed by a Dunnett's multiple comparisons test. *p<0.05, **p<0.01 and ***p<0.001, while ns denotes non-significance, where p>0.05. n = 3, from two independent experiments.*

4.9 Mutation of the GCP16 binding interface sites does not disrupt the co-immunoprecipitation of zDHHC9

After exploring the effects of mutating the binding interface sites in GCP16 or zDHHC9 on protein S-acylation and stability, the ability of the GCP16 interface mutants to interact with zDHHC9 was examined in a co-immunoprecipitation experiment. HEK293T cells were co-transfected with HA-zDHHC9, together with EGFP-tagged GCP16 WT, interface mutants 1, 2, 3, 4a/b, 1-4a/b, or EGFP as a control. Cell lysates were incubated with GFP-Trap® Agarose beads, and eluted proteins were examined by immunoblotting (Figure 4.11B). The results show that zDHHC9 was co-immunoprecipitated with all GCP16 interface mutant constructs, including 1-4a/b, which has all the binding interfaces disrupted. No zDHHC9 co-immunoprecipitation was seen with the EGFP negative control (Figure 4.11B). Statistical analysis in Figure 4.11C suggested that GCP16 interface mutants 4a/b and 1-4a/b had increased levels of zDHHC9 co-immunoprecipitation, but this is likely affected by the much lower expression levels of these two constructs, compared with GCP16 WT, as data is quantified as HA/EGFP signal intensity in the immunoprecipitation samples. The incredibly high values of 4a/b and 1-4a/b also influenced the statistical comparison of zDHHC9 co-immunoprecipitation between GCP16 WT and EGFP control.

A.

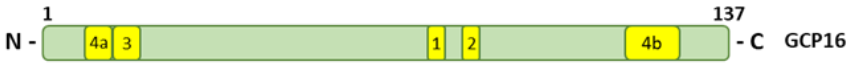

Interface mutants of **GCP16**	
1:	Y76A
2:	Y86A
3:	R16A/Y18A
4a/b:	K11A/F13A/R118A/R121A/E124A
1-4a/b:	K11A/F13A/R16A/Y18A/Y76A/Y86A/R118A/R121A/E124A

B.

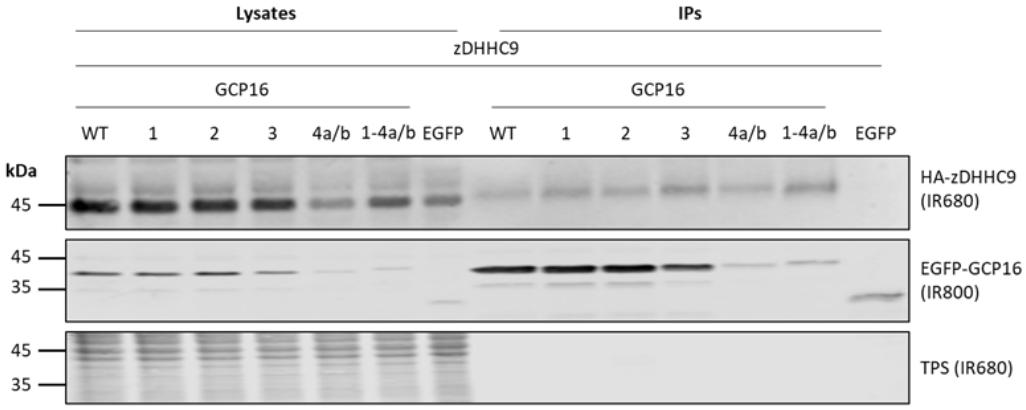

C.

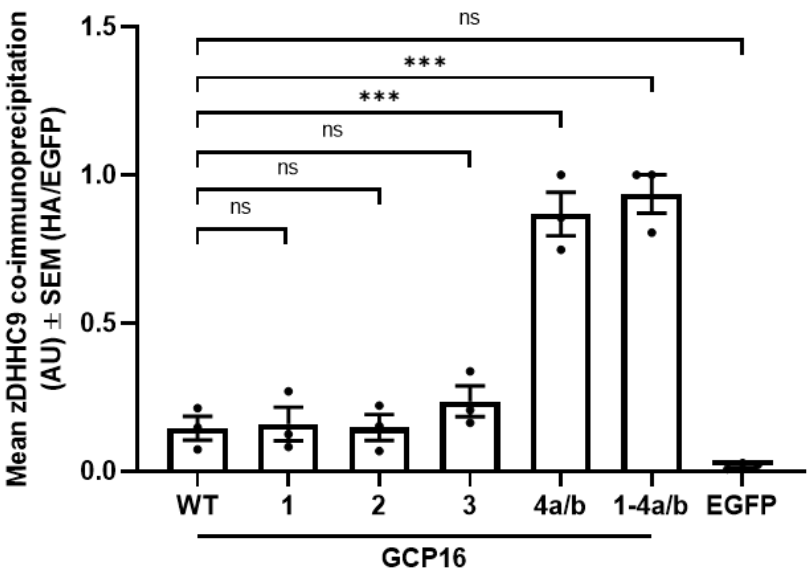

Figure 4.11 Mutation of the GCP16 binding interface sites does not disrupt co-immunoprecipitation of zDHHC9.

(A) *Schematic of the GCP16 interface mutant constructs, designed based on the cryo-EM structure of the zDHHC9/GCP16 protein complex.* ***(B)*** *HEK293T cells were co-transfected with HA-tagged zDHHC9 and EGFP-tagged GCP16 WT, 1, 2, 3, 4a/b, or 1-4a/b. The EGFP plasmid was used as a negative control. The EGFP-tagged proteins (IR800) were immunoprecipitated using anti-EGFP beads and detected by immunoblotting, along with co-immunoprecipitated HA-tagged proteins (IR680). The position of molecular weight markers (kDa) is shown on the left.* ***(C)*** *Quantified data show the mean (± SEM) of the HA-zDHHC9 (IR680) intensity value divided by the corresponding intensity value of the EGFP signal (IR800) in each IP sample. The data has been normalised to the highest value of each experiment, which was set to 1. Statistical significance was analysed using an ordinary one-way ANOVA, followed by a Dunnett's multiple comparisons test. *p<0.05, **p<0.01 and ***p<0.001, while ns denotes non-significance, where p>0.05. n = 3, from two independent experiments.*

4.10 Investigating the interaction between GCP16 and zDHHC9 using different approaches

The results of the immunoprecipitation experiments with the binding interface mutants of GCP16 were somewhat unexpected. Although these results may suggest that there is an alternative mode of binding between GCP16 and zDHHC9, additional immunoprecipitation experiments were undertaken under more stringent conditions to confirm the previoius findings. For this, four different wash buffers were compared, which contained either 1% Triton X-100, 1% Triton X-100 with 250 mM NaCl, 1% Triton X-100 with 500 mM NaCl, or 1% NP40. HEK293T cells were co-transfected with HA-zDHHC9, together with EGFP-tagged GCP16 WT, 1-4a/b, or EGFP as a control. Cell lysates were incubated with GFP-Trap® Agarose beads, washed three times in the buffers above and eluted in 0.1 M glycine pH 2. Immunoblotting analysis of the recovered samples indicated that binding of zDHHC9 to wild-type or 1-4a/b GCP16 was not disrupted under any of the conditions tested, even when high salt conditions were used (Figure 4.12A).

In a second experiment, we treated transfected cells with the proteasome inhibitor MG132 (Figure 4.12B) to prevent excessive degradation of interface mutants 3 and 4a/b. This was done in an attempt to equalise expression levels of these mutants with GCP16 WT and therefore to allow for a more direct quantitative comparison of zDHHC9 binding. After transfection, cells were incubated with 10 μM of MG132 for approximately 16 hours, and cell lysates were then incubated with GFP-Trap® Agarose beads, and the eluted proteins were examined by immunoblotting. Quantified data showed that zDHHC9 was co-immunoprecipitated with wild-type GCP16 and both interface mutants 3 and 4a/b, whereas there was no binding of the EGFP negative control. The expression of 4a/b GCP16 was still lower than GCP16 WT, which resulted in an increase in zDHHC9 co-immunoprecipitation levels when the data were quantified. GCP16 binding interface mutant 3 also showed higher zDHHC9 co-immunoprecipitation levels compared to GCP16 WT, while its expression level was similar.

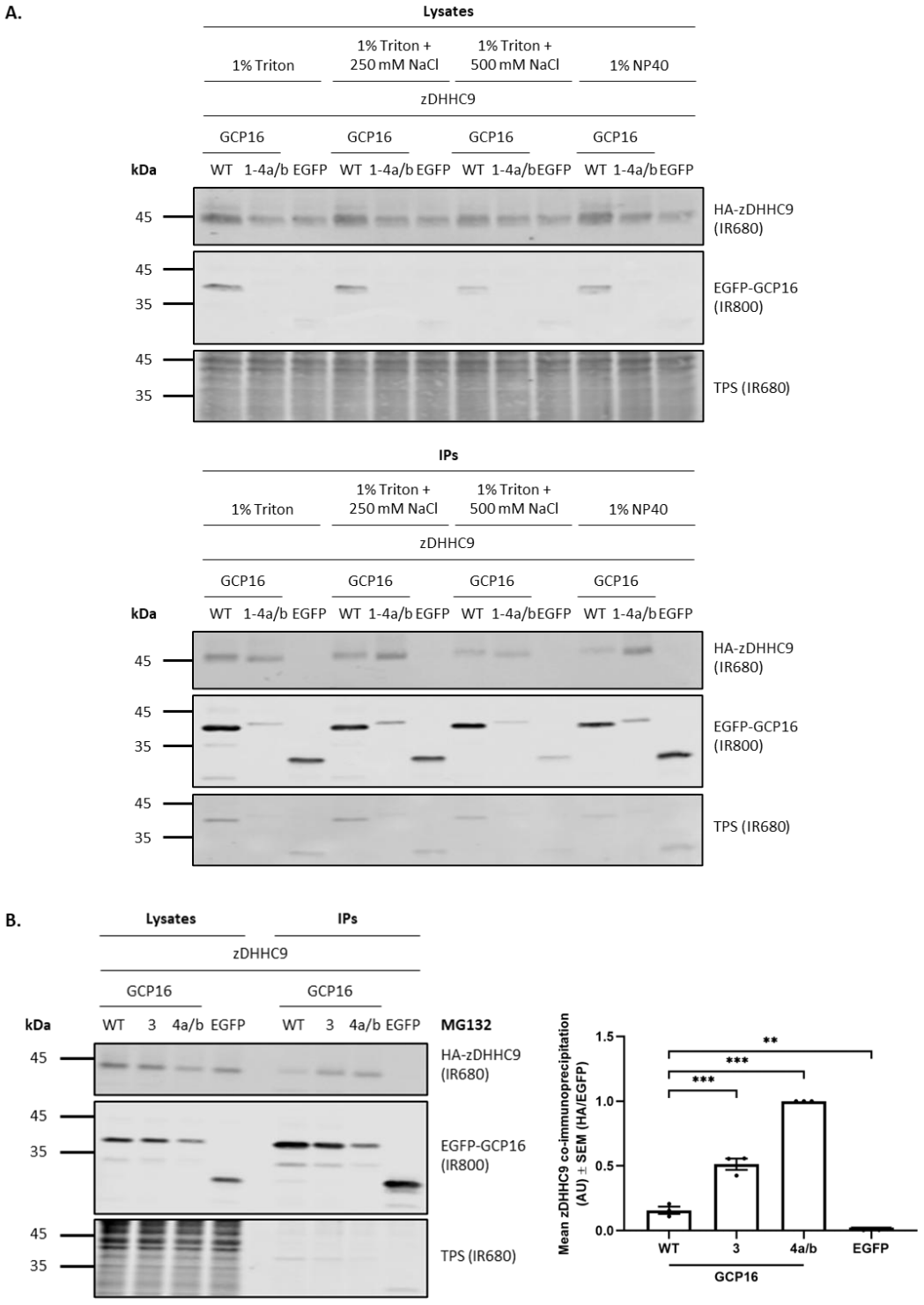
A.
Lysates
1% Triton
1% Triton + 250 mM NaCl
1% Triton + 500 mM NaCl
1% NP40
zDHHC9
GCP16
kDa
WT 1-4a/b EGFP
45
35
HA-zDHHC9 (IR680)
EGFP-GCP16 (IR800)
TPS (IR680)
IPs
B.
Lysates
IPs
zDHHC9
GCP16
kDa
WT 3 4a/b EGFP
MG132
HA-zDHHC9 (IR680)
EGFP-GCP16 (IR800)
TPS (IR680)
Mean zDHHC9 co-immunoprecipitation (AU) ± SEM (HA/EGFP)
1.5
1.0
0.5
0.0
**
***
***
WT
3
4a/b
EGFP
GCP16

Figure 4.12 Analysis of zDHHC9/GCP16 co-immunoprecipitation using different buffer conditions and when equalising GCP16 expression with MG132.

(A) *HEK293T cells were co-transfected with HA-tagged zDHHC9 and EGFP-tagged GCP16 WT, 1-4a/b, or EGFP as a control. The EGFP-tagged proteins (IR800) were immunoprecipitated using anti-EGFP beads along with co-immunoprecipitated HA-tagged proteins (IR680) and were washed three times with either 1% Triton X-100, 1% Triton X-100 with 250 mM NaCl, 1% Triton X-100 with 500 mM NaCl, or 1% NP40. Subsequently, the samples were eluted with 50 µl of 0.1 M glycine (pH 2) for 30 minutes, rotating. The samples were then centrifudged and the supernatant was retrieved in a new Eppendorf and 17 µl of 4x SDS with 100 mM DTT was added to elute the captured EGFP-tagged proteins and any co-immunoprecipitated zDHHC9, along with 1 µl of saturated Tris to raise the pH. Proteins were then and detected by immunoblotting.* ***(B)*** *HEK293T cells were co-transfected with HA-tagged zDHHC9, and EGFP-tagged GCP16 WT, 3 or 4a/b, or EGFP as a control. After transfection, the cells were incubated with 10 µM of MG132 for 16 hours. The EGFP-tagged proteins (IR800) were immunoprecipitated using anti-EGFP beads and detected by immunoblotting, along with co-immunoprecipitated HA-tagged proteins (IR680). Quantified data show the mean (± SEM) of the HA-zDHHC9 (IR680) intensity value divided by the corresponding intensity value of the EGFP signal (IR800) in each IP sample. The data has been normalised to the highest value of each experiment, which was set to 1. Statistical significance was analysed using an ordinary one-way ANOVA, followed by a Dunnett's multiple comparisons test. *p<0.05, **p<0.01 and ***p<0.001, while ns denotes non-significance, where p>0.05. n = 3, from two independent experiments. The position of molecular weight markers (kDa) is shown on the left.*

4.11 Mutation of the binding interfaces in both GCP16 and zDHHC9 does not disrupt co-immunoprecipitation

Since all our previous efforts to disrupt binding to zDHHC9 using GCP16 binding interface mutants have failed, the interaction of the GCP16 1-4a/b mutant with a zDHHC9 1-4a/b binding interface mutant was examined in another co-immunoprecipitation experiment. This experiment ensured that all identified binding interface sites in both proteins, based on the cryo-EM protein structure, were mutated.

HEK293T cells were co-transfected with either HA-tagged zDHHC9 WT, or zDHHC9 1-4a/b, together with EGFP-tagged GCP16 WT, 1-4a/b, or EGFP as a negative control. Cell lysates were incubated with GFP-Trap® Agarose beads, and the eluted proteins were examined by immunoblotting. As seen in Figure 4.13B, both GCP16 WT and GCP161-4a/b were able to co-immunoprecipitate zDHHC9 WT, as well as the zDHHC9 1-4a/b mutant. No binding was detected with the EGFP negative control. Quantified data in Figure 4.13C shows that GCP16 WT can bind to zDHHC9 1-4a/b to a similar extent as to zDHHC9 WT. GCP16 mutant 1-4a/b showed higher levels of zDHHC9 WT and zDHHC9 1-4a/b co-immunoprecipitation, and again, this was presumably due to its lower protein expression.

A.

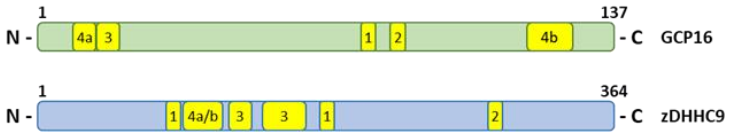

zDHHC9 1-4a/b interface mutant
R85A, D100A, E101A, F104A, F129A, P150A, E163A, Y183A, P292A

Interactions between GCP16 and zDHHC9 interfaces		
Interface	**GCP16 residues**	**zDHHC9 residues**
1:	Y76	R85/Y183
2:	Y86	P292
3:	R16/Y18	F129/P150/E163
4a:	K11/F13	D100/F104
4b:	R118/R121/E124	E101

B.

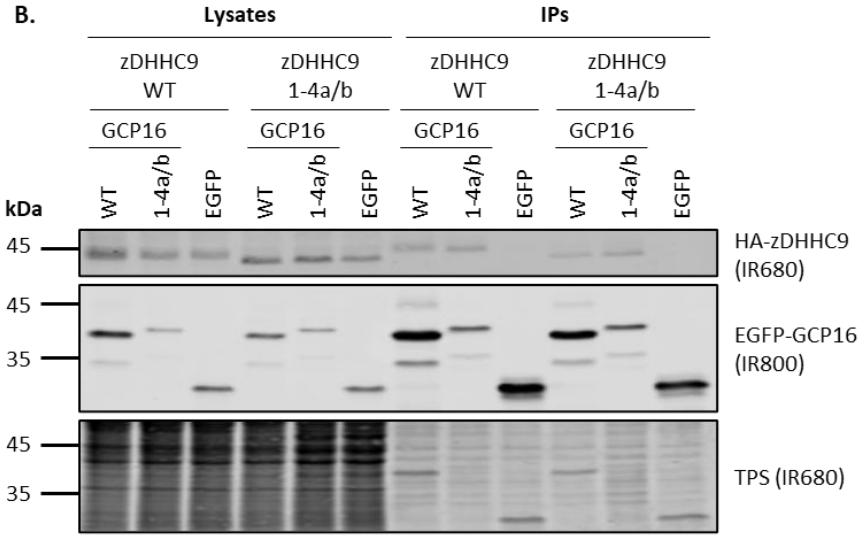

C.

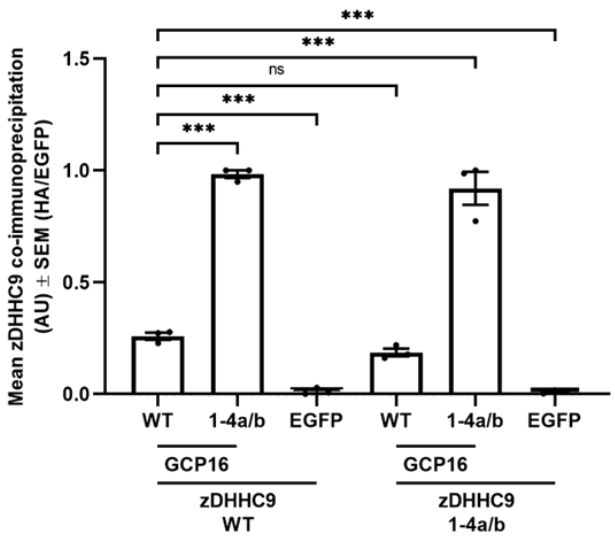

Figure 4.13 Mutation of the binding interface sites in both GCP16 and zDHHC9 does not disrupt binding.

(A) *Schematic of the GCP16 and zDHHC9 interface mutant constructs, highlighting the interacting residues of each binding interface, designed based on the cryo-EM structure of the zDHHC9/GCP16 protein complex.* ***(B)*** *HEK293T cells were co-transfected with HA-tagged zDHHC9 WT or zDHHC9 1-4a/b interface mutant, and EGFP-tagged GCP16 WT, or 1-4a/b. The EGFP plasmid was used as a negative control. The EGFP-tagged proteins (IR800) were immunoprecipitated using anti-EGFP beads and detected by immunoblotting, along with co-immunoprecipitated HA-tagged proteins (IR680). The position of molecular weight markers (kDa) is shown on the left.* ***(C)*** *Quantified data show the mean (± SEM) of the HA-zDHHC9 (IR680) intensity value divided by the corresponding intensity value of the EGFP signal (IR800) in each IP sample. The data has been normalised to the highest value of each experiment, which was set to 1. Statistical significance was analysed using an ordinary one-way ANOVA, followed by a Dunnett's multiple comparisons test. *p<0.05, **p<0.01 and ***p<0.001, while ns denotes non-significance, where p>0.05. n = 3, from three independent experiments.*

4.12 AlphaFold protein structure prediction of wild-type and mutant zDHHC9/GCP16 protein complex

To further elucidate the results from Figure 4.13, which suggested that formation of the zDHHC9/GCP16 complex is not disturbed when all binding interfaces are mutated in both proteins, AphaFold was used to visualise the mutant zDHHC9/GCP16 complex and compare it to that of the wild-type proteins. Initial modelling of wild-type and mutant zDHHC9/GCP16 was conducted by Dr Kimon Lemonidis (University of Glasgow) using AlphaFold3 (Jumper *et al*., 2021, Varadi *et al*., 2022, Abramson *et al*., 2024, Varadi *et al*., 2024).

Surprisingly, the 1-4a/b interface mutant complex of zDHHC9/GCP16 was predicted to interact in a similar way as the wild-type complex, which was in agreement with our experimental data (Figure 4.13). AlphaFold predicted just some slight conformational changes between the two models. The main difference was in the overall confidence of the models, which is reflected in the predicted aligned error (PAE) plots, as well as

the predicted template modelling scores (pTM) and in the interface predicted template modelling scores (ipTM). PAE is a measure of confidence in the relative position of two residues within the predicted structure, measured in Ångströms (Å). It is an indication of how well packed the domains are and if their relative placement in the predicted structure is correct. pTM and ipTM are measures of evaluating the accuracy of the prediction and how confident AlphaFold is regarding the whole structure and the interactions between different subunits forming the protein complex, respectively. For pTM, scores above 0.5 mean that the overall prediction might be similar to the true structure. For ipTM, scores higher than 0.8 represent confident predictions, while anything below 0.6 is considered a failed prediction. ipTM values between 0.6 and 0.8 reflect uncertainty around the prediction.

The PAE plot for the two models seemed similar, but the 1-4a/b interface mutant zDHHC9/GCP16 prediction model showed higher expected error. The pTM scores of both wild-type and mutant zDHHC9/GCP16 complexes were above 0.5, with that of the WT complex being higher than that of the mutant complex, at 0.77 and 0.68, respectively. The ipTM score of WT zDHHC9/GCP16 was 0.81, suggesting strong confidence in the prediction regarding the relative positions of the subunits forming the protein complex. However, the ipTM score of the 1-4a/b interface mutant zDHHC9/GCP16 complex was 0.54, suggesting that the predicted position of the subunits could be wrong. Notably, the mutant complex also had more regions with low per-residue confidence score (pLDDT), which can negatively affect the ipTM score, even if the overall structure prediction is accurate (Figure 4.14).

zDHHC9 WT / GCP16 WT

zDHHC9 1-4a/b / GCP16 1-4a/b

ipTM = 0.81 pTM = 0.77

ipTM = 0.54 pTM = 0.68

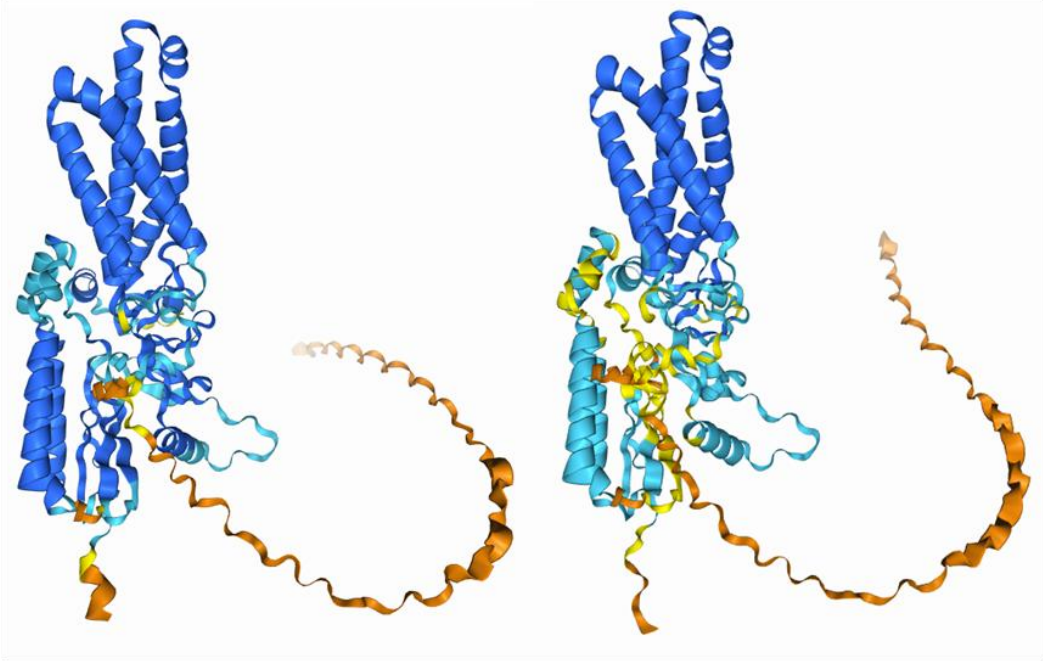

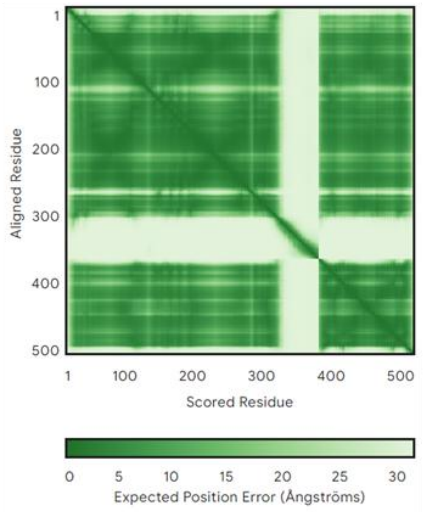

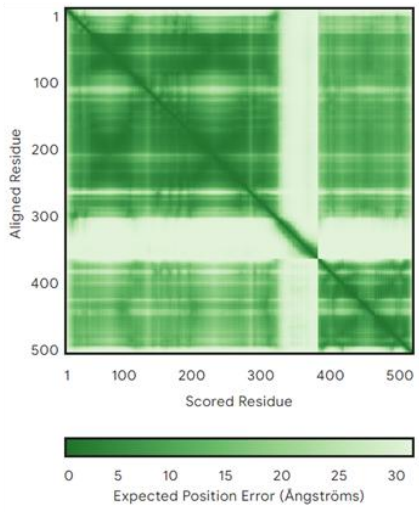

Figure 4.14 AlphaFold protein structure prediction of wild-type and mutant zDHHC9/GCP16 protein complex.

Protein structure predictions of mouse zDHHC9 (UniProt ID: P59268) interacting with human GCP16 (UniProt ID: Q7Z5G4), and mouse zDHHC9 binding interface mutant 1-4a/b, interacting with human GCP16 binding interface mutant 1-4a/b, adapted from outputs generated using AlphaFold3 by DeepMind and EMBL-EBI (Jumper et al., 2021, Varadi et al., 2022, Abramson et al., 2024, Varadi et al., 2024). For every prediction model, AlphaFold produces a predicted alignment error (PAE) plot, pTM and ipTM scores, and a per-residue confidence score (pLDDT) between 0 and 100 that is illustrated with the use of a coloured scale. Regions with very low pLDDT (< 50) may be unstructured in isolation.

4.13 Analysis of the interaction between GCP16 binding interface mutants containing charged amino acid substitutions and zDHHC9

After inspection of the protein structure prediction for wild-type zDHHC9/GCP16 complex, we noticed that the binding interfaces were predominantly hydrophobic and likely supported by additional weaker interactions of neighbouring residues. Hence, it might be possible that the alanine substitutions we introduced, although weakening the overall interaction to a certain extent, were still able to preserve the hydrophobicity required for complex formation. Therefore, we decided to replace key residues in the zDHHC9-binding interfaces of GCP16 with charged amino acids, aspartic acid (Asp, D) or lysine (Lys, K), to produce more disruptive GCP16 mutants.

While introducing either charge may work in disrupting the hydrophobicity of the binding interfaces, by examining the overall charge of zDHHC9 where GCP16 binds to, we concluded that replacing interacting residues in the amino acid region 70-90 of GCP16 with positively charged lysine and interacting residues in the amino acid regions 10-20 and 115-125 of GCP16 with negatively charged aspartic acid, would maximise disruption. We therefore introduced the following substitutions in GCP16 binding interface mutants 4a/b and 1-4a/b; GCP16 4a/b (D): K11D, F13D, R118D, R121D, and E124A, GCP16 1-4a/b (D/K): K11D, F13D, R16D, Y18D, Y76K, Y86K, R118D, R121D, and E124A. AlphaFold3 was first used to predict the binding of these charged GCP16 mutants to wild-type zDHHC9, conducted by Dr Kimon Lemonidis

(University of Glasgow) (Jumper *et al*., 2021, Varadi *et al*., 2022, Abramson *et al*., 2024, Varadi *et al*., 2024).

Figure 4.15 shows the protein structure predictions generated for the interaction between wild-type zDHHC9 and either wild-type GCP16, GCP16 4a/b (D), or GCP16 1-4a/b (D/K). The overall confidence of the models is reflected in the predicted alignment error plots, as well as the pTM and ipTM scores and the pLDDT. The zDHHC9 WT/GCP16 4a/b (D) protein complex prediction had high pTM and ipTM scores of 0.74 and 0.8, respectively, which were really similar to those for the zDHHC9 WT/GCP16 WT protein complex prediction, 0.77 and 0.81, respectively (Figure 4.14). The two models also had similar PAE plots with low expected error. Such metrics suggest confidence in the overall structure, as well as in the interactions between different subunits of the protein complex. The zDHHC9 WT/GCP16 1-4a/b (D/K) protein complex prediction, on the other hand, had extremely low pTM and ipTM scores of 0.54 and 0.23, respectively, along with a PAE plot with high expected error. These scores suggest that the software has very little confidence in the two proteins interacting. Additionally, the zDHHC9 WT/GCP16 1-4a/b (D/K) model included the most regions with low pLDDT, while some were found in the zDHHC9 WT/GCP16 4a/b (D) and very few in the zDHHC9 WT/GCP16 WT prediction models (Figure 4.15).

Taking into account all the above metrics of confidence, we concluded that GCP16 4a/b (D) could still bind to zDHHC9, while GCP16 1-4a/b (D/K) might be able to disrupt binding to zDHHC9.

zDHHC9 WT / GCP16 WT

ipTM = 0.81 pTM = 0.77

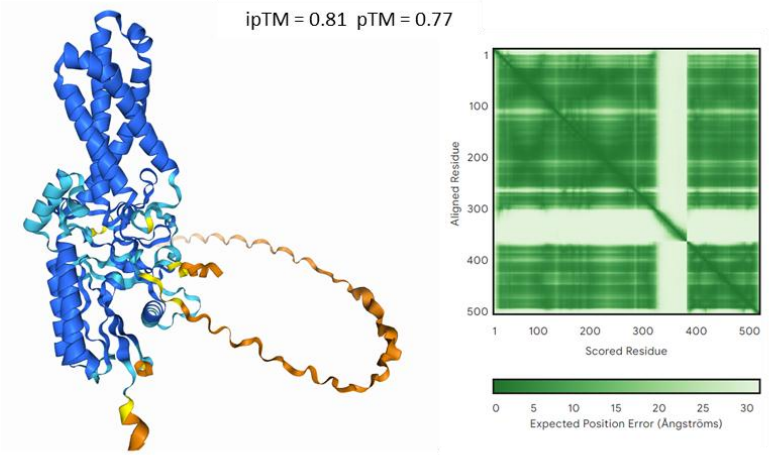

zDHHC9 WT / GCP16 4a/b (D)

ipTM = 0.80 pTM = 0.74

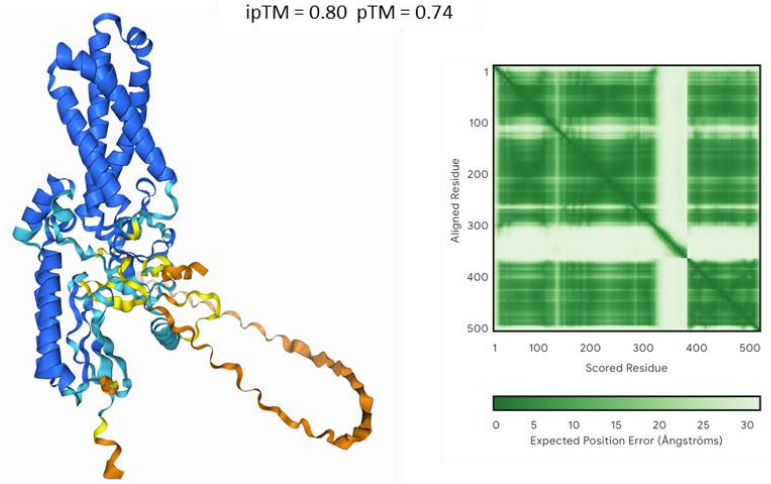

zDHHC9 WT / GCP16 1-4a/b (D/K)

ipTM = 0.23 pTM = 0.54

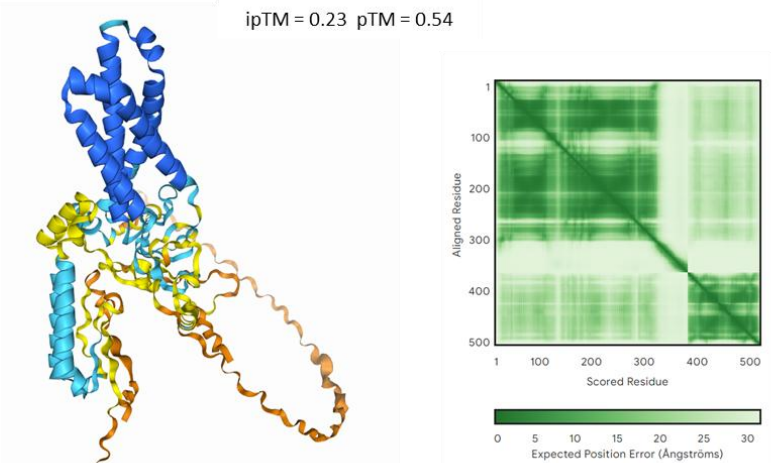

Very high (pLDDT > 90)	Confident (90 > pLDDT > 70)	Low (70 > pLDDT > 50)	Very low (pLDDT < 50)

Figure 4.15 AlphaFold protein structure prediction of the interaction between charged GCP16 binding interface mutants and zDHHC9.

Protein structure predictions of mouse zDHHC9 (UniProt ID: P59268) interacting with either human GCP16 (UniProt ID: Q7Z5G4), human GCP16 binding interface mutant 4a/b (D) (K11D/F13D/R118D/R121D/E124A), or human GCP16 binding interface mutant 1-4a/b (D/K) (K11D/F13D/R16D/Y18D/Y76K/Y86K/R118D/R121D/E124A), adapted from outputs generated using AlphaFold3 by DeepMind and EMBL-EBI (Jumper et al., 2021, Varadi et al., 2022, Abramson et al., 2024, Varadi et al., 2024). For every prediction model, AlphaFold produces a predicted alignment error (PAE) plot, pTM and ipTM scores, and a per-residue confidence score (pLDDT) between 0 and 100 that is illustrated with the use of a coloured scale. Regions with very low pLDDT (< 50) may be unstructured in isolation.

Following on the hypothesis that GCP16 binding interface mutant 4a/b (D) was still able to interact with zDHHC9, while substitution of all key residues with charged amino acids in GCP16 1-4a/b (D/K) was able to disrupt the interaction, these GCP16 mutants were examined in a co-immunoprecipitation experiment.

HEK293T cells were co-transfected with HA-zDHHC9 WT, along with EGFP-tagged GCP16 WT, 4a/b, 4a/b (D), 1-4a/b, 1-4a/b (D/K), or EGFP as a negative control. Cell lysates were incubated with GFP-Trap® Agarose beads, and the eluted proteins were examined by immunoblotting. As indicated in Figure 4.16B, zDHHC9 was successfully co-immunoprecipitated with GCP16 WT and all mutants used - 4a/b, 4a/b (D), 1-4a/b, 1-4a/b (D/K), while no co-immunoprecipitation was seen with the EGFP negative control. The lower expression of the mutants compared to GCP16 WT resulted in seemingly higher zDHHC9 co-immunoprecipitation levels when the data was quantified, which also affected the statistical comparison of zDHHC9 co-immunoprecipitation between GCP16 WT and EGFP (Figure 4.16C). All in all, even the introduction of more disruptive charged mutations in the binding interfaces of GCP16 could not disrupt interaction with zDHHC9.

A.

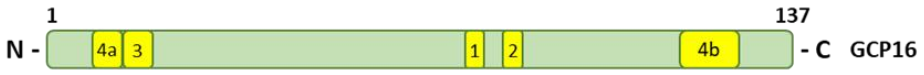

Interface mutants of **GCP16**	
4a/b:	K11A/F13A/R118A/R121A/E124A
4a/b (D):	K11D/F13D/R118D/R121D/E124A
1-4a/b:	K11A/F13A/R16A/Y18A/Y76A/Y86A/R118A/R121A/E124A
1-4a/b (D/K):	K11D/F13D/R16D/Y18D/Y76K/Y86K/R118D/R121D/E124A

B.

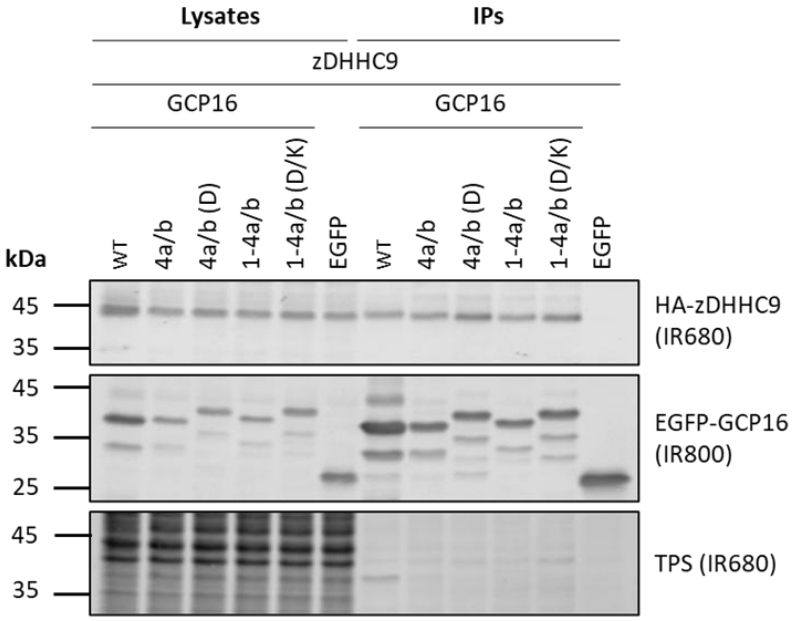

C.

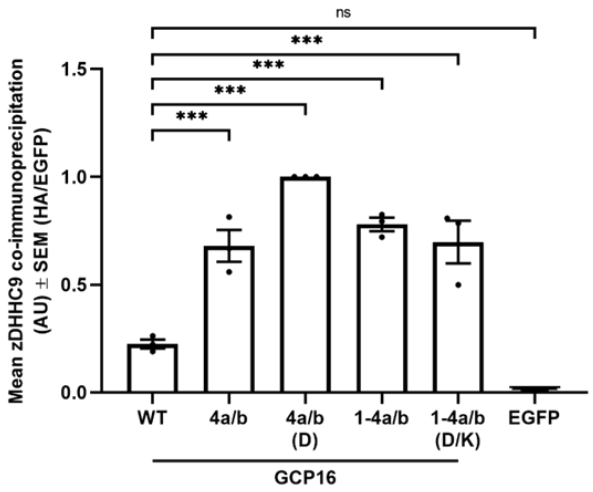

Figure 4.16 Co-immunoprecipitation of GCP16 interface mutant constructs containing charged amino acid residues.

(A) *Schematic of the GCP16 interface mutant constructs used, noting the charged amino acid substitutions that were introduced based on the AlphaFold structure prediction of the zDHHC9/GCP16 protein complex.* ***(B)*** *HEK293T cells were co-transfected with HA-tagged zDHHC9 and EGFP-tagged GCP16 WT, 4a/b, 4a/b (D), 1-4a/b, or 1-4a/b (D/K). The EGFP plasmid was used as a negative control. The EGFP-tagged proteins (IR800) were immunoprecipitated using anti-EGFP beads and detected by immunoblotting, along with co-immunoprecipitated HA-tagged proteins (IR680). The position of molecular weight markers (kDa) is shown on the left.* ***(C)*** *Quantified data show the mean (± SEM) of the HA-zDHHC9 (IR680) intensity value divided by the corresponding intensity value of the EGFP signal (IR800) in each IP sample. The data has been normalised to the highest value of each experiment, which was set to 1. Statistical significance was analysed using an ordinary one-way ANOVA, followed by a Dunnett's multiple comparisons test. *p<0.05, **p<0.01 and ***p<0.001, while ns denotes non-significance, where p>0.05. n = 3, from two independent experiments.*

4.14 The GCP16 interface mutant can bind to both mouse and human zDHHC9

The zDHHC9 construct used in all experiments in this thesis is from mouse. It is very unlikely that there are significant differences between mouse and human zDHHC9 in binding to GCP16, considering the high amino acid similarity of the two species as seen in 4.17A (the two species differ in only six amino acids at the C-terminal tail of the protein). Nevertheless, mouse and human zDHHC9 were compared in a co-immunoprecipitation experiment with wild-type GCP16 and GCP16 binding interface mutant 1-4a/b.

HEK293T cells were co-transfected with mouse HA-zDHHC9, or human HA-zDHHC9, along with EGFP-tagged GCP16 WT, 1-4a/b, or EGFP as a negative control. Cell lysates were incubated with GFP-Trap® Agarose beads, and the eluted proteins were examined by immunoblotting. Results showed that GCP16 WT and 1-4a/b were able to co-immunoprecipitate both mouse and human zDHHC9 to equal levels (Figure 4.17C).

A.


Mouse zDHHC9 MSVMVVRKKVTRKWEKLPGRNTFCCDGRVMMARQKGIFYLTLFLILGTCTLFFAFECRYLAVQLSPAIP 69
Human zDHHC9 MSVMVVRKKVTRKWEKLPGRNTFCCDGRVMMARQKGIFYLTLFLILGTCTLFFAFECRYLAVQLSPAIP 69
Mouse zDHHC9 VFAAMLFLFSMATLLRTSFSDPGVIPRALPDEAAFIEMEIEATNGAVPQGQRPPPRIKNFQINNQIVKL 138
Human zDHHC9 VFAAMLFLFSMATLLRTSFSDPGVIPRALPDEAAFIEMEIEATNGAVPQGQRPPPRIKNFQINNQIVKL 138
Mouse zDHHC9 KYCYTCKIFRPPRASHCSICDNCVERFDHHCPWVGNCVGKRNYRYFYLFILSLSLLTIYVFAFNIVYVA 207
Human zDHHC9 KYCYTCKIFRPPRASHCSICDNCVERFDHHCPWVGNCVGKRNYRYFYLFILSLSLLTIYVFAFNIVYVA 207
Mouse zDHHC9 LKSLKIGFLETLKETPGTVLEVLICFFTLWSVVGLTGFHTFLVALNQTTNEDIKGSWTGKNRVQNPYSH 276
Human zDHHC9 LKSLKIGFLETLKETPGTVLEVLICFFTLWSVVGLTGFHTFLVALNQTTNEDIKGSWTGKNRVQNPYSH 276
Mouse zDHHC9 GNIVKNCCEVLCGPLPPSVLDRRGILPLEESGSRPPSTQETSSSLLPQSPASTEHMNSNEMAEDTSIPE 345
Human zDHHC9 GNIVKNCCEVLCGPLPPSVLDRRGILPLEESGSRPPSTQETSSSLLPQSPAPTEHLNSNEMPEDSSTPE 345
Mouse zDHHC9 EMPPPEPPEPPQEASEAEK 364
Human zDHHC9 EMPPPEPPEPPQEAAEAEK 364

B.

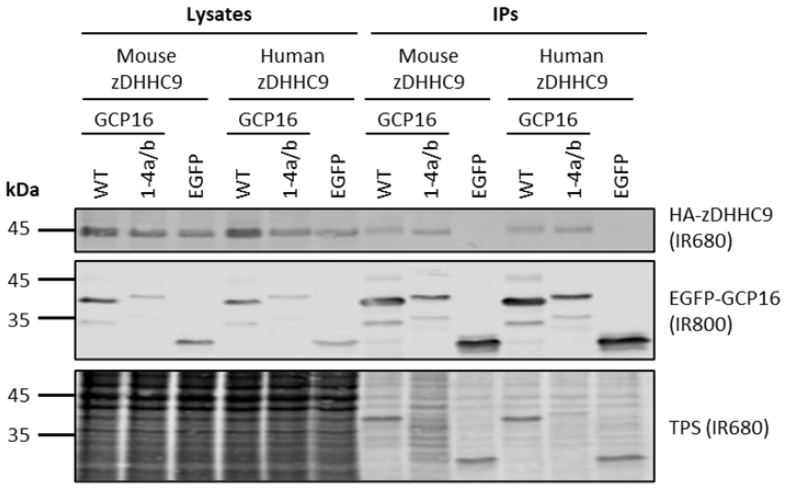
Lysates
IPs
Mouse zDHHC9
Human zDHHC9
Mouse zDHHC9
Human zDHHC9
GCP16
WT
1-4a/b
EGFP
kDa
45
45
35
45
35
HA-zDHHC9 (IR680)
EGFP-GCP16 (IR800)
TPS (IR680)

C.

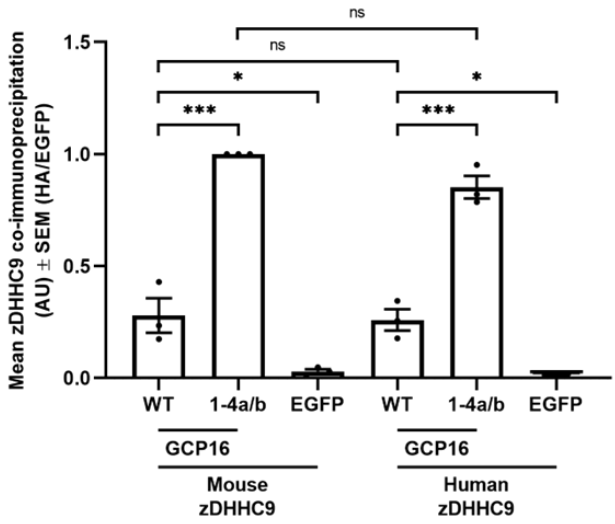
Mean zDHHC9 co-immunoprecipitation (AU) ± SEM (HA/EGFP)
1.5
1.0
0.5
0.0
ns
ns
*
*
***
***
WT
1-4a/b
EGFP
WT
1-4a/b
EGFP
GCP16
GCP16
Mouse zDHHC9
Human zDHHC9

Figure 4.17 The GCP16 interface mutant can bind to both mouse and human zDHHC9.

(A) *Amino acid sequence alignment of mouse zDHHC9 (UniProt ID: P59268) and human zDHHC9 (UniProt ID: Q9Y397), generated using the Clustal Omega multiple sequence alignment program through the align tool from UniProt (UniProt, 2025).* ***(B)*** *HEK293T cells were co-transfected with HA-tagged mouse or human zDHHC9, and EGFP-tagged GCP16 WT, or 1-4a/b. The EGFP plasmid was used as a negative control. The EGFP-tagged proteins (IR800) were immunoprecipitated using anti-EGFP beads and detected by immunoblotting, along with co-immunoprecipitated HA-tagged proteins (IR680). The position of molecular weight markers (kDa) is shown on the left.* ***(C)*** *Quantified data show the mean (± SEM) of the HA-zDHHC9 (IR680) intensity value divided by the corresponding intensity value of the EGFP signal (IR800) in each IP sample. The data has been normalised to the highest value of each experiment, which was set to 1. Statistical significance was analysed using an ordinary one-way ANOVA, followed by a Tukey's multiple comparisons test. *p<0.05, **p<0.01 and ***p<0.001, while ns denotes non-significance, where p>0.05. n = 3, from three independent experiments.*

4.15 The GCP16 binding interface mutant 4a/b is rapidly degraded by the proteasome

When the stability of all GCP16 binding interface mutants were examined in a cycloheximide experiment, it was observed that binding interface mutants 1, 3, and 4a/b had decreased stability when compared to the wild-type protein. This decrease in stability was more significant for mutants 3 and 4a/b (Figure 4.6C). To examine if this reflected increased proteasomal degradation of the mutant GCP16, HEK293T cells were transfected with EGFP (control), EGFP-tagged GCP16 WT, binding interface mutants 3, or 4a/b, together with either PEF-BOS-HA as a control, or HA-zDHHC9. Cells were then either incubated with DMSO as a vehicle control or with the MG132 proteasomal inhibitor for 16 hours, and protein levels were subsequently examined by immunoblotting (Figure 4.18). Protein expression after 16 hours of proteasomal inhibition by MG132 was quantified relative to the DMSO vehicle control expression. Quantified data in Figure 4.18B shows that while the expression of

GCP16 binding interface mutant 3 was not influenced by proteasomal inhibition, the expression of binding interface mutant 4a/b was significantly increased following MG132 treatment, compared to wild-type GCP16. This increase was seen both with and without zDHHC9 co-expression. On the other hand, MG132 had no effects on the expression of zDHHC9, irrespective of which GCP16 construct the enzyme was co-expressed with.

The effects of MG132 on FLAG-tagged GCP16 interface mutant constructs was also examined to confirm the above findings. HEK293T cells were transfected with FLAG-tagged GCP16 WT, binding interface mutants 1, 2, 3, or 4a/b, and treated with either DMSO or MG132 as described above (Figure 4.18C). Notably, the significantly lower molecular weight of the FLAG-tag fused to the constructs (approximately 1 kDa tag, compared to 27 kDa for EGFP) enabled the resolution of two separate bands for each GCP16 construct. We assume that the lower band corresponds to the non-acylated form of GCP16, whereas the upper represents the S-acylated form. For the wild-type protein and binding interface mutants 1 and 2, both bands appear more intense after MG132 treatment, and the ratio of S-acylated (upper band) and non-acylated (lower band) protein levels appears unchanged compared to the control. For interface binding mutants 3 and 4a/b however, MG132 treatment significantly increased the presence of the non-acylated (lower band) form of the protein, suggesting that this form of the proteins is especially susceptible to proteasomal degradation.

A.

Interface mutants of **GCP16**	
1:	Y76A
2:	Y86A
3:	R16A/Y18A
4a/b:	K11A/F13A/R118A/R121A/E124A

B.

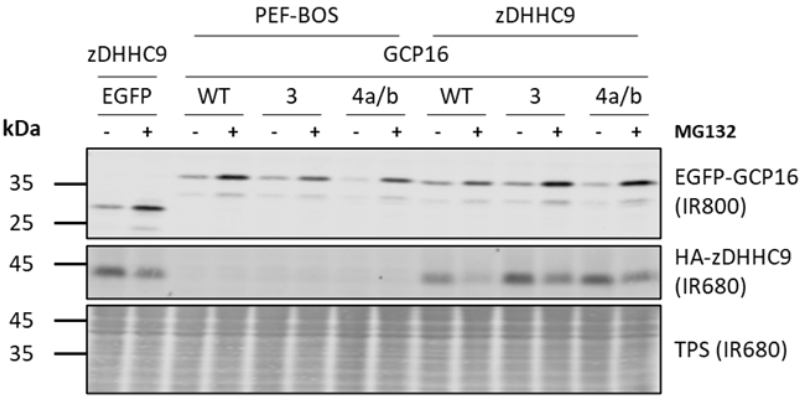

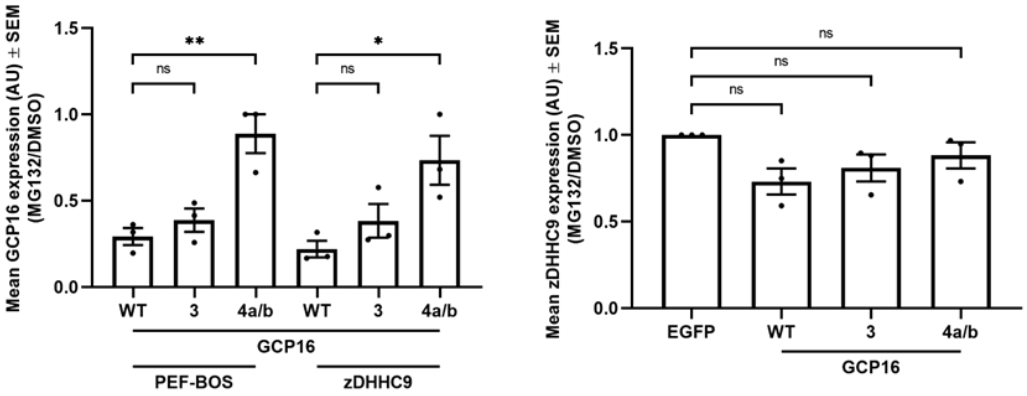

C.

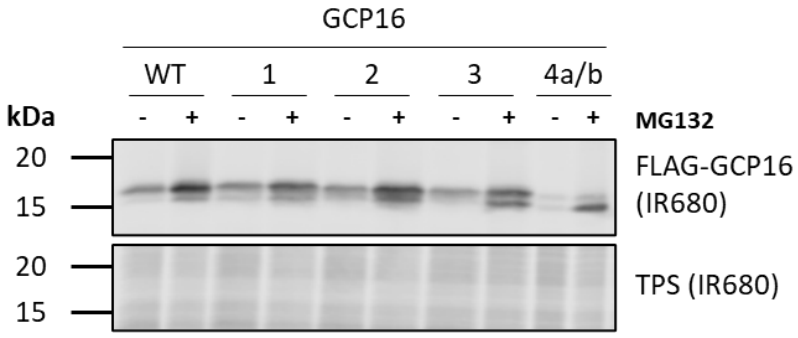

Figure 4.18 Effect of proteasomal inhibition with MG132 on GCP16 binding interface mutants and zDHHC9.

(A) *Schematic of the GCP16 binding interface mutant constructs used, designed based on the cryo-EM structure of the zDHHC9/GCP16 protein complex. HEK293T cells were co-transfected with* ***(B)*** *PEF-BOS-HA (empty plasmid control), or HA-tagged zDHHC9, together with EGFP, EGFP-tagged GCP16 WT, binding interface mutants 3, or 4a/b.* ***(C)*** *HEK293T cells were transfected with FLAG-tagged GCP16 WT, binding interface mutants 1, 2, 3, or 4a/b. In both experiments, cells were incubated with either DMSO as a vehicle control, or with 10 μM of MG132 for 16 hours. The cells were lysed, and expression levels were detected by immunoblotting. The position of molecular weight markers (kDa) is shown on the left. Quantified data shows the mean protein expression (± SEM) after 16 hours of MG132 treatment, relative to the corresponding DMSO control value and to the total protein stain levels of each sample. Data has been normalised to the highest value of each experiment, which was set to 1. Statistical significance was analysed using an ordinary one-way ANOVA, followed by a Dunnett's multiple comparisons test. *p<0.05, **p<0.01 and ***p<0.001, while ns denotes non-significance, where p>0.05. n = 3, from three independent experiments.*

4.16 The amino acid region 60-90 of GCP16 promotes proteasomal degradation

After observing that the GCP16 interface binding mutant 4a/b is rapidly degraded by the proteasome, it was examined whether there is a certain region within GCP16 responsible for driving protein degradation. Therefore, the effects of MG132 on the expression levels of EGFP-tagged GCP16 truncation mutants were examined to identify any rapidly-degrading construct. HEK293 cells were transfected with either EGFP control, EGFP-tagged GCP16 1-130, 1-60, 1-90, 1-120, or the full-length GCP16 WT. Cells were then incubated with DMSO as a vehicle control or treated with the MG132 proteasomal inhibitor for 16 hours, and protein levels were examined by immunoblotting (Figure 4.19A).

The quantified results suggest that amino acids 1-30 and 1-60 of GCP16 did not affect EGFP expression, whereas addition of amino acids 1-90 and 1-120 led to a significant decrease in expression that was then reversed by MG132 proteasomal inhibition.

Interestingly, the increased degradation of 1-90 and 1-120 regions of GCP16 was also seen in Chapter 3 in a cycloheximide experiment assessing protein stability (Figure 3.6). In Chapter 3, the hydrophobic character of the 60-90 region was also highlighted in a Kyte-Doolittle hydropathy analysis, with the main S-acylated cysteines, Cys-69 and Cys-72, also present in this region (Figure 3.14). It is therefore proposed that the 60-90 region promotes protein degradation when GCP16 is not stabilised by S-acylation.

To explore this idea further, cysteine-to-alanine mutants of GCP16 were also examined. Interestingly, the effects of MG132 on the C69A/C72A/C81A mutant were not significantly different from the EGFP control (Figure 4.19B). This finding suggests that enhanced degradation of the truncated forms of GCP16 in Figure 4.19A is occurring due to the presence of non-acylated cysteines, and that S-acylation of these residues stabilises the protein.

A.

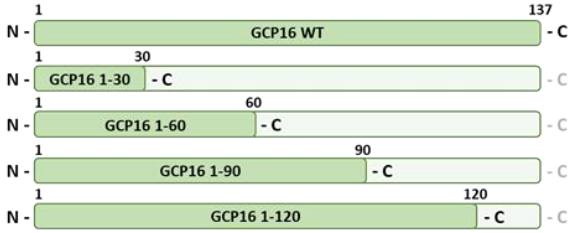
1
137
N -
GCP16 WT
- C
1
30
GCP16 1-30
60
GCP16 1-60
90
GCP16 1-90
120
GCP16 1-120

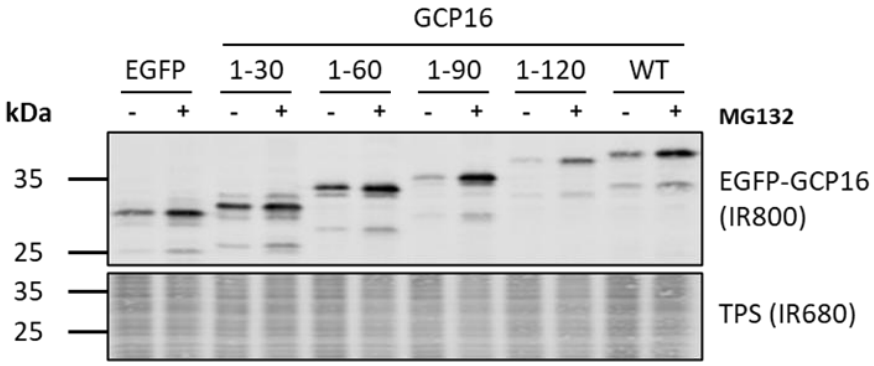
GCP16
EGFP
1-30
1-60
1-90
1-120
WT
kDa
MG132
35
25
EGFP-GCP16
(IR800)
TPS (IR680)

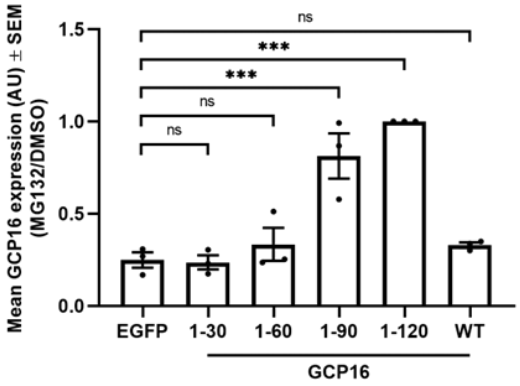
Mean GCP16 expression (AU) ± SEM
(MG132/DMSO)
ns
***
***
ns
ns
EGFP
1-30
1-60
1-90
1-120
WT
GCP16

B.

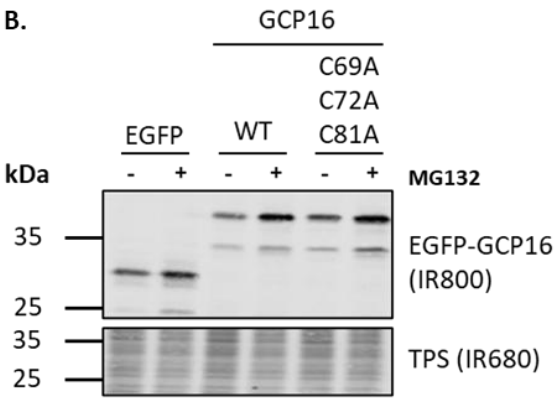
GCP16
C69A
C72A
C81A
EGFP
WT
kDa
MG132
35
25
EGFP-GCP16
(IR800)
TPS (IR680)

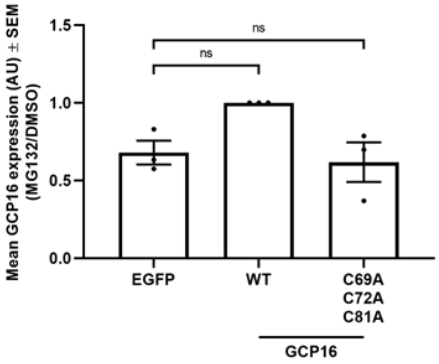
Mean GCP16 expression (AU) ± SEM
(MG132/DMSO)
ns
ns
EGFP
WT
C69A
C72A
C81A
GCP16

Figure 4.19 The amino acid region 60-90 in GCP16 promotes degradation.

(A) *Schematic of the GCP16 truncation mutant constructs used. HEK293T cells were transfected with EGFP (control), EGFP-tagged GCP16 1-130, 1-60, 1-90, 1-120, or WT.* ***(B)*** *HEK293T cells were transfected with EGFP (control), EGFP-tagged GCP16 WT, or C69A/C72A/C81A. In both experiments, cells were incubated with either DMSO as a vehicle control, or with 10 μM of MG132 for 16 hours. The cells were lysed, and expression levels were detected by immunoblotting. The position of molecular weight markers (kDa) is shown on the left. Quantified data show the mean protein expression (± SEM) after 16 hours of MG132 treatment, relative to the corresponding DMSO control value and to the total protein stain levels of each sample. Data has been normalised to the highest value of each experiment, which was set to 1. Statistical significance was analysed using an ordinary one-way ANOVA, followed by a Dunnett's multiple comparisons test. *p<0.05, **p<0.01 and ***p<0.001, while ns denotes non-significance, where p>0.05. n = 3, from two independent experiments*.

4.17 Mutations in binding interfaces 3 and 4a/b of GCP16 inhibit the activity of the zDHHC9/GCP16 complex in rat hippocampal neurons

Finally, the effects of disrupting the S-acylation and stability of zDHHC9 and GCP16 on the functional properties of the zDHHC9/GCP16 protein complex were examined. Enhancing the expression of both zDHHC9 and GCP16 has previously been shown to promote increased dendrite growth in rat hippocampal neurons (Shimell *et al.*, 2019).

To investigate the effect of wild-type and mutant GCP16 on the activity of zDHHC9, rat hippocampal neuron cultures were transfected with HA-zDHHC9 along with either FLAG-tagged GCP16 WT, or GCP16 binding interface mutant 3 or 4a/b. CaMK2a-EGFP was also transfected to allow the visualisation of excitatory neurons. Cells were then fixed, immunostained and imaged on an Evident IX83 inverted microscope. Individual transfected neurons were then selected for analysis of dendrite length. For this, cells were selected in which the intensity of wild-type and mutant GCP16 and co-expressed zDHHC9 in different cultures was similar (i.e. where the intensity of staining of GCP16 WT in one culture was similar to that of mutant GCP16 in a different culture,

under identical microscope settings). This approach allowed a more direct comparison of the functional effects of the wild-type and mutant GCP16 at similar levels of expression. As shown in the representative images and the quantified data in Figure 4.20, wild-type GCP16 co-expressed with zDHHC9 promoted a significant increase in dendrite length compared to the control, as shown previously (Shimell *et al.*, 2019). In contrast, neither GCP16 binding interface mutant 3 nor 4a/b increased dendrite growth, despite confirmation of their similar expression levels by fluorescence intensity quantification in the analysed neurons.

A.

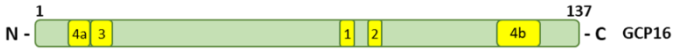

Interface mutants of **GCP16**	
3:	R16A/Y18A
4a/b:	K11A/F13A/R118A/R121A/E124A

B.

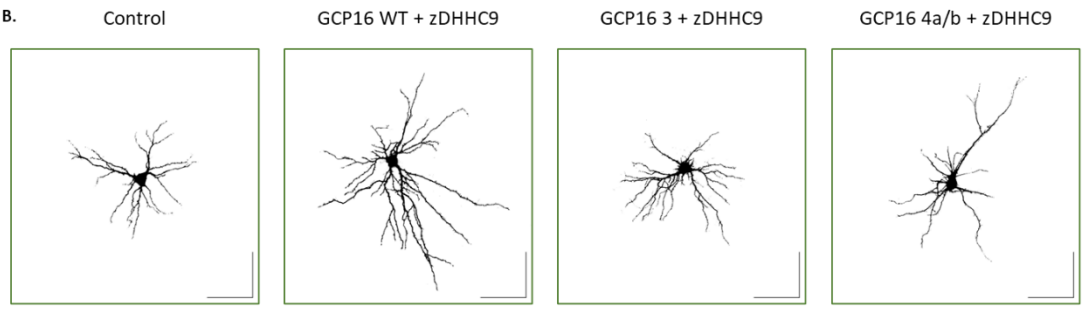

C.

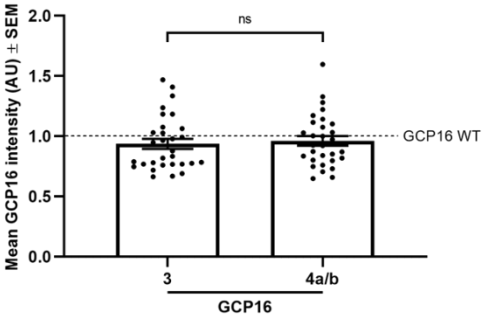

D.

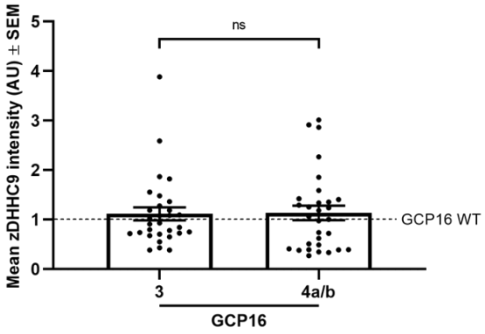

E.

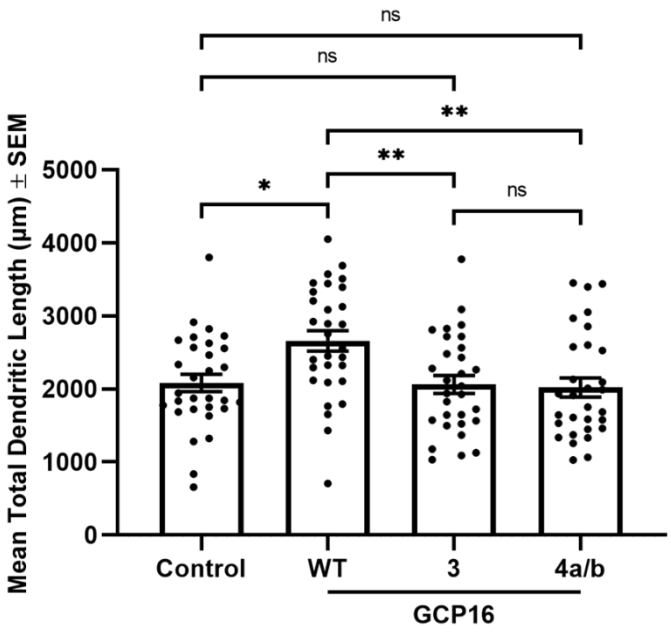

Figure 4.20 Mutations in binding interfaces 3 and 4a/b of GCP16 inhibit the activity of zDHHC9 in rat hippocampal neurons.

(A) *Schematic of the GCP16 binding interface mutant constructs used.* ***(B)*** *Representative binarised mask images (imaged at 20X magnification) of the EGFP channel of transfected rat hippocampal neurons used to measure total dendritic length using the SimpleNeuriteTracer (SNT) plugin (Arshadi et al., 2021) on Image J software (version v1.54p) (Schneider et al., 2012). Scale bar = 100 µm.* ***(C-D)*** *Mean protein intensity (± SEM) was calculated using the mean grey value for the FLAG-GCP16 WT and mutant constructs and HA-zDHHC9 channels within the EGFP mask in ImageJ. Values were normalised to GCP16 WT, which was set to 1. Statistical significance was determined using an unpaired t-test.* ***(E)*** *Quantified data show the mean total dendritic length (µm) (± SEM) measured in SNT after manually tracing dendritic arbors using the mask images. Statistical significance was determined using a one-way ANOVA followed by a Tukey's multiple comparisons test. *p<0.05, **p<0.01 and ***p<0.001, while ns denotes non-significance, where p>0.05. n = 30, from three separate cultures.*

Following on from the finding that GCP16 binding interface mutants 3 and 4a/b do not support dendrite growth in rat hippocampal neurons when co-expressed with zDHHC9, it was next investigated if these GCP16 mutants exhibited dominant-negative activity. This might be predicted if the mutants were able to bind to zDHHC9 but without the usual functional regulation of the enzyme. To investigate any potential dominant effects of the mutants on zDHHC9 activity, rat hippocampal neuron cultures were transfected with FLAG-tagged GCP16 WT, binding interface mutants 3, or 4a/b. Quantified data in Figure 4.21 shows that WT GCP16 expression without co-expression of zDHHC9 did not affect dendrite growth in accordance with the observations by Shimell *et al.* (2019) (Shimell *et al.*, 2019). Binding interface mutants 3 and 4a/b also showed no significant difference in dendrite length, suggesting that the mutants do not display any dominant inhibition effects on the activity of endogenous zDHHC9.

A.

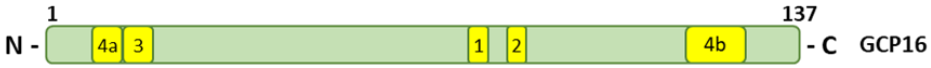

Interface mutants of **GCP16**	
3:	R16A/Y18A
4a/b:	K11A/F13A/R118A/R121A/E124A

B.

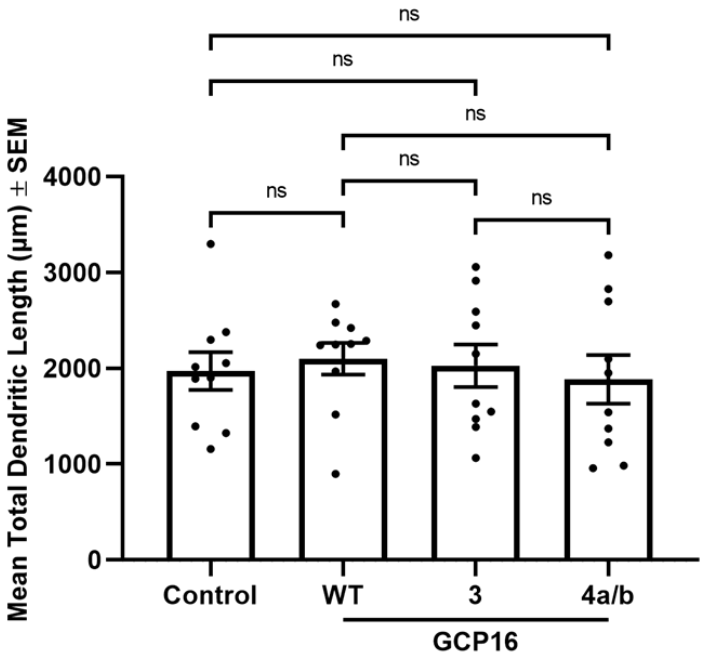

Figure 4.21 Mutations in binding interfaces 3 and 4a/b of GCP16 do not display any dominant negative effects on the activity of endogenous zDHHC9 in rat hippocampal neurons.

(A) *Schematic of the GCP16 binding interface mutant constructs used.* ***(B)*** *Quantified data show the mean total dendritic length (µm) (± SEM) measured using the SimpleNeuriteTracer (SNT) plugin (Arshadi et al., 2021) on Image J software (version v1.54p) (Schneider et al., 2012), after manually tracing dendritic arbors using the mask images. Statistical significance was determined using a one-way ANOVA followed by a Tukey's multiple comparisons test. *p<0.05, **p<0.01 and ***p<0.001, while ns denotes non-significance, where p>0.05. n = 10, from one culture.*

Discussion

Although it is well accepted that GCP16 plays an essential role in the regulation of zDHHC9, there is little published information on how the formation of this protein complex affects the stability and S-acylation of the proteins in a cellular environment. In particular, there has been no investigation of the reciprocal effects of zDHHC9 on its accessory protein, GCP16. This chapter builds on Chapter 3 by exploring the effects of amino acid substitutions in the identified binding interfaces of GCP16 and zDHHC9 on S-acylation, protein stability, and protein complex formation. The key findings show that binding interfaces 3 and 4a/b of GCP16 are essential for the functional effects of this protein on the complex. Specifically, replacing key amino acids in these interfaces with alanine leads to reduced S-acylation of GCP16 and zDHHC9, and reduced stability of both proteins. Surprisingly, however, co-immunoprecipitation experiments did not uncover any loss of binding with either the GCP16 mutants or with corresponding interface mutations introduced into zDHHC9. Furthermore, the co-immunoprecipitation of the mutants was also not disrupted by either more stringent immunoprecipitation buffer conditions or by the introduction of more disruptive (charged) amino acid substitutions into the binding interfaces of GCP16. Moreover, a region within GCP16 was identified that drives protein degradation of non-acylated forms of the protein with intact cysteines. Finally, experiments in rat hippocampal neurons showed that binding interface mutations in GCP16 inhibited the ability of the zDHHC9/GCP16 complex to promote dendrite growth.

Analysis of the AlphaFold protein structure prediction for zDHHC9/GCP16

At the outset of the work described in this chapter, the cryo-EM structure of the zDHHC9/GCP16 complex was not yet published (Yang *et al.*, 2024). Therefore, AlphaFold was used to predict protein regions involved in the interaction between zDHHC9 and GCP16 (Jumper *et al.*, 2021, Varadi *et al.*, 2022, Varadi *et al.*, 2024). Through investigation of the AlphaFold structure, two predicted zDHHC9-binding residues within GCP16 were identified: Tyr-76, which formed a Pi stack with Tyr-183 of zDHHC9, and Arg-121, which formed a hydrogen bond with Glu-101 of zDHHC9 (Figure 4.1). Substitution of these residues in GCP16 to alanine (Y76A/R121A), a

non-polar, hydrophobic amino acid that does not form H-bonds, did not disrupt binding with zDHHC9, or the S-acylation of GCP16, but showed a decreased ability to stabilise zDHHC9 S-acylation (Figure 4.2). As there was some effect of substituting these residues, a more disruptive mutant, where Arg-121, was replaced with the negatively charged glutamic acid, was designed (GCP16 Y76A/R121E). It was predicted that switching the overall charge could result in repulsion of the interacting amino acids, however, this mutant was no more disruptive than the Y76A/R121A mutant on the interaction with zDHHC9, or on GCP16 S-acylation. A third mutant generated based on AlphaFold protein structure prediction, Y76A/F79A/R121A, did show a decrease in both GCP16 and zDHHC9 S-acylation (Figure 4.4), but it did not affect the interaction between the two proteins in immunoprecipitation assays either (Figure 4.3).

AlphaFold has been a major advancement in the protein structure field, and in this case, it was able to successfully highlight residues that were later shown by Yang *et al.* (2024) to be involved in the zDHHC9/GCP16 complex. However, as the software was primarily trained on monomers, it is more accurate for monomeric predictions than for protein complexes. Another limitation is that its performance tends to drop for transient or small interface interactions, and it can also struggle with intrinsically disordered regions and conformational changes caused by co-factors, ions, ligands, or PTMs. It is also unaware of environmental settings that affect binding, such as membrane orientation. Therefore, AlphaFold's confidence metrics require careful interpretation and can only be seen as hypotheses to be validated, not as definitive evidence of interaction (Bagdonas *et al.*, 2021, EMBL-EBI, 2025).

Mutations in binding interfaces 3 and 4a/b of GCP16 disrupt the reciprocal S-acylation and stabilisation of zDHHC9 and GCP16

After the initiation of this project, Yang *et al.* (2024) published the cryo-EM structure of the zDHHC9/GCP16 protein complex. The reported structure highlighted four main binding interfaces promoting the interaction between the two proteins. Interestingly, the interacting residues that were previously identified using AlphaFold were included in the binding interfaces reported in the cryo-EM structure. The findings by Yang *et al.* (2024) allowed the study to progress from AlphaFold protein structure predictions to generating specific amino acid substitutions of the four binding interfaces identified in the cryo-EM structure (Yang *et al.*, 2024). These GCP16 binding interface mutants

were examined in a range of assays to determine the importance of specific contact sites for interaction, S-acylation, and protein stability.

Amino acid substitutions showed that residues in both the N-terminal and C-terminal regions of GCP16 encompassing binding interfaces 3 and 4a/b were essential for GCP16 and zDHHC9 S-acylation (Figure 4.5) and protein stability (Figure 4.6). Mutation of interface 3, which includes amino acid residues in the N-terminal region, decreased the S-acylation of GCP16 by approximately 50%, while mutation of interface 4a/b, which spans both the N- and C-terminal regions of the protein, completely abolished GCP16 S-acylation (Figure 4.5). These results agree with results in Chapter 3, which showed that short truncations to both the N-terminal region (aa 11-20 which include residues identified in binding interfaces 3 and 4a) and C-terminal region (aa 127-128 found at the very end of the β3' strand, in close proximity to E124 which stabilises residues K11 and R118 in binding interface 4a/b) of GCP16 disrupted S-acylation. The use of the 4b mutant, which only contains amino acid substitutions in the C-terminal region of binding interface 4a/b, showed that although this mutant did not affect GCP16 S-acylation, it was unable to stabilise zDHHC9 S-acylation and also decreased the stability of both GCP16 and zDHHC9 (Figure 4.7). In addition, both GCP16 interface mutants 3 and 4a/b were unable to stabilise zDHHC9 S-acylation (Figure 4.5) and displayed reduced stability and a decreased ability to stabilise the zDHHC9 protein (Figure 4.6). Overall, these results highlighted the importance of binding interfaces 3 and 4a/b for S-acylation and stability of both proteins.

The study by Yang *et al.* (2024) indicated that a protein complex of zDHHC9 and GCP16 binding interface mutant 1 (Y76A) had reduced catalytic activity against purified H-Ras (Yang *et al.*, 2024). In our analyses, we found that this mutant behaved similarly to wild-type GCP16 in terms of S-acylation of GCP16, but that it could not stabilise zDHHC9 S-acylation and it had a decreased stability when in a complex with zDHHC9, along with a reduced ability to stabilise the enzyme. The reduced catalytic activity reported by Yang *et al.* (2024) is reflected by the inability of the mutant to stabilise the autoacylated intermediate of zDHHC9, which also might be the reason for the observed decrease in stability of both GCP16 binding interface mutant 1 and zDHHC9. Tyrosine-76 of GCP16 interacts with residues found in TMD2 and TMD3 of zDHHC9 (R85 and Y183, respectively), the transmembrane domains on either side of the catalytic loop containing the DHHC and zinc finger domains. Moreover, R85 of

zDHHC9, one of the residues interacting with Y76 of GCP16, is part of a positively charged patch formed by R85, R179 and R298 of zDHHC9 that facilitates the interaction with a phospholipid, stabilising the conformation of TMD2, TMD3 and the PPII helix of zDHHC9 and modulating the spatial topology of the enzyme (Yang *et al.*, 2024). It is surprising that GCP16 interface mutant 1 has decreased stability but no change in S-acylation, as S-acylation is generally linked to protein stability. Interestingly, the three proline residues (P290, P292 and P293) in the PPII helix of zDHHC9 dock into a groove in GCP16 (Yang *et al.*, 2024), so substitution of Y76 to alanine in GCP16 (binding interface mutant 1) could disrupt the association of the phospholipid with the positively patch of zDHHC9 via disrupting R85, which then impairs the stabilising effect of this association, which could subsequently disrupt the interaction of the PPII helix of zDHHC9 with GCP16. Therefore, the decrease in protein stability of binding interface mutant 1 might be linked to possible conformational changes described above and not to the S-acylation of GCP16. Also, these stabilising interactions can rationalise why disruption of either Y76 or R85 impairs the enzymatic activity of the complex.

Another important finding from the alanine substitution analysis of the binding interfaces within GCP16 was that interface mutant 2 (Y86A) had similar S-acylation as that seen for wild-type GCP16 (Figure 4.5) and was the only binding interface mutant that retained its protein stability and the ability to stabilise zDHHC9 (Figure 4.6), despite not being able to stabilise the S-acylation of zDHHC9. The binding interface 2 is composed of tyrosine-86 of GCP16 interacting with proline-292 in the PPII helix of zDHHC9, whereas proline-290 and proline-293 in the PPII helix are also inserted into two negatively charged pockets on GCP16 (Yang *et al.*, 2024). It is assumed that substituting Y86 with alanine might not be disruptive enough to break the interaction of the PPII helix with the charged pockets of GCP16, hence why the mutant can retain its S-acylation and reciprocal effects on stability. It would be interesting to substitute Y86 with a positively charged amino acid, while also including positively charged substitutions in the pocket of GCP16 that have the potential to switch the weak negative charge of the pocket and inhibit the interaction with the PPII helix of zDHHC9. Nonetheless, the binding interface mutant 2 was not able to stabilise the S-acylation of zDHHC9, suggesting that the enhancing effect of GCP16 on zDHHC9 S-acylation might be more susceptible to conformational changes and that the singular Y86A substitution is enough to disrupt it.

The analysis of the 4b mutant (R118A/R121A/E124A) was interesting as it is S-acylated, but its stability and that of zDHHC9 are reduced (Figure 4.7). We are not certain how binding interface mutant 4b retains its S-acylation, as we hypothesised that alanine substitutions in the C-terminal region, especially on the β3' strand (aa 122-127), would disrupt S-acylation, based on results from the analyses performed in Chapter 3. One possibility is that when single point mutations are introduced, rather than truncations, amino acids in proximity to E124, or even the introduced alanine, may be able to form additional contacts with zDHHC9 that allow S-acylation to occur. As for the decreased stability of this mutant, we believe that it is linked to direct conformational changes, rather than the S-acylation of GCP16, as for binding interface mutant 1. Through AlphaFold analysis, we observed that E124, found on the β3' strand of the C-terminal region of GCP16, forms a hydrogen bond with K11 which is located on the β1' strand of the N-terminal region of the protein, bringing the two regions together. Therefore, the substitutions introduced in GCP16 binding interface mutant 4b could disrupt the β-sheet formation of the protein and decrease its stability.

A zDHHC9 binding interface mutant disrupts the reciprocal S-acylation and stability of zDHHC9 and GCP16

The binding interface residues of zDHHC9 reported by the cryo-EM study (Yang *et al.*, 2024) include P150, a residue that is part of a motif juxtaposed to the catalytic DHHC motif, and that is conserved between yeast Erf2 and mammalian zDHHC9 (Raymond *et al*., 2007, Mitchell *et al*., 2014). In Erf2, the sequence RPPR (which includes the proline at a similar position to P150 in human zDHHC9) is involved in substrate S-acylation after the initial formation of the autoacylated intermediate (Mitchell *et al.*, 2010, Mitchell *et al.*, 2014), while a P150S zDHHC9 mutant was autoacylated to a lesser extent than wild-type, resulting in lower catalytic activity (Mitchell *et al.*, 2014). Indeed, the P150S substitution is known to cause intellectual disability in humans, confirming the importance of this residue *in vivo* (Raymond *et al.*, 2007). As expected (due to a P150A substitution), the zDHHC9 binding interface mutant 1-4a/b was unable to S-acylate GCP16, and it also failed to form an autoacylated intermediate (Figure 4.8). Reciprocal stabilisation of GCP16 and zDHHC9 was also disrupted by the zDHHC9 1-4a/b mutant (Figure 4.9). As only a single binding interface mutant of zDHHC9, which had substitutions at key sites in all interfaces was analysed in this chapter, it is unclear if the loss of protein stability would

be seen with a single P150A substitution, but it would be interesting to examine this to assess how changes in the extent of enzyme autoacylation are linked to the stability of zDHHC9.

A study by Nguyen *et al.* (2023) demonstrated that catalytically inactive zDHHS9 is aggregated when expressed alone, but GCP16 co-expression increases the stability and monodispersity of the mutant in FSEC analyses, at levels similar to the wild-type enzyme (Nguyen *et al.*, 2023). However, the authors did not examine the stabilising effects of the mutant enzyme on GCP16. To investigate whether the stabilising effect on GCP16 depends on the catalytic activity of zDHHC9, we used the catalytically inactive zDHHA9 mutant in a cycloheximide experiment to directly assess the protein's stability. We observed that zDHHA9 was unable to stabilise GCP16 (Figure 4.10), similarly to the zDHHC9 1-4a/b binding interface mutant (Figure 4.9). This proposes that the zDHHC9-mediated stabilisation of GCP16 requires an intact interaction (Figure 4.6), as well as a catalytically active enzyme (Figure 4.10), while GCP16-mediated stabilisation of zDHHC9 is independent of the S-acylation activity of the enzyme (Nguyen *et al*., 2023).

Mutation of the binding interfaces within zDHHC9 and GCP16 does not perturb protein complex formation

Surprisingly, even though substitutions in binding interfaces 3 and 4a/b have dramatic effects on the S-acylation and protein stability of both GCP16 and zDHHC9, co-immunoprecipitation assays using all binding interface mutants of GCP16, including 1-4a/b, showed that the interaction with zDHHC9 was not disrupted (Figure 4.11).

To further examine the interaction, the salt and detergent conditions in the immunoprecipitation wash buffer were also modified. Triton X-100 and NP40 are commonly used non-ionic detergents of similar strength. Low salt concentrations of 50 – 130 mM of NaCl allow for the detection of weak interactions but can also result in non-specific binding. Increasing the salt concentration up to 500 mM of NaCl makes the washing steps harsher and disrupts weak or non-specific binding, while strong interactors are not affected (Gerace and Moazed, 2014). Therefore, a moderate salt concentration of 250 mM and a high salt concentration of 500 mM, along with 1% Triton X-100, were used to determine whether the interaction of zDHHC9 with GCP16 interface mutant 1-4a/b could be disrupted under these conditions. The results

showed that binding of zDHHC9 to GCP16 1-4a/b was not disrupted by any of these different washing conditions (Figure 4.12A). Indeed, binding was still detected even when interface mutations were introduced into all binding interfaces of both GCP16 and zDHHC9 (Figure 4.13).

To better understand why these binding interface mutants were still interacting, AlphaFold analysis was undertaken to visualise the predicted binding between zDHHC9 1-4a/b and GCP16 1-4a/b mutant constructs and compare it to the wild-type protein complex. When the interaction between zDHHC9 and GCP16 with all binding interfaces mutated was examined, AlphaFold predicted some disruption in their association, which was indicated in the lower metrics of confidence (Figure 4.14). However, this was not enough to prevent the formation of the complex, as was previously determined experimentally (Figure 4.13). Further analysis of the binding interfaces revealed their highly hydrophobic nature, which then led to the hypothesis that the alanine substitutions that were introduced, although weakening the overall interaction to a certain degree, were still able to preserve the hydrophobicity required for the formation of the complex. If the AlphaFold predictions are correct and the proteins do still bind, it is possible that their effects on the S-acylation and stability of GCP16 and zDHHC9 within the complex, might be linked to local conformation changes. Another theory is that there is a secondary binding site that is uncovered when the main binding interfaces are disrupted.

Based on the results of the AlphaFold analysis outlined above, it was also examined whether more disruptive amino acid substitutions are predicted to affect the zDHHC9/GCP16 interaction. In Figure 4.15, AlphaFold was used to visualise the zDHHC9/GCP16 interaction after substituting binding interface residues with charged aspartic acid and lysine residues. Substitution of all binding interfaces within GCP16 with charged amino acids (GCP16 1-4a/b (D/K)) was predicted to disrupt binding between the two proteins (Figure 4.15). However, this prediction was invalidated after experimental co-immunoprecipitation analysis, which indicated that the GCP16 alanine substitution mutant (1-4a/b) and aspartic acid/lysine substitution mutant (1-4a/b (D/K)) with all binding interfaces mutated demonstrated a similar capacity to bind to zDHHC9 (Figure 4.16).

Mouse zDHHC9 has been used throughout this project, together with human GCP16. Therefore, it was important to confirm that the effects seen with the mouse enzyme were also observed for the human zDHHC9. The results in Figure 4.17 proved that

the two species of zDHHC9 interact with GCP16 in the same way, and both can bind to GCP16 1-4a/b. This is not surprising, as the amino acid differences between the two species are minimal and only limited to 6 residues present in the far C-terminal region of zDHHC9 (Figure 4.17A) that have not been reported to be part of the binding interfaces of the zDHHC9/GCP16 cryo-EM structure.

The non-acylated GCP16 binding interface mutant 4a/b is rapidly degraded by the proteasome

A limitation faced throughout this project in co-immunoprecipitation experiments has been the unequal expression of EGFP-tagged proteins that are being compared in some experiments. Changes in protein expression affect the quantification of co-immunoprecipitated protein levels, since the intensity value of the co-immunoprecipitated protein (HA-zDHHC) is divided by the corresponding intensity value of the captured EGFP-tagged protein in each sample. In a study performed on Golga7b and zDHHC5 by Woodley and Collins (2019), they demonstrated that treatment of a mutant Golga7b construct with MG132, a protease inhibitor, inhibited its degradation and increased its expression (Woodley and Collins, 2019). Therefore, we incubated the transfected cells with MG132 to prevent protein degradation and equalise the expression of wild-type and mutant GCP16 constructs. Although the expression levels of the GCP16 binding interface mutant 3 and 4a/b constructs was increased after MG132 treatment, they still did not reach the same levels as the corresponding wild-type construct. Hence, it was not possible to examine binding of zDHHC9 to equal amounts of EGFP-tagged GCP16. The expression of GCP16 binding interface mutant 3 at levels was somewhat comparable to GCP16 WT, and higher zDHHC9 co-immunoprecipitation levels were observed for this mutant construct than for GCP16 WT (Figure 4.12B). While the mutants may switch to a different binding mode that has a higher affinity when the binding interfaces are mutated, we do not favour this possibility. How else, then, might unequal expression of EGFP-GCP16 proteins affect the quantification of binding? The level of GCP16 expression may be very much higher than the level of zDHHC9 expression in our transfected cells. In this case, there is an excess of free GCP16, such that reducing the levels of this protein does not affect the amount of zDHHC9 that can be captured by co-immunoprecipitation. As our approach to quantification is to divide the HA-zDHHC9 signal by the EGFP-GCP16 signal in immunoprecipitate samples, this may

lead to an over-estimation of binding for EGFP-GCP16 mutants with low expression, and in this case, it may be more accurate to quantify the data simply based on HA-zDHHC9 signal in the IP samples. However, it would be important to undertake a detailed analysis of the relative expression levels of GCP16 and zDHHC9 before considering this alternative quantitative approach, and without evidence of vastly different expression levels, we believe that the approach taken in the thesis is appropriate.

As MG132 proteasomal inhibition seemed to increase the expression of GCP16 binding interface mutants 3 and 4a/b in the co-immunoprecipitation experiment, this suggested that they were being degraded by the proteasome. This was tested in an experiment using MG132 inhibition, which showed that the expression of binding interface mutant 4a/b (but not mutant 3) was enhanced by MG132, suggesting that this mutant is particularly susceptible to degradation (Figure 4.18B).

When examining the effects of MG132 treatment on FLAG-tagged GCP16 binding interface constructs 1, 2, 3, and 4a/b, two distinct immunoreactive bands were observed, that are assumed to represent the non-acylated and S-acylated state of the proteins. MG132 treatment caused an apparent increase in the lower, non-acylated band of mutants 3 and 4a/b, the only two interface mutants with disrupted S-acylation profiles (Figure 4.5). This suggests that the non-acylated form of the protein is more prone to degradation, while S-acylation of GCP16 might offer a protective stabilising effect (Figure 4.18C).

The amino acid region 60-90 in GCP16 promotes degradation by the proteasome

Another key finding of this chapter is that GCP16 amino acid region 1-90 and 1-120 promoted the degradation of EGFP, while the region 1-60 did not affect the expression of the EGFP tag (Figure 4.19A). This finding validates our previous observation that 1-90 and 1-120 truncated mutants of GCP16 have a significantly reduced stability in cycloheximide assays from Chapter 3. We assessed the role of the cysteines found in the hydrophobic region 60-90 that drives protein degradation using alanine substitutions at position 69, 72, and 81, in another MG132 experiment. The non-acylated triple cysteine-to-alanine mutant did not affect protein expression when compared to the EGFP control (Figure 4.19B). Therefore, it is proposed that non-acylated GCP16 with intact cysteines is associated with the membrane via direct

cysteine interactions (e.g. the 1-26 truncation mutant) but that membrane association in the absence of S-acylation leads to degradation. The 60-90 region of GCP16 is part of the α2' and α3' helices that are embedded in the membrane, while Cys-69 and Cys-72 are also found on the α2' helix (Yang *et al.*, 2024). Therefore, it makes sense to assume that the hydrophobic domain can mediate membrane association before S-acylation if the cysteines are intact, and when the cysteines are S-acylated, the membrane interaction may become tighter and more secure, shielding the protein from degradation via ubiquitination by membrane-bound E3 ligases.

Mutations in GCP16 binding interfaces 3 and 4a/b disrupt the function of zDHHC9/GCP16 in dendrite growth assays

Mutations in the *ZDHHC9* gene cause intellectual disability and childhood epilepsy (Raymond *et al.*, 2007, Baker *et al.*, 2015). The two point mutations associated with XLID are R148W and P150S substitutions in the DHHC-CRD (Raymond *et al.*, 2007, Mitchell *et al.*, 2014, Shimell *et al.*, 2019). It was shown that zDHHC9 knockdown in hippocampal neuron cultures resulted in reduced dendrite growth and fewer inhibitory synapses (Shimell *et al.*, 2019). These effects were proposed to be mediated by reduced S-acylation of two different substrates. Specifically, the S-acylation of Ras was linked to promoting dendrite growth, while the S-acylation of TC10 was linked to promoting inhibitory synapse formation. Moreover, the same study by Shimell *et al.* (2019) demonstrated that overexpression of both zDHHC9 and GCP16 was able to enhance dendrite growth through Ras S-acylation. Thus, to investigate the role of GCP16 binding interfaces 3 and 4a/b for the functional activity of the zDHHC9/GCP16 protein complex, we compared the effects of wild-type and mutant GCP16 on dendrite length in hippocampal neurons. For this comparison, neurons were selected with similar expression levels of wild-type and mutant GCP16 constructs, as well as zDHHC9 expression. This was to rule out the possibility of any functional differences being the result of the proteins having unequal expression. Using this approach, it was confirmed that co-expression of zDHHC9 with wild-type GCP16 promotes dendrite growth, while co-expression with GCP16 interface mutants 3 and 4a/b had no effect on dendrite length (Figure 4.20). These findings confirm the regulatory role of the zDHHC9/GCP16 complex in neuronal morphology and show the involvement of the amino acid residues found within binding interfaces 3 and 4a/b of GCP16 for the functional interaction with zDHHC9. Indeed, this is the first demonstration that the

effects of combined zDHHC9 and GCP16 expression on dendrite growth require their functional interaction.

To examine whether GCP16 binding interface mutants 3 and 4a/b could exert dominant negative inhibition on dendrite growth, an alternative assay was used in which only wild-type or mutant GCP16 was overexpressed in hippocampal neuron cultures. It was hypothesised that if GCP16 mutant 3 or 4a/b had a strong affinity for endogenous zDHHC9 (e.g., through an alternative binding mode), it might be possible to see a decrease in dendrite length compared to the control. In Figure 4.21, it was indicated that overexpression of wild-type GCP16 alone had no effect on dendrite length, as Shimell *et al.* (2019) has previously demonstrated, and similarly mutants 3 and 4a/b did not exhibit any dominant negative effects on endogenous zDHHC9. This observation suggests that either the mutants do not interact with zDHHC9 at all in neurons, or that they cannot compete with endogenous WT GCP16 for binding to the enzyme, or that they bind to zDHHC9 through an alternative binding mode that does not inhibit the activity of the enzyme.

Future directions

There are several areas that should be explored in future work that follow on from the results in this chapter. Perhaps the most surprising finding was that physical interaction between zDHHC9/GCP16 did not appear to be affected by any binding interface mutant, despite their clear effects on S-acylation and stability. This may indicate that there is another mode of zDHHC9/GCP16 interaction. However, it is also possible that the co-immunoprcipitation assays are not sensitive enough to detect changes in binding, and therefore it would be interesting to use alternative binding assays, including the use of purified proteins that would allow a more accurate determination of binding kinetics and affinities than is possible using co-immunoprecipitation. Moreover, it would be interesting to investigate whether the enhanced protein degradation of GCP16 binding interface mutant 4a/b is ubiquitylation-dependent by substituting the lysine residues in the construct with arginine residues. Another important area would be to examine the effects of interface mutants on substrate S-acylation in cells, for example, testing how substitutions in interfaces 1 and 2 (which have less effect on S-acylation) impact the modification of proteins such as Ras and TC10. As S-acylation of N-Ras is important for the effects of zDHHC9/GCP16 on dendrite growth, the inability of binding interface mutants 3

and 4a/b of GCP16 to support dendrite growth implies that complexes containing these mutants are not able to mediate N-Ras S-acylation. As the experiments involve co-expression of zDHHC9 and GCP16, it would also be interesting to generate the interface mutants in the endogenous genes by CRISPR, as this would allow all analyses to be performed at endogenous expression levels.

CHAPTER 5

BROADER ANALYSIS OF

THE INTERACTIONS OF GCP16

Chapter 5 - Broader analysis of the interactions of GCP16

Introduction

Generally, S-acylation is mediated through the interaction of a zDHHC enzyme with its cognate substrate protein and requires a fatty acyl-CoA donor. However, some zDHHC enzymes also require additional proteins for their S-acylation activity (Salaun *et al.*, 2020). GCP16 is an important accessory protein for zDHHC9, but it has been reported to also form complexes with other zDHHC enzymes such as zDHHC5 and zDHHC8 (Ko *et al.*, 2019). Indeed, zDHHC14 and zDHHC18, which are closely related to zDHHC9, were recently reported to require GCP16 to prevent their oligomerisation/aggregation and for effective enzymatic activity (Nguyen *et al.*, 2023, Yang *et al.*, 2024). Additionally, a homologue of GCP16, Golga7b, has been shown to form a complex with zDHHC5, regulating its activity and localisation (Woodley and Collins, 2019).

The specific role of GCP16 in these zDHHC enzyme complexes in mammalian cells has not been well defined. The observation of Ko *et al.* (2019) that GCP16 interacts not only with zDHHC9, but also with zDHHC5 and zDHHC8 in co-immunoprecipitation experiments (Ko *et al.*, 2019) was surprising, as GCP16 has been characterised as a Golgi-associated protein (Ohta *et al.*, 2003) and yet zDHHC5 is present at the plasma membrane (Ohno *et al.*, 2006). However, the study by Ko *et al.* (2019) demonstrated that GCP16 had a plasma membrane localisation in both control and zDHHC5 KO HT-1080 cells. The co-immunoprecipitation of both zDHHC9 and zDHHC5 with GCP16 in HEK293T cells suggested that GCP16 may exist in different functional pools found in distinct subcellular compartments (Ko *et al.*, 2019, Salaun *et al.*, 2020).

The study of Nguyen *et al.* (2023) showed that there is an important role for the C-terminus of zDHHC9 and specific S-acylated cysteines in GCP16 interaction. Co-expression and affinity co-purification analysis from Sf9 cells suggested that the zDHHC9 C-terminal triple cysteine region (Cys-283, Cys-284, Cys-288) is required for GCP16 interaction. Cysteine-288 in particular, was shown to be crucial for GCP16-mediated stabilisation of zDHHC9. The same study then showed via FSEC that all zDHHC enzymes containing the C-terminal cysteine motif, namely zDHHC14, zDHHC18, zDHHC8, and zDHHC5, are stabilised by GCP16 (Nguyen *et al.*, 2023). Although GCP16 can impart functional regulation on zDHHC enzymes that are closely

related to zDHHC9, there is less known about how this accessory protein might affect other zDHHC enzymes that co-distribute with zDHHC9 at the Golgi. For example, the potential interactions of GCP16 with enzymes such as zDHHC3 and zDHHC7, which are active against a broad range of proteins, has not been examined. Although these enzymes are not well conserved with zDHHC9 in the C-terminal region, GCP16 does form contacts with the DHHC domain of zDHHC9 (Yang *et al.*, 2024), which might suggest possible interaction/regulation of less well-conserved zDHHC enzymes by DHHC domain contacts.

Understanding the broader interactions of GCP16 with zDHHC enzymes is important not only from the perspective of gaining a better appreciation of how S-acylation dynamics are regulated in cells, but also from the perspective of developing new zDHHC enzyme inhibitors. The lack of selective inhibitors for zDHHC enzymes has been a major barrier to the progress of the field of S-acylation. Commonly used S-acylation inhibitors include 2-bromopalmitate, but this molecule is characterised by low selectivity and high cytotoxicity and cannot be used to target individual zDHHC enzymes (Davda *et al.*, 2013). There have been efforts to identify novel inhibitors through high-throughput screens, like the palmitoyl-transferase probe assay that uses palmitoyl-CoA mimetic probes that fluoresce when processed by zDHHC enzymes (Qiu *et al.*, 2022). In addition, there is also some ongoing work to target specific substrate interactions of zDHHC enzymes to reach selective inhibition, like Genistein, which binds to the ankyrin repeat domain that zDHHC17 uses for substrate recognition via the zDABM motif that proved to inhibit the S-acylation of MAP2K4 (Lemonidis *et al.*, 2015a, Chen *et al.*, 2020). Targeting the zDHHC9/GCP16 interaction may provide a novel strategy to mediate selective inhibition of zDHHC9, or a subset of zDHHC enzymes, and therefore, it is important to understand the wider interactions of this accessory protein.

The main aims of this chapter were to: (i) investigate the interaction, S-acylation and stability of GCP16 with other zDHHC enzymes; and (ii) analyse the potential use of peptide inhibitors derived from the sequence of GCP16 to disrupt the formation of the zDHHC9/GCP16 protein complex.

Results

5.1 Confirmation of GCP16 binding to zDHHC14 and zDHHC18

Previous work showed that in the absence of GCP16, zDHHC14 and zDHHC18 form enzymatically inactive aggregates in Sf9 cell lysates, similar to those observed with zDHHC9 (Nguyen *et al.*, 2023). GCP16 co-purification was required for the correct folding and catalytic activity of zDHHC14 and zDHHC18, which was assessed using purified H-Ras and [^{3}H] palmitoyl-CoA (Nguyen *et al.*, 2023). Furthermore, Yang *et al.* (2024) showed that both zDHHC14 and zDHHC18 can co-purify with GCP16 in Expi293F cells, and that the purified complexes are enzymatically active against H-Ras and N-Ras proteins (Yang *et al.*, 2024). Therefore, the first step in examining the broader interactions of GCP16 with zDHHC enzymes was to confirm that zDHHC14 and zDHHC18 could be captured by GCP16 in co-immunoprecipitation assays in mammalian cells. In addition, we also compared their binding to the GCP16 interface mutant 1-4a/b.

HEK293T cells were co-transfected with either HA-tagged zDHHC9, zDHHC14, or zDHHC18, together with EGFP-tagged GCP16 WT, binding interface mutant 1-4a/b, or EGFP as a control. Cell lysates were incubated with GFP-Trap® Agarose beads, and eluted proteins were examined by immunoblotting (Figure 5.1). Immunoblot results showed that both GCP16 WT and the GCP16 binding interface mutant 1-4a/b were successfully co-immunoprecipitated with zDHHC9, zDHHC14, and zDHHC18. In fact, zDHHC18 appeared to be more strongly co-immunoprecipitated with GCP16 1-4a/b than with the wild-type GCP16 protein (Figure 5.1B). In addition, analysis of the lysate samples indicates that whereas both zDHHC9 and zDHHC14 have higher expression levels with GCP16 wild-type than the 1-4a/b mutant or EGFP, the level of zDHHC18 was the same in all transfection lysates. This might imply that zDHHC18 is not stabilised by GCP16 interaction, unlike the other two enzymes. However, as this experiment was only performed once, it will be important to confirm the findings that are presented. All in all, these results confirm binding of GCP16 to zDHHC enzymes that are closely related to zDHHC9.

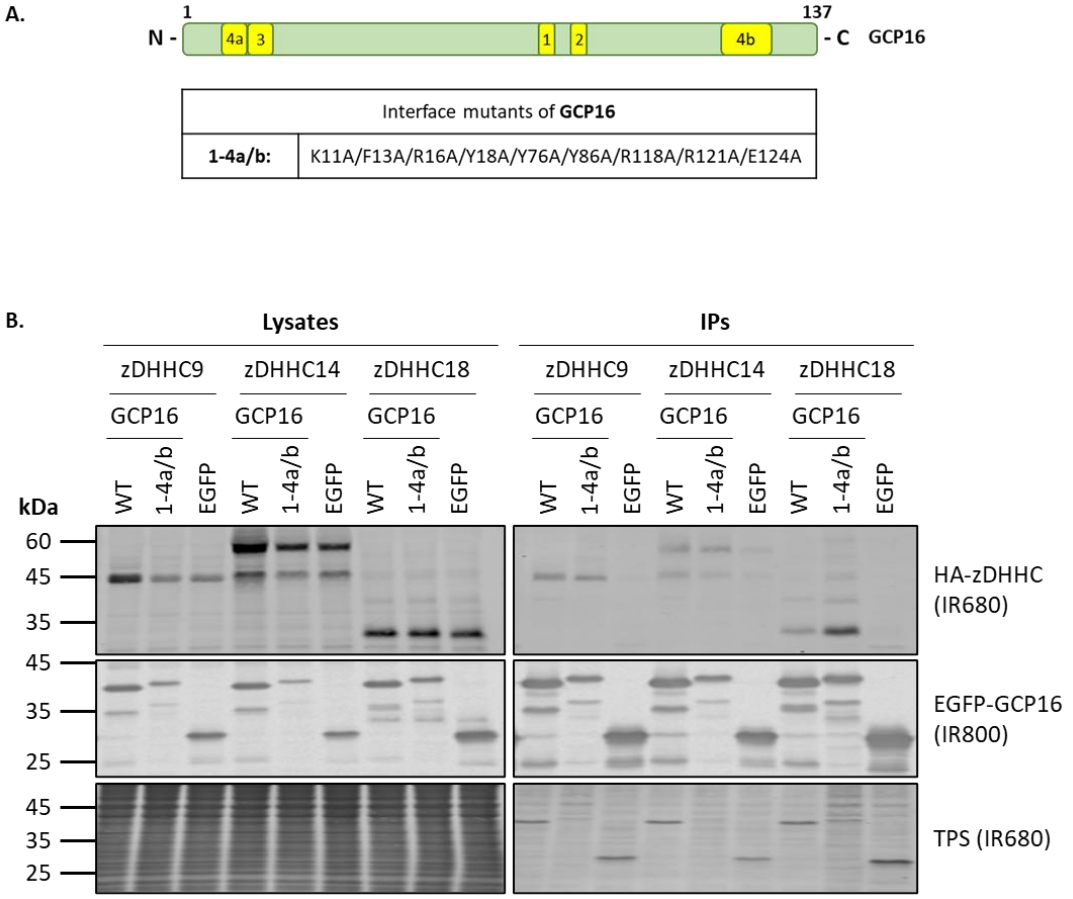

Figure 5.1 GCP16 wild-type and interface mutant can co-immunoprecipitate other zDHHC enzymes that are evolutionarily similar to zDHHC9.

(A) *Schematic of the GCP16 interface mutant construct used.* ***(B)*** *HEK293T cells were co-transfected with EGFP-tagged GCP16 WT, or 1-4a/b, together with HA-tagged zDHHC9, zDHHC14, or zDHHC18. The EGFP empty plasmid was used as a negative control. The EGFP-tagged proteins (IR800) were immunoprecipitated using anti-EGFP beads and detected by immunoblotting, along with co-immunoprecipitated HA-tagged proteins (IR680). The position of molecular weight markers (kDa) is shown on the left.*

5.2 GCP16 can co-immunoprecipitate other Golgi-localised zDHHC enzymes

The analysis in section 5.1, together with the work of Nguyen *et al.* (2023), and Yang *et al.* (2024) (Nguyen *et al.*, 2023, Yang *et al.*, 2024) confirm that GCP16 interacts with zDHHC enzymes that are closely linked to zDHHC9. However, the wider interaction of GCP16 with zDHHC enzymes has not been explored, and this is especially true for other Golgi-localised enzymes. Fluorescence microscopy and colocalisation analysis with the Golgi marker GM130 indicated that zDHHC3 and zDHHC7 are localised to the Golgi, similar to zDHHC9 (Ohno *et al.*, 2006). To investigate if GCP16 can interact with these other Golgi enzymes, HEK293T cells were co-transfected with EGFP-GCP16 or EGFP as a control, together with HA-tagged zDHHC3, zDHHC7, or zDHHC9 for a co-immunoprecipitation experiment. Cell lysates were incubated with GFP-Trap® Agarose beads, and eluted proteins were examined by immunoblotting, as described above (Figure 5.2). Sequence alignment of zDHHC9, zDHHC3, and zDHHC7 in Figure 5.2A highlights the limited similarity between these three enzymes outside of the conserved DHHC domain, with the lowest similarity being in the C-terminal region. The immunoblot results in Figure 5.2B show that all three enzymes were co-immunoprecipitated with EGFP-GCP16, while no co-immunoprecipitation was detected with the EGFP negative control. Quantified data in Figure 5.2C indicates that the highest co-immunoprecipitation levels were seen with zDHHC9, and since all three zDHHC enzymes were expressed at comparable levels, we could conclude that GCP16 binds to zDHHC9 more strongly than to zDHHC3 or zDHHC7. This observation suggests that there is a degree of selectivity in the zDHHC9/GCP16 interaction. Nevertheless, given that zDHHC3 and zDHHC7 show a stronger interaction with EGFP-GCP16 than with EGFP, these results do suggest that GCP16 may have a broader impact on Golgi-localised enzymes. Another point worth noting is that when comparing the cell lysate samples, zDHHC9 was more highly expressed in the presence of GCP16 than EGFP, whereas GCP16 co-expression did not affect the levels of zDHHC3 and zDHHC7. Thus, in addition to having a stronger interaction with zDHHC9, GCP16 may specifically stabilise this enzyme.

A.

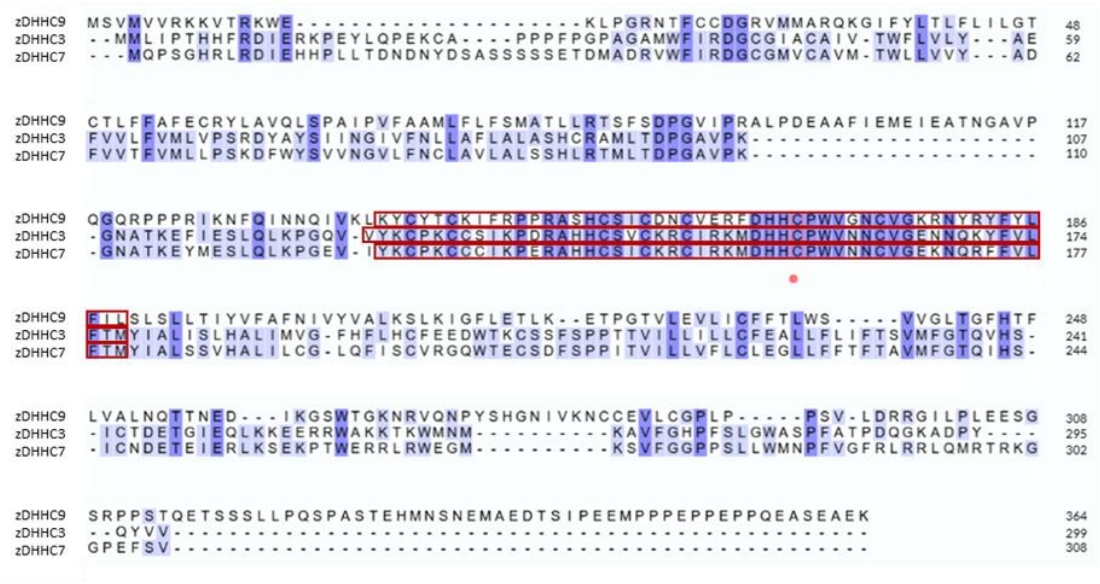
zDHHC9
zDHHC3
zDHHC7

B.

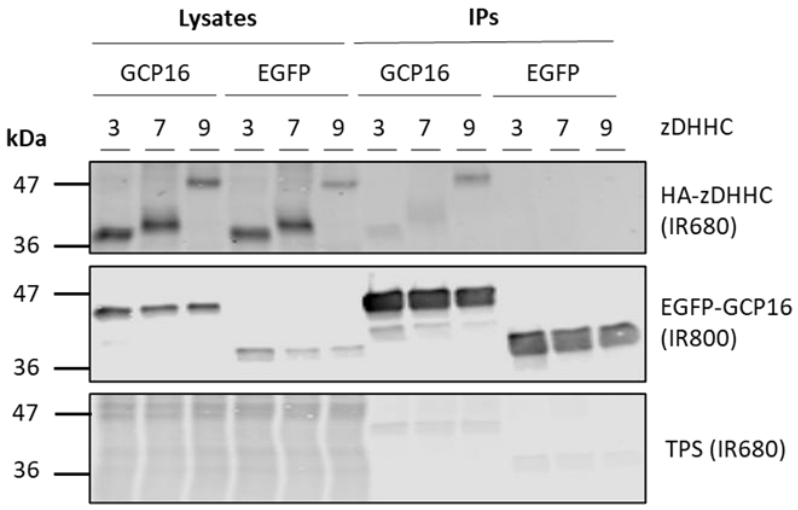
Lysates
IPs
GCP16
EGFP
GCP16
EGFP
kDa
3 7 9 3 7 9 3 7 9 3 7 9
zDHHC
47
36
HA-zDHHC (IR680)
EGFP-GCP16 (IR800)
TPS (IR680)

C.

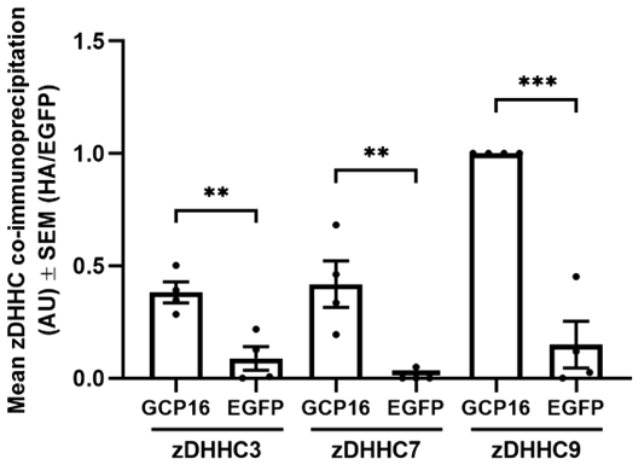
Mean zDHHC co-immunoprecipitation (AU) ± SEM (HA/EGFP)
1.5
1.0
0.5
0.0
**
**
***
GCP16 EGFP GCP16 EGFP GCP16 EGFP
zDHHC3
zDHHC7
zDHHC9

Figure 5.2 GCP16 can co-immunoprecipitate several Golgi-localised zDHHC enzymes.

(A) *Amino acid sequence alignment of mouse zDHHC9 (UniProt ID: P59268), zDHHC3 (UniProt ID: Q8R173), and zDHHC7 (UniProt ID: Q91WU6), generated using the Clustal Omega multiple sequence alignment program through the align tool from UniProt (UniProt, 2025). The amino acid similarity between the enzymes is highlighted, while their DHHC domain is indicated by a red border, and their active site is highlighted by a red circle.* ***(B)*** *HEK293T cells were co-transfected with EGFP-tagged GCP16 and HA-tagged zDHHC3, zDHHC7 or zDHHC9. The EGFP empty plasmid was used as a negative control. The EGFP-tagged proteins (IR800) were immunoprecipitated using anti-EGFP beads and detected by immunoblotting, along with co-immunoprecipitated HA-tagged proteins (IR680). The position of molecular weight markers (kDa) is shown on the left.* ***(C)*** *Quantified data show the mean (± SEM) intensity value of the HA-tagged proteins (IR680), divided by the corresponding intensity value of the EGFP signal (IR800) in each IP sample. The data has been normalised to the highest value of each experiment, which was set to 1. Statistical significance was analysed using unpaired t-tests, where *p<0.05, **p<0.01, and ***p<0.001, while ns denotes non-significance, where p>0.05. n = 4, from three independent experiments.*

5.3 GCP16 does not affect the protein stability of other Golgi-localised zDHHC enzymes

As noted in Figure 5.2, the expression levels of zDHHC3 and zDHHC7 in HEK293 cell lysates appeared to be similar in the absence and presence of GCP16. To confirm whether GCP16 has any effects on the stability of these Golgi-localised enzymes, HEK293T cells were co-transfected with HA-tagged zDHHC3, zDHHC7, or zDHHC9, together with EGFP or EGFP-tagged GCP16. Cells were then either lysed at 0 hours or incubated with cycloheximide protein synthesis inhibitor for 8 hours, and protein levels were examined by immunoblotting (Figure 5.3). Quantified data and statistical analysis showed that GCP16 co-expression significantly increased the stability of zDHHC9, but had no effect on the stability of zDHHC3 or zDHHC7 (Figure 5.3A), confirming our hypothesis. The reciprocal stabilisation of GCP16 by the enzymes was

also examined, as we showed previously that zDHHC9 could enhance the stability of GCP16. However, the results of this analysis were inconclusive due to high variation between the individual experimental repeats (Figure 5.3B). Thus, at this stage, we can only state with certainty that GCP16 imparts specific stabilisation on zDHHC9 and not zDHHC3 or zDHHC7, whereas further investigation of the effects of the enzymes on GCP16 stability is required.

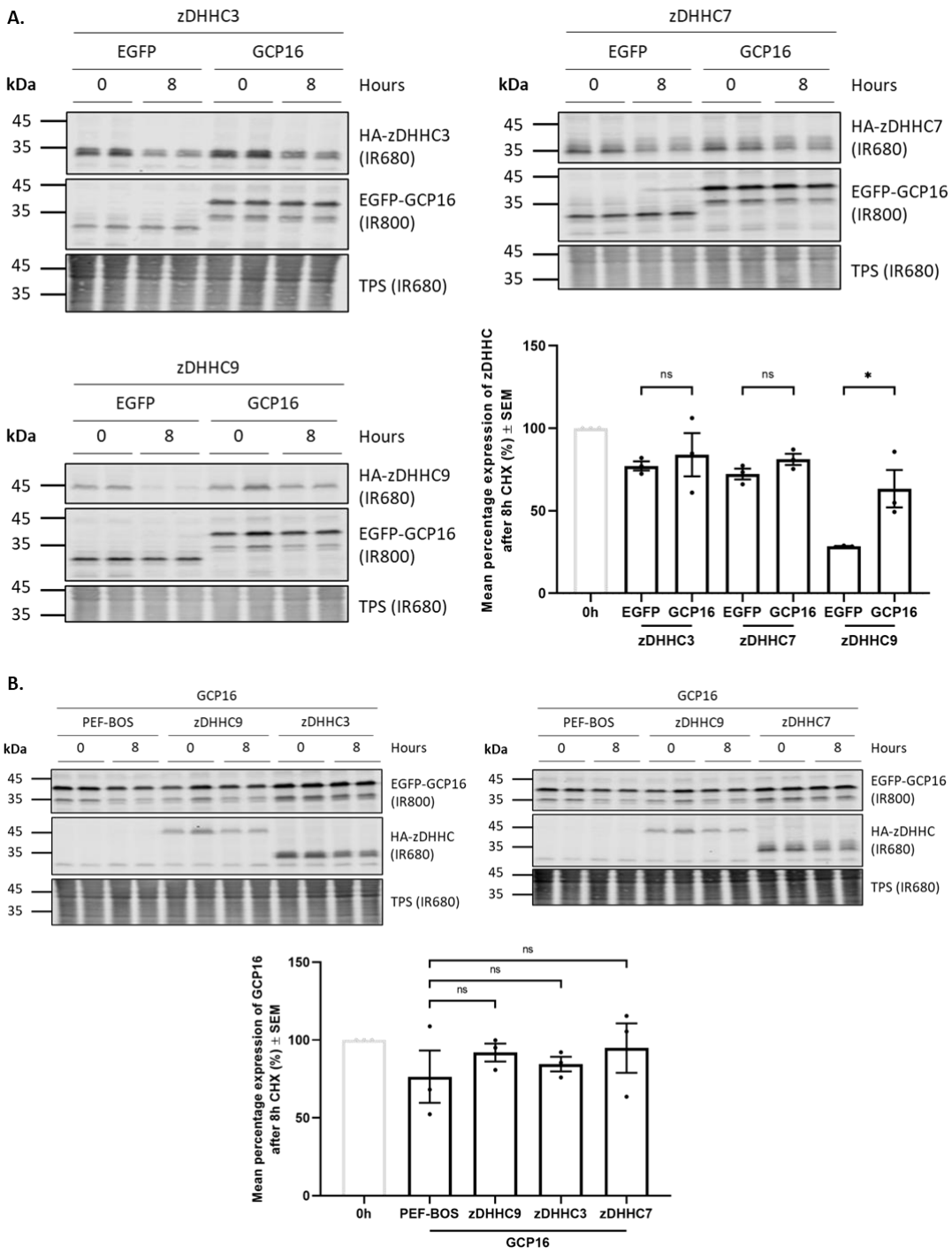
A.
zDHHC3
EGFP
GCP16
kDa
0
8
0
8
Hours
45
35
HA-zDHHC3
(IR680)
EGFP-GCP16
(IR800)
TPS (IR680)
zDHHC7
HA-zDHHC7
(IR680)
zDHHC9
HA-zDHHC9
(IR680)
Mean percentage expression of zDHHC after 8h CHX (%) ± SEM
150
100
50
0
ns
*
0h
EGFP
GCP16
zDHHC3
zDHHC7
zDHHC9
B.
PEF-BOS
zDHHC9
zDHHC3
zDHHC7
EGFP-GCP16
(IR800)
HA-zDHHC
(IR680)
TPS (IR680)
Mean percentage expression of GCP16 after 8h CHX (%) ± SEM
PEF-BOS
zDHHC9
zDHHC3
zDHHC7
GCP16

Figure 5.3 GCP16 stabilises zDHHC9 but not zDHHC3 or zDHHC7.

*HEK293T cells were co-transfected with HA-tagged zDHHC3, zDHHC7, or zDHHC9, along with EGFP, or EGFP-tagged GCP16. The PEF-BOS-HA empty plasmid was used as a control. Lysates were collected at 0 hours or after 8 hours of incubation with 50 µg/ml cycloheximide (CHX). Protein expression levels were detected by immunoblotting. The position of molecular weight markers (kDa) is shown on the left. Quantified data show the mean percentage protein expression (± SEM) after 8 hours of CHX treatment, quantified relative to the corresponding 0-hour value and normalised to the total protein stain levels of each sample. Statistical significance was analysed using an unpaired t-test, or an ordinary one-way ANOVA, followed by a Dunnett's multiple comparisons test where appropriate. *p<0.05, **p<0.01 and ***p<0.001, while ns denotes non-significance, where p>0.05. n = 3, from two independent experiments.*

5.4 Reciprocal effects on S-acylation are seen between GCP16 and zDHHC9, but not between GCP16 and zDHHC3

We showed in previous results chapters that co-expression of GCP16 and zDHHC9 leads to an increase in the S-acylation of each protein. Here, we examined whether these reciprocal effects on S-acylation are also seen with zDHHC3 and GCP16. HEK293T cells were co-transfected with HA-tagged zDHHC9 or zDHHC3, together with EGFP or EGFP-tagged GCP16. Cells were labelled with either palmitic acid as a control or palmitic acid azide and processed for click chemistry detection of S-acylation using alkyne mPEG (5 kDa). The protein samples were then resolved by SDS-PAGE, while immunoblot analysis allowed for the visualisation of the proteins and the detection of S-acylation (Figure 5.4). The results in Figure 5.4A show that while GCP16 co-expression significantly enhanced the S-acylation of zDHHC9, it had no effect on zDHHC3 S-acylation. Both zDHHC9 and zDHHC3, however, cause a similar increase in GCP16 S-acylation (Figure 5.4B). Thus, the interaction of GCP16 with zDHHC9 is required for the S-acylation of this enzyme and has reciprocal effects on the S-acylation of GCP16, but while GCP16 is S-acylated by zDHHC3, their interaction has no effect on zDHHC3 S-acylation.

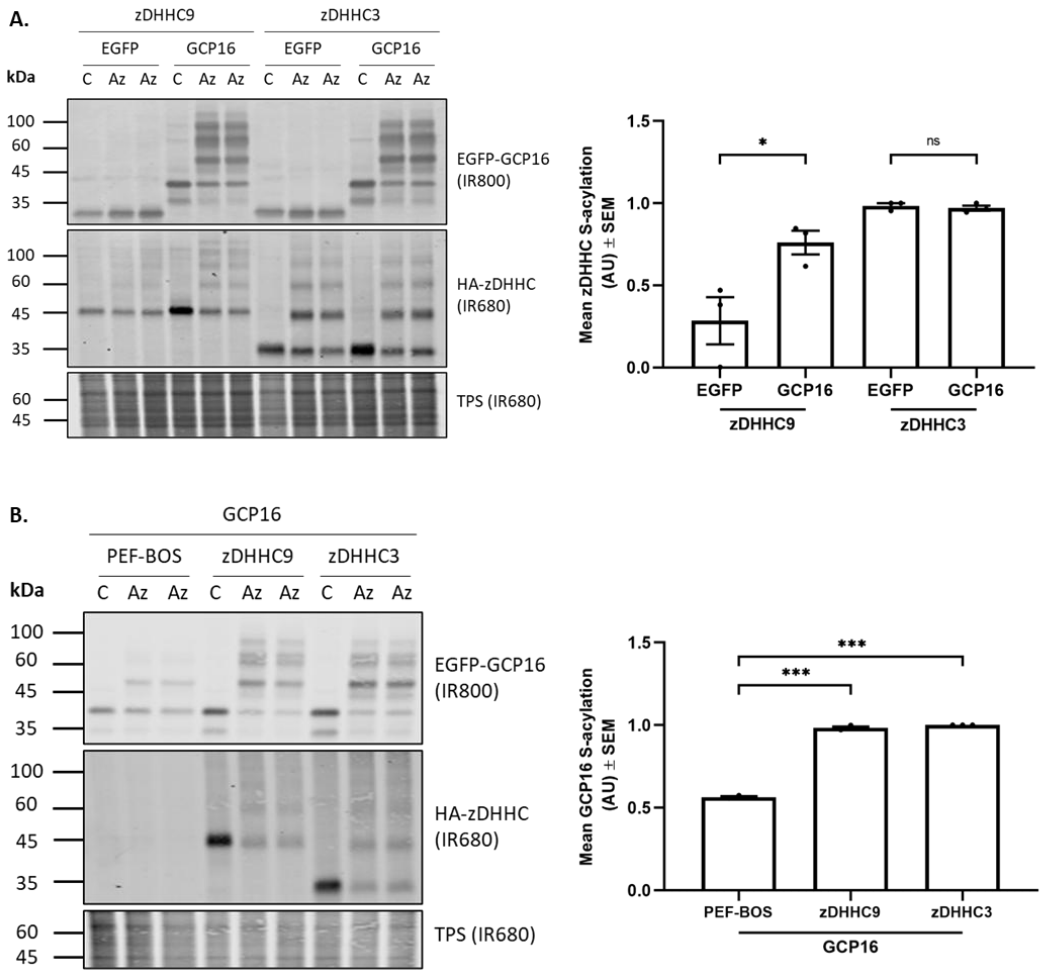
A.
zDHHC9
zDHHC3
EGFP
GCP16
EGFP
GCP16
kDa
C Az Az C Az Az C Az Az C Az Az
100
60
45
35
EGFP-GCP16
(IR800)
HA-zDHHC
(IR680)
TPS (IR680)
Mean zDHHC S-acylation
(AU) ± SEM
*
ns
EGFP
GCP16
EGFP
GCP16
zDHHC9
zDHHC3
B.
GCP16
PEF-BOS
zDHHC9
zDHHC3
Mean GCP16 S-acylation
(AU) ± SEM
***
***
PEF-BOS
zDHHC9
zDHHC3
GCP16

Figure 5.4 Reciprocal S-acylation is seen with GCP16 and zDHHC9, but not zDHHC3.

*HEK293T cells were co-transfected with HA-tagged zDHHC9 or zDHHC3, together with EGFP (empty plasmid control) or EGFP-tagged GCP16. The PEF-BOS-HA empty plasmid was used as a control. Cells were labelled with palmitic acid (C16:0) as a control (C) or palmitic acid azide (Az-C16:0) for 4 hours and were then lysed and clicked using alkyne mPEG (5 kDa). S-acylation is indicated by band shifts in Az samples. The position of molecular weight markers (kDa) is shown on the left. Quantified data show the mean percentage (± SEM) intensity values of the S-acylated substrates. The S-acylated bands were quantified as a percentage of total expression for each substrate incubated with the palmitic acid azide. The data has been normalised to the highest value of each experiment, which was set to 1. Statistical significance was analysed using an unpaired t-test, or an ordinary one-way ANOVA, followed by a Dunnett's multiple comparisons test where appropriate. *p<0.05, **p<0.01 and ***p<0.001, while ns denotes non-significance, where p>0.05. n = 3, from three independent experiments.*

5.5 S-acylation of GCP16 by zDHHC3 is disrupted by binding interface mutations

We next examined if zDHHC3 also requires intact binding interfaces for the S-acylation of GCP16, as we have shown for zDHHC9. HEK293T cells were co-transfected with HA-tagged zDHHC9 or zDHHC3, together with EGFP, EGFP-tagged GCP16 WT, or binding interface mutant 1-4a/b. Cells were labelled and processed for click chemistry using alkyne mPEG (5 kDa) as described above. The protein samples were then resolved by SDS-PAGE, followed by immunoblotting (Figure 5.5). As per previous experiments, S-acylation was completely abolished with GCP16 binding interface mutant 1-4a/b when co-expressed with zDHHC9, and there was no stabilisation of zDHHC9 S-acylation by the mutant (Figure 5.5B). In addition, zDHHC3 also showed a substantial reduction in its ability to S-acylate this mutant, although there was slightly more S-acylation than seen with zDHHC9. Neither the wild-type nor the mutant GCP16 construct affected the S-acylation status of zDHHC3 (Figure 5.5C). This data suggests that zDHHC3 requires the same binding interfaces as zDHHC9 to

mediate efficient S-acylation of GCP16. Another possibility is that the structural conformation of the GCP16 binding interface mutant 1-4a/b is excessively disrupted, in a way that S-acylation by highly active zDHHC3 is prevented, even though the interaction between the proteins may be less specific than the zDHHC9/GCP16 interaction.

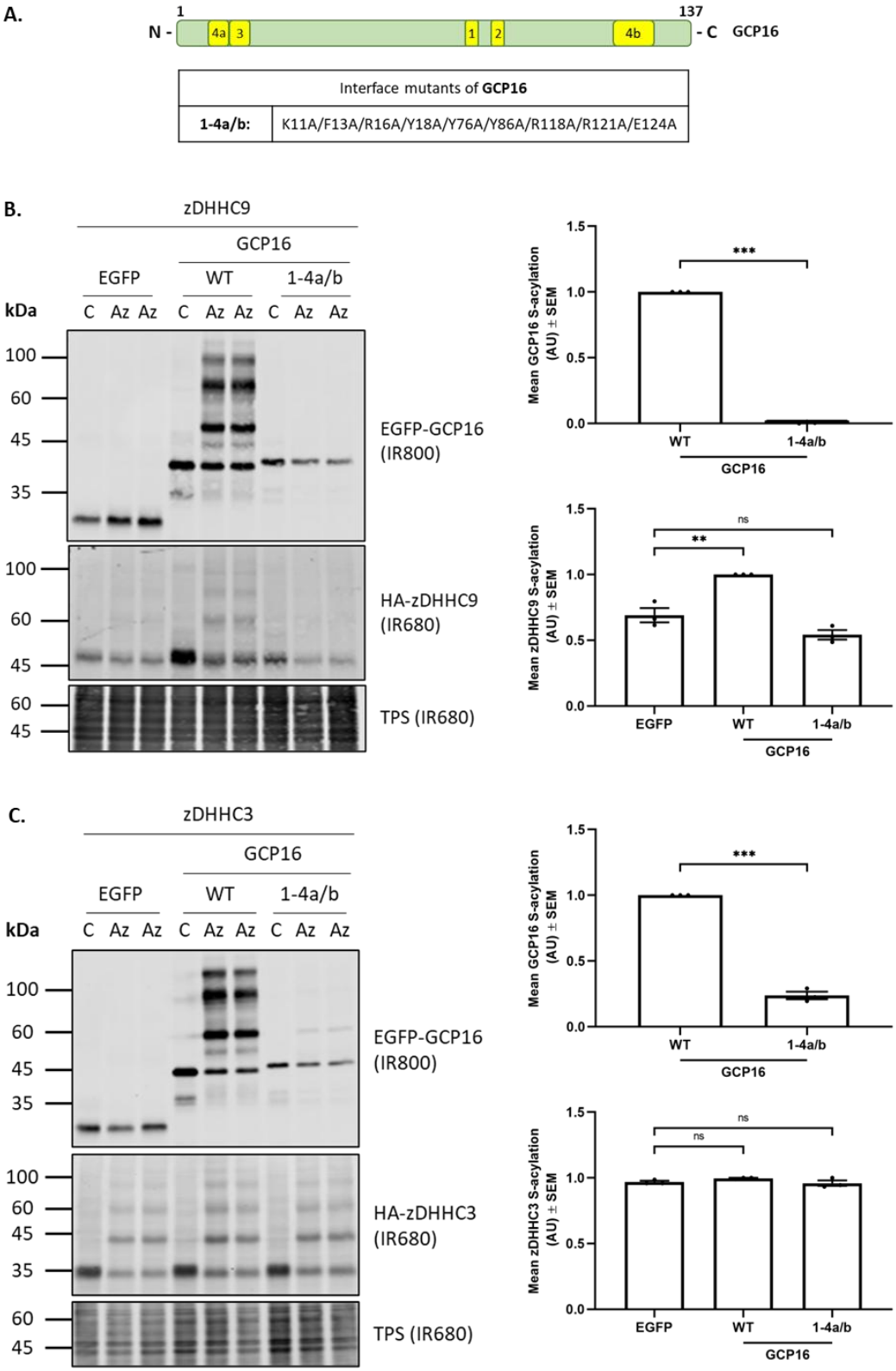
A.
1
137
N -
4a
3
1
2
4b
- C
GCP16
Interface mutants of GCP16
1-4a/b:
K11A/F13A/R16A/Y18A/Y76A/Y86A/R118A/R121A/E124A
B.
zDHHC9
GCP16
EGFP
WT
1-4a/b
kDa
C Az Az C Az Az C Az Az
100
60
45
35
EGFP-GCP16
(IR800)
HA-zDHHC9
(IR680)
TPS (IR680)
Mean GCP16 S-acylation
(AU) ± SEM
***
WT
1-4a/b
GCP16
Mean zDHHC9 S-acylation
(AU) ± SEM
ns
**
EGFP
C.
zDHHC3
HA-zDHHC3
(IR680)
Mean zDHHC3 S-acylation
(AU) ± SEM

Figure 5.5 GCP16 interface mutant 1-4a/b cannot be S-acylated by zDHHC3.

(A) *Schematic of the GCP16 interface mutant construct used. HEK293T cells were co-transfected with EGFP (empty plasmid control), EGFP-tagged GCP16 WT, or 1-4a/b, and either* ***(B)*** *HA-zDHHC9, or* ***(C)*** *HA-zDHHC3. Cells were labelled with palmitic acid (C16:0) as a control (C) or palmitic acid azide (Az-C16:0) for 4 hours and were then lysed and clicked using alkyne mPEG (5 kDa). S-acylation is indicated by band shifts in Az samples. The position of molecular weight markers (kDa) is shown on the left. Quantified data show the mean percentage (± SEM) intensity values of the S-acylated substrates. The S-acylated bands were quantified as a percentage of total expression for each substrate incubated with the palmitic acid azide. The data has been normalised to the highest value of each experiment, which was set to 1. Statistical significance was analysed using an unpaired t-test, or an ordinary one-way ANOVA, followed by Dunnett's multiple comparisons test where appropriate. *p<0.05, **p<0.01 and ***p<0.001, while ns denotes non-significance, where p>0.05. n = 3, from three independent experiments.*

5.6 Developing chimeric mutants of zDHHC9-zDHHC3 to better understand the specific effects of GCP16 on zDHHC9

The results above show that GCP16 binds more strongly to zDHHC9 than to zDHHC3. In addition, the effects of GCP16 on zDHHC9 stabilisation and S-acylation are not seen with zDHHC3. To better understand how these differences may arise, especially the effects on zDHHC9 S-acylation, we examined whether there was something specific about the DHHC domain that led to a requirement for GCP16 to stabilise the S-acylation of zDHHC9. To do this, we designed mutants of zDHHC9 in which amino acids in the DHHC domain were replaced by corresponding residues present at the same position in zDHHC3 (Figure 5.6A). By analysing these mutants, it should be possible to determine if switching any of these residues led to stabilisation of zDHHC9 S-acylation in the absence of GCP16, similarly to zDHHC3.

The first step towards characterising the zDHHC9 mutants was to compare their co-immunoprecipitation with EGFP-GCP16 to that of wild-type zDHHC9. Cell lysates expressing wild-type zDHHC9, the chimeric mutants, or wild-type zDHHC3, together with EGFP or EGFP-GCP16 were incubated with GFP-Trap® Agarose beads, and

eluted proteins were examined by immunoblotting (Figure 5.6B). Figure 5.6B shows that all mutants were co-immunoprecipitated with GCP16, while there was no binding detected with the EGFP negative control. Quantified data and statistical analysis showed that co-immunoprecipitation levels of zDHHC3 with GCP16 were significantly decreased compared to the levels seen for zDHHC9 WT. The chimeric mutant 3.2 with amino acid substitutions introduced at the start of the DHHC domain, at residues 145-148 (KIFR to CSIK), showed the lowest co-immunoprecipitation levels with GCP16 and the largest decrease when compared to zDHHC9 WT (Figure 5.6B).

A.

DHHC domain mutants of zDHHC9:

3.1: YKCPKCKIFRPPRASHCSICDNCVERFDHHCPWVGNCVGKRNYRYFYLFIL

3.2: KYCYTCCSIKPPRASHCSICDNCVERFDHHCPWVGNCVGKRNYRYFYLFIL

3.3: KYCYTCKIFRPPRASHCSVCKRCVERFDHHCPWVGNCVGKRNYRYFYLFIL

3.4: KYCYTCKIFRPPRASHCSICDNCIRKMDHHCPWVGNCVGKRNYRYFYLFIL

3.5: KYCYTCKIFRPPRASHCSICDNCVERFDHHCPWVGNCVGENNQKYFYLFIL

B.

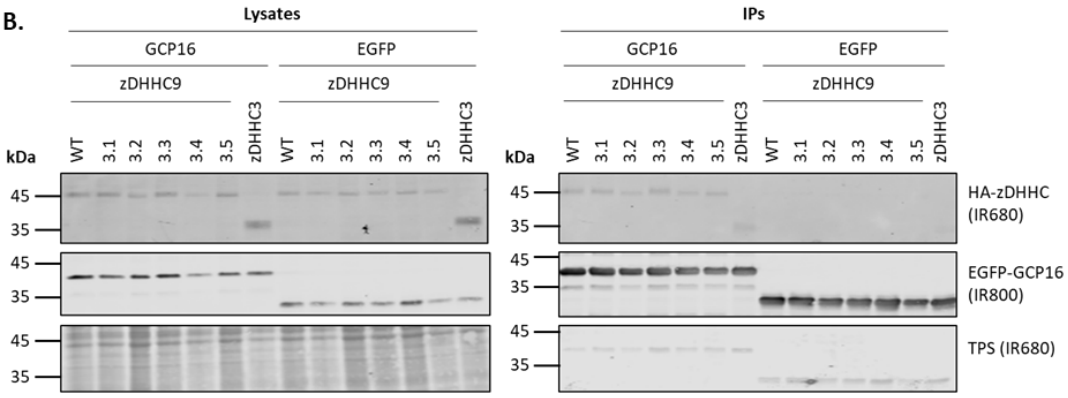

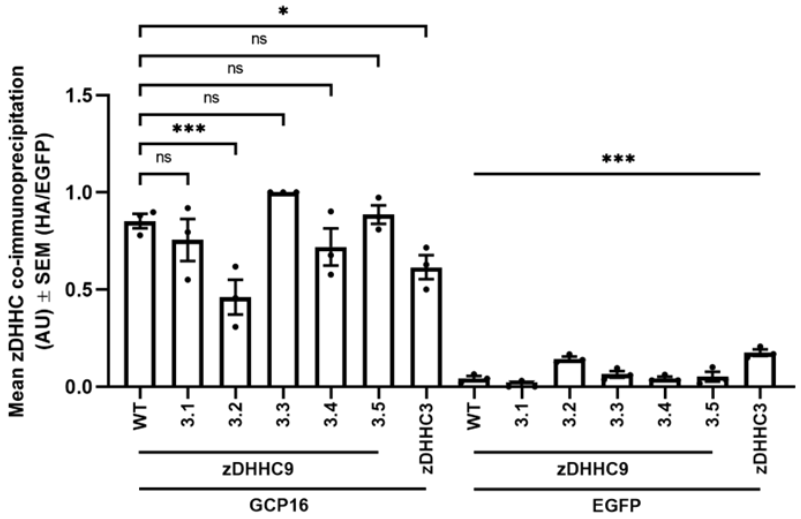

Figure 5.6 Co-immunoprecipitation of zDHHC9 DHHC domain mutant constructs with GCP16.

(A) *Amino acid sequence alignment of the DHHC domains of mouse zDHHC9 (amino acids 139-189) (UniProt ID: P59268) and zDHHC3 (amino acids 127-177) (UniProt ID: Q8R173), generated using the Clustal Omega multiple sequence alignment program through the align tool from UniProt (UniProt, 2025). Identical amino acids are highlighted in purple, while the substitutions made in the zDHHC9 DHHC domain based on the sequence of zDHHC3 are shown in red.* ***(B)*** *HEK293T cells were co-transfected with EGFP-tagged GCP16 and either HA-tagged zDHHC9 WT, 3.1, 3.2, 3.3, 3.4, 3.5, or zDHHC3. The EGFP empty plasmid was used as a negative control. The EGFP-tagged proteins (IR800) were immunoprecipitated using anti-EGFP beads and detected by immunoblotting, along with co-immunoprecipitated HA-tagged proteins (IR680). The position of molecular weight markers (kDa) is shown on the left. Quantified data show the mean (± SEM) intensity value of the HA-tagged proteins (IR680), divided by the corresponding intensity value of the EGFP signal (IR800) in each IP sample. The data has been normalised to the highest value of each experiment, which was set to 1. Statistical significance was analysed using an ordinary one-way ANOVA, followed by a Dunnett's multiple comparisons test. *p<0.05, **p<0.01 and ***p<0.001, while ns denotes non-significance, where p>0.05. n = 3, from two independent experiments.*

We next undertook a click chemistry experiment to investigate whether any of the DHHC domain substitutions made in zDHHC9 affect the reciprocal effects on GCP16 S-acylation. HEK293T cells were co-transfected with EGFP or EGFP-GCP16, together with either HA-tagged zDHHC9, zDHHC3, or the DHHC domain mutants shown in Figure 5.7A. Cells were labelled with either palmitic acid as a control or palmitic acid azide and processed for click chemistry detection of S-acylation using alkyne mPEG (5 kDa). The protein samples were then resolved by SDS-PAGE, followed by immunoblotting.

We first investigated the ability of the mutants to S-acylate GCP16 to determine whether they were still catalytically active. Quantified data in Figure 5.7B showed that only the wild-type enzymes and zDHHC9 DHHC mutant 3.3 with amino acid substitutions at residues 157-160 (ICDN to VCKR) significantly increased the levels

of GCP16 S-acylation. In contrast, the other mutants had no significant effect on GCP16 S-acylation. Regarding S-acylation of zDHHC9, none of the mutants showed a switch in profile to that seen with zDHHC3, i.e. robust S-acylation with no effect of GCP16 co-expression (Figure 5.7C). Although this experiment should be repeated, the results shown in Figure 5.7 suggest that none of the DHHC domain mutants change the overall S-acylation profile to mimic zDHHC3. However, as many of the mutations led to a loss of zDHHC9 activity, more precise amino acid substitutions should be examined to hopefully prevent this from occurring.

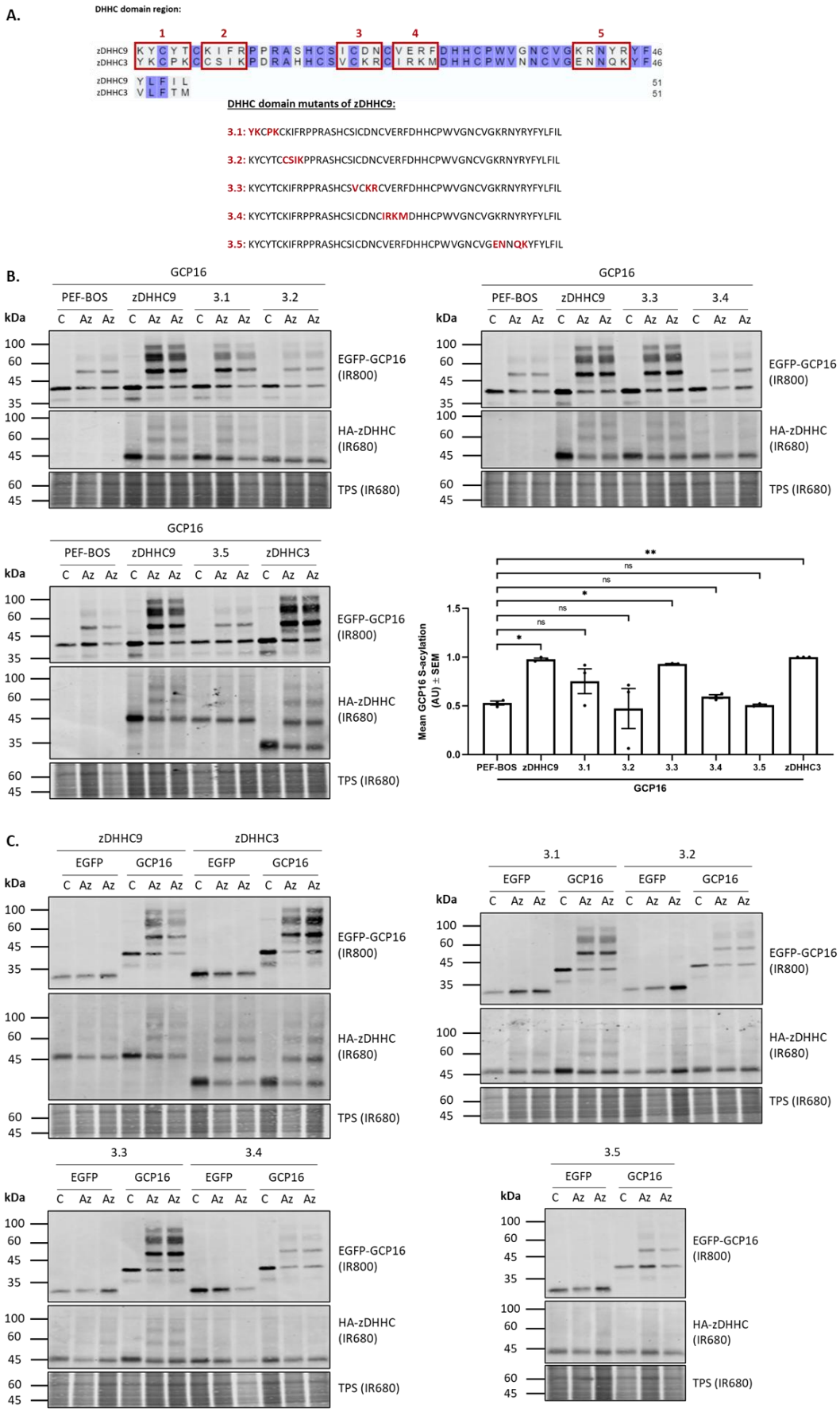
A.
DHHC domain region:
1
2
3
4
5
zDHHC9 K Y C Y T C K I F R P P R A S H C S I C D N C V E R F D H H C P W V G N C V G K R N Y R Y F 46
zDHHC3 Y K C P K C C S I K P D R A H H C S V C K R C I R K M D H H C P W V N N C V G E N N Q K Y F 46
zDHHC9 Y L F I L 51
zDHHC3 V L F T M 51
DHHC domain mutants of zDHHC9:
3.1: YKCPKCKIFRPPRASHCSICDNCVERFDHHCPWVGNCVGKRNYRYFYLFIL
3.2: KYCYTCCSIKPPRASHCSICDNCVERFDHHCPWVGNCVGKRNYRYFYLFIL
3.3: KYCYTCKIFRPPRASHCSVCKRCVERFDHHCPWVGNCVGKRNYRYFYLFIL
3.4: KYCYTCKIFRPPRASHCSICDNCIRKMDHHCPWVGNCVGKRNYRYFYLFIL
3.5: KYCYTCKIFRPPRASHCSICDNCVERFDHHCPWVGNCVGENNQKYFYLFIL
B.
GCP16
PEF-BOS
zDHHC9
3.1
3.2
3.3
3.4
3.5
zDHHC3
kDa
C Az Az
100
60
45
35
EGFP-GCP16 (IR800)
HA-zDHHC (IR680)
TPS (IR680)
Mean GCP16 S-acylation (AU) ± SEM
1.5
1.0
0.5
0.0
*
**
ns
C.
zDHHC9
zDHHC3
EGFP
GCP16

Figure 5.7 S-acylation profiles of zDHHC9 DHHC domain mutant constructs.

(A) *Amino acid sequence alignment of the DHHC domains of mouse zDHHC9 (amino acids 139-189) (UniProt ID: P59268) and zDHHC3 (amino acids 127-177) (UniProt ID: Q8R173), generated using the Clustal Omega multiple sequence alignment program through the align tool from UniProt (UniProt, 2025). Identical amino acids are highlighted in purple, while the substitutions made in the zDHHC9 DHHC domain based on the sequence of zDHHC3 are shown in red.* ***(B-C)*** *HEK293T were co-transfected with EGFP (empty plasmid control) or EGFP-GCP16, and either HA-tagged zDHHC9, zDHHC3, 3.1, 3.2, 3.3, 3.4, or 3.5. PEF-BOS-HA empty plasmid was used as a control. Cells were labelled with palmitic acid (C16:0) as a control (C) or palmitic acid azide (Az-C16:0) for 4 hours and were then lysed and clicked using alkyne mPEG (5 kDa). S-acylation is indicated by band shifts in Az samples. The position of molecular weight markers (kDa) is shown on the left. Quantified data show the mean percentage (± SEM) intensity values of the S-acylated substrates. The S-acylated bands were quantified as a percentage of total expression for each substrate incubated with the palmitic acid azide. The data has been normalised to the highest value of each experiment, which was set to 1. Statistical significance was analysed using ordinary one-way ANOVA, followed by Dunnett's multiple comparisons test. *p<0.05, **p<0.01 and ***p<0.001, while ns denotes non-significance, where p>0.05. n = 3, from three independent experiments.*

5.7 The N-terminal region of GCP16 is involved in homodimerisation

There is evidence that zDHHC enzymes can form higher molecular weight oligomers that influence enzyme activity (Lai and Linder, 2013), and indeed GCP16 was previously reported to influence the aggregation/oligomerisation of zDHHC9 (Nguyen *et al.*, 2023). Given the importance of GCP16 in regulating zDHHC9, and its wider interactions with other zDHHC enzymes, we were interested in whether this accessory protein also forms dimers or other oligomers, which might provide a new perspective on its interaction with zDHHC enzymes. Initial co-immunoprecipitation experiments suggested that this might be the case, and so we compared the co-immunoprecipitation of HA-GCP16 with a number of EGFP-tagged GCP16 truncation mutants to identify what regions of GCP16 might be undergoing self-association.

HEK293T cells were co-transfected with HA-tagged GCP16, along with EGFP-tagged GCP16 WT, 1-30, 1-60, 1-90, or 91-137. EGFP was used as a negative control. To investigate protein binding, cell lysates were incubated with GFP-Trap® Agarose beads, and eluted proteins were examined by immunoblotting (Figure 5.8A). Immunoblot results showed that HA-GCP16 was successfully co-immunoprecipitated with EGFP-GCP16 WT, indicating the formation of a homodimer. EGFP-tagged GCP16 1-60 and 1-90 were also able to co-immunoprecipitate HA-GCP16, as seen by the bands detected on the immunoblot. However, quantified data and statistical analysis showed that the GCP16 co-immunoprecipitation seen with GCP16 truncation mutant 1-60 was not significantly different from the negative EGFP control, while GCP16 co-immunoprecipitation levels with GCP16 truncation mutant 1-90 were significantly higher – but this was linked to the lower expression of the EGFP-tagged truncation mutant (Figure 5.8A). At this point, we are not able to confirm whether the amino acid region 30-60 of GCP16 is involved in homodimerisation but it does appear that the N-terminal region of the protein mediates homodimerisation.

It was also investigated whether the zDHHC9 binding interfaces within GCP16 were involved in the homodimerisation of GCP16. For this, HEK293T cells were co-transfected with HA-tagged GCP16, along with EGFP-tagged GCP16 WT, or binding interface mutant 3, 4b, 4a/b, or 1-4a/b. EGFP was used as a negative control. To investigate protein binding, cell lysates were treated as described above for Figure 5.8A. Immunoblot results showed that HA-GCP16 was co-immunoprecipitated with the GCP16 WT control and all interface mutants used, whereas there was no binding detected for the EGFP negative control (Figure 5.8B).

A.

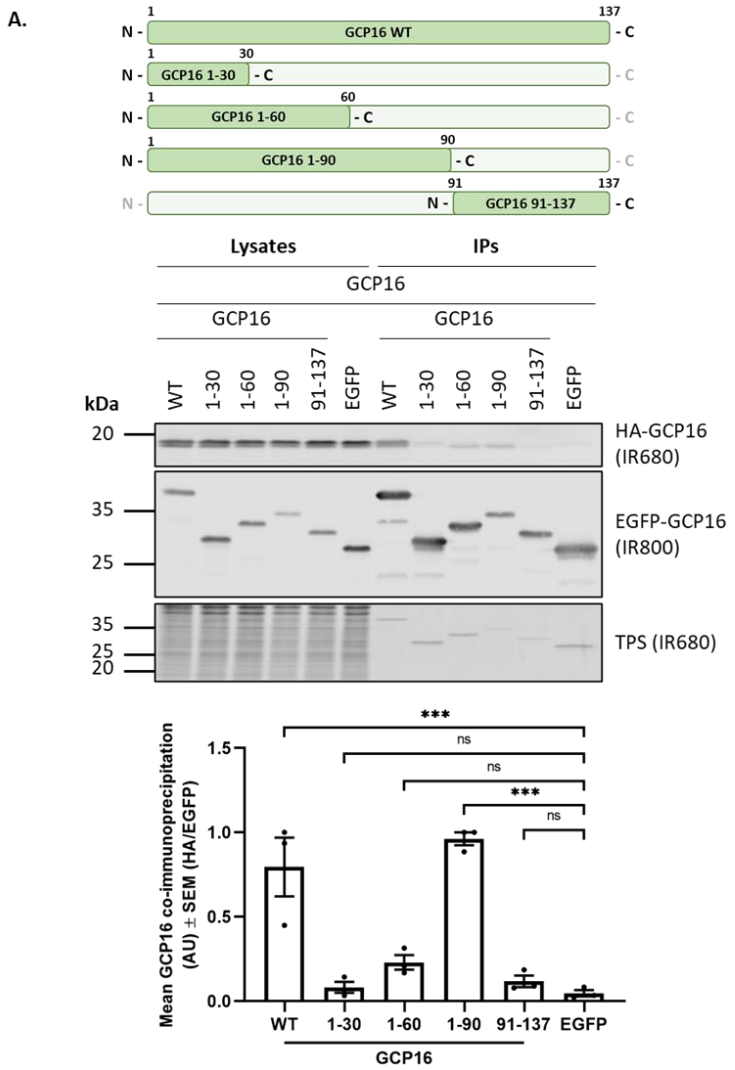

B.

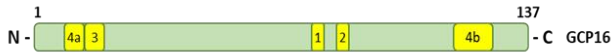

Interface mutants of **GCP16**	
3:	R16A/Y18A
4b:	R118A/R121A/E124A
4a/b:	K11A/F13A/R118A/R121A/E124A
1-4a/b:	K11A/F13A/R16A/Y18A/Y76A/Y86A/R118A/R121A/E124A

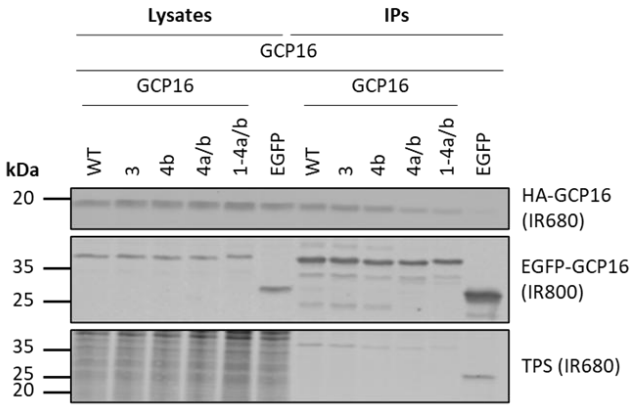

Figure 5.8 The N-terminal region of GCP16 is involved in homodimerisation.

(A) *Schematic showing the GCP16 truncation mutants used. HEK293T cells were co-transfected with HA-tagged GCP16, together with EGFP-tagged GCP16 WT, 1-30, 1-60, 1-90, or 91-137. The EGFP empty plasmid was used as a negative control. The EGFP-tagged proteins (IR800) were immunoprecipitated using anti-EGFP beads and detected by immunoblotting, along with co-immunoprecipitated HA-tagged proteins (IR680). The position of molecular weight markers (kDa) is shown on the left. Quantified data show the mean (± SEM) intensity value of the HA-tagged proteins (IR680), divided by the corresponding intensity value of the EGFP signal (IR800) in each IP sample. The data has been normalised to the highest value of each experiment, which was set to 1. Statistical significance was analysed using an ordinary one-way ANOVA, followed by a Dunnett's multiple comparisons test. *p<0.05, **p<0.01 and ***p<0.001, while ns denotes non-significance, where p>0.05. n = 3, from three independent experiments.* ***(B)*** *Schematic of the GCP16 interface mutant constructs used, designed based on the cryo-EM structure of the zDHHC9/GCP16 protein complex. HEK293T cells were co-transfected with HA-tagged GCP16, together with EGFP-tagged GCP16 WT, 3, 4b, 4a/b, or 1-4a/b. The EGFP empty plasmid was used as a negative control. The EGFP-tagged proteins (IR800) were immunoprecipitated using anti-EGFP beads and detected by immunoblotting, along with co-immunoprecipitated HA-tagged proteins (IR680). The position of molecular weight markers (kDa) is shown on the left.*

5.8 Investigating if targeting specific domains of GCP16 to the Golgi complex can disrupt the zDHHC9/GCP16 protein complex

The overarching aim of this project was to generate enough knowledge on the zDHHC9/GCP16 interaction to develop peptide inhibitors with high selectivity for zDHHC9 that could disrupt the formation of the complex and selectively inhibit the activity of zDHHC9. To provide an initial insight into whether this was possible, a set of three peptides was designed based on the amino acid sequence of GCP16. One of these contained amino acids 1-60 (with an alanine substitution at Cys-24 to block S-acylation), and encompasses a key region involved in interfaces 3 (R16/Y18) and 4 (K11/F13) of the interaction with zDHHC9. The other two peptides contained either

amino acids 91-124 or 91-137. Both of these contain a region involved in interface 4 (R118/R121/E124) interaction with zDHHC9, but previous analysis showed that 91-137 could co-immunoprecipitate zDHHC9, whereas 91-124 could not. These peptides were then fused to a 10-amino acid Golgi-localisation sequence (GLS), FLWRIFCFRK (Navarro and Cheeseman, 2022), separated by two copies of a Gly(4)-Ser flexible linker. These constructs were cloned into a plasmid that encodes an N-terminal mCherry tag and are referred to as: GLS, the Golgi localisation sequence with no GCP16 peptide fused to it; GLS-1, which contains amino acids 1-60 of GCP16; GLS-2, containing amino acids 91-124 of GCP16; and GLS-3, which includes amino acids 91-137 of GCP16 (Figure 5.9A).

To investigate the ability of these constructs to act as inhibitors of the zDHHC9/GCP16 complex, a co-immunoprecipitation experiment with GCP16 and zDHHC9 was designed to assess effects on binding, together with a cycloheximide experiment to test if the peptides can decrease the stability of zDHHC9 or GCP16. HEK293T cells were co-transfected with EGFP-GCP16, along with HA-zDHHC9 and either mCherry-tagged GLS, GLS-1, GLS-2, or GLS-3. The EGFP and mCherry empty plasmids were used as controls. For co-immunoprecipitation analysis, cell lysates were incubated with GFP-Trap® Agarose beads, and eluted proteins were examined by immunoblotting (Figure 5.9B). For cycloheximide analysis, cells were either lysed at 0 hours or incubated with cycloheximide protein synthesis inhibitor for 8 hours, and protein levels were then examined by immunoblotting (Figure 5.9C).

The immunoblot results in Figure 5.9B showed that the GLS control peptide inhibitor did not affect zDHHC9 co-immunoprecipitation with GCP16, as expected. However, zDHHC9 was also efficiently co-immunoprecipitated in the presence of GLS-1, GLS-2, and GLS-3. It was noted that GCP16 and zDHHC9 appear to be more highly expressed with all of the GLS constructs (compare lysate samples), compared to the mCherry controls, indicating there might be a stabilising effect on the proteins by these constructs.

The results of the cycloheximide experiments showed that the Golgi-localisation peptides, including the GLS control, seemed to increase the stability of GCP16 when co-expressed with zDHHC9. However, as this experiment was only repeated twice, statistical analysis could not be performed, and it is uncertain whether this increase is significantly different from co-expression with the mCherry empty plasmid and zDHHC9. As for zDHHC9 stability, GCP16 co-expression seemed to increase the

stability of zDHHC9, as expected. Co-expression with the Golgi-localisation peptides did not appear to influence the effect of GCP16 on zDHHC9 stability, although this should be confirmed after repeating the experiment and performing statistical analysis (Figure 5.9C).

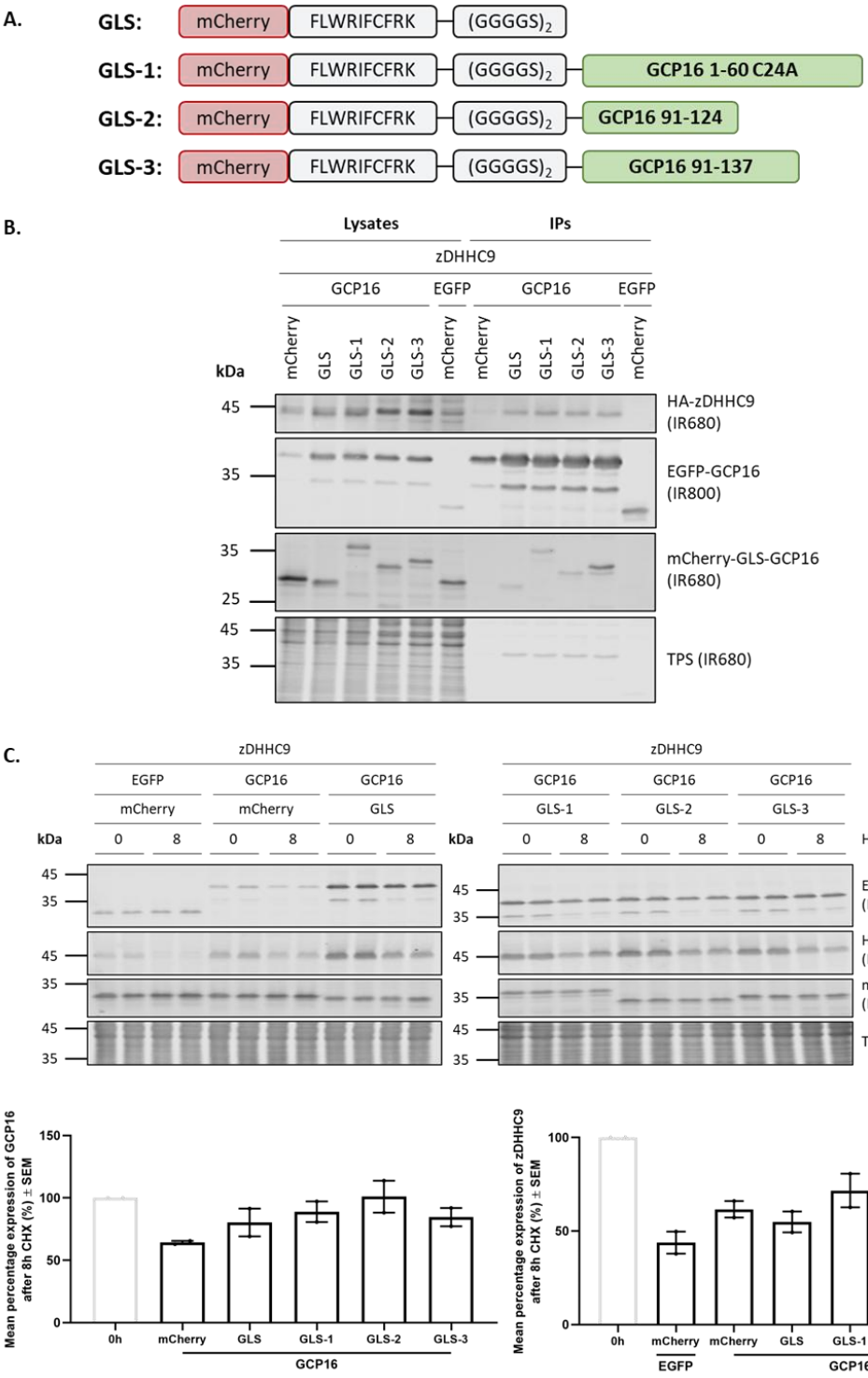
A.
GLS:
mCherry
FLWRIFCFRK
(GGGGS)2
GLS-1:
GCP16 1-60 C24A
GLS-2:
GCP16 91-124
GLS-3:
GCP16 91-137
B.
Lysates
IPs
zDHHC9
GCP16
EGFP
mCherry
GLS
GLS-1
GLS-2
GLS-3
kDa
45
35
25
HA-zDHHC9 (IR680)
EGFP-GCP16 (IR800)
mCherry-GLS-GCP16 (IR680)
TPS (IR680)
C.
Hours
0
8
EGFP-GCP16 (IR800)
HA-zDHHC9 (IR680)
mCherry-GLS-GCP16 (IR680)
TPS (IR680)
Mean percentage expression of GCP16 after 8h CHX (%) ± SEM
Mean percentage expression of zDHHC9 after 8h CHX (%) ± SEM
0h
GCP16
EGFP

Figure 5.9 Investigating the effects of Golgi-localised GCP16 peptides on zDHHC9/GCP16 complex formation and stability.

(A) *Schematic of the mCherry-tagged, Golgi-localised peptide inhibitors used, based on the amino acid sequence of GCP16; GLS, GLS-1, GLS-2, and GLS-3.* ***(B)*** *HEK293T cells were co-transfected with EGFP-GCP16, along with HA-zDHHC9 and either mCherry-tagged GLS, GLS-1, GLS-2, or GLS-3. The EGFP and mCherry empty plasmids were used as controls. The EGFP-tagged proteins (IR800) were immunoprecipitated using anti-EGFP beads and detected by immunoblotting, along with any co-immunoprecipitated proteins. The position of molecular weight markers (kDa) is shown on the left.* ***(C)*** *HEK293T cells were co-transfected with EGFP-GCP16, along with HA-zDHHC9 and either mCherry-tagged GLS, GLS-1, GLS-2, or GLS-3. The EGFP and mCherry empty plasmids were used as controls. Lysates were collected at 0 hours, or after 8 hours of incubation with 50 µg/ml cycloheximide (CHX). Protein expression levels were detected by immunoblotting. The position of molecular weight markers (kDa) is shown on the left. Quantified data show the mean percentage protein expression (± SEM) after 8 hours of CHX treatment, quantified relative to the corresponding 0-hour value and normalised to the total protein stain levels of each sample. n = 2, from two independent experiments.*

The Golgi-localisation peptides were then used in a single click chemistry experiment with zDHHC9 and GCP16 to assess their S-acylation and the S-acylation of the zDHHC9/GCP16 complex. HEK293T cells were co-transfected with HA-zDHHC9, along with EGFP-GCP16 and either mCherry-tagged GLS, GLS-1, GLS-2, or GLS-3. Cells were labelled with either palmitic acid as a control or palmitic acid azide and processed for click chemistry using alkyne mPEG (5 kDa). The protein samples were then resolved by SDS-PAGE, followed by immunoblotting. For GCP16, we did not detect any noticeable effect on S-acylation by any of the peptide constructs (Figure 5.10B). Unfortunately, in this experiment, the S-acylation of zDHHC9 was not visible, and therefore no conclusions could be drawn about the effects of the peptides on zDHHC9 S-acylation. Interestingly, all of the GLS peptides were S-acylated, and this is consistent with the work that discovered this localisation sequence, which reported that Golgi localisation is dependent on the S-acylation of the cysteine residue in the 10-amino acid sequence (Navarro and Cheeseman, 2022).

Overall, the GLS peptides were not found to have any clear inhibitory effects on zDHHC9/GCP16 complex formation, S-acylation or stability. However, it will be important to repeat these experiments to allow statistical analysis to be performed.

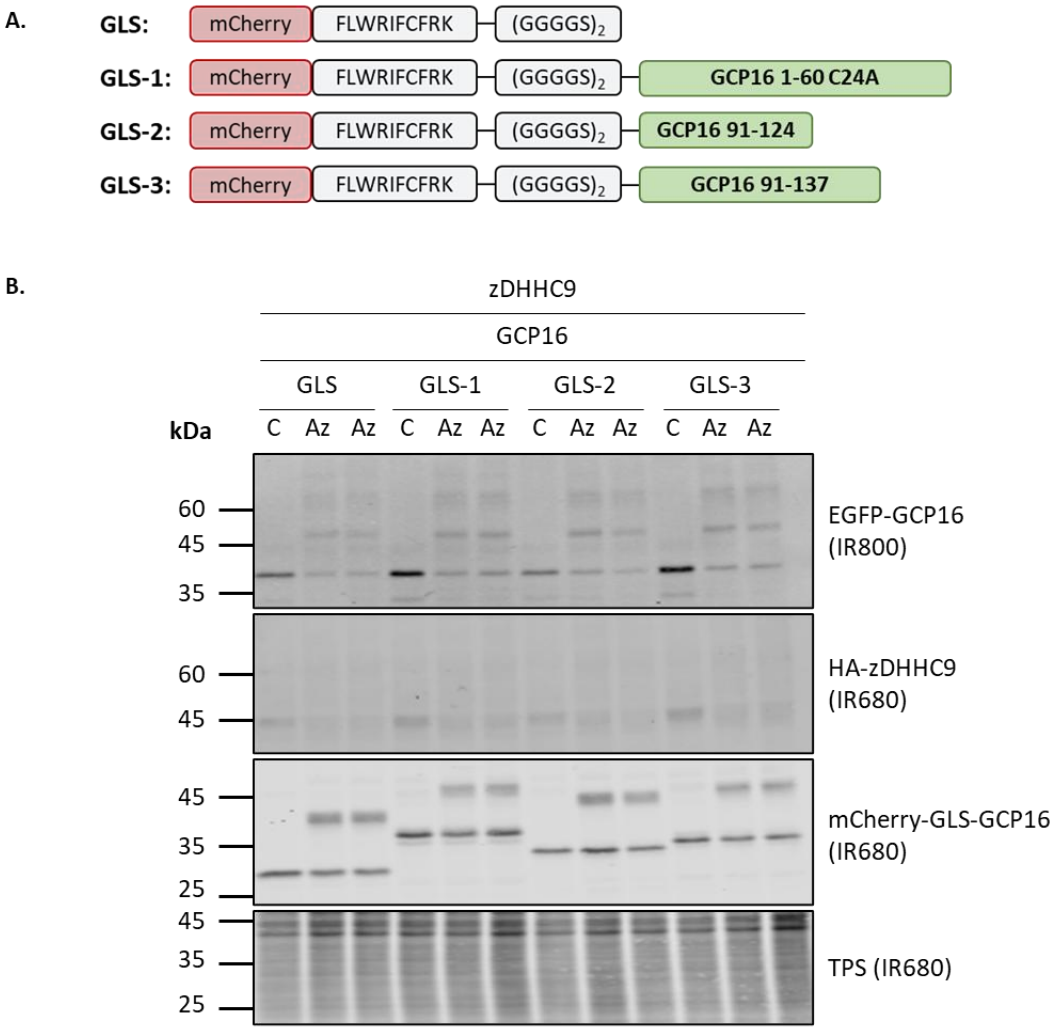

Figure 5.10 Investigating the effects of Golgi-localised GCP16 peptides on zDHHC9/GCP16 complex S-acylation.

(A) *Schematic of the mCherry-tagged, Golgi-localised peptide inhibitors used, based on the amino acid sequence of GCP16; GLS, GLS-1, GLS-2, and GLS-3.* ***(B)*** *HEK293T cells were co-transfected with HA-zDHHC9, along with EGFP-GCP16, and either mCherry-tagged GLS, GLS-1, GLS-2, or GLS-3. Cells were labelled with palmitic acid (C16:0) as a control (C) or palmitic acid azide (Az-C16:0) for 4 hours and were then lysed and clicked using alkyne mPEG (5 kDa). S-acylation is indicated by band shifts in Az samples. The position of molecular weight markers (kDa) is shown on the left.*

Discussion

This chapter has provided new insights into the broader interactions of GCP16 with zDHHC enzymes. The findings presented suggest that: (i) GCP16 binds to zDHHC14 and zDHHC18; (ii) GCP16 also interacts with the more distantly related Golgi enzymes zDHHC3 and zDHHC7; (iii) the reciprocal effects of zDHHC9/GCP16 complex formation on stability and S-acylation are not seen with zDHHC3 and zDHHC7; and (iv) GCP16 can form dimers/oligomers, which appear to involve the N-terminal region of the protein but not the identified zDHHC9 binding interfaces. The preliminary experiments that explored the effects of Golgi-localised GCP16 fragments on the zDHHC9/GCP16 complex were not conclusive, but there were no obvious effects of these constructs on the functional interaction between zDHHC9 and GCP16.

GCP16 can interact with but not stabilise Golgi-localised zDHHC enzymes evolutionary distinct from zDHHC9

Co-immunoprecipitation results in Figure 5.2 demonstrate that GCP16 can interact with zDHHC3 and zDHHC7, two Golgi-localised zDHHC enzymes that are distantly related to zDHHC9. However, cycloheximide analysis of protein stability demonstrated that GCP16 co-expression had no significant effect on the stability of zDHHC3 or zDHHC7, while the stability of zDHHC9 was significantly increased (Figure 5.3). This finding highlights a clear distinction in the relationship of GCP16 with zDHHC9, versus these other Golgi-localised zDHHC enzymes. Our findings agree with Nguyen *et al.* (2023), who used fluorescence-detection size exclusion chromatography analysis of crude HEK cell lysates to study the expression of zDHHC enzymes in the absence or presence of GCP16. Their results showed that GCP16 only increased the expression and monodispersity of enzymes that share a conserved C-terminal cysteine motif: zDHHC9, zDHHC18, zDHHC14, zDHHC8, and zDHHC5, but had no effect on zDHHC3 and zDHHC20 expression (Nguyen *et al.*, 2023).

Furthermore, experiments performed using purified proteins from infected Sf9 cells in [^{3}H] palmitoyl-CoA radiolabelling assays showed that in the absence of GCP16, zDHHC14 and zDHHC18 form enzymatically inactive aggregates, similarly to zDHHC9 (Nguyen *et al.*, 2023). The overall similar findings of cycloheximide chase

experiments and the aggregation assays of Nguyen *et al.* (2023), show that zDHHC9 monodispersity and aggregation are closely linked to the stability of the enzyme in intact cells.

Like zDHHC9, the co-immunoprecipitation of zDHHC14 and zDHHC18 was not affected by introducing amino acid substitutions to destroy the zDHHC9 binding interfaces in GCP16 (Figure 5.1). This result implies that either binding to zDHHC14 and zDHHC18 is mediated by different amino acid residues outside of the zDHHC9-binding interfaces, or that the same residues are involved in the interaction as for zDHHC9, but there is a second binding site that allows a different mechanism of interaction. Co-immunoprecipitation of zDHHC18 actually seemed to be stronger with the GCP16 1-4a/b mutant than with the wild-type GCP16, however, this result will require further validation and statistical analysis.

zDHHC3 can S-acylate GCP16, but GCP16 has no effect on zDHHC3 S-acylation

Results in this chapter showed that GCP16 is robustly S-acylated by zDHHC3. This observation was not surprising, as zDHHC3 is well established to have high activity and a broad substrate selectivity profile (Lemonidis *et al.*, 2014). Previous work has shown that zDHHC3 is also active against other soluble proteins, such as SNAP25 and CSP (Greaves *et al.*, 2008, Greaves *et al.*, 2009). As with zDHHC9, the S-acylation of GCP16 was perturbed by the introduction of amino acid substitutions to disrupt the 4 binding interfaces, and the GCP16 mutant 1-4a/b was not S-acylated by either zDHHC9 or zDHHC3 (Figure 5.5). Thus, even though zDHHC3 is a highly active enzyme with a broad substrate profile, it is not able to S-acylate the cysteines in GCP16 when the zDHHC9-binding interfaces are disrupted. This might suggest that the zDHHC3 and zDHHC9 share a similar mechanism for the recognition and S-acylation of GCP16, despite there being different effects of GCP16 on the S-acylation of the two enzymes. However, another possibility is that the amino acid substitutions introduced into the GCP16 interface mutant 1-4a/b are too disruptive to allow the S-acylation of the protein, or perhaps the mutant is degraded too quickly to be efficiently S-acylated, since we concluded that GCP16 interface mutant 4a/b is susceptible to protein degradation by the proteasome (Figure 4.18).

Although zDHHC9 requires GCP16 for stabilisation of its S-acylated state, zDHHC3 is robustly S-acylated without GCP16 (Figure 5.4). This suggests that the S-acylated

intermediate of zDHHC3 is either more susceptible to formation or less prone to thioester cleavage than the autoacylated state of zDHHC9. This may reflect differences in the DHHC domains of these enzymes responsible for autoacylation.

Swapping small sections of the DHHC domain that are unique to zDHHC9 with those of zDHHC3 does not affect binding to GCP16 but perturbs the activity of the enzyme

As both zDHHC3 and zDHHC9 can interact with GCP16 but there are differences in stabilisation of enzyme S-acylation, the catalytic DHHC domains of these enzymes were more closely examined. In our efforts to identify which amino acids of the DHHC domain region unique to zDHHC9 might be responsible for its unique S-acylation profile and dependency on GCP16 association for catalytic activity, mutations were incorporated in the DHHC domain of zDHHC9 to resemble that of zDHHC3 (Figure 5.6A). The ability of these chimeric mutants to interact with and mediate reciprocal S-acylation of GCP16 was then examined. Co-immunoprecipitation results in Figure 5.6B showed that all of the chimeric mutants were still able to interact with GCP16. Although this is not surprising (as both enzymes co-immunoprecipitate GCP16), we did expect to see a modest reduction in binding if the DHHC domain was responsible for the differences between zDHHC9 and zDHHC3, as GCP16 associates with zDHHC3 more weakly that with zDHHC9.

The cryo-EM structure of the zDHHC9/GCP16 complex identified Pro-150, Glu-163, and Tyr-183 within the DHHC domain of zDHHC9 as interacting residues with GCP16 (Yang *et al.*, 2024). Pro-150 was not included in the mutations introduced, while Glu-163, and Tyr-183 were mutated as part of different mutant constructs (mutants 3.4 and 3.5, respectively). Chimeric mutant 3.2 with amino acid substitutions at residues 145-148 (KIFR to CSIK) did show decreased binding compared to zDHHC9, resembling the levels seen with zDHHC3 co-expression (Figure 5.6B). An explanation for this could be that the substitutions introduced might affect the ability of nearby Pro-150 to interact with GCP16. However, it should be noted that mutant 3.2 was present at lower levels in the lysate samples, which could account for its lower levels of co-immunoprecipitation. At the same time, this lower expression could reflect a loss of functional interaction with GCP16.

Investigation of the ability of these mutants to S-acylate GCP16 in a click chemistry experiment showed that the 3.2 mutant lost its catalytic activity (Figure 5.7B). In fact,

the only mutant that remained catalytically active against GCP16 was 3.3, with amino acid substitutions at residues 157-160 (ICDN to VCKR). This mutant, however, did not adopt the S-acylation profile of zDHHC3, which is S-acylated with both EGFP control and GCP16 co-expression, and instead was still dependent on GCP16 co-expression for S-acylation stability, similarly to zDHHC9 (Figure 5.7C). This suggests that the amino acid residues 157-160 (IXDN) are not essential for the catalytic activity of zDHHC9, rather than the amino acid residues VCKR of zDHHC3 facilitating the robust S-acylation of the enzyme independently of GCP16 co-expression.

On the other hand, in addition to the DHHC domain, the differences in the S-acylation profiles of zDHHC9 and zDHHC3 with GCP16 might also be a consequence of their different C-terminal regions. The cryo-EM structure of zDHHC9/GCP16 revealed that cysteine-288 of the C-terminal cysteine motif in zDHHC9 mediates the attachment of a palmitate that is inserted near TMDs 2 and 3 and the α2' helix of GCP16, facilitating membrane association and stabilising the complex. S-acylation of Cys-288 is critical for the overall structure of the enzyme, and its mutation disrupts the catalytic activity of zDHHC9 (Yang *et al.*, 2024). Therefore, perhaps the distinct zDHHC3 domain can enhance the stability of the autoacylated intermediate or shield it from hydrolysis more effectively than the C-terminal region of zDHHC9.

Ko *et al.* (2019) showed that GCP16 and zDHHC5 display reciprocal stabilisation in HT-1080 and HEK293T cells, using genetic knockouts and immunoblotting analysis of endogenous proteins. The same study noted that while a catalytically inactive mutant of zDHHC5 (zDHHS5) could form a complex with GCP16, a C-terminal cysteine-to-serine mutant of the enzyme could not. Mutation of the cysteine residues of the conserved C-terminal cysteine motif of zDHHC5 also failed to stabilise endogenous GCP16 in immunoblot analysis of zDHHC5 KO HEK293T cells, whereas the zDHHS5 mutant could (Ko *et al.*, 2019). This is another example of a zDHHC enzyme whose C-terminal region is implicated in reciprocal stabilisation when in a complex with GCP16, while their interaction is independent of catalytic activity, similarly to zDHHC9. Our findings from Chapter 4, however, suggested that the catalytically inactive mutant of zDHHC9 (zDHHA9) could not stabilise GCP16 (Figure 4.10). On that account, it may also be interesting to examine how swapping the C-terminal regions of zDHHC3 and zDHHC9 affects their different S-acylation profiles with GCP16 in future work.

The N-terminal region of GCP16 is involved in homodimerisation

Another interesting finding presented in this chapter is the observed homodimerisation of GCP16, which seems to require the N-terminus of the protein. At this point, we are unable to conclude whether the amino acid region 30-60 or 60-90 is mediating the interaction, due to the difference in expression of the 1-60 and 1-90 truncation mutants that affects the quantification of co-immunoprecipitation levels (Figure 5.8A). Nevertheless, based on the results of another co-immunoprecipitation experiment shown in Figure 5.8B, we assume that the zDHHC9-binding interfaces within GCP16 are not involved in protein dimerisation. It has previously been shown that zDHHC3 undergoes dimerisation and/or oligomerisation (Lai and Linder, 2013), with the oligomeric form of the enzyme suggested to have reduced S-acylation activity. It is possible, therefore, that the homodimerisation of GCP16 can contribute to the functional regulation of zDHHC9 by regulating the oligomeric status of the enzyme. It might also provide a mechanism for the assembly of multi-zDHHC assemblies and facilitate the hetero-oligomerisation of zDHHC enzymes. However, in light of the findings of Nguyen *et al.* (2023), who showed that GCP16 reduces oligomerisation/aggregation of zDHHC enzymes (Nguyen *et al.*, 2023), it might also be that dimerisation of GCP16 is incompatible with the formation of zDHHC-GCP16 enzyme complexes. This could be investigated by determining if over-expression of zDHHC9 can outcompete the formation of GCP16 dimers.

Investigating the effects of targeting segments of GCP16 to the Golgi complex on the formation and stability of the zDHHC9/GCP16 complex

It was hypothesised that by uncovering detailed information about the formation of the zDHHC9/GCP16 complex and how this affects the functional regulation of both proteins, we would be able to use this information to develop novel peptide inhibitors that selectively block the interaction. Such inhibitors would provide important new tools for the field that could provide proof-of-principle that the zDHHC9/GCP16 complex is a valid target for drug discovery. The development of selective zDHHC inhibitors is an important challenge for the field, given the links between S-acylation and diseases such as cancer and neurodevelopmental disorders. By targeting the zDHHC9/GCP16 complex, it might be possible to get selective inhibition of this enzyme, or a small subset of GCP16-dependent zDHHC enzymes.

Navarro and Cheeseman (2022) identified a 10-amino acid motif within the alternative open reading frame of the mRNA of the centromere protein CENP-R that facilitates Golgi localisation. The peptide sequence is FLWRIFCFRK, with S-acylation of the central cysteine residue being responsible for Golgi localisation (Navarro and Cheeseman, 2022). This peptide sequence was employed to try to target segments of GCP16 to the Golgi to determine if they could disrupt the formation of the zDHHC9/GCP16 complex and its functional properties. The Golgi-localisation sequence was fused to different regions found in GCP16; 1-60 C24A (GLS-1), 91-124 (GLS-2), or 91-137 (GLS-3). As these experiments were performed at the very end of the project, it was not possible to undertake a detailed analysis of these effects. Nevertheless, we did not observe any clear effects on binding, stability, or S-acylation, and indeed, zDHHC9 S-acylation was only weakly detected such that no conclusions were possible on the effects of the peptides on this parameter. Interestingly, an S-acylated band was detected for all GLS peptides, most likely representing the S-acylation of the cysteine at position 7 in the GLS sequence. In follow-up experiments, it will be important to establish that the GLS sequence leads to Golgi localisation, which should be done by undertaking immunofluorescence co-localisation experiments with a Golgi marker protein such as GM130.

Future work should also undertake a more detailed analysis of GCP16 peptides. For example, shorter peptides that correspond to regions involved in interface 3 and 4 interactions could be more potent; for example, residues 11-20 from GCP16 would include amino acids involved in interactions with both of these interfaces. These shorter peptides may be better able to integrate into the complex and disrupt the interaction. It is also possible that the mCherry tag added to the peptides limits their ability to interact with zDHHC9, and so a short tag could also be employed in follow-up work. However, when the GCP16 segments used in this analysis were originally selected, we were cognisant of the likely requirement to ensure that these sequences adopted the correct folding, and this should be considered when examining the effects of shorter peptide sequences.

Limitations and future directions

One of the main limitations of the work presented in this chapter is that a number of the analyses were performed towards the end of the project, and it was not possible to repeat them a sufficient time for statistical analysis to be performed. Future work

should certainly include investigating the binding of the Golgi-localisation peptides in more depth and whether they associate with GCP16 or zDHHC9. Here, it will be important to confirm that the peptides localise correctly to the Golgi, for example, by using immunofluorescence co-localisation analysis against a Golgi marker protein, such as GM130. A much larger set of peptides should be examined, and a short tag used. Indeed, it would be useful to start by designing a set of peptides that could be tested for their ability to interfere with the binding of purified zDHHC9 and GCP16. After selecting the most potent peptides, these could be fused to GLS and then developed into a cell-permeable format for the delivery into cells. Other work should also look more closely at why zDHHC9 but not zDHHC3 requires GCP16 for stabilisation of its S-acylated state. In particular, it will be interesting to compare the effects of swapping the C-terminal regions of these enzymes downstream of the 4th TMD.

CHAPTER 6

GENERAL DISCUSSION

Chapter 6 - General discussion

S-acylation is a common lipid post-translational modification, and since its identification in 1979 (Schmidt and Schlesinger, 1979) it has been deemed as a key dynamic regulator of approximately 20% of the human proteome. Even though the enzymes mediating S-acylation were identified over two decades ago, their crystal structure and the characterisation of their molecular mechanism have only been revealed in the last decade (Mitchell *et al.*, 2010, Rana *et al.*, 2018a, Rana *et al.*, 2018b). Indeed, our knowledge of substrate selectivity and regulation of zDHHC enzymes is still quite rudimentary. Considering the myriad of physiological processes that S-acylation and zDHHC enzymes are involved in, and the number of diseases their dysregulation is associated with, a critical area in the field of S-acylation is the development of selective inhibitors that can be utilised experimentally to further our knowledge on the role of zDHHC enzymes, and that can eventually lead the way to new therapeutic approaches. The work presented in this thesis outlines a detailed analysis of the functional relationship between zDHHC9 and its accessory protein GCP16. The zDHHC9/GCP16 protein complex has been correlated with Ras-driven cancers (Swarthout *et al.*, 2005, Liu *et al.*, 2016, Busquets-Hernandez and Triola, 2021), while mutations in *ZDHHC9* cause neurological disorders, including X-linked intellectual disability and epilepsy (Raymond *et al.*, 2007, Shimell *et al.*, 2019). The dependency of zDHHC9 on the association with GCP16 for catalytic activity could be exploited as a method to selectively modulate the activity of the enzyme. Therefore, we hypothesised that developing a more refined understanding of the mechanisms of their interaction could highlight novel ways to mediate inhibition of zDHHC9.

The bidirectional effects of the zDHHC9/GCP16 complex on S-acylation and stability

The first key finding of this project was that zDHHC9 and GCP16 have a bidirectional relationship. Previous work on the zDHHC9/GCP16 protein complex was performed using purified proteins and mainly focused on the regulatory effects of GCP16 on zDHHC9. Here, it was demonstrated that co-expression of zDHHC9 and GCP16 in mammalian cells results in enhanced S-acylation and stability of *both* proteins.

The effects of GCP16 on the S-acylation of zDHHC9 were first reported by Swarthout *et al.* (2005) using purified proteins. They demonstrated that the autoacylation and

catalytic activity of zDHHC9 are dependent on the association with GCP16 (Swarthout *et al.*, 2005). A later study elucidated that GCP16 protects the autoacylated intermediate of zDHHC9 from hydrolysis (Mitchell *et al.*, 2014). Our study is the first to show that GCP16 also affects the S-acylated status of zDHHC9 in live cells. In fact, the click mPEG assay that was used to study S-acylation revealed that zDHHC9 underwent several band shifts, indicating that it is modified on multiple cysteines, and that this multi-S-acylated state of zDHHC9 is enhanced by GCP16 co-expression. Therefore, it is possible that stabilising the S-acylation of the catalytic cysteine in the DHHC domain of zDHHC9, then allows the enzyme to autoacylate the other available cysteines. In fact, Yang *et al.* (2024) identified three cysteines within zDHHC9, C24, C25, and C288, whose S-acylation directly influences the structure of the enzyme and therefore its catalytic activity (Yang *et al.*, 2024).

Ohta *et al.* (2003) reported that cysteine-69 and cysteine-72 are the main S-acylation sites within GCP16, as a double alanine substitution of these residues substantially reduced S-acylation (Ohta *et al.*, 2003). However, our results showed that although C69 and C72 appear to be the main S-acylated residues, C24 or C81 are also likely to be S-acylated, albeit at lower levels. This multiple S-acylation of GCP16 was also apparent from the number of band shifts that we observed in click chemistry experiments. Specifically, two clear bands were seen when GCP16 was expressed alone, while zDHHC9 co-expression resulted in at least three visible band shifts for GCP16. It is surprising to note that this, to our knowledge, is the first time that GCP16 has been shown to be a substrate of zDHHC9. Thus, GCP16 is both a substrate and a regulator of zDHHC9.

Both the N- and C-terminal regions are essential for GCP16 S-acylation and for its ability to stabilise the S-acylation of zDHHC9, as seen through truncation analyses. The cryo-EM structure of the zDHHC9/GCP16 protein complex that was reported by Yang *et al.* (2024) while this project was in progress revealed that amino acid residues involved in the binding interfaces are in fact found in both N- and C-terminal regions of GCP16. However, the authors did not explore the effects of introducing amino acid changes into these regions of GCP16 on formation or stability of the zDHHC9/GCP16 complex. Our analysis showed that binding interfaces 3 and 4a/b, present at the N- and C-terminus of GCP16, are important for the S-acylation of GCP16, whereas substitutions in interfaces 1 (Y76A) and 2 (Y86A) found in the middle of the protein had no effect on GCP16 S-acylation. On the other hand, all of the binding interface

mutants of GCP16 disrupted the S-acylation of zDHHC9, with interface mutants 3 and 4a/b actually reducing zDHHC9 S-acylation below control levels, suggesting some possible dominant-negative activity. Both binding interface 3 and 4a/b involve interactions that stabilise the zinc finger motifs of zDHHC9, either directly or indirectly (Yang *et al.*, 2024), which could explain why mutations introduced in these constructs were the most disruptive, as the zinc finger motifs are critical for the stability and catalytic activity of zDHHC enzymes (Gottlieb *et al*., 2015).

Another key observation of this project is that the stability of both zDHHC9 and GCP16 is increased when the proteins are co-expressed. This is in agreement with previous findings about the yeast orthologues Erf2 and Erf4 (Lobo *et al.*, 2002), and purified zDHHC9, which is prone to proteolysis in the absence of GCP16 (Swarthout *et al.*, 2005), or susceptible to aggregation (Nguyen *et al.*, 2023). In our alanine substitution analyses of the binding interfaces within GCP16, we observed that mutations in binding interfaces 1, 3, and 4a/b within GCP16 inhibited the stability of zDHHC9, while the constructs were also less stable themselves. In contrast, GCP16 binding interface mutant 2 (Y86A) had normal S-acylation and was the only binding interface mutant that retained its protein stability and the ability to stabilise zDHHC9. By examining the interactions in binding interface 2, we concluded that mutating Y86 could potentially disrupt the interaction with proline-292 in the PPII helix of zDHHC9, but the docking of proline-290 and proline-293, also found in the PPII helix, into the two negatively charged pockets of GCP16 is most probably not affected. These residual interactions in the second binding interface are probably the reason why the GCP16 interface mutant 2 is still S-acylated and also retains reciprocal stabilising effects. In future analyses, it would be interesting to replace Y86 with a positively charged amino acid and also incorporate positively charged substitutions in the interacting pockets of GCP16 that could switch the weak negative charge and prevent the interaction with the PPII helix of zDHHC9.

Yang *et al.* (2024) demonstrated that a protein complex of zDHHC9 and GCP16 binding interface mutant 1 (Y76A) had reduced catalytic activity against purified H-Ras (Yang *et al.*, 2024). We found that although GCP16 binding interface mutant 1 (Y76A) is S-acylated, its stability is significantly reduced when in a complex with zDHHC9, while it also has a reduced ability to stabilise the enzyme. Although we initially found it surprising that GCP16 interface mutant 1 had reduced stability while its S-acylation levels were not altered, we rationalised these effects by examining the

cryo-EM structure of zDHHC9 and GCP16 more closely. Tyrosine-76 in GCP16 interacts with R85 and Y183 in zDHHC9, found in TMD2 and TMD3 respectively, enclosing the catalytic loop that contains the DHHC-CRD and zinc finger motifs. Additionally, R85 in zDHHC9, one of the interacting residues of Y76 in GCP16, belongs to a positively charged patch formed by R85, R179 and R298 that facilitates the interaction with a phospholipid. The phospholipid attachment stabilises the conformation of TMD2, TMD3 and the PPII helix of zDHHC9 and modulates the spatial topology of the enzyme (Yang *et al.*, 2024). More importantly for the case of Y76 in GCP16, the PPII helix of zDHHC9 docks into a groove found in GCP16, hence substitution of Y76 to alanine could disrupt the interaction with R85 which could then disrupt the attachment of the phospholipid and as a result destabilise both zDHHC9 and GCP16. Therefore, perhaps the decrease in protein stability seen with GCP16 binding interface mutant 1 is linked to conformational changes like the ones described above and not to the S-acylation of GCP16. Also, these stabilising interactions could explain why mutation of either Y76 in GCP16 or R85 in zDHHC9 inhibit the catalytic activity of the complex, as reported by Yang *et al.* (2024) (Yang *et al.*, 2024).

A catalytically inactive zDHHS9 mutant demonstrated increased aggregation when expressed alone, while GCP16 enhanced its stability and monodispersity (Nguyen *et al.*, 2023). Similarly, the GCP16 binding interface mutant 2 enhanced the protein stability of zDHHC9, even though the enzyme failed to autoacylate and was therefore not enzymatically active. The enzymatically inactive zDHHA9 and zDHHC9 binding interface mutant 1-4a/b were unable to S-acylate or stabilise GCP16, while the GCP16 binding interface 1 which was efficiently S-acylated was not stabilised by zDHHC9 due to conformational changes in their association. All in all, we suggest that GCP16-mediated stabilisation of zDHHC9 is independent of the S-acylation activity of the enzyme, while the stability of GCP16 is paralleled by its S-acylation and interaction with zDHHC9. This is in contrast to the increase in GCP16 stability seen with zDHHS5 (Ko *et al.*, 2019), suggesting that the effects of the zDHHC9/GCP16 interaction might be unique in requiring both S-acylation and complex formation for the stabilisation of GCP16 but only complex formation for the stabilisation of zDHHC9.

The unidirectional relationship between GCP16 and other zDHHC enzymes

GCP16 is also reported to be an accessory protein for zDHHC enzymes that are evolutionary related to zDHHC9, including zDHHC14, zDHHC18, zDHHC8, and

zDHHC5 (Ko *et al.*, 2019, Nguyen *et al.*, 2023, Yang *et al.*, 2024). In fact, similarly to zDHHC9, GCP16 is required for the catalytic activity of zDHHC14 and zDHHC18 and to prevent their aggregation (Nguyen *et al.*, 2023). We confirmed the co-immunoprecipitation of zDHHC14 and zDHHC18 with GCP16, as well as with the GCP16 binding interface mutant 1-4a/b. Moreover, we revealed that GCP16 can also interact with the highly active Golgi-localised zDHHC3 and zDHHC7 enzymes, even though these isoforms are not closely related to zDHHC9. However, the relationship of GCP16 with zDHHC3 and zDHHC7 differs from that with zDHHC9, as GCP16 co-expression has no effect on their stability after protein synthesis inhibition. This is explained by examining the C-terminal region of the enzymes. Nguyen *et al.* (2023) proposed that a C-terminal cysteine motif present in zDHHC enzymes that are closely related to zDHHC9 is essential for the stabilising effect of GCP16 (Nguyen *et al.*, 2023), while another study also demonstrated that the co-immunoprecipitation and reciprocal stability of GCP16 and zDHHC5 are dependent on the C-terminal cysteines of zDHHC5 (Ko *et al.*, 2019). The cryo-EM structure revealed that the S-acylation of the C-terminal cysteine motif of zHHC9 and, in particular Cys-288, is essential for the activity and stability of the zDHHC9/GCP16 complex. S-acylation of Cys-288 promotes the membrane association of the α3' helix of zDHHC9 in a pocket adjacent to TMD2 and TMD3 that flank the cytosolic region which includes the DHHC-CRD. Moreover, Cys-288 is part of a cysteine cluster formed by Cys-283, Cys-284, and Cys-288 in zDHHC9 and Cys-69 and Cys-72 in GCP16, which promotes the close association with the α2' helix of GCP16, thereby enhancing the stability of the complex (Yang *et al.*, 2024).

When examining the relationship between GCP16 and the highly active enzyme zDHHC3 further, we observed that co-expression with zDHHC3 enhanced the S-acylation of GCP16 to levels almost identical to those seen with zDHHC9. On the other hand, zDHHC3 was robustly S-acylated in the absence of GCP16 and adding the accessory protein did not affect the autoacylated state of this enzyme. This exhibits a unidirectional relationship in which only GCP16 is affected by zDHHC3, as opposed to the reciprocal effects seen for zDHHC9 and GCP16.

We attempted to identify what characteristics distinguish the relationship of zDHHC3 and zDHHC9 with GCP16 in terms of their S-acylation by swapping regions in the DHHC domain of zDHHC9 that are specific to this isoform with those of zDHHC3. None of the zDHHC9 DHHC mutants that were analysed adopted the S-acylation

profile of zDHHC3 that is unaffected by GCP16 co-expression, but considering the involvement of the C-terminal cysteines in the zDHHC9/GCP16 complex, we assume that the distinct profiles of zDHHC3 and zDHHC9 could be a result of differences in both their DHHC and C-terminal domains, and future work should certainly examine how replacing or removing the cysteine rich motif in the C-terminal domain of zDHHC9 affects the dependency on GCP16.

S-acylation is not required for GCP16 membrane association, but it protects the protein from degradation

It has been long thought that the S-acylation of Cys-69 and Cys-72 mediate the membrane association of GCP16, as cysteine to alanine mutants showed decreased membrane association in fractionation experiments and caused the redistribution of GCP16 from the Golgi to the cytoplasm (Ohta *et al.*, 2003). While we confirmed that substitution of C69 and C72 reduce the membrane localisation of GCP16, we concluded that membrane association is directly mediated by the cysteine residues, rather than their S-acylation. This is because a C-terminal truncation mutant of GCP16 that was not S-acylated (1-126), and an S-acylated C-terminal truncation mutant (1-128) were both localised to the membrane similarly to the wild-type protein. This was even observed in the absence of zDHHC9, to ensure that the membrane association seen for GCP16 was not influenced by the direct association with zDHHC9. Previous studies on SNAP25 and CSP proposed that the cysteine residues might have a primary role in membrane association by mediating a transient interaction before the proteins are S-acylated (Greaves *et al.*, 2008, Greaves *et al.*, 2009). Therefore, we suggest that the membrane association of GCP16 is mediated by the strong intrinsic membrane affinity of cysteines and surrounding residues. In fact, the 60-90 region of GCP16, in which C69 and C72 are found, has strong hydrophobicity, further suggesting that this region of the protein could facilitate membrane association prior to S-acylation of the cysteine residues. The cryo-EM structure revealed that the 60-90 region of GCP16 is part of the α2’ and α3’ helices that are embedded in the membrane, with C69 and C72 found on the α2’ helix (Yang *et al.*, 2024).

Notably, we detected that the 60-90 region of GCP16 enhanced the proteasomal degradation of EGFP in the absence of S-acylation. On the other hand, a cysteine to alanine mutant of all cysteines found in the 60-90 region (C69A/C72A/C81A), whose mutation completely abolishes GCP16 S-acylation, did not affect protein expression

levels after MG132 proteasomal inhibition. This resulted in the hypothesis that non-acylated GCP16 with intact cysteines is localised to the membrane via direct cysteine interactions, and that this mode of membrane interaction is associated with rapid degradation of GCP16. In contrast, the S-acylation of these cysteines protects the proteins, perhaps by promoting a tighter and more secure membrane interaction that prevents recognition by membrane-bound ubiquitylation enzymes.

When assessing the proteasomal degradation of the GCP16 binding interface mutants using MG132, we found that mutant 4a/b was also rapidly degraded. This agrees with our hypothesis that S-acylation shields the protein from degradation, as this mutant is completely non-acylated and yet has intact cysteines. Further supporting our proposal, we specifically detected increased expression of the lower, non-acylated band of 4a/b upon MG132 inhibition of proteasomal degradation, which highlights the susceptibility of the non-acylated form of GCP16 to degradation. It would be really interesting to see if cysteine substitution in the 4/b mutant of GCP16 can reverse its stability to resemble that of GCP16.

Mutations in GCP16 binding interfaces 3 and 4a/b disrupt the function of zDHHC9/GCP16 in dendrite growth assays

Mutations in *zDHHC9* cause X-linked intellectual disability and childhood epilepsy (Raymond *et al.*, 2007, Baker *et al.*, 2015). It was later shown that zDHHC9 knockdown in hippocampal neuron cultures leads to reduced dendrite growth and inhibitory synapse formation. Specifically, the S-acylation of Ras was linked to promoting dendrite growth, while the S-acylation of TC10 was linked to promoting inhibitory synapse formation, and both are mediated by the activity of zDHHC9 and GCP16 (Shimell *et al.*, 2019). In our analyses, we identified GCP16 interface mutants 3 and 4a/b as the most disruptive for the reciprocal stability and S-acylation of both proteins, and these mutants also inhibited the effect of zDHHC9 in rat hippocampal neurons in promoting dendritic growth. This finding confirms the importance of the amino acid residues within binding interfaces 3 and 4a/b for the function of zDHHC9 in normal neuronal development and is the first demonstration that the effects of combined zDHHC9 and GCP16 expression on dendrite growth require their functional interaction.

The inability of GCP16 binding interface mutant 2 to stabilise the S-acylation of zDHHC9 suggests that the single substitution included in this mutant (Y86A) is sufficient to inhibit the enhancing effect of GCP16 on zDHHC9 S-acylation without affecting the stability of the complex. This marks GCP16 binding interface mutant 2 as an interesting construct to use in future functional experiments.

Limitations and future directions

In this thesis, the first detailed analysis of the interaction between zDHHC9 and GCP16 in mammalian cells is presented, highlighting important regions and residues for the S-acylation, stability, and function of the complex. A surprising finding was that the physical interaction between zDHHC9/GCP16 did not appear to be affected by any binding interface mutant despite their clear effects on S-acylation and stability, and even after stringent immunoprecipitation buffer conditions, or the introduction of more disruptive (charged) amino acid substitutions into the binding interfaces of GCP16. Therefore, we believe that there might be another mode of binding, other than the ones presented in the cryo-EM structure. In future analyses, alternative and more sensitive binding approaches should be used to confirm this, like a FRET assay.

Additionally, Ras S-acylation should be investigated after zDHHC9 co-expression with the GCP16 binding interface mutants to confirm their effect on the function of the complex. Most importantly, since the experiments performed in this thesis involve protein overexpression, the findings presented should be confirmed using CRISPR to engineer endogenous genes and modify protein expression.

Although we did not identify potential peptide inhibitors for the regulation of the zDHHC9/GCP16 complex, the findings of this thesis significantly expand the knowledge about the mechanisms and outcomes of complex formation. Future work should focus on the identification of short Golgi-localised peptides that mimic GCP16, to be tested in binding and S-acylation assays for their ability to outcompete GCP16 and perturb the activity of zDHHC9. Targeting the zDHHC9/GCP16 complex remains an intriguing approach towards the selective inhibition of this enzyme, which might, in the future, be a useful strategy in treating Ras-driven cancers.

CHAPTER 7

REFERENCES

Chapter 7 - References

ABRAMI, L., AUDAGNOTTO, M., HO, S., MARCAIDA, M. J., MESQUITA, F. S., ANWAR, M. U., SANDOZ, P. A., FONTI, G., POJER, F., DAL PERARO, M. & VAN DER GOOT, F. G. 2021. Palmitoylated acyl protein thioesterase APT2 deforms membranes to extract substrate acyl chains. *Nat Chem Biol,* 17**,** 438-447.

ABRAMI, L., DALLAVILLA, T., SANDOZ, P. A., DEMIR, M., KUNZ, B., SAVOGLIDIS, G., HATZIMANIKATIS, V. & VAN DER GOOT, F. G. 2017. Identification and dynamics of the human ZDHHC16-ZDHHC6 palmitoylation cascade. *Elife,* 6.

ABRAMI, L., KUNZ, B., IACOVACHE, I. & VAN DER GOOT, F. G. 2008. Palmitoylation and ubiquitination regulate exit of the Wnt signaling protein LRP6 from the endoplasmic reticulum. *Proc Natl Acad Sci U S A,* 105**,** 5384-9.

ABRAMI, L., LEPPLA, S. H. & VAN DER GOOT, F. G. 2006. Receptor palmitoylation and ubiquitination regulate anthrax toxin endocytosis. *J Cell Biol,* 172**,** 309-20.

ABRAMSON, J., ADLER, J., DUNGER, J., EVANS, R., GREEN, T., PRITZEL, A., RONNEBERGER, O., WILLMORE, L., BALLARD, A. J., BAMBRICK, J., BODENSTEIN, S. W., EVANS, D. A., HUNG, C. C., O'NEILL, M., REIMAN, D., TUNYASUVUNAKOOL, K., WU, Z., ZEMGULYTE, A., ARVANITI, E., BEATTIE, C., BERTOLLI, O., BRIDGLAND, A., CHEREPANOV, A., CONGREVE, M., COWEN-RIVERS, A. I., COWIE, A., FIGURNOV, M., FUCHS, F. B., GLADMAN, H., JAIN, R., KHAN, Y. A., LOW, C. M. R., PERLIN, K., POTAPENKO, A., SAVY, P., SINGH, S., STECULA, A., THILLAISUNDARAM, A., TONG, C., YAKNEEN, S., ZHONG, E. D., ZIELINSKI, M., ZIDEK, A., BAPST, V., KOHLI, P., JADERBERG, M., HASSABIS, D. & JUMPER, J. M. 2024. Accurate structure prediction of biomolecular interactions with AlphaFold 3. *Nature,* 630**,** 493-500.

AHONEN, T. J., NG, C. P., FARINHA, B., ALMEIDA, B., VICTOR, B. L., REYNOLDS, C., KALSO, E., YLI-KAUHALUOMA, J., GREAVES, J. & MOREIRA, V. M. 2023. Probing the Interactions of Thiazole Abietane Inhibitors with the Human Serine Hydrolases ABHD16A and ABHD12. *ACS Med Chem Lett,* 14**,** 1404-1410.

AHONEN, T. J., SAVINAINEN, J. R., YLI-KAUHALUOMA, J., KALSO, E., LAITINEN, J. T. & MOREIRA, V. M. 2018. Discovery of 12-Thiazole Abietanes as Selective Inhibitors of the Human Metabolic Serine Hydrolase hABHD16A. *ACS Med Chem Lett,* 9**,** 1269-1273.

ANWAR, M. U. & VAN DER GOOT, F. G. 2023. Refining S-acylation: Structure, regulation, dynamics, and therapeutic implications. *J Cell Biol,* 222.

APPELS, N. M., BEIJNEN, J. H. & SCHELLENS, J. H. 2005. Development of farnesyl transferase inhibitors: a review. *Oncologist,* 10**,** 565-78.

ARDITO, F., GIULIANI, M., PERRONE, D., TROIANO, G. & LO MUZIO, L. 2017. The crucial role of protein phosphorylation in cell signaling and its use as targeted therapy (Review). *Int J Mol Med,* 40**,** 271-280.

ARSHADI, C., GUNTHER, U., EDDISON, M., HARRINGTON, K. I. S. & FERREIRA, T. A. 2021. SNT: a unifying toolbox for quantification of neuronal anatomy. *Nat Methods,* 18**,** 374-377.

AZIZI, S. A., LAN, T., DELALANDE, C., KATHAYAT, R. S., BANALES MEJIA, F., QIN, A., BROOKES, N., SANDOVAL, P. J. & DICKINSON, B. C. 2021. Development of an Acrylamide-Based Inhibitor of Protein S-Acylation. *ACS Chem Biol,* 16**,** 1546-1556.

BAGDONAS, H., FOGARTY, C. A., FADDA, E. & AGIRRE, J. 2021. The case for post-predictional modifications in the AlphaFold Protein Structure Database. *Nat Struct Mol Biol,* 28**,** 869-870.

BAKER, K., ASTLE, D. E., SCERIF, G., BARNES, J., SMITH, J., MOFFAT, G., GILLARD, J., BALDEWEG, T. & RAYMOND, F. L. 2015. Epilepsy, cognitive deficits and neuroanatomy in males with ZDHHC9 mutations. *Ann Clin Transl Neurol,* 2**,** 559-69.

BARTELS, D. J., MITCHELL, D. A., DONG, X. & DESCHENES, R. J. 1999. Erf2, a novel gene product that affects the localization and palmitoylation of Ras2 in Saccharomyces cerevisiae. *Mol Cell Biol,* 19**,** 6775-87.

BATES, G. P., DORSEY, R., GUSELLA, J. F., HAYDEN, M. R., KAY, C., LEAVITT, B. R., NANCE, M., ROSS, C. A., SCAHILL, R. I., WETZEL, R., WILD, E. J. & TABRIZI, S. J. 2015. Huntington disease. *Nat Rev Dis Primers,* 1**,** 15005.

BERCHTOLD, L. A., STORLING, Z. M., ORTIS, F., LAGE, K., BANG-BERTHELSEN, C., BERGHOLDT, R., HALD, J., BRORSSON, C. A., EIZIRIK, D. L., POCIOT, F., BRUNAK, S. & STORLING, J. 2011. Huntingtin-interacting protein 14 is a type 1 diabetes candidate protein regulating insulin secretion and beta-cell apoptosis. *Proc Natl Acad Sci U S A,* 108**,** E681-8.

BLANC, M., DAVID, F. P. A. & VAN DER GOOT, F. G. 2019. SwissPalm 2: Protein S-Palmitoylation Database. *Methods Mol Biol,* 2009**,** 203-214.

BLASKOVIC, S., BLANC, M. & VAN DER GOOT, F. G. 2013. What does S-palmitoylation do to membrane proteins? *FEBS J,* 280**,** 2766-74.

BOLLU, L. R., KATREDDY, R. R., BLESSING, A. M., PHAM, N., ZHENG, B., WU, X. & WEIHUA, Z. 2015. Intracellular activation of EGFR by fatty acid synthase dependent palmitoylation. *Oncotarget,* 6**,** 34992-5003.

BRIGIDI, G. S., SANTYR, B., SHIMELL, J., JOVELLAR, B. & BAMJI, S. X. 2015. Activity-regulated trafficking of the palmitoyl-acyl transferase DHHC5. *Nat Commun,* 6**,** 8200.

BUSQUETS-HERNANDEZ, C., RIBO, S., GRATACOS-BATLLE, E., CARBAJO, D., TSIOTSIA, A., BLANCO-CANOSA, J. B., CHAMBERLAIN, L. H. & TRIOLA, G. 2024. Quantitative analysis of protein lipidation and acyl-CoAs reveals substrate preferences of the S-acylation machinery. *Chem Sci,* 15**,** 12845-12855.

BUSQUETS-HERNANDEZ, C. & TRIOLA, G. 2021. Palmitoylation as a Key Regulator of Ras Localization and Function. *Front Mol Biosci,* 8**,** 659861.

BUTLER, L., LOCATELLI, C., ALLAGIOTI, D., LOUSA, I., LEMONIDIS, K., TOMKINSON, N. C. O., SALAUN, C. & CHAMBERLAIN, L. H. 2023. S-acylation of Sprouty and SPRED proteins by the S-acyltransferase zDHHC17 involves a novel mode of enzyme-substrate interaction. *J Biol Chem,* 299**,** 102754.

BUTLER, W. & HUANG, J. 2021. Glycosylation Changes in Prostate Cancer Progression. *Front Oncol,* 11**,** 809170.

CALERO, G., GUPTA, P., NONATO, M. C., TANDEL, S., BIEHL, E. R., HOFMANN, S. L. & CLARDY, J. 2003. The crystal structure of palmitoyl protein thioesterase-2 (PPT2) reveals the basis for divergent substrate specificities of the two lysosomal thioesterases, PPT1 and PPT2. *J Biol Chem,* 278**,** 37957-64.

CAMP, L. A. & HOFMANN, S. L. 1993. Purification and properties of a palmitoyl-protein thioesterase that cleaves palmitate from H-Ras. *J Biol Chem,* 268**,** 22566-74.

CHAMBERLAIN, L. H. & SHIPSTON, M. J. 2015. The physiology of protein S-acylation. *Physiol Rev,* 95**,** 341-76.

CHAMBERLAIN, L. H., SHIPSTON, M. J. & GOULD, G. W. 2021. Regulatory effects of protein S-acylation on insulin secretion and insulin action. *Open Biol,* 11**,** 210017.

CHEN, S., HAN, C., MIAO, X., LI, X., YIN, C., ZOU, J., LIU, M., LI, S., STAWSKI, L., ZHU, B., SHI, Q., XU, Z. X., LI, C., GODING, C. R., ZHOU, J. & CUI, R. 2019. Targeting MC1R depalmitoylation to prevent melanomagenesis in redheads. *Nat Commun,* 10**,** 877.

CHEN, X., HAO, A., LI, X., YE, K., ZHAO, C., YANG, H., MA, H., HU, L., ZHAO, Z., HU, L., YE, F., SUN, Q., ZHANG, H., WANG, H., YAO, X. & FANG, Z. 2020. Activation of JNK and p38 MAPK Mediated by ZDHHC17 Drives Glioblastoma Multiforme Development and Malignant Progression. *Theranostics,* 10**,** 998-1015.

DALLAVILLA, T., ABRAMI, L., SANDOZ, P. A., SAVOGLIDIS, G., HATZIMANIKATIS, V. & VAN DER GOOT, F. G. 2016. Model-Driven Understanding of Palmitoylation Dynamics: Regulated Acylation of the Endoplasmic Reticulum Chaperone Calnexin. *PLoS Comput Biol,* 12**,** e1004774.

DANIOTTI, J. L., PEDRO, M. P. & VALDEZ TAUBAS, J. 2017. The role of S-acylation in protein trafficking. *Traffic,* 18**,** 699-710.

DAS, A. K., BELLIZZI, J. J., 3RD, TANDEL, S., BIEHL, E., CLARDY, J. & HOFMANN, S. L. 2000. Structural basis for the insensitivity of a serine enzyme (palmitoyl-protein thioesterase) to phenylmethylsulfonyl fluoride. *J Biol Chem,* 275**,** 23847-51.

DAVDA, D., EL AZZOUNY, M. A., TOM, C. T., HERNANDEZ, J. L., MAJMUDAR, J. D., KENNEDY, R. T. & MARTIN, B. R. 2013. Profiling targets of the irreversible palmitoylation inhibitor 2-bromopalmitate. *ACS Chem Biol,* 8**,** 1912-7.

DAVIS, M. W. & JORGENSEN, E. M. 2022. ApE, A Plasmid Editor: A Freely Available DNA Manipulation and Visualization Program. *Front Bioinform,* 2**,** 818619.

DU, K., MURAKAMI, S., SUN, Y., KILPATRICK, C. L. & LUSCHER, B. 2017. DHHC7 Palmitoylates Glucose Transporter 4 (Glut4) and Regulates Glut4 Membrane Translocation. *J Biol Chem,* 292**,** 2979-2991.

DUNCAN, J. A. & GILMAN, A. G. 1998. A cytoplasmic acyl-protein thioesterase that removes palmitate from G protein alpha subunits and p21(RAS). *J Biol Chem,* 273**,** 15830-7.

EMBL-EBI. 2025. *Strengths and limitations of AlphaFold2* [Online]. Available: https://www.ebi.ac.uk/training/online/courses/alphafold/an-introductory-guide-to-its-strengths-and-limitations/strengths-and-limitations-of-alphafold/ [Accessed June 2025].

ERNST, A. M., SYED, S. A., ZAKI, O., BOTTANELLI, F., ZHENG, H., HACKE, M., XI, Z., RIVERA-MOLINA, F., GRAHAM, M., REBANE, A. A., BJORKHOLM, P., BADDELEY, D., TOOMRE, D., PINCET, F. & ROTHMAN, J. E. 2018. S-Palmitoylation Sorts Membrane Cargo for Anterograde Transport in the Golgi. *Dev Cell,* 47**,** 479-493 e7.

FARNSWORTH, C. C., SEABRA, M. C., ERICSSON, L. H., GELB, M. H. & GLOMSET, J. A. 1994. Rab geranylgeranyl transferase catalyzes the geranylgeranylation of adjacent cysteines in the small GTPases Rab1A, Rab3A, and Rab5A. *Proc Natl Acad Sci U S A,* 91**,** 11963-7.

FREDERICKS, G. J., HOFFMANN, F. W., HONDAL, R. J., ROZOVSKY, S., URSCHITZ, J. & HOFFMANN, P. R. 2018. Selenoprotein K Increases Efficiency of DHHC6 Catalyzed Protein Palmitoylation by Stabilizing the Acyl-DHHC6 Intermediate. *Antioxidants (Basel),* 7.

FREDERICKS, G. J., HOFFMANN, F. W., ROSE, A. H., OSTERHELD, H. J., HESS, F. M., MERCIER, F. & HOFFMANN, P. R. 2014. Stable expression and function of the

inositol 1,4,5-triphosphate receptor requires palmitoylation by a DHHC6/selenoprotein K complex. *Proc Natl Acad Sci U S A,* 111**,** 16478-83.

FROMER, M., POCKLINGTON, A. J., KAVANAGH, D. H., WILLIAMS, H. J., DWYER, S., GORMLEY, P., GEORGIEVA, L., REES, E., PALTA, P., RUDERFER, D. M., CARRERA, N., HUMPHREYS, I., JOHNSON, J. S., ROUSSOS, P., BARKER, D. D., BANKS, E., MILANOVA, V., GRANT, S. G., HANNON, E., ROSE, S. A., CHAMBERT, K., MAHAJAN, M., SCOLNICK, E. M., MORAN, J. L., KIROV, G., PALOTIE, A., MCCARROLL, S. A., HOLMANS, P., SKLAR, P., OWEN, M. J., PURCELL, S. M. & O'DONOVAN, M. C. 2014. De novo mutations in schizophrenia implicate synaptic networks. *Nature,* 506**,** 179-84.

FUKATA, M., FUKATA, Y., ADESNIK, H., NICOLL, R. A. & BREDT, D. S. 2004. Identification of PSD-95 palmitoylating enzymes. *Neuron,* 44**,** 987-96.

GERACE, E. & MOAZED, D. 2014. Coimmunoprecipitation of proteins from yeast. *Methods Enzymol,* 541**,** 13-26.

GONZALEZ MONTORO, A., CHUMPEN RAMIREZ, S. & VALDEZ TAUBAS, J. 2015. The canonical DHHC motif is not absolutely required for the activity of the yeast S-acyltransferases Swf1 and Pfa4. *J Biol Chem,* 290**,** 22448-59.

GONZALEZ MONTORO, A., QUIROGA, R., MACCIONI, H. J. & VALDEZ TAUBAS, J. 2009. A novel motif at the C-terminus of palmitoyltransferases is essential for Swf1 and Pfa3 function in vivo. *Biochem J,* 419**,** 301-8.

GORENBERG, E. L., MASSARO TIEZE, S., YUCEL, B., ZHAO, H. R., CHOU, V., WIRAK, G. S., TOMITA, S., LAM, T. T. & CHANDRA, S. S. 2022. Identification of substrates of palmitoyl protein thioesterase 1 highlights roles of depalmitoylation in disulfide bond formation and synaptic function. *PLoS Biol,* 20**,** e3001590.

GORLEKU, O. A., BARNS, A. M., PRESCOTT, G. R., GREAVES, J. & CHAMBERLAIN, L. H. 2011. Endoplasmic reticulum localization of DHHC palmitoyltransferases mediated by lysine-based sorting signals. *J Biol Chem,* 286**,** 39573-84.

GOTTLIEB, C. D., ZHANG, S. & LINDER, M. E. 2015. The Cysteine-rich Domain of the DHHC3 Palmitoyltransferase Is Palmitoylated and Contains Tightly Bound Zinc. *J Biol Chem,* 290**,** 29259-69.

GREAVES, J., CARMICHAEL, J. A. & CHAMBERLAIN, L. H. 2011. The palmitoyl transferase DHHC2 targets a dynamic membrane cycling pathway: regulation by a C-terminal domain. *Mol Biol Cell,* 22**,** 1887-95.

GREAVES, J. & CHAMBERLAIN, L. H. 2006. Dual role of the cysteine-string domain in membrane binding and palmitoylation-dependent sorting of the molecular chaperone cysteine-string protein. *Mol Biol Cell,* 17**,** 4748-59.

GREAVES, J. & CHAMBERLAIN, L. H. 2011. DHHC palmitoyl transferases: substrate interactions and (patho)physiology. *Trends Biochem Sci,* 36**,** 245-53.

GREAVES, J., GORLEKU, O. A., SALAUN, C. & CHAMBERLAIN, L. H. 2010. Palmitoylation of the SNAP25 protein family: specificity and regulation by DHHC palmitoyl transferases. *J Biol Chem,* 285**,** 24629-38.

GREAVES, J., LEMONIDIS, K., GORLEKU, O. A., CRUCHAGA, C., GREFEN, C. & CHAMBERLAIN, L. H. 2012. Palmitoylation-induced aggregation of cysteine-string protein mutants that cause neuronal ceroid lipofuscinosis. *J Biol Chem,* 287**,** 37330-9.

GREAVES, J., MUNRO, K. R., DAVIDSON, S. C., RIVIERE, M., WOJNO, J., SMITH, T. K., TOMKINSON, N. C. & CHAMBERLAIN, L. H. 2017. Molecular basis of fatty acid selectivity in the zDHHC family of S-acyltransferases revealed by click chemistry. *Proc Natl Acad Sci U S A,* 114**,** E1365-E1374.

GREAVES, J., PRESCOTT, G. R., FUKATA, Y., FUKATA, M., SALAUN, C. & CHAMBERLAIN, L. H. 2009. The hydrophobic cysteine-rich domain of SNAP25 couples with downstream residues to mediate membrane interactions and recognition by DHHC palmitoyl transferases. *Mol Biol Cell,* 20**,** 1845-54.

GREAVES, J., SALAUN, C., FUKATA, Y., FUKATA, M. & CHAMBERLAIN, L. H. 2008. Palmitoylation and membrane interactions of the neuroprotective chaperone cysteine-string protein. *J Biol Chem,* 283**,** 25014-26.

GUO, Q., CHEN, C., WANG, Y., GUO, L. & SHANG, S. 2025. Multi-Omics Mendelian Randomization Identifies a DNA Methylation-ZDHHC20-Immune Axis Associated With Schizophrenia Risk. *Brain Behav,* 15**,** e70722.

HANCOCK, J. F., MAGEE, A. I., CHILDS, J. E. & MARSHALL, C. J. 1989. All ras proteins are polyisoprenylated but only some are palmitoylated. *Cell,* 57**,** 1167-77.

HAO, J. W., WANG, J., GUO, H., ZHAO, Y. Y., SUN, H. H., LI, Y. F., LAI, X. Y., ZHAO, N., WANG, X., XIE, C., HONG, L., HUANG, X., WANG, H. R., LI, C. B., LIANG, B., CHEN, S. & ZHAO, T. J. 2020. CD36 facilitates fatty acid uptake by dynamic palmitoylation-regulated endocytosis. *Nat Commun,* 11**,** 4765.

HE, M., ABDI, K. M. & BENNETT, V. 2014. Ankyrin-G palmitoylation and betaII-spectrin binding to phosphoinositide lipids drive lateral membrane assembly. *J Cell Biol,* 206**,** 273-88.

HELLSTEN, E., VESA, J., OLKKONEN, V. M., JALANKO, A. & PELTONEN, L. 1996. Human palmitoyl protein thioesterase: evidence for lysosomal targeting of the enzyme and disturbed cellular routing in infantile neuronal ceroid lipofuscinosis. *EMBO J,* 15**,** 5240-5.

HOMMA, Y., HIRAGI, S. & FUKUDA, M. 2021. Rab family of small GTPases: an updated view on their regulation and functions. *FEBS J,* 288**,** 36-55.

HUANG, K., SANDERS, S., SINGARAJA, R., ORBAN, P., CIJSOUW, T., ARSTIKAITIS, P., YANAI, A., HAYDEN, M. R. & EL-HUSSEINI, A. 2009. Neuronal palmitoyl acyl transferases exhibit distinct substrate specificity. *FASEB J,* 23**,** 2605-15.

HUANG, K., SANDERS, S. S., KANG, R., CARROLL, J. B., SUTTON, L., WAN, J., SINGARAJA, R., YOUNG, F. B., LIU, L., EL-HUSSEINI, A., DAVIS, N. G. & HAYDEN, M. R. 2011. Wild-type HTT modulates the enzymatic activity of the neuronal palmitoyl transferase HIP14. *Hum Mol Genet,* 20**,** 3356-65.

HUANG, K., YANAI, A., KANG, R., ARSTIKAITIS, P., SINGARAJA, R. R., METZLER, M., MULLARD, A., HAIGH, B., GAUTHIER-CAMPBELL, C., GUTEKUNST, C. A., HAYDEN, M. R. & EL-HUSSEINI, A. 2004. Huntingtin-interacting protein HIP14 is a palmitoyl transferase involved in palmitoylation and trafficking of multiple neuronal proteins. *Neuron,* 44**,** 977-86.

HUTTLIN, E. L., TING, L., BRUCKNER, R. J., GEBREAB, F., GYGI, M. P., SZPYT, J., TAM, S., ZARRAGA, G., COLBY, G., BALTIER, K., DONG, R., GUARANI, V., VAITES, L. P., ORDUREAU, A., RAD, R., ERICKSON, B. K., WUHR, M., CHICK, J., ZHAI, B., KOLIPPAKKAM, D., MINTSERIS, J., OBAR, R. A., HARRIS, T., ARTAVANIS-TSAKONAS, S., SOWA, M. E., DE CAMILLI, P., PAULO, J. A., HARPER, J. W. & GYGI, S. P. 2015. The BioPlex Network: A Systematic Exploration of the Human Interactome. *Cell,* 162**,** 425-440.

JANOSI, L., LI, Z., HANCOCK, J. F. & GORFE, A. A. 2012. Organization, dynamics, and segregation of Ras nanoclusters in membrane domains. *Proc Natl Acad Sci U S A,* 109**,** 8097-102.

JENNINGS, B. C. & LINDER, M. E. 2012. DHHC protein S-acyltransferases use similar ping-pong kinetic mechanisms but display different acyl-CoA specificities. *J Biol Chem,* 287**,** 7236-45.

JENNINGS, B. C., NADOLSKI, M. J., LING, Y., BAKER, M. B., HARRISON, M. L., DESCHENES, R. J. & LINDER, M. E. 2009. 2-Bromopalmitate and 2-(2-hydroxy-5-nitro-benzylidene)-benzo[b]thiophen-3-one inhibit DHHC-mediated palmitoylation in vitro. *J Lipid Res,* 50**,** 233-42.

JIANG, H., ZHANG, X., CHEN, X., ARAMSANGTIENCHAI, P., TONG, Z. & LIN, H. 2018. Protein Lipidation: Occurrence, Mechanisms, Biological Functions, and Enabling Technologies. *Chem Rev,* 118**,** 919-988.

JUMPER, J., EVANS, R., PRITZEL, A., GREEN, T., FIGURNOV, M., RONNEBERGER, O., TUNYASUVUNAKOOL, K., BATES, R., ZIDEK, A., POTAPENKO, A., BRIDGLAND, A., MEYER, C., KOHL, S. A. A., BALLARD, A. J., COWIE, A., ROMERA-PAREDES, B., NIKOLOV, S., JAIN, R., ADLER, J., BACK, T., PETERSEN, S., REIMAN, D., CLANCY, E., ZIELINSKI, M., STEINEGGER, M., PACHOLSKA, M., BERGHAMMER, T., BODENSTEIN, S., SILVER, D., VINYALS, O., SENIOR, A. W., KAVUKCUOGLU, K., KOHLI, P. & HASSABIS, D. 2021. Highly accurate protein structure prediction with AlphaFold. *Nature,* 596**,** 583-589.

KADKOVA, A., RADECKE, J. & SORENSEN, J. B. 2019. The SNAP-25 Protein Family. *Neuroscience,* 420**,** 50-71.

KARVE, T. M. & CHEEMA, A. K. 2011. Small changes huge impact: the role of protein posttranslational modifications in cellular homeostasis and disease. *J Amino Acids,* 2011**,** 207691.

KHAN, A. H. & SMITH, D. J. 2021. Cost-Effective Mapping of Genetic Interactions in Mammalian Cells. *Front Genet,* 12**,** 703738.

KHARBANDA, A., WALTER, D. M., GUDIEL, A. A., SCHEK, N., FELDSER, D. M. & WITZE, E. S. 2020. Blocking EGFR palmitoylation suppresses PI3K signaling and mutant KRAS lung tumorigenesis. *Sci Signal,* 13.

KIM, S. J., ZHANG, Z., SARKAR, C., TSAI, P. C., LEE, Y. C., DYE, L. & MUKHERJEE, A. B. 2008. Palmitoyl protein thioesterase-1 deficiency impairs synaptic vesicle recycling at nerve terminals, contributing to neuropathology in humans and mice. *J Clin Invest,* 118**,** 3075-86.

KO, P. J. & DIXON, S. J. 2018. Protein palmitoylation and cancer. *EMBO Rep,* 19.

KO, P. J., WOODROW, C., DUBREUIL, M. M., MARTIN, B. R., SKOUTA, R., BASSIK, M. C. & DIXON, S. J. 2019. A ZDHHC5-GOLGA7 Protein Acyltransferase Complex Promotes Nonapoptotic Cell Death. *Cell Chem Biol,* 26**,** 1716-1724 e9.

KONG, E., PENG, S., CHANDRA, G., SARKAR, C., ZHANG, Z., BAGH, M. B. & MUKHERJEE, A. B. 2013. Dynamic palmitoylation links cytosol-membrane shuttling of acyl-protein thioesterase-1 and acyl-protein thioesterase-2 with that of proto-oncogene H-ras product and growth-associated protein-43. *J Biol Chem,* 288**,** 9112-25.

KYTE, J. & DOOLITTLE, R. F. 1982. A simple method for displaying the hydropathic character of a protein. *J Mol Biol,* 157**,** 105-32.

LAI, J. & LINDER, M. E. 2013. Oligomerization of DHHC protein S-acyltransferases. *J Biol Chem,* 288**,** 22862-70.

LAN, T., DELALANDE, C. & DICKINSON, B. C. 2021. Inhibitors of DHHC family proteins. *Curr Opin Chem Biol,* 65**,** 118-125.

LEE, J. Y., DILONES, S., MAUJEAN, T., ASAD, M., MOHD, A., AUSLANDER, N., BRADY, D. C., BURSLEM, G. M. & WITZE, E. S. 2024. A selective S-acyltransferase inhibitor suppresses tumor growth. *bioRxiv*.

LEMONIDIS, K., GORLEKU, O. A., SANCHEZ-PEREZ, M. C., GREFEN, C. & CHAMBERLAIN, L. H. 2014. The Golgi S-acylation machinery comprises zDHHC

enzymes with major differences in substrate affinity and S-acylation activity. *Mol Biol Cell,* 25**,** 3870-83.
LEMONIDIS, K., SANCHEZ-PEREZ, M. C. & CHAMBERLAIN, L. H. 2015a. Identification of a Novel Sequence Motif Recognized by the Ankyrin Repeat Domain of zDHHC17/13 S-Acyltransferases. *J Biol Chem,* 290**,** 21939-50.
LEMONIDIS, K., WERNO, M. W., GREAVES, J., DIEZ-ARDANUY, C., SANCHEZ-PEREZ, M. C., SALAUN, C., THOMSON, D. M. & CHAMBERLAIN, L. H. 2015b. The zDHHC family of S-acyltransferases. *Biochem Soc Trans,* 43**,** 217-21.
LIN, D. T. & CONIBEAR, E. 2015. ABHD17 proteins are novel protein depalmitoylases that regulate N-Ras palmitate turnover and subcellular localization. *Elife,* 4**,** e11306.
LIN, Z., AGARWAL, S., TAN, S., SHI, H., LU, X., TAO, Z., DONG, X., WU, X., ZHAO, J. C. & YU, J. 2023. Palmitoyl acyltransferase ZDHHC7 inhibits androgen receptor and suppresses prostate cancer. *Oncogene,* 42**,** 2126-2138.
LINDER, M. E. & DESCHENES, R. J. 2007. Palmitoylation: policing protein stability and traffic. *Nat Rev Mol Cell Biol,* 8**,** 74-84.
LINDER, M. E. & JENNINGS, B. C. 2013. Mechanism and function of DHHC S-acyltransferases. *Biochem Soc Trans,* 41**,** 29-34.
LINDWASSER, O. W. & RESH, M. D. 2002. Myristoylation as a target for inhibiting HIV assembly: unsaturated fatty acids block viral budding. *Proc Natl Acad Sci U S A,* 99**,** 13037-42.
LIU, P., JIAO, B., ZHANG, R., ZHAO, H., ZHANG, C., WU, M., LI, D., ZHAO, X., QIU, Q., LI, J. & REN, R. 2016. Palmitoylacyltransferase Zdhhc9 inactivation mitigates leukemogenic potential of oncogenic Nras. *Leukemia,* 30**,** 1225-8.
LIU, Y., BRIDGES, R., WORTHAM, A. & KULESZ-MARTIN, M. 2012. NF-kappaB repression by PIAS3 mediated RelA SUMOylation. *PLoS One,* 7**,** e37636.
LIU, Z. Y., LAN, T., TANG, F., HE, Y. Z., LIU, J. S., YANG, J. Z., CHEN, X., WANG, Z. F. & LI, Z. Q. 2023. ZDHHC15 promotes glioma malignancy and acts as a novel prognostic biomarker for patients with glioma. *BMC Cancer,* 23**,** 420.
LOBO, S., GREENTREE, W. K., LINDER, M. E. & DESCHENES, R. J. 2002. Identification of a Ras palmitoyltransferase in Saccharomyces cerevisiae. *J Biol Chem,* 277**,** 41268-73.
LONG, J. Z. & CRAVATT, B. F. 2011. The metabolic serine hydrolases and their functions in mammalian physiology and disease. *Chem Rev,* 111**,** 6022-63.
LORD, C. C., THOMAS, G. & BROWN, J. M. 2013. Mammalian alpha beta hydrolase domain (ABHD) proteins: Lipid metabolizing enzymes at the interface of cell signaling and energy metabolism. *Biochim Biophys Acta,* 1831**,** 792-802.
MACLAINE, N. J. & HUPP, T. R. 2011. How phosphorylation controls p53. *Cell Cycle,* 10**,** 916-21.
MALGAPO, M. I. P. & LINDER, M. E. 2021. Substrate recruitment by zDHHC protein acyltransferases. *Open Biol,* 11**,** 210026.
MARTIN, B. R. & CRAVATT, B. F. 2009. Large-scale profiling of protein palmitoylation in mammalian cells. *Nat Methods,* 6**,** 135-8.
MCCLURG, U. L. & ROBSON, C. N. 2015. Deubiquitinating enzymes as oncotargets. *Oncotarget,* 6**,** 9657-68.
MENG, X., TEMPLETON, C., CLEMENTI, C. & VEIT, M. 2023. The role of an amphiphilic helix and transmembrane region in the efficient acylation of the M2 protein from influenza virus. *Sci Rep,* 13**,** 18928.
MESQUITA, F. S., ABRAMI, L., BRACQ, L., PANYAIN, N., MERCIER, V., KUNZ, B., CHUAT, A., CARLEVARO-FITA, J., TRONO, D. & VAN DER GOOT, F. G. 2023. SARS-CoV-2

hijacks a cell damage response, which induces transcription of a more efficient Spike S-acyltransferase. *Nat Commun,* 14**,** 7302.

MITCHELL, D. A., HAMEL, L. D., ISHIZUKA, K., MITCHELL, G., SCHAEFER, L. M. & DESCHENES, R. J. 2012. The Erf4 subunit of the yeast Ras palmitoyl acyltransferase is required for stability of the Acyl-Erf2 intermediate and palmitoyl transfer to a Ras2 substrate. *J Biol Chem,* 287**,** 34337-48.

MITCHELL, D. A., HAMEL, L. D., REDDY, K. D., FARH, L., RETTEW, L. M., SANCHEZ, P. R. & DESCHENES, R. J. 2014. Mutations in the X-linked intellectual disability gene, zDHHC9, alter autopalmitoylation activity by distinct mechanisms. *J Biol Chem,* 289**,** 18582-92.

MITCHELL, D. A., MITCHELL, G., LING, Y., BUDDE, C. & DESCHENES, R. J. 2010. Mutational analysis of Saccharomyces cerevisiae Erf2 reveals a two-step reaction mechanism for protein palmitoylation by DHHC enzymes. *J Biol Chem,* 285**,** 38104-14.

MITCHELL, D. A., VASUDEVAN, A., LINDER, M. E. & DESCHENES, R. J. 2006. Protein palmitoylation by a family of DHHC protein S-acyltransferases. *J Lipid Res,* 47**,** 1118-27.

NADOLSKI, M. J. & LINDER, M. E. 2007. Protein lipidation. *FEBS J,* 274**,** 5202-10.

NATALE, F., SPINELLI, M., RINAUDO, M., GULISANO, W., NIFO SARRAPOCHIELLO, I., ACETO, G., PUZZO, D., FUSCO, S. & GRASSI, C. 2024. Inhibition of zDHHC7-driven protein S-palmitoylation prevents cognitive deficits in an experimental model of Alzheimer's disease. *Proc Natl Acad Sci U S A,* 121**,** e2402604121.

NAVARRO, A. P. & CHEESEMAN, I. M. 2022. Identification of a Golgi-localized peptide reveals a minimal Golgi-targeting motif. *Mol Biol Cell,* 33**,** ar110.

NGUYEN, P. L., GREENTREE, W. K., KAWATE, T. & LINDER, M. E. 2023. GCP16 stabilizes the DHHC9 subfamily of protein acyltransferases through a conserved C-terminal cysteine motif. *Front Physiol,* 14**,** 1167094.

NORITAKE, J., FUKATA, Y., IWANAGA, T., HOSOMI, N., TSUTSUMI, R., MATSUDA, N., TANI, H., IWANARI, H., MOCHIZUKI, Y., KODAMA, T., MATSUURA, Y., BREDT, D. S., HAMAKUBO, T. & FUKATA, M. 2009. Mobile DHHC palmitoylating enzyme mediates activity-sensitive synaptic targeting of PSD-95. *J Cell Biol,* 186**,** 147-60.

OHNO, Y., KIHARA, A., SANO, T. & IGARASHI, Y. 2006. Intracellular localization and tissue-specific distribution of human and yeast DHHC cysteine-rich domain-containing proteins. *Biochim Biophys Acta,* 1761**,** 474-83.

OHTA, E., MISUMI, Y., SOHDA, M., FUJIWARA, T., YANO, A. & IKEHARA, Y. 2003. Identification and characterization of GCP16, a novel acylated Golgi protein that interacts with GCP170. *J Biol Chem,* 278**,** 51957-67.

OLSON, E. N., TOWLER, D. A. & GLASER, L. 1985. Specificity of fatty acid acylation of cellular proteins. *J Biol Chem,* 260**,** 3784-90.

PALSULEDESAI, C. C. & DISTEFANO, M. D. 2015. Protein prenylation: enzymes, therapeutics, and biotechnology applications. *ACS Chem Biol,* 10**,** 51-62.

PASKEVICIUS, T., FARRAJ, R. A., MICHALAK, M. & AGELLON, L. B. 2023. Calnexin, More Than Just a Molecular Chaperone. *Cells,* 12.

PERCHERANCIER, Y., PLANCHENAULT, T., VALENZUELA-FERNANDEZ, A., VIRELIZIER, J. L., ARENZANA-SEISDEDOS, F. & BACHELERIE, F. 2001. Palmitoylation-dependent control of degradation, life span, and membrane expression of the CCR5 receptor. *J Biol Chem,* 276**,** 31936-44.

PHILIPPE, J. M. & JENKINS, P. M. 2019. Spatial organization of palmitoyl acyl transferases governs substrate localization and function. *Mol Membr Biol,* 35**,** 60-75.

PLAIN, F., HOWIE, J., KENNEDY, J., BROWN, E., SHATTOCK, M. J., FRASER, N. J. & FULLER, W. 2020. Control of protein palmitoylation by regulating substrate recruitment to a zDHHC-protein acyltransferase. *Commun Biol,* 3**,** 411.

PREININGER, A. M., KAYA, A. I., GILBERT, J. A., 3RD, BUSENLEHNER, L. S., ARMSTRONG, R. N. & HAMM, H. E. 2012. Myristoylation exerts direct and allosteric effects on Galpha conformation and dynamics in solution. *Biochemistry,* 51**,** 1911-24.

PRIOR, I. A., HOOD, F. E. & HARTLEY, J. L. 2020. The Frequency of Ras Mutations in Cancer. *Cancer Res,* 80**,** 2969-2974.

PRIOR, I. A., MUNCKE, C., PARTON, R. G. & HANCOCK, J. F. 2003. Direct visualization of Ras proteins in spatially distinct cell surface microdomains. *J Cell Biol,* 160**,** 165-70.

QIU, T., AZIZI, S. A., BROOKES, N., LAN, T. & DICKINSON, B. C. 2022. A High-Throughput Fluorescent Turn-On Assay for Inhibitors of DHHC Family Proteins. *ACS Chem Biol,* 17**,** 2018-2023.

RAJALINGAM, K., SCHRECK, R., RAPP, U. R. & ALBERT, S. 2007. Ras oncogenes and their downstream targets. *Biochim Biophys Acta,* 1773**,** 1177-95.

RAMAZI, S. & ZAHIRI, J. 2021. Posttranslational modifications in proteins: resources, tools and prediction methods. *Database (Oxford),* 2021.

RANA, M. S., KUMAR, P., LEE, C. J., VERARDI, R., RAJASHANKAR, K. R. & BANERJEE, A. 2018a. Fatty acyl recognition and transfer by an integral membrane S-acyltransferase. *Science,* 359.

RANA, M. S., LEE, C. J. & BANERJEE, A. 2018b. The molecular mechanism of DHHC protein acyltransferases. *Biochem Soc Trans,* 47**,** 157-167.

RAPPU, P., SALO, A. M., MYLLYHARJU, J. & HEINO, J. 2019. Role of prolyl hydroxylation in the molecular interactions of collagens. *Essays Biochem,* 63**,** 325-335.

RAYMOND, F. L., TARPEY, P. S., EDKINS, S., TOFTS, C., O'MEARA, S., TEAGUE, J., BUTLER, A., STEVENS, C., BARTHORPE, S., BUCK, G., COLE, J., DICKS, E., GRAY, K., HALLIDAY, K., HILLS, K., HINTON, J., JONES, D., MENZIES, A., PERRY, J., RAINE, K., SHEPHERD, R., SMALL, A., VARIAN, J., WIDAA, S., MALLYA, U., MOON, J., LUO, Y., SHAW, M., BOYLE, J., KERR, B., TURNER, G., QUARRELL, O., COLE, T., EASTON, D. F., WOOSTER, R., BOBROW, M., SCHWARTZ, C. E., GECZ, J., STRATTON, M. R. & FUTREAL, P. A. 2007. Mutations in ZDHHC9, which encodes a palmitoyltransferase of NRAS and HRAS, cause X-linked mental retardation associated with a Marfanoid habitus. *Am J Hum Genet,* 80**,** 982-7.

REN, W., SUN, Y. & DU, K. 2015. Glut4 palmitoylation at Cys223 plays a critical role in Glut4 membrane trafficking. *Biochem Biophys Res Commun,* 460**,** 709-14.

RESH, M. D. 2017. Palmitoylation of proteins in cancer. *Biochem Soc Trans,* 45**,** 409-416.

ROCKS, O., GERAUER, M., VARTAK, N., KOCH, S., HUANG, Z. P., PECHLIVANIS, M., KUHLMANN, J., BRUNSVELD, L., CHANDRA, A., ELLINGER, B., WALDMANN, H. & BASTIAENS, P. I. 2010. The palmitoylation machinery is a spatially organizing system for peripheral membrane proteins. *Cell,* 141**,** 458-71.

ROCKS, O., PEYKER, A., KAHMS, M., VERVEER, P. J., KOERNER, C., LUMBIERRES, M., KUHLMANN, J., WALDMANN, H., WITTINGHOFER, A. & BASTIAENS, P. I. 2005. An acylation cycle regulates localization and activity of palmitoylated Ras isoforms. *Science,* 307**,** 1746-52.

RODENBURG, R. N. P., SNIJDER, J., VAN DE WATERBEEMD, M., SCHOUTEN, A., GRANNEMAN, J., HECK, A. J. R. & GROS, P. 2017. Stochastic palmitoylation of accessible cysteines in membrane proteins revealed by native mass spectrometry. *Nat Commun,* 8**,** 1280.

ROTH, A. F., FENG, Y., CHEN, L. & DAVIS, N. G. 2002. The yeast DHHC cysteine-rich domain protein Akr1p is a palmitoyl transferase. *J Cell Biol,* 159**,** 23-8.

ROTH, A. F., WAN, J., BAILEY, A. O., SUN, B., KUCHAR, J. A., GREEN, W. N., PHINNEY, B. S., YATES, J. R., 3RD & DAVIS, N. G. 2006. Global analysis of protein palmitoylation in yeast. *Cell,* 125**,** 1003-13.

SALAUN, C., LOCATELLI, C., ZMUDA, F., CABRERA GONZALEZ, J. & CHAMBERLAIN, L. H. 2020. Accessory proteins of the zDHHC family of S-acylation enzymes. *J Cell Sci,* 133.

SALAUN, C., RITCHIE, L., GREAVES, J., BUSHELL, T. J. & CHAMBERLAIN, L. H. 2017. The C-terminal domain of zDHHC2 contains distinct sorting signals that regulate intracellular localisation in neurons and neuroendocrine cells. *Mol Cell Neurosci,* 85**,** 235-246.

SALAUN, C., TOMKINSON, N. C. O. & CHAMBERLAIN, L. H. 2023. The endoplasmic reticulum-localized enzyme zDHHC6 mediates S-acylation of short transmembrane constructs from multiple type I and II membrane proteins. *J Biol Chem,* 299**,** 105201.

SAMARZIJA, I. 2021. Post-Translational Modifications That Drive Prostate Cancer Progression. *Biomolecules,* 11.

SCHMIDT, M. F. & SCHLESINGER, M. J. 1979. Fatty acid binding to vesicular stomatitis virus glycoprotein: a new type of post-translational modification of the viral glycoprotein. *Cell,* 17**,** 813-9.

SCHNEIDER, C. A., RASBAND, W. S. & ELICEIRI, K. W. 2012. NIH Image to ImageJ: 25 years of image analysis. *Nat Methods,* 9**,** 671-5.

SEHNAL, D., BITTRICH, S., DESHPANDE, M., SVOBODOVA, R., BERKA, K., BAZGIER, V., VELANKAR, S., BURLEY, S. K., KOCA, J. & ROSE, A. S. 2021. Mol* Viewer: modern web app for 3D visualization and analysis of large biomolecular structures. *Nucleic Acids Res,* 49**,** W431-W437.

SHIMELL, J. J., GLOBA, A., SEPERS, M. D., WILD, A. R., MATIN, N., RAYMOND, L. A. & BAMJI, S. X. 2021. Regulation of hippocampal excitatory synapses by the Zdhhc5 palmitoyl acyltransferase. *J Cell Sci,* 134.

SHIMELL, J. J., SHAH, B. S., CAIN, S. M., THOUTA, S., KUHLMANN, N., TATARNIKOV, I., JOVELLAR, D. B., BRIGIDI, G. S., KASS, J., MILNERWOOD, A. J., SNUTCH, T. P. & BAMJI, S. X. 2019. The X-Linked Intellectual Disability Gene Zdhhc9 Is Essential for Dendrite Outgrowth and Inhibitory Synapse Formation. *Cell Rep,* 29**,** 2422-2437 e8.

SIMANSHU, D. K., NISSLEY, D. V. & MCCORMICK, F. 2017. RAS Proteins and Their Regulators in Human Disease. *Cell,* 170**,** 17-33.

SIMONATI, A. & WILLIAMS, R. E. 2022. Neuronal Ceroid Lipofuscinosis: The Multifaceted Approach to the Clinical Issues, an Overview. *Front Neurol,* 13**,** 811686.

SINGARAJA, R. R., HADANO, S., METZLER, M., GIVAN, S., WELLINGTON, C. L., WARBY, S., YANAI, A., GUTEKUNST, C. A., LEAVITT, B. R., YI, H., FICHTER, K., GAN, L., MCCUTCHEON, K., CHOPRA, V., MICHEL, J., HERSCH, S. M., IKEDA, J. E. & HAYDEN, M. R. 2002. HIP14, a novel ankyrin domain-containing protein, links huntingtin to intracellular trafficking and endocytosis. *Hum Mol Genet,* 11**,** 2815-28.

SONG, L. & LUO, Z. Q. 2019. Post-translational regulation of ubiquitin signaling. *J Cell Biol,* 218**,** 1776-1786.

SOYOMBO, A. A. & HOFMANN, S. L. 1997. Molecular cloning and expression of palmitoyl-protein thioesterase 2 (PPT2), a homolog of lysosomal palmitoyl-

protein thioesterase with a distinct substrate specificity. *J Biol Chem,* 272**,** 27456-63.

SUN, Y., LI, X., YIN, C., ZHANG, J., LIANG, E., WU, X., NI, Y., ARBESMAN, J., GODING, C. R. & CHEN, S. 2023. AMPK Phosphorylates ZDHHC13 to Increase MC1R Activity and Suppress Melanomagenesis. *Cancer Res,* 83**,** 1062-1073.

SWARTHOUT, J. T., LOBO, S., FARH, L., CROKE, M. R., GREENTREE, W. K., DESCHENES, R. J. & LINDER, M. E. 2005. DHHC9 and GCP16 constitute a human protein fatty acyltransferase with specificity for H- and N-Ras. *J Biol Chem,* 280**,** 31141-8.

TABACZAR, S., CZOGALLA, A., PODKALICKA, J., BIERNATOWSKA, A. & SIKORSKI, A. F. 2017. Protein palmitoylation: Palmitoyltransferases and their specificity. *Exp Biol Med (Maywood),* 242**,** 1150-1157.

THOMAS, G. M. & HAYASHI, T. 2013. Smarter neuronal signaling complexes from existing components: how regulatory modifications were acquired during animal evolution: evolution of palmitoylation-dependent regulation of AMPA-type ionotropic glutamate receptors. *Bioessays,* 35**,** 929-39.

THOMAS, G. M., HAYASHI, T., CHIU, S. L., CHEN, C. M. & HUGANIR, R. L. 2012. Palmitoylation by DHHC5/8 targets GRIP1 to dendritic endosomes to regulate AMPA-R trafficking. *Neuron,* 73**,** 482-96.

TIAN, L., MCCLAFFERTY, H., KNAUS, H. G., RUTH, P. & SHIPSTON, M. J. 2012. Distinct acyl protein transferases and thioesterases control surface expression of calcium-activated potassium channels. *J Biol Chem,* 287**,** 14718-25.

TIAN, Y., LI, W., ZHAI, Q., YU, Y., YUAN, J., MA, Y., YANG, J., LI, M., CHANG, W., LI, W., HUANG, K., SUN, C., ZENG, C., SUN, Y., GU, J., ZHANG, H., LI, D., YU, Y., HU, L., ZHANG, P., MA, B., ZHENG, J., LI, P., GUO, F. & SUN, Y. 2025. Pharmacological Targeting of DHHC9-Mediated STRN4 Palmitoylation to Suppress YAP-Driven Cancer Metastasis. *J Cell Mol Med,* 29**,** e70815.

TOMATIS, V. M., TRENCHI, A., GOMEZ, G. A. & DANIOTTI, J. L. 2010. Acyl-protein thioesterase 2 catalyzes the deacylation of peripheral membrane-associated GAP-43. *PLoS One,* 5**,** e15045.

TORTOSA, E., ADOLFS, Y., FUKATA, M., PASTERKAMP, R. J., KAPITEIN, L. C. & HOOGENRAAD, C. C. 2017. Dynamic Palmitoylation Targets MAP6 to the Axon to Promote Microtubule Stabilization during Neuronal Polarization. *Neuron,* 94**,** 809-825 e7.

TOYODA, T., SUGIMOTO, H. & YAMASHITA, S. 1999. Sequence, expression in Escherichia coli, and characterization of lysophospholipase II. *Biochim Biophys Acta,* 1437**,** 182-93.

TSUTSUMI, R., FUKATA, Y., NORITAKE, J., IWANAGA, T., PEREZ, F. & FUKATA, M. 2009. Identification of G protein alpha subunit-palmitoylating enzyme. *Mol Cell Biol,* 29**,** 435-47.

UNIPROT, C. 2025. UniProt: the Universal Protein Knowledgebase in 2025. *Nucleic Acids Res,* 53**,** D609-D617.

VALDEZ-TAUBAS, J. & PELHAM, H. 2005. Swf1-dependent palmitoylation of the SNARE Tlg1 prevents its ubiquitination and degradation. *EMBO J,* 24**,** 2524-32.

VARADI, M., ANYANGO, S., DESHPANDE, M., NAIR, S., NATASSIA, C., YORDANOVA, G., YUAN, D., STROE, O., WOOD, G., LAYDON, A., ZIDEK, A., GREEN, T., TUNYASUVUNAKOOL, K., PETERSEN, S., JUMPER, J., CLANCY, E., GREEN, R., VORA, A., LUTFI, M., FIGURNOV, M., COWIE, A., HOBBS, N., KOHLI, P., KLEYWEGT, G., BIRNEY, E., HASSABIS, D. & VELANKAR, S. 2022. AlphaFold Protein Structure Database: massively expanding the structural coverage of

protein-sequence space with high-accuracy models. *Nucleic Acids Res,* 50**,** D439-D444.

VARADI, M., BERTONI, D., MAGANA, P., PARAMVAL, U., PIDRUCHNA, I., RADHAKRISHNAN, M., TSENKOV, M., NAIR, S., MIRDITA, M., YEO, J., KOVALEVSKIY, O., TUNYASUVUNAKOOL, K., LAYDON, A., ZIDEK, A., TOMLINSON, H., HARIHARAN, D., ABRAHAMSON, J., GREEN, T., JUMPER, J., BIRNEY, E., STEINEGGER, M., HASSABIS, D. & VELANKAR, S. 2024. AlphaFold Protein Structure Database in 2024: providing structure coverage for over 214 million protein sequences. *Nucleic Acids Res,* 52**,** D368-D375.

VARTAK, N., PAPKE, B., GRECCO, H. E., ROSSMANNEK, L., WALDMANN, H., HEDBERG, C. & BASTIAENS, P. I. 2014. The autodepalmitoylating activity of APT maintains the spatial organization of palmitoylated membrane proteins. *Biophys J,* 106**,** 93-105.

VERKRUYSE, L. A. & HOFMANN, S. L. 1996. Lysosomal targeting of palmitoyl-protein thioesterase. *J Biol Chem,* 271**,** 15831-6.

VERMA, S., HOFFMANN, F. W., KUMAR, M., HUANG, Z., ROE, K., NGUYEN-WU, E., HASHIMOTO, A. S. & HOFFMANN, P. R. 2011. Selenoprotein K knockout mice exhibit deficient calcium flux in immune cells and impaired immune responses. *J Immunol,* 186**,** 2127-37.

WANG, M. & CASEY, P. J. 2016. Protein prenylation: unique fats make their mark on biology. *Nat Rev Mol Cell Biol,* 17**,** 110-22.

WARD, A. F., BRAUN, B. S. & SHANNON, K. M. 2012. Targeting oncogenic Ras signaling in hematologic malignancies. *Blood,* 120**,** 3397-406.

WEST, S. J., BOEHNING, D. & AKIMZHANOV, A. M. 2022. Regulation of T cell function by protein S-acylation. *Front Physiol,* 13**,** 1040968.

WHITE, R. B., WILD, A. R., O'LEARY, T. P., THOMPSON, A. J., FLIBOTTE, S., PENG, A., ROGALSKI, J. C., MAIR, M., DERHAMI, N. & BAMJI, S. X. 2025. The X-Linked Intellectual Disability Gene, ZDHHC9 , Is Important for Oligodendrocyte Subtype Determination and Myelination. *Glia,* 73**,** 1452-1466.

WILSON, A. L., ERDMAN, R. A., CASTELLANO, F. & MALTESE, W. A. 1998. Prenylation of Rab8 GTPase by type I and type II geranylgeranyl transferases. *Biochem J,* 333 (Pt 3)**,** 497-504.

WON, S. J., CHEUNG SEE KIT, M. & MARTIN, B. R. 2018. Protein depalmitoylases. *Crit Rev Biochem Mol Biol,* 53**,** 83-98.

WOODLEY, K. T. & COLLINS, M. O. 2019. S-acylated Golga7b stabilises DHHC5 at the plasma membrane to regulate cell adhesion. *EMBO Rep,* 20**,** e47472.

YANAI, A., HUANG, K., KANG, R., SINGARAJA, R. R., ARSTIKAITIS, P., GAN, L., ORBAN, P. C., MULLARD, A., COWAN, C. M., RAYMOND, L. A., DRISDEL, R. C., GREEN, W. N., RAVIKUMAR, B., RUBINSZTEIN, D. C., EL-HUSSEINI, A. & HAYDEN, M. R. 2006. Palmitoylation of huntingtin by HIP14 is essential for its trafficking and function. *Nat Neurosci,* 9**,** 824-31.

YANG, A., LIU, S., ZHANG, Y., CHEN, J., FAN, Y., WANG, F., ZOU, Y., FENG, S., WU, J. & HU, Q. 2024. Regulation of RAS palmitoyltransferases by accessory proteins and palmitoylation. *Nat Struct Mol Biol,* 31**,** 436-446.

YEH, D. C., DUNCAN, J. A., YAMASHITA, S. & MICHEL, T. 1999. Depalmitoylation of endothelial nitric-oxide synthase by acyl-protein thioesterase 1 is potentiated by Ca(2+)-calmodulin. *J Biol Chem,* 274**,** 33148-54.

YUAN, M., SONG, Z. H., YING, M. D., ZHU, H., HE, Q. J., YANG, B. & CAO, J. 2020. N-myristoylation: from cell biology to translational medicine. *Acta Pharmacol Sin,* 41**,** 1005-1015.

ZHA, J., WEILER, S., OH, K. J., WEI, M. C. & KORSMEYER, S. J. 2000. Posttranslational N-myristoylation of BID as a molecular switch for targeting mitochondria and apoptosis. *Science,* 290**,** 1761-5.

ZHANG, M. M. & HANG, H. C. 2017. Protein S-palmitoylation in cellular differentiation. *Biochem Soc Trans,* 45**,** 275-285.

ZHAO, L., LOBO, S., DONG, X., AULT, A. D. & DESCHENES, R. J. 2002. Erf4p and Erf2p form an endoplasmic reticulum-associated complex involved in the plasma membrane localization of yeast Ras proteins. *J Biol Chem,* 277**,** 49352-9.

ZINGLER, P., SARCHEN, V., GLATTER, T., CANING, L., SAGGAU, C., KATHAYAT, R. S., DICKINSON, B. C., ADAM, D., SCHNEIDER-BRACHERT, W., SCHUTZE, S. & FRITSCH, J. 2019. Palmitoylation is required for TNF-R1 signaling. *Cell Commun Signal,* 17**,** 90.

ZMUDA, F. & CHAMBERLAIN, L. H. 2020. Regulatory effects of post-translational modifications on zDHHC S-acyltransferases. *J Biol Chem,* 295**,** 14640-14652.

ZVERINA, E. A., LAMPHEAR, C. L., WRIGHT, E. N. & FIERKE, C. A. 2012. Recent advances in protein prenyltransferases: substrate identification, regulation, and disease interventions. *Curr Opin Chem Biol,* 16**,** 544-52.

Appendix I

ANALYSIS OF THE INTERACTION OF ZDHHC9 WITH ITS ACCESSORY PROTEIN GCP16

[1]Despoina Allagioti, [1]Nicholas C.O. Tomkinson, [2]Rami N. Hannoush and [1]Luke H. Chamberlain
[1]Strathclyde Institute of Pharmacy and Biomedical Sciences, University of Strathclyde, Glasgow, Scotland, UK
[2]Department of Early Discovery Biochemistry, Genentech, South San Francisco, California 94080, United States

University of Strathclyde Glasgow

BACKGROUND

Ras proteins regulate growth factor signalling pathways, and hyper-activating mutations in *RAS* genes result in uncontrolled cell division and oncogenesis. S-acylation of H-Ras and N-Ras controls their membrane association, intracellular localization, and signaling activity, and targeting this modification could represent a strategy to inhibit mutant Ras proteins.

zDHHC9 has been reported to S-acylate Ras proteins, and the enzymatic activity of this enzyme depends on its association with GCP16. Recent work reported the cryoEM structure of the zDHHC9-GCP16 complex.

The aim of this project (which was initiated before the zDHHC9-GCP16 cryoEM structure was reported) is to study the zDHHC9-GCP16 interaction and to use the information generated to design peptide inhibitors that disrupt protein complex formation. We hypothesize that these peptide inhibitors will perturb the activity of zDHHC9 and the corresponding S-acylation of Ras, down-regulating the activity of this signalling molecule.

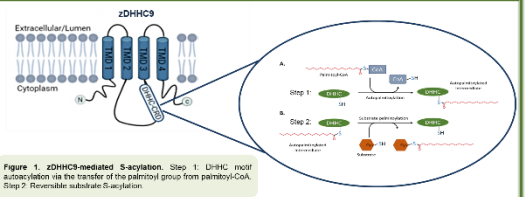

Figure 1. zDHHC9-mediated S-acylation. Step 1: DHHC motif autoacylation via the transfer of the palmitoyl group from palmitoyl-CoA. Step 2: Reversible substrate S-acylation.

METHODS

Cell culture (HEK 293T) → Transfection → Click chemistry (Figures 2 & 3) Cycloheximide (Figure 4) Immunoprecipitation (Figure 5) → Protein detection by immunoblotting

RESULTS

1. The N- and C-terminal regions of GCP16 are important for GCP16 and zDHHC9 S-acylation

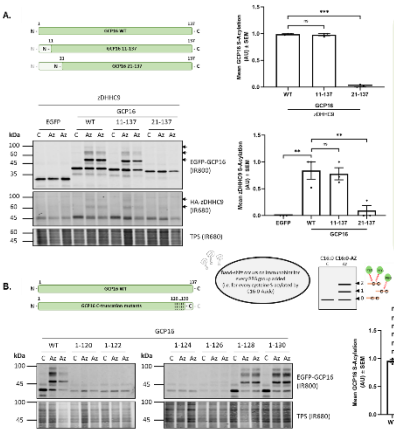

Figure 2. S-acylation of GCP16 N- and C-terminal mutants and their effect on the stability of zDHHC9 S-acylation, detected using click-mPEG. HEK 293T cells were co-transfected with **(A)** EGFP, EGFP-tagged GCP16 WT, 11-137, or 21-137, and HA-tagged zDHHC9, or with **(B)** EGFP-tagged GCP16 WT, 1-120, 1-122, 1-124, 1-126, 1-128, or 1-130. In both experiments, cells were labelled with palmitic acid as a control (C), or with palmitic acid-azide (Az) for 4 hours and were then lysed and clicked using Alkyne-mPEG. S acylation is indicated by band-shifts in Az samples. Quantified data shows the mean S acylation values +/- SEM. Statistical significance was analysed using a one-way ANOVA, followed by a Dunnett's multiple comparisons test against GCP16 WT (**p>0.1,***p<0.001, n = 3 (A), n = 4 (B)).

2. Analysis of key residues within GCP16 for the S-acylation of both GCP16 and zDHHC9

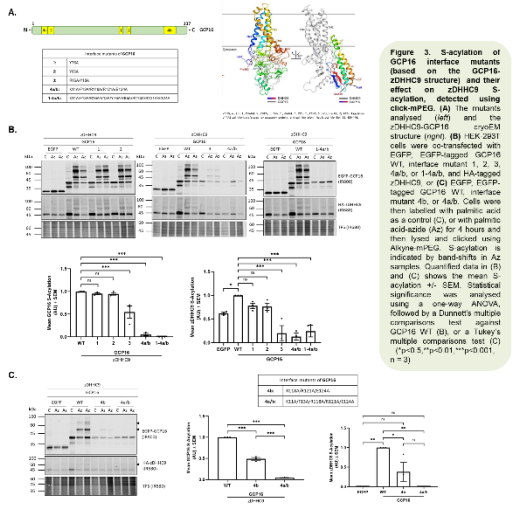

Figure 3. S-acylation of GCP16 interface mutants (based on the GCP16-zDHHC9 structure) and their effect on zDHHC9 S-acylation, detected using click-mPEG. (A) The mutants analysed (left) and the zDHHC9-GCP16 cryoEM structure (right). **(B)** HEK 293T cells were co-transfected with EGFP, EGFP-tagged GCP16 WT, interface mutant 1, 2, 3, 4a/b, or 1-4a/b, and HA-tagged zDHHC9, or **(C)** EGFP, EGFP-tagged GCP16 WT, interface mutant 4b, or 4a/b. Cells were then labelled with palmitic acid as a control (C), or with palmitic acid-azide (Az) for 4 hours and then lysed and clicked using Alkyne-mPEG. S-acylation is indicated by band-shifts in Az samples. Quantified data in (B) and (C) shows the mean S-acylation +/- SEM. Statistical significance was analysed using a one-way ANOVA, followed by a Dunnett's multiple comparisons test against GCP16 WT (B), or a Tukey's multiple comparisons test (C) (*p<0.5,**p<0.01,***p<0.001, n = 3)

3. The binding interface residues affect the protein stability of GCP16 and its ability to stabilise zDHHC9

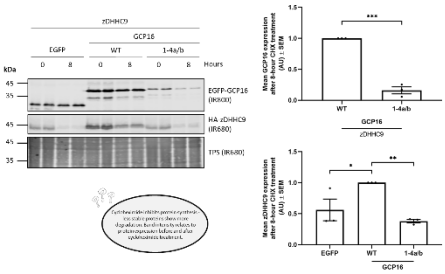

Figure 4. Expression of zDHHC9 in the presence of GCP16 binding interface mutant, after cycloheximide treatment. HEK 293T cells were co-transfected with EGFP, EGFP-tagged GCP16 WT, or interface mutant 1-4a/b, and HA-tagged zDHHC9. Cells were collected at 0 hour or treated with cycloheximide (CHX) for 8 hours. Intensity values for each sample were divided by the corresponding intensity value of the TPS in each sample (EGFP or HA/TPS). Quantified data shows the mean (± SEM) protein expression levels, calculated by dividing the 8h signal over that of the 0h and normalized to the highest value in each experiment, which was set to 1. Statistical significance was analysed using a one-way ANOVA, followed by a Dunnett's multiple comparisons test against GCP16 WT, or an unpaired t-test. (*p<0.5,**p<0.01,***p<0.001, n = 3)

4. Co-immunoprecipitation of zDHHC9 by GCP16 is not affected by introducing the binding interface mutations

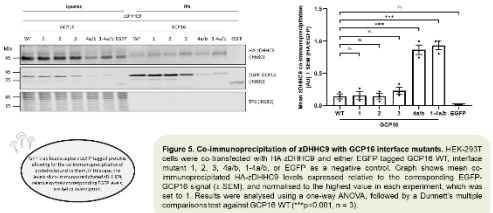

Figure 5. Co-immunoprecipitation of zDHHC9 with GCP16 interface mutants. HEK-293T cells were co-transfected with HA-zDHHC9 and either EGFP-tagged GCP16 WT, interface mutant 1, 2, 3, 4a/b, 1-4a/b, or EGFP as a negative control. Graph shows mean co-immunoprecipitated HA-zDHHC9 levels expressed relative to the corresponding EGFP-GCP16 signal (± SEM), and normalised to the highest value in each experiment, which was set to 1. Results were analysed using a one-way ANOVA, followed by a Dunnett's multiple comparisons test against GCP16 WT (***p<0.001, n = 3).

CONCLUSIONS

1A. Amino acid residues 12-20 in the N-terminus of GCP16 are important for its S-acylation and for stabilizing zDHHC9 S-acylation (Figure 2).

1B. No S-acylation is detected with the C-terminal truncation mutants 1-120, 1-122, 1-124, or 1-126, even though all S-acylation sites are present. GCP16 S-acylation is recovered with C-terminal mutant 1-128, suggesting an important role of the C-terminal region in facilitating S-acylation of the protein (Figure 2).

2. GCP16 interface mutants 3 and 4b show a decrease in S-acylation, while mutants 4a/b and 1-4a/b completely abolish protein S-acylation. zDHHC9 S-acylation is decreased when co-expressed with GCP16 mutants 3, 4b, 4a/b, or 1-4a/b. This suggests that both the N- and C-terminal regions of GCP16 are involved in GCP16 and zDHHC9 S-acylation and highlights important residues within GCP16 – K11, F13, R16, Y18, R118, R121, E124 (Figure 3).

3. GCP16 interface mutant 1-4a/b is less stable, compared to the WT protein. It has been shown that GCP16 WT can stabilize zDHHC9, but a decrease in zDHHC9 protein stability is seen when the protein is co-expressed with GCP16 1-4a/b (Figure 4).

4. Although the interface mutants disrupt the S-acylation of both GCP16 and zDHHC9, no loss of binding is detected in co-immunoprecipitation assays. It might be that additional mutations need to be introduced to fully displace the protein and disrupt the complex formation, or that additional factors present in the cell lysate can stabilize interactions of the mutant proteins (Figure 5).

MRS Medical Research Scotland — Funding a healthier future
Genentech
University of Strathclyde Glasgow
Chamberlain Lab
despoinaallagioti
despoina.allagioti.2017@uni.strath.ac.uk

Appendix II

TARGETING ZDHHC9 INTERACTIONS AS A NOVEL THERAPEUTIC STRATEGY

[1]Despoina Allagioti, [1]Nicholas Tomkinson, [2]Rami Hannoush and [1]Luke Chamberlain
[1]Strathclyde Institute of Pharmacy and Biomedical Sciences, University of Strathclyde, Glasgow, Scotland, UK
[2]Genentech, Inc., San Francisco, CA, USA

University of Strathclyde Glasgow

BACKGROUND

zDHHC9-mediated S-acylation controls the membrane association and signaling activity of Ras proteins.
Over-activation of the Ras signaling pathway results in uncontrolled cell division and cancer progression.

zDHHC9 activity depends on the binding with GCP16, however, little is known about this protein complex.

The aim of this project is to study the zDHHC9-GCP16 interaction and to use the information generated to design peptide inhibitors that disrupt the complex formation.

The hypothesis is that disrupting the zDHHC9-GCP16 interaction will inhibit the S-acylation activity of zDHHC9, perturbing the downstream signalling effects of Ras in cancer disease states.

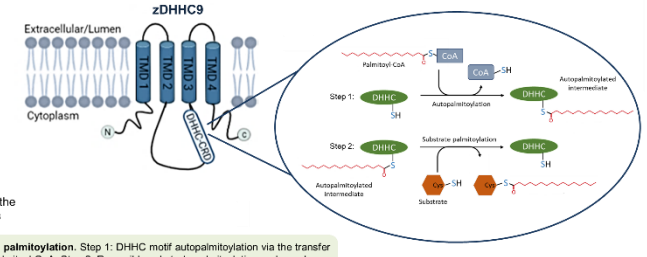

Figure 1. zDHHC9-mediated palmitoylation. Step 1: DHHC motif autopalmitoylation via the transfer of the palmitoyl group from palmitoyl-CoA. Step 2: Reversible substrate palmitoylation and membrane association. In the case of Ras, the cell signalling pathway is activated.

METHODS

Cell culture (HEK-293T) → Transfection → RUSH and Immunoprecipitation (Figure 2), Immunoprecipitation (Figures 3 and 5), Click chemistry (Figure 4) → Western Blotting

RESULTS

1. Controlling the localisation of zDHHC9 using RUSH

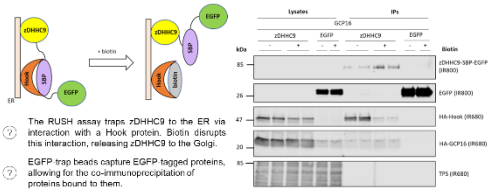

The RUSH assay traps zDHHC9 to the ER via interaction with a Hook protein. Biotin disrupts this interaction, releasing zDHHC9 to the Golgi.

EGFP trap beads capture EGFP tagged proteins, allowing for the co-immunoprecipitation of proteins bound to them.

Figure 2. Combined RUSH and immunoprecipitation assay of zDHHC9 and GCP16. HEK-293T cells were co-transfected with HA-GCP16 and Hook-zDHHC9-SBP-EGFP or EGFP-C2 as a negative control. Co-immunoprecipitation of HA-Hook and HA-GCP16 were detected -/+ 6-hour incubation with biotin (100μM).

2. Identification of two potential zDHHC9-interaction sites within GCP16

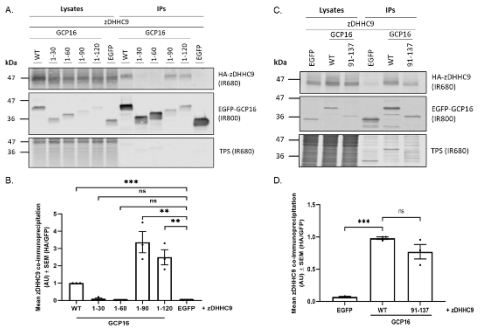

Figure 3. Co-immunoprecipitation of zDHHC9 with GCP16 mutants. HEK-293T cells were co-transfected with HA-zDHHC9 and either (A) EGFP-tagged GCP16 WT, 1-30, 1-60, 1-90, 1-120 or EGFP as a negative control or (C) EGFP-tagged GCP16 WT, 91-137 or EGFP as a negative control. Graphs show mean co-immunoprecipitated HA-zDHHC9 levels (± SEM), normalised to GCP16 WT which was set to 1. Results were analysed by unpaired t-tests (**p<0.01,***p<0.001, ns=non-significant, n = 3).

3. Binding of GCP16 1-90 to zDHHC9 is not sufficient for a functional interaction

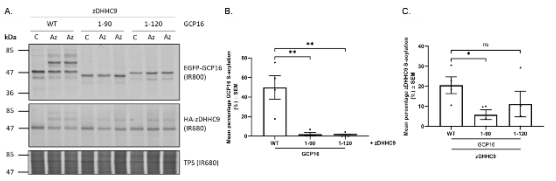

Figure 4. S-acylation of GCP16 1-90 and 1-120 and their effect on the stability of zDHHC9 S-acylation, detected using click-mPEG. HEK-293T cells were co-transfected with EGFP-tagged GCP16 WT, 1-90 and 1-120 and HA-tagged zDHHC9. Cells were labelled with Palmitic acid Azide (Az) or Palmitic acid as a control (C) for 4 hours and were then lysed and clicked using Alkyne-mPEG. S-acylation is indicated by band-shifts in Az samples. Quantified data shows the mean percentage intensity values (± SEM) of the S-acylated substrates. Results were analysed by unpaired t-tests (**p<0.01,***p<0.001,ns=non-significant, n = 4)

4. GCP16 interacts more strongly with zDHHC9 than with other zDHHC enzyme isoforms

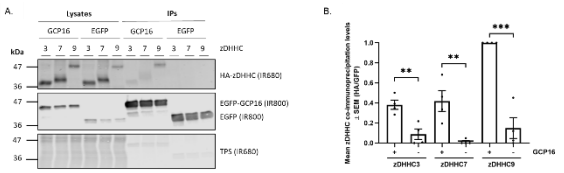

Figure 5. Co-immunoprecipitation of zDHHC3, zDHHC7 and zDHHC9 with GCP16. HEK-293T cells were co-transfected with HA-tagged zDHHC3, zDHHC7 or zDHHC9 and EGFP-tagged GCP16 or EGFP as a negative control. Graph shows mean co-immunoprecipitated HA-zDHHC levels (± SEM), normalised to the highest value which was set to 1. Statistical significance was analysed by unpaired t-tests (**p<0.01,***p<0.001, n = 4).

CONCLUSIONS

1. GCP16 is co-immunoprecipitated with zDHHC9 while zDHHC9 is trapped in the ER, indicating that the zDHHC9/GCP16 complex may form in the ER and move to the Golgi upon biotin-induced release (Figure 2).

2. zDHHC9 is co-immunoprecipitated with GCP16 1-90 and 1-120 but not 1-60 (Figure 3A), suggesting that the 60-90 amino acid region of GCP16 is important for binding to zDHHC9. However, zDHHC9 is also co-immunoprecipitated with GCP16 91-137, indicating that there is a potential second binding site for zDHHC9 within the 91-137 GCP16 region.

3. Although both GCP16 1-90 and 1-120 include all four S-acylation sites, they are not S-acylated (Figure 4B). This suggests that amino acids 121-137 of the C-terminal domain of GCP16 are important for GCP16 S-acylation. The decreased stability of zDHHC9 S-acylation in the presence of GCP16 1-90 (Figure 4C) implies that binding of GCP16 1-90 is not sufficient for a functional interaction between the two proteins, highlighting the potential importance of the second binding site within GCP16. Both zDHHC9-interaction sites could be within the 1-120 GCP16 region.

4. GCP16 is co-immunoprecipitated with other zDHHC enzyme isoforms that share a conserved DHHC domain, suggesting that the DHHC domain is involved in binding to GCP16. However, zDHHC9 shows increased specificity towards GCP16 and stronger binding (Figure 5).

despoinaallagioti
despoina.allagioti.2017@uni.strath.ac.uk